

MAGNESIUM AND AZ91 ALLOY BASED CAST COMPOSITES AND THEIR TRIBOLOGICAL CHARACTERISTICS

A THESIS

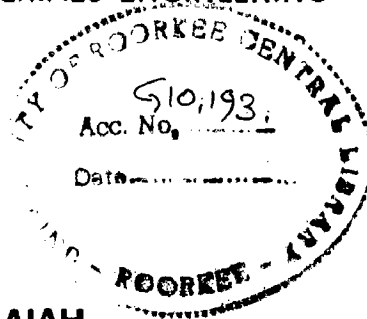
*Submitted in fulfilment of the
requirements for the award of the degree*

of

DOCTOR OF PHILOSOPHY

in

METALLURGICAL AND MATERIALS ENGINEERING



By

RAMALINGAIAH



**DEPARTMENT OF METALLURGICAL AND MATERIALS ENGINEERING
UNIVERSITY OF ROORKEE
ROORKEE-247 667 (INDIA)**

SEPTEMBER, 1999

UNIVERSITY OF ROORKEE
ROORKEE
CANDIDATE'S DECLARATION

I hereby certify that the work which is being presented in the thesis entitled **"MAGNESIUM AND AZ91 ALLOY BASED CAST COMPOSITES AND THEIR TRIBOLOGICAL CHARACTERISTICS"** in fulfilment of the requirement for the award of the Degree of Doctor of Philosophy, submitted in the Department of Metallurgical and Materials Engineering of the University is an authentic record of my own work carried out during a period from ~~Aug~~, 1996 to September, 1999 under the supervision of Dr. S. Ray.

The matter presented in this thesis has not been submitted by me for the award of any other degree of this or any other University.



(Ramalingaiah)

This is to certify that the above statement made by the candidate is correct to the best of my knowledge.

Date: 23 sept 1999



(Dr.S.Ray)

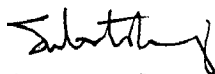
Professor

Department of Metallurgical and Material Engineering

University of Roorkee

Roorkee 247667 (U.P.)India

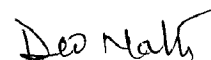
The Ph.D. Viva-Voice examination of **Ramalingaiah** Research Scholar, has been held on 14-8-2000



Signature of
Supervisor



Signature of
Head of Department



Signature of
External Examiner

ABSTRACT

The composites are tailor made materials designed to possess the required spectrum of properties for a given application. The constituents are chosen and combined to result in a composite which has properties not generally available in the constituents alone. The constituent which is spatially continuous in a composite, is called the matrix and the other constituents which are generally discontinuous, are dispersed in the matrix. The dispersed constituents may have different size, shape and orientations in a matrix. A composite may contain particles with length to diameter ratio around unity or fibers that has high length to diameter ratio. The fibers may be long and aligned along the length of the composite or may be short and aligned or random. Fibers which are expensive constituents compared to particles, may result in anisotropic properties disliked by designers. A composite containing particles dispersed in a matrix, often has isotropic properties and is relatively cheaper and attractive to industries. Solidification synthesis of composites decreases the processing cost of the composites and thus, provides the basic motive for pursuing cast particulate composites.

Weight saving is the prime mover for application of composites in space, aerospace and automobile industries. Since magnesium is about thirty five percent lighter than even aluminium, there is increasing use of magnesium and its alloys in aerospace and automobile industries. But magnesium and its alloy are of low modulus and medium strength. It is possible to add a small amount of reinforcement into magnesium or its alloy and improve their modulus and strength significantly while maintaining their density

close to the original value. (It is easy to fabricate magnesium and its alloys by a number of conventional techniques.) (Magnesium and its alloys are, therefore, attractive as a matrix for designing lightweight composites which may have considerable potential for future applications.)

(Engines including those used in vehicles, use a number of bearings.) In addition, there are components like valve seat where tribological properties like friction and wear are important factors deciding their service life. (By replacing the currently used denser alloys based on lead, tin, copper or iron in components by lightweight materials it is possible to achieve reduction in the weight of such engines resulting in considerable fuel economy. Magnesium or its alloys being soft materials, may provide a suitable matrix of a composite for developing bearing by incorporating hard load bearing constituents in it.) In the present study, the matrices of commercial magnesium and AZ91 alloy have been chosen for developing composites. The dispersed constituents are either steel wool or alumina which are considerably harder than the chosen matrix and are relatively cheap. Iron has insignificant solubility in magnesium and thus, has a high chemical compatibility with the matrix. But alumina may react with magnesium at the processing temperatures and has, therefore, a relatively poor chemical compatibility with magnesium and its alloys. A hybrid composite containing both alumina and graphite has also been synthesized and investigated.

The friction and wear in composites during its dry sliding against the counterface of hardened steel depends on the nature, extent and strength of contacts between the

asperities of the mating surfaces. The hardness of the materials in sliding contact determine the extent of real area of contact. Higher hardness and low interfacial strength at contact decreases both friction and wear. Steel wool may result in high hardness in the composite but when in contact with the counterface of hardened steel, may create contacts of high interfacial strength. Alumina is expected to impart hardness in the composite and at the same time, it will result in low interfacial strength contact with the steel counterface. Adding graphite to the composite containing alumina will decrease the interfacial strength further if it spread on the sliding surface. The present study also focuses on the synergy between the matrix and the dispersed constituents during dry sliding of composites and its effect on the observed friction and wear behaviour which may enrich our understanding of the material aspects of friction and wear.

In the present study, composites based on magnesium and AZ91 alloy have been synthesized by solidification processing. The composites containing dispersed steel wool or alumina have been characterized by microstructures and mechanical properties. The friction and wear behaviour of these composites under dry sliding condition have been determined. A hybrid composite containing alumina and graphite has also been synthesized and its tribological properties have been evaluated under dry sliding condition. (Chapter 1 contains the introductory remarks underscoring the technological importance of the problem under investigation.)

(Chapter-2 contains critical review of the existing literature) on the solidification processing of composites in general, and the techniques of vacuum infiltration and

squeeze casting in particular, since the synthesis of composites has been carried out in this study following these two techniques. Apart from information on magnesium, its common alloying elements and their effect on properties, phase diagrams and microstructure, relevant to this study, this chapter also reviews the existing knowledge base on the mechanical properties of magnesium and AZ91 alloy based composites, their friction and wear behaviour under dry sliding condition.

(Chapter 3 deals with the experimental procedures followed in the present investigation. The details of the vacuum casting and squeeze casting set-up and the parameters used for the synthesis of composites have been outlined. The methods used to determine the chemical composition of the composites and their densities are given. The method for carrying out X-ray diffraction analysis to identify the phase constituents has been described and these experiments have been supplemented by the results of electron probe microanalysis (EPMA) of selected sites in the microstructure. The procedure followed for investigating microstructures has also been outlined. Hardness and uniaxial tensile tests have been carried out following methods described in this chapter. The friction and dry sliding wear in the matrix materials and the composites have been determined by tests carried out in pin-on-disc machine against a counterface of En-32 steel hardened to HRC 62 to 65, following procedures outlined in this section. The applied normal load at sliding contact has been varied in the range between 0.5 to 2.5 kg for the composites containing steel wool but the composites containing alumina and both alumina and graphite have been tested at loads in the range between 2.5 to 5.5 kg. For all the tests the sliding speed has been maintained at 1 m/s. The wear debris generated during

sliding have been observed under stereo-optical microscope. The test surfaces after sliding have been examined under scanning electron microscope (SEM).

(Chapter-4 describes the results on magnesium and AZ91 alloy) matrix composites containing steel wool, (their mechanical) and tribological (properties). The distribution of steel wool in the composites has generally been inhomogeneous with steel wool rich and steel wool deficient areas. The solidification structures developed in these two areas are different. The Brinell hardness measurements indicate an increasing hardness with steel wool content. The ultimate tensile strength also increases similarly with steel wool content. The ultimate tensile strength in magnesium-steel wool composite increases by about 30% between 4.5 and 6.5 vol % of steel wool and it may be indicative of the role of mechanical and frictional restraint in steel wool during deformation.

The cumulative volume loss during dry sliding of the composites containing steel wool increases linearly with sliding distance at different loads following Archard's law. The coefficient of friction decreases rapidly with load which may be explained on the basis of the extent of cover provided by the transfer layer at lower loads and the softening of the matrix at higher loads. X-ray diffraction analysis indicates that the transfer layer contains amorphous and mixed oxides which will have lower adhesion with the counterface and thus, the coefficient of friction may decrease. The wear rate has not varied linearly with load although linear variation is predicted by Archard's law and this variation has been represented by two linear segments with a discontinuity that has been

attributed to softening of the matrix due to frictional heating and its effect on the transfer layer.

The wear rate in the composites has been calculated at different loads on the basis of estimated sharing of load and superposition of wear rates in the constituent phases. But the calculated values are much higher compared to those observed experimentally which has been attributed to the observed synergy between the constituent phases during dry sliding. At higher loads, the sliding surface has not revealed the presence of steel wool strands. The flow of softer matrix during sliding has covered the steel wool strands decreasing the overall friction. The real area of contact should also decrease because of higher hardness due to the presence of steel wool underlying the surface layer. This interaction between steel wool and commercial magnesium in these composites is of immense importance in decreasing the observed wear rates compared to the calculated ones. The wear coefficient which may be interpreted as wear rate per unit real area of contact, does not change significantly between the matrix and the composites. The composites has higher hardness that results in significant reduction in real area of contact which provides a major advantage in the composites. In wear coefficient, because of its definition, decrease in real area of contact becomes a disadvantage.

Chapter-5 describes the results on magnesium and AZ91 alloy matrix composites containing alumina, their mechanical and tribological properties. The distribution of alumina particles and the matrix microstructure have been characterized by optical microscopy. The phase constituents have been determined by X-ray diffraction and

EPMA. During processing of the composites at elevated temperatures, there is evidence of chemical reaction between the alumina particles and molten magnesium. The hardnesses have been measured in terms of Brinell hardness and Vickers microhardness for both the composites and the Brinell hardness increases with the alumina content.

The cumulative volume loss during dry sliding of the composites containing alumina increases more or less linearly with sliding distance at different loads following Archard's law. The coefficient of friction is higher at lower contact loads and it decreases with increasing load similar to that observed in composites containing steel wool. At lower loads, the cumulative volume loss and wear rate at different loads in magnesium-21 vol% alumina composites are significantly lower than those in both commercial magnesium and magnesium-23 vol% alumina composites. The variation of wear rate with load in magnesium-21 vol% alumina composites is more or less linear and distinct from the nonlinear variation observed in either magnesium or magnesium-23 vol% alumina composites. In the AZ91 alloy based composites, it is observed that the volume loss in the composite containing 16 vol% alumina is significantly lower than the other two composites containing 14 and 24 vol% alumina. The volume loss in the magnesium-21 vol% alumina composites is similar but lower than that in the AZ91 alloy based composite containing 16 vol% alumina. The wear rate increases more or less linearly in all the AZ91 alloy based composites investigated here but the wear rates observed in the composite containing 16 vol% alumina are considerably lower than those in the other two composites at similar loads. The extent of chemical reaction during processing and its

consequences appear to be responsible for this observed anomalous behaviour where composites of intermediate composition are showing better wear resistance.

Chapter-6 describes the results on magnesium and AZ91 alloy based hybrid composites containing particles of both alumina and graphite, their mechanical and tribological properties. The relative particle content in these hybrid composites could not be controlled during solidification processing as these particles of graphite and alumina have different densities and surface properties. The graphite level in the three magnesium based composites investigated are around 0.3 vol% only. In AZ91 alloy based composites the graphite contents are around 0.4 vol%. The Brinell hardness in these composites increases generally with the alumina content. The Vickers microhardness of primary phase increases by a little with alumina content but that observed in alumina decreases.

The cumulative volume loss during dry sliding of the composites containing alumina increases more or less linearly with sliding distance at different loads following Archard's law. If one compares the results on the coefficient of friction in magnesium based hybrid composites with those containing alumina alone, the hybrid composites containing 13 vol% alumina and that containing 15 vol% alumina shows the effect of graphite in terms of decreased coefficient of friction but the wear in these composites are relatively higher than that observed in the composite containing 18 vol% alumina. In the alloy based composites if one compares the results on hybrid composite containing 16 vol% alumina with the composite containing 16 vol% alumina alone, the volume loss in wear is a little higher in the hybrid composite but the coefficient of friction in it does not

indicate any effect of graphite. The wear rates in the hybrid composites are nonlinear excepting for the case of alloy based composite containing 17 vol% alumina.

Chapter-7 presents the major conclusions of the current study on the solidification processing, microstructure, mechanical properties and tribological behaviour of the magnesium and AZ91 alloy based composites containing steel wool, alumina or alumina and graphite together.

ACKNOWLEDGMENTS

(I express my deep sense of gratitude to Dr.Subrata Ray, professor of Metallurgical and Materials Engineering, for his valuable guidance and insightful advice. I have greatly benefited from his knowledge and experience throughout this work. His valuable and prompt remarks at the time of preparation of the manuscript are especially appreciated.)

I am grateful to the Quality Improvement Programme for providing me an opportunity to pursue this research and to the Magnagement of my College for the encouragement and support I received during the duration of this work.

(Thanks go to the technician staff of the Metallurgical Department for their help during casting and preparing the specimens.) Special thanks go to Mr.A Singh, MP, VP, SKS, AHK, SG, SSG, BDS and JS who have helped him in all possible ways during the experimental work. I also thank the staff of the University service and Instrumentation Centre, University of Roorkee for their assistance and cooperation.

I would like to express my reverence and great admiration for my parents, to whom I owe everything. They have been a guiding force all my life and I have tried to measure up to their expectations. I humbly dedicate this work to them.

When hurdles appeared insurmountable and targets unachievable, the encouragement and camaraderie of friends helped keep things in perspective. My sincere thanks to the many friends who helped lighten the burden, specially R.Tyagi, Prakash B.G, Bhowmik, S.B.Sharma, Dr.J.Devaraju, P.S.Puttaswamy, B.M.Manjunath, S.Prashanth, Satish Anngeri, V.T.Venkateshaiah, Basavarajappa and Narendra.Kumar.

Finally, I would like to thank my wife S.G. Anitha, and son A.R.Mohan, daughter A.R. Deepa for being an incessant source of inspiration and support. They found the power to encourage and support me and radiate strength and determination to help me overcome even the most daunting situation. I express my sincere gratitude for their forbearance and stoicism in the face of many inconveniences and long absences.

Ramalingaiah

CONTENTS

	Page. No.
Candidate's Declaration	i
Abstract	iii
Acknowledgments	xiii
Contents	xv
List of Figures	xxi
List of Tables	xxxiii
Notation	xxxvii
Chapter 1 Introduction	1
1.1 Introduction	1
Chapter 2 Literature Review	7
2.1 Magnesium and its Alloy	7
2.1.1 Alloying in Commercial Cast Magnesium Alloys	7
2.1.2 Properties of Magnesium and its Alloys	10
2.1.3 The Physical Properties of Dispersoids	11
(a) Mild Steel	
(b) Alumina	
(c) Graphite	
2.1.4 Solidification Processing of Magnesium Composites	13
2.1.4.1 Vacuum Infiltration	13
2.1.4.2 Squeeze Casting	14
2.1.4.3 Squeeze Casting of Magnesium Based Composite	18
2.1.4.4 Stir Casting	19
2.1.5 Magnesium Aluminium and Magnesium Zinc Alloys	21
(a) Microstructure and Phase Diagram of Mg-Al Alloys	
(b) Microstructure and Phase Diagram of Mg-Zn Alloys	
(c) Microstructure and Phase Diagram of Ternary Magnesium Alloys	

2.1.6	Mechanical Properties of Magnesium Alloys and Composites	24
	(a) Hardness of Magnesium Alloys and Composites	
	(b) Tensile Properties of Magnesium Alloys and Composites	
2.1.7	Friction and Dry Sliding Wear	36
	(a) Friction and its origin	
	(b) Dry Sliding Wear	
	(c) Friction and Dry Sliding Wear	
Chapter 3	Experimental Work	51
3.1	Slection of Matrix Alloy	51
3.2	Slection of Dispersoids	52
3.3	Solidification Processing of Composites	56
	3.3.1 Vacuum Casting	56
	3.3.2 Squeeze Casting	58
3.4	Determination of Chemical Composition and Densities	58
3.5	Metallography	59
3.6	Estimation of Dispersoid Content	59
3.7	X-Ray Diffraction Electron Probe Micro-Analysis (EPMA)	61
3.8	Hardness and Tensile Testing	62
	(a) Hardness Testing	
	(b) Tensile Testing	
3.9	Dry Sliding Wear Test	63
3.10	Microscopic Examinations	65
	3.10.1 Examination of Sliding Surface	65
	3.10.2 Examination of Wear Debris	65
Chapter 4	Magnesium Based Metal-Metal Composites	67
4.1	Results	67
	4.1.1 Chemical Composition	67

4.1.2	Density of Composites and Steel-Wool Content	67
4.1.3	Microstructure of the Composites	68
	(a) Magnesium Based Composite	
	(b) Magnesium AZ91 Alloy Based Composite	
4.1.4	Hardness of the Composites	79
4.1.5	Tensile Properties	86
4.1.6	Dry Sliding Friction and Wear	87
	(a) Magnesium-Steel Wool Composites	
	(b) Magnesium AZ91 Alloy-Steel Wool Composites	
4.1.7	Examination of Sliding Surface and Wear Debris	108
	(a) Commercial Magnesium and Steel Wool Composite	
	(b) AZ91 Magnesium Alloy and Steel Wool Composite	
4.1.8	Estimation of Wear Rate	124
4.2	Discussion	129
Chapter 5	Magnesium Based Metal-Ceramic Composites	141
5.1	Results	141
5.1.1	Chemical Composition	141
5.1.2	Density of Composites and Alumina Content	141
5.1.3	Microstructure of the Composites	143
	(a) Magnesium-Alumina-Composites	
	(b) AZ91 Alloy-Alumina-Composites	
5.1.4	Electron Probe Microanalysis (EPMA)	147
5.1.5	X-Ray Diffraction Studies	152
5.1.6	Hardness of the Composites	156
5.1.7	Dry Sliding Friction and Wear	159
	(a) Magnesium-Alumina-Composites	
	(b) AZ91 Alloy-Alumina-Composites	
5.1.8	Examination of Sliding Surface and Wear Debris	170
	(a) Magnesium-Alumina-Composites	
	(b) AZ91 Alloy-Alumina-Composites	

5.2	Discussion	176
Chapter 6	Hybrid Composite Bearing Graphite and Alumina	191
6.1	Results	191
6.1.1	Chemical Composition	191
6.1.2	Density of Composites and Particle Content	191
6.1.3	Microstructure of the Composites	192
(a)	Magnesium-Alumina-Graphite-Composites	
(b)	AZ91 Alloy-Alumina-Graphite-Composites	
6.1.4	Electron Probe Microanalysis (EPMA)	200
6.1.5	X-Ray Diffraction Studies	206
6.1.6	Hardness of the Composites	208
6.1.7	Dry Sliding Friction and Wear	212
(a)	Magnesium Based Hybrid Composites	
(b)	AZ91 Alloy Based Hybrid Composites	
6.1.8	Examination of Sliding Surface and Wear Debris	223
(a)	Hybrid Magnesium-Alumina-Graphite	
(b)	Hybrid AZ91 Alloy-Alumina-Graphite	
6.2	Discussion	228
Chapter 7	Conculsion	241
7.1	The composite containing steelwool	241
7.2	The composite containing Alumina	242
7.3	The hybrid composite containing Alumina and Grapite	244
References		247

List of Figures

	Page No.	
Fig. 2.1	Equilibrium diagrams and the mechanical properties of Magnesium alloys.	8
Fig. 2.2	Schematic diagram of the direct squeeze casting process.	15
Fig. 2.3	Schematic diagram of the indirect squeeze casting process.	16
Fig. 2.4	Equilibrium phase diagram of Mg-Al alloy system.	22
Fig. 2.5	Equilibrium phase diagram of Mg-Zn alloy system	23
Fig. 2.6	The solvus surfaces in magnesium alloys with aluminium and zinc.	25
Fig. 2.7	The six stages in coefficient of friction versus distance slid relationship.	38
Fig. 3.1	Part of equilibrium phase diagram of Mg-Fe alloy system showing solubility of Fe in liquid Mg.	53
Fig. 3.2	The standard free energies formation of various oxides, as a function of temperature.	54
Fig. 3.3	Phase diagram for the system MgO-Al ₂ O ₃ .	55
Fig. 3.4	Vacuum casting set-up used in present study.	57
Fig. 3.5	Squeeze casting set-up used in present study.	57
Fig. 3.6	The test specimens machined out from the cast ingots.	60
Fig. 3.7	Dimensions of the tensile specimens	64
Fig. 4.1	Microstructure of vacuum infiltrated commercial magnesium based composite containing 4.5 vol% steel wool, showing transverse section of steel wool strands in the matrix of commercial magnesium; X125.	70
Fig. 4.2	Microstructure of vacuum infiltrated commercial magnesium based composite containing 4.5 vol% steel wool, showing shrinkage cavity at the boundary of infiltrating streams; X250.	70
Fig. 4.3	Microstructure of commercial magnesium cast by vacuum infiltration showing bright primary phase and relatively dark interdendritic areas; X250.	71

Fig. 4.4	Microstructure of commercial magnesium cast by vacuum infiltration showing solute rich interdendritic area containing dark precipitates; X250.	71
Fig. 4.5	Microstructure of vacuum infiltrated commercial magnesium based composite containing 5.5 vol% steel wool, showing steel wool strands in the matrix of commercial magnesium; X125.	72
Fig. 4.6	Microstructure of vacuum infiltrated commercial magnesium based composite containing 5.5 vol% steel wool, showing shrinkage cavities at the boundary of infiltration streams; X125.	72
Fig. 4.7	Microstructure of vacuum infiltrated commercial magnesium based composite containing 5.5 vol% steel wool, showing relatively dark solute rich area; X125.	73
Fig. 4.8	Microstructure of vacuum infiltrated commercial magnesium based composite containing 5.5 vol% steel wool, showing steel wool in focus, containing ferrite and a little pearlite; X625.	73
Fig. 4.9	Microstructure of vacuum infiltrated commercial magnesium based composite containing 6.0 vol% steel wool, showing both transverse and longitudinal sections of steel wool strands in the matrix of commercial magnesium; X62.5.	75
Fig. 4.10	Microstructure of vacuum infiltrated commercial magnesium based composite containing 6.0 vol% steel wool, showing steel wool strands surrounding a location in the matrix of commercial magnesium; X250.	75
Fig. 4.11	Microstructure of vacuum infiltrated commercial magnesium based composite containing 6.5 vol% steel wool, showing different sections of steel wool strands in the matrix of commercial magnesium; X125.	76
Fig. 4.12	Microstructure of vacuum infiltrated commercial magnesium based composite containing 6.5 vol% steel wool, showing streams relatively darker marks in the last freezing area of the boundary of commercial magnesium; X250.	76
Fig. 4.13	Microstructure of vacuum infiltrated AZ91 alloy based composite containing 5.0 vol% steel wool, showing clustering of steel wool strands in the matrix of dendritically solidified AZ91 alloy; X250.	77

Fig. 4.14	Microstructure of vacuum infiltrated AZ91 alloy based composite containing 5.0 vol% steel wool, showing steel wool strands in the matrix of AZ91 alloy; where the last freezing liquid shows divorced eutectic; X625.	77
Fig. 4.15	Microstructure of AZ91 alloy cast by vacuum infiltration showing primary phase dendrites and interdendritic area of divorced eutectic; X250.	78
Fig. 4.16	Microstructure of vacuum infiltrated AZ91 alloy based composite containing 6.0 vol% steel wool, showing steel wool strands well distributed in the matrix of AZ91 alloy; Mag X125.	78
Fig. 4.17	Microstructure of vacuum infiltrated AZ91 alloy based composite containing 6.0 vol% steel wool, showing a thick network of solute rich phase touching steel wool strands in the matrix of AZ91 alloy; X625.	80
Fig. 4.18	Microstructure of vacuum infiltrated AZ91 alloy based composite containing 6.0 vol% steel wool, showing steel wool strands in the matrix of AZ91 alloy where there is a thick network of solute rich phase; X625.	80
Fig. 4.19	Microstructure of vacuum infiltrated AZ91 alloy based composite containing 7.0 vol% steel wool, showing steel wool strands in the matrix of AZ91 alloy; X125.	81
Fig. 4.20	Microstructure of vacuum infiltrated AZ91 alloy based composite containing 8.0 vol% steel wool, showing steel wool strands in the matrix of AZ91 alloy; X125.	81
Fig. 4.21	The variation of Brinell hardness with volume percent of steel wool in commercial magnesium and AZ91 alloy based composites containing steel wool.	83
Fig. 4.22	The variation of Vicker hardness with volume percent of steel wool in composites based on commercial magnesium.	85
Fig. 4.23	The variation of Vicker hardness with volume percent of steel wool in composites based on AZ91 alloy.	85
Fig. 4.24	The variation of Ultimate tensile strength (UTS) with volume percent of steel wool in commercial magnesium and AZ91 alloy based composites containing steel wool.	88

Fig. 4.25	The variation of cumulative volume loss with sliding distance in commercial magnesium under a constant sliding speed of 1.0 m/s.	89
Fig. 4.26	The variation of cumulative volume loss with sliding distance in commercial magnesium based composite containing 4.5 vol% of steel wool under a fixed sliding speed of 1.0 m/s.	89
Fig. 4.27	The variation of cumulative volume loss with sliding distance in commercial magnesium based composite containing 5.5 vol% of steel wool under a fixed sliding speed of 1.0 m/s.	90
Fig. 4.28	The variation of cumulative volume loss with sliding distance in commercial magnesium based composite containing 6.0 vol% of steel wool under a fixed sliding speed of 1.0 m/s.	90
Fig. 4.29	The variation of cumulative volume loss with sliding distance in commercial magnesium based composite containing 6.5 vol% of steel wool under a fixed sliding speed of 1.0 m/s.	91
Fig. 4.30	The variation of wear rate with normal load for commercial magnesium at a fixed sliding speed of 1.0 m/s.	91
Fig. 4.31	The variation of wear rate with normal load in commercial magnesium based composite containing 4.5 vol% of steel wool at a fixed sliding speed of 1.0 m/s.	93
Fig. 4.32	The variation of wear rate with normal loads in commercial magnesium based composite containing 5.5 vol% of steel wool at a fixed sliding speed of 1.0m/s.	93
Fig. 4.33	The variation of wear rate with normal loads in commercial magnesium based composite containing 6.0 vol% of steel wool at a fixed sliding speed of 1.0 m/s.	94
Fig. 4.34	The variation of wear rate with normal loads in commercial magnesium based composite containing 6.5 vol% of steel wool at a fixed sliding speed of 1.0 m/s.	94
Fig. 4.35	The variation of average coefficient of friction with sliding distance in commercial magnesium under a constant sliding speed of 1.0 m/s.	95
Fig. 4.36	The variation of average coefficient of friction with sliding distance in commercial magnesium based composite containing 4.5 vol% of steel wool under a fixed sliding speed of 1.0 m/s.	95

Fig. 4.37	The variation of average coefficient of friction with sliding distance in commercial magnesium based composite containing 5.5 vol% of steel wool under a fixed sliding speed of 1.0 m/s.	97
Fig. 4.38	The variation of average coefficient of friction with sliding distance in commercial magnesium based composite containing 6.0 vol% of steel wool under a fixed sliding speed of 1.0 m/s.	97
Fig. 4.39	The variation of average coefficient of friction with sliding distance in commercial magnesium based composite containing 6.5 vol% of steel wool under a fixed sliding speed of 1.0 m/s.	98
Fig. 4.40 (a)	The variation of average coefficient of friction with normal load for commercial magnesium at a fixed sliding speed of 1.0 m/s.	99
Fig. 4.40 (b)	The variation of average coefficient of friction with normal load in commercial magnesium based composite containing 4.5 vol% of steel wool at a fixed sliding speed of 1.0 m/s.	99
Fig. 4.40 (c)	The variation of average coefficient of friction with normal load in commercial magnesium based composite containing 5.5 vol% of steel wool at a fixed sliding speed of 1.0 m/s.	99
Fig. 4.40 (d)	The variation of average coefficient of friction with normal load in commercial magnesium based composite containing 6.0 vol% of steel wool at a fixed sliding speed of 1.0 m/s.	100
Fig. 4.40 (e)	The variation of average coefficient of friction with normal load in commercial magnesium based composite containing 6.5 vol% of steel wool at a fixed sliding speed of 1.0 m/s.	100
Fig. 4.41	The variation of cumulative volume loss with sliding distance in AZ91 alloy under a constant sliding speed of 1.0 m/s.	101
Fig. 4.42	The variation of cumulative volume loss with sliding distance in AZ91 alloy based composite containing 5.0 vol% of steel wool under a fixed sliding speed of 1.0 m/s.	101
Fig. 4.43	The variation of cumulative volume loss with sliding distance in AZ91 alloy based composite containing 6.0 vol% of steel wool under a fixed sliding speed of 1.0 m/s.	102
Fig. 4.44	The variation of cumulative volume loss with sliding distance in AZ91 alloy based composite containing 7.0 vol% of steel wool under a fixed sliding speed of 1.0 m/s.	102

Fig. 4.45	The variation of cumulative volume loss with sliding distance in AZ91 alloy based composite containing 8.0 vol% of steel wool under a fixed sliding speed of 1.0 m/s.	103
Fig. 4.46	The variation of wear rate with normal load for AZ91 alloy at a fixed sliding speed of 1.0 m/s.	103
Fig. 4.47	The variation of wear rate with normal load in AZ91 alloy based composite containing 5.0 vol% of steel wool at a fixed sliding speed of 1.0 m/s.	105
Fig. 4.48	The variation of wear rate with normal load in AZ91 alloy based composite containing 6.0 vol% of steel wool at a fixed sliding speed of 1.0 m/s.	105
Fig. 4.49	The variation of wear rate with normal load in AZ91 alloy based composite containing 7.0 vol% of steel wool at a fixed sliding speed of 1.0 m/s.	106
Fig. 4.50	The variation of wear rate with normal load in AZ91 alloy based composite containing 8.0 vol% of steel wool at a fixed sliding speed of 1.0 m/s.	106
Fig. 4.51	The variation of average coefficient of friction with sliding distance in AZ91 alloy under a constant sliding speed of 1.0 m/s.	107
Fig. 4.52	The variation of average coefficient of friction with sliding distance in AZ91 alloy based composite containing 5.0 vol% of steel wool under a fixed sliding speed of 1.0 m/s.	107
Fig. 4.53	The variation of average coefficient of friction with sliding distance in AZ91 alloy based composite containing 6.0 vol% of steel wool under a fixed sliding speed of 1.0 m/s.	109
Fig. 4.54	The variation of average coefficient of friction with sliding distance in AZ91 alloy based composite containing 7.0 vol% of steel wool under a fixed sliding speed of 1.0 m/s.	109
Fig. 4.55	The variation of average coefficient of friction with sliding distance in AZ91 alloy based composite containing 8.0 vol% of steel wool under a fixed sliding speed of 1.0 m/s.	110
Fig. 4.56 (a)	The variation of average coefficient of friction with normal load for AZ91 alloy at a fixed sliding speed of 1.0 m/s.	111
Fig. 4.56 (b)	The variation of average coefficient of friction with normal load in AZ91 alloy based composite containing 5.0 vol% of steel wool at a fixed sliding speed of 1.0 m/s.	111

Fig. 4.56 (c) The variation of average coefficient of friction with normal load in AZ91 alloy based composite containing 6.0 vol% of steel wool at a fixed sliding speed of 1.0 m/s.	111
Fig. 4.56 (d) The variation of average coefficient of friction with normal load in AZ91 alloy based composite containing 7.0 vol% of steel wool at a fixed sliding speed of 1.0 m/s.	112
Fig. 4.56 (e) The variation of average coefficient of friction with normal load in AZ91 alloy based composite containing 8.0 vol% of steel wool at a fixed sliding speed of 1.0 m/s.	112
Fig. 4.57 (a) SEM micrographs of the surface of commercial magnesium after sliding at a normal load of 0.5kg, X77.	114
Fig. 4.57 (b) SEM micrographs of the surface of commercial magnesium after sliding at a normal load of 2.5kg, X77.	114
Fig. 4.57 (c) SEM micrographs of the surface of commercial magnesium after sliding at a normal load of 2.5 kg of, X200.	114
Fig. 4.57 (d) SEM micrographs of the surface of commercial magnesium after sliding at a normal load of 2.5kg, X400.	114
Fig. 4.58 (a) SEM micrographs of the surface of commercial magnesium based composite containing 4.5 vol% of steel wool after sliding at a normal load of 0.5kg, X77.	115
Fig. 4.58 (b) SEM micrographs of the surface of commercial magnesium based composite containing 4.5 vol% of steel wool after sliding at a normal load of 2.5kg, X77.	115
Fig. 4.58 (c) SEM micrographs of the surface of commercial magnesium based composite containing 4.5 vol% of steel wool after sliding at a normal load of 0.5kg, X300.	115
Fig. 4.58 (d) SEM micrographs of the surface of commercial magnesium based composite containing 4.5 vol% of steel wool after sliding at a normal load of 2.5kg, X400.	115
Fig. 4.59 (a) Stereo microphotograph showing the wear debris of commercial magnesium, generated during dry sliding against steel disc at load of 0.5 kg ; X16.	116

Fig. 4.59 (b) Stereo microphotograph showing the wear debris of commercial magnesium, generated during dry sliding against steel disc at load of 2.5 kg ; X16.	116
Fig. 4.60 (a) Stereo microphotograph showing the wear debris of commercial magnesium based composite containing 4.5 vol% of steel wool, generated during dry sliding against steel disc at load of 0.5 kg ; X16.	117
Fig. 4.60 (b) Stereo microphotograph showing the wear debris of commercial magnesium based composite containing 4.5 vol% of steel wool, generated during dry sliding against steel disc at load of 2.5 kg ; X16.	117
Fig. 4.61 (a) SEM micrographs of the surface of AZ91 alloy after sliding at a normal load of 0.5kg, X77.	120
Fig. 4.61 (b) SEM micrographs of the surface of AZ91 alloy after sliding at a normal load of 2.5kg, X77.	120
Fig. 4.61 (c) SEM micrographs of the surface of AZ91 alloy after sliding at a normal load of 0.5kg, X200.	120
Fig. 4.61 (d) SEM micrographs of the surface of AZ91 alloy after sliding at a normal load of 2.5kg, X200.	120
Fig. 4.62(a) SEM micrographs of the surface of AZ91 alloy based composite containing 6.0 vol% steel wool at a normal load of 0.5 kg, X77.	121
Fig. 4.62(b) SEM micrographs of the surface of AZ91 alloy based composite containing 6.0 vol% steel wool at a normal load of 2.5 kg, X77.	121
Fig. 4.62(c) SEM micrographs of the surface of AZ91 alloy based composite containing 6.0 vol% steel wool at a normal load of 0.5 kg, X400.	121
Fig. 4.62(d) SEM micrographs of the surface of AZ91 alloy based composite containing 6.0 vol% steel wool at a normal load of 2.5 kg, X400.	121
Fig. 4.63 (a) Stereo microphotograph showing the wear debris of AZ91 alloy, generated during dry sliding against steel disc at different load of 0.5 kg, X16.	122
Fig. 4.63 (b) Stereo microphotograph showing the wear debris of AZ91 alloy, generated during dry sliding against steel disc at different load of 2.5 kg, X16.	122

Fig. 4.64 (a) Stereo microphotograph showing the wear debris of AZ91 alloy based composite containing 5.0 vol% of steelwool, genrated during dry sliding against steel disc at different load of 0.5 kg; X16.	123
Fig. 4.64 (b) Stereo microphotograph showing the wear debris of AZ91 alloy based composite containing 5.0 vol% of steel wool, genrated during dry sliding against steel disc at different load of 2.5 kg, X16.	123
Fig. 4.65 The calculated and experimental variation of wear rate with normal load in commercial magnesium based composite containing 4.5 vol% of steel wool at a fixed sliding speed of 1.0 m/s.	127
Fig. 4.66 The calculated and experimental variation of wear rate with normal load in commercial magnesium based composite contaning 5.5 vol% of steel wool at a fixed sliding speed of 1.0 m/s.	127
Fig. 4.67 The calculated and experimental variation of wear rate with normal load in commercial magnesium based composite contaning 6.0 vol% of steel wool at a fixed sliding speed of 1.0 m/s.	128
Fig. 4.68 The variation of wear rate with normal load for calculated and experimental result of in commercial magnesium based composite contaning 6.5 vol% of steel wool at a fixed sliding speed of 1.0 m/s.	128
Fig. 4.69 The calculated and experimental variation of wear rate with normal load in AZ91 alloy based composite contaning .0 vol% of steel wool at a fixed sliding speed of 1.0 m/s.	130
Fig. 4.70 The calculated and experimental variation of wear rate with normal load in AZ91 alloy based composite contaning 6.0 vol% of steel wool at a fixed sliding speed of 1.0 m/s.	130
Fig. 4.71 The calculated and experimental variation of wear rate with normal load in AZ91 alloy based composite contaning 7.0 vol% of steel wool at a fixed sliding speed of 1.0 m/s.	131
Fig. 4.72 The calculated and experimental variation of wear rate with normal load in AZ91alloy based composite contaning 8.0 vol% of steel wool at a fixed sliding speed of 1.0 m/s.	131
Fig. 5.1 Microstructure of Squeeze cast composite based on commercial magnesium containing 23 vol % of alumina, showing fairly uniform distribution of alumina particles in the matrix of commercial magnesium; X62.5.	143

Fig. 5.2	Microstructure of Squeeze cast composite based on commercial magnesium containing 23 vol % of alumina, showing fairly uniform distribution of alumina particles of different sizes in the matrix of commercial magnesium; X125.	143
Fig. 5.3	Microstructure of Squeeze cast composite based on commercial magnesium containing 23 vol % of alumina, showing network solute rich phase at the boundary of particles and in the matrix; X250.	145
Fig. 5.4	Microstructure of Squeeze cast composite based on commercial magnesium containing 23 vol % of alumina, a network of a phase in the matrix of commercial magnesium and irregular surface of the alumina particles; X625.	145
Fig. 5.5	Microstructure of Squeeze cast composite based on commercial magnesium containing 21 vol % of alumina, showing the particles rich and the particle deficient regions in the matrix of commercial magnesium; X62.5	146
Fig. 5.6	Microstructure of Squeeze cast composite based on commercial magnesium containing 21 vol % of alumina, boundaries of stream and relatively darker phases at the boundary of particles that is relatively more regular; X625.	146
Fig. 5.7	Microstructure of Squeeze cast composite based on AZ91 alloy containing 16 vol % of alumina, showing the inhomogenous particle distribution characterised by particle rich and the particle deficient regions in the matrix of AZ91 alloy; X62.5	148
Fig. 5.8	Microstructure of Squeeze cast composite based on AZ91 alloy containing 16 vol % of alumina, showing dendrites in the particle deficient regions in the matrix of AZ91 alloy and lamellar eutectic in the last freezing liquid; X250.	148
Fig. 5.9	Microstructure of Squeeze cast composite based on AZ91 alloy containing 16 vol % of alumina, showing irregular surface of the particles and lamellar eutectic rich and the particle deficient regions in the matrix of AZ91 alloy; X625.	149
Fig. 5.10 (a)	EPMA line scan for aluminium between two alumina particles in commercial magnesium based composite containing 23 vol% of alumina.	150
Fig. 5.10 (b)	EPMA line scan for aluminium between two alumina particles in commercial magnesium based composite containing 21 vol% of alumina	151

Fig. 5.11 (a) X-ray diffraction patterns of commercial magnesium and alumina particles used for synthesis of composites.	153
Fig. 5.11 (b) X-ray diffraction patterns of commercial magnesium based composites and AZ91 alloy based composites containing alumina particles used for synthesis of composites.	154
Fig. 5.12 The variation of Brinell hardness with volume percent of alumina in commercial magnesium based composites and AZ91 alloy based composites.	158
Fig. 5.13 The variation of Vickers hardness with volume percent of alumina in AZ91 alloy based composites.	158
Fig. 5.14 The variation of cumulative volume loss with sliding distance in commercial magnesium, during dry sliding under a constant sliding speed of 1.0 m/s against counterface of hardened steel.	160
Fig. 5.15 The variation of cumulative volume loss with sliding distance in commercial magnesium based composite containing 21 vol% of alumina, during dry sliding under a constant sliding speed of 1.0 m/s against counterface of hardened steel.	160
Fig. 5.16 The variation of cumulative volume loss with sliding distance in commercial magnesium based composite containing 23 vol% of alumina, during dry sliding under a constant sliding speed of 1.0 m/s against counterface of hardened steel.	161
Fig. 5.17 The variation of wear rate with normal load for commercial magnesium, during dry sliding at a fixed sliding speed of 1.0 m/s against counterface of hardened steel.	161
Fig. 5.18 The variation of wear rate with normal load in commercial magnesium based composite containing 21 vol% of alumina, during dry sliding at a fixed sliding speed of 1.0 m/s against counterface of hardened steel.	162
Fig. 5.19 The variation of wear rate with normal load in commercial magnesium based composite containing 23 vol% of alumina, during dry sliding at a fixed sliding speed of 1.0 m/s against counterface of hardened steel.	162
Fig. 5.20 The variation of coefficient of friction with sliding distance in commercial magnesium, during dry sliding under a constant sliding speed of 1.0 m/s against counterface of hardened steel.	163

- Fig. 5.21 The variation of coefficient of friction with sliding distance in commercial magnesium based composite containing 21 vol% of alumina, during dry sliding under a constant sliding speed of 1.0 m/s against counterface of hardened steel. 163
- Fig. 5.22 The variation of coefficient of friction with sliding distance in commercial magnesium based composite containing 23 vol% of alumina, during dry sliding under a constant sliding speed of 1.0 m/s against counterface of hardened steel. 164
- Fig. 5.23 The variation of coefficient of friction averaged over sliding distance, with normal load for commercial magnesium, during dry sliding at a fixed sliding speed of 1.0 m/s against counterface of hardened steel. 164
- Fig. 5.24 The variation of coefficient of friction averaged over sliding distance, with normal load in commercial magnesium based composite containing 21 vol% of alumina, during dry sliding at a fixed sliding speed of 1.0 m/s against counterface of hardened steel. 166
- Fig. 5.25 The variation of coefficient of friction averaged over sliding distance, with normal load in commercial magnesium based composite containing 23 vol% of alumina, during dry sliding at a fixed sliding speed of 1.0 m/s against counterface of hardened steel. 166
- Fig. 5.26 The variation of cumulative volume loss with sliding distance in AZ91 alloy based composite containing 14 vol% of alumina, during dry sliding under a constant sliding speed of 1.0 m/s against counterface of hardened steel. 167
- Fig. 5.27 The variation of cumulative volume loss with sliding distance in AZ91 alloy based composite containing 16 vol% of alumina, during dry sliding under a constant sliding speed of 1.0 m/s against counterface of hardened steel. 167
- Fig. 5.28 The variation of cumulative volume loss with sliding distance in AZ91 alloy based composite containing 24 vol% of alumina, during dry sliding under a constant sliding speed of 1.0 m/s against counterface of hardened steel. 168
- Fig. 5.29 The variation of wear rate with normal load for AZ91 alloy based composite containing 14 vol% of alumina, during dry sliding at a fixed sliding speed of 1.0 m/s against counterface of hardened steel. 168

- Fig. 5.30 The variation of wear rate with normal load for AZ91 alloy based composite containing 16 vol% of alumina, during dry sliding at a fixed sliding speed of 1.0 m/s against counterface of hardened steel. 169
- Fig. 5.31 The variation of wear rate with normal loads in AZ91 alloy based composite containing 24 vol% of alumina, during dry sliding at a fixed sliding speed of 1.0 m/s against counterface of hardened steel. 169
- Fig. 5.32 The variation of coefficient of friction with sliding distance for AZ91 alloy based composite containing 14 vol% of alumina, during dry sliding under a constant sliding speed of 1.0 m/s against counterface of hardened steel. 171
- Fig. 5.33 The variation of coefficient of friction with sliding distance in AZ91 alloy based composite containing 16 vol% of alumina, during dry sliding under a constant sliding speed of 1.0 m/s against counterface of hardened steel. 171
- Fig. 5.34 The variation of coefficient of friction with sliding distance in AZ91 alloy based composite containing 24 vol% of alumina, during dry sliding under a constant sliding speed of 1.0 m/s against counterface of hardened steel. 172
- Fig. 5.35 The variation of coefficient of friction averaged over sliding distance, with normal load in AZ91 alloy based hybrid composite containing 14 vol% of alumina, during dry sliding at a fixed sliding speed of 1.0 m/s against counterface of hardened steel. 172
- Fig. 5.36 The variation of coefficient of friction averaged over sliding distance, with normal load in AZ91 alloy based composite containing 16 vol% of alumina, during dry sliding at a fixed sliding speed of 1.0 m/s against counterface of hardened steel. 173
- Fig. 5.37 The variation of coefficient of friction averaged over sliding distance, with normal load in AZ91 alloy based hybrid composite containing 24 vol% of alumina, during dry sliding at a fixed sliding speed of 1.0 m/s against counterface of hardened steel. 173
- Fig. 5.38 (a) SEM micrograph of the surface of commercial magnesium based composite containing 21 vol% of alumina, after dry sliding at a normal load of 2.5 kg, X77. 174
- Fig. 5.38 (b) SEM micrograph of the surface of commercial magnesium based composite containing 21 vol% of alumina, after dry sliding at a normal load of 2.5 kg, X200. 174

Fig. 5.38 (c) SEM micrograph of the surface of commercial magnesium based composite containing 21 vol% of alumina, after dry sliding at a normal load of 2.5 kg, X400.	174
Fig. 5.39 (a) SEM micrograph of the surface of commercial magnesium based composite containing 21 vol% of alumina, after dry sliding at a normal load of 5.5 kg, X77.	175
Fig. 5.39 (b) SEM micrograph of the surface of commercial magnesium based composite containing 21 vol% of alumina, after dry sliding at a normal load of 5.5 kg, X200.	175
Fig. 5.39 (c) SEM micrograph of the surface of commercial magnesium based composite containing 21 vol% of alumina, after dry sliding at a normal load of 5.5 kg, X400.	175
Fig. 5.40 (a) Stereo microphotograph showing the wear debris of commercial magnesium based composite containing 21 vol% of alumina, generated during dry sliding against steel disc at load of 2.5 kg; X16.	177
Fig. 5.40 (b) Stereo microphotograph showing the wear debris of magnesium based composite containing 21 vol% of alumina, generated dry sliding against steel disc at load of 5.5 kg; X16.	177
Fig. 5.41 (a) SEM micrograph of the surface of AZ91 alloy based composite containing 16 vol% of alumina, after dry sliding at a normal load of 2.5 kg; X77.	178
Fig. 5.41 (b) SEM micrograph of the surface of AZ91 alloy based composite containing 16 vol% of alumina, after dry sliding at a normal load of 2.5 kg; X200.	178
Fig. 5.41 (c) SEM micrograph of the surface of AZ91 alloy based composite containing 16 vol% of alumina, after dry sliding at a normal load of 2.5 kg; X400.	178
Fig. 5.42 (a) SEM micrograph of the surface of AZ91 alloy based composite containing 16 vol% of alumina, after dry sliding at a normal load of 5.5 kg; X77.	179
Fig. 5.42 (b) SEM micrograph of the surface of AZ91 alloy based composite containing 16 vol% of alumina, after dry sliding at a normal load of 5.5 kg; X200.	179

Fig. 5.42 (c)	SEM micrograph of the surface of AZ91 alloy based composite containing 16 vol% of alumina, after dry sliding at a normal load of 2.5 kg; X400.	179
Fig. 5.43(a)	Stereo microphotograph showing the wear debris of AZ91 alloy based composite containing 16 vol% of alumina, generated during dry sliding against steel disc at different load of 2.5 kg; X16.	180
Fig. 5.43(b)	Stereo microphotograph showing the wear debris of AZ91 alloy based composite containing 16 vol% of alumina, generated during dry sliding against steel disc at different load of 5.5 kg; X16.	180
Fig. 6.1	Microstructure of Squeeze cast hybrid composite based on commercial magnesium containing 13 vol % of alumina and ~0.3 vol% of graphite, showing fairly uniform particle distribution; X62.5.	193
Fig. 6.2	Microstructure of Squeeze cast hybrid composite based on commercial magnesium containing 13 vol % of alumina and ~0.3 vol% of graphite, showing longer but smaller graphite particles along with a relatively darker phase in the bright matrix; X250.	193
Fig. 6.3	Microstructure of Squeeze cast hybrid composite based on commercial magnesium containing 13 vol % of alumina and ~0.3 vol% of graphite, show paricle rich areas where particle distribution is fairly uniform; X625.	195
Fig. 6.4	Microstructure of Squeeze cast hybrid composite based on commercial magnesium containing 15 vol % of alumina and ~0.3 vol% of graphite, showing darker regions of geraphite flakes only in certain regions; X62.5.	195
Fig. 6.5	Microstructure of Squeeze cast hybrid composite based on commercial magnesium containing 15 vol % of alumina and ~0.3 vol% of graphite, showing the geraphite flakes and solute rich phase; X250.	196
Fig. 6.6	Microstructure of Squeeze cast hybrid composite based on commercial magnesium containing 15 vol % of alumina and ~0.3 vol% of graphite, showing dark geraphite flakes and less dark solute rich phase in bright matrix; X625.	196
Fig. 6.7	Microstructure of Squeeze cast hybrid composite based on commercial magnesium containing 18 vol % of alumina and ~0.3 vol% of graphite, showing both particle rich and particle deficient regions; X62.5.	197

Fig. 6.8	Microstructure of Squeeze cast hybrid composite based on commercial magnesium containing 18 vol % of alumina and ~ 0.3 vol% of graphite, showing relatively darker phase surrounding the alumina particles; X250.	197
Fig. 6.9	Microstructure of Squeeze cast hybrid composite based on commercial magnesium containing 18 vol % of alumina and ~ 0.3 vol% of graphite, showing graphite particles in the relatively darker solute rich area and irregular particle boundaries; X625.	198
Fig. 6.10	Microstructure of Squeeze cast hybrid composite based on AZ91 alloy containing 16 vol % of alumina and ~ 0.4 vol% of graphite, show the highly inhomogenous particle distribution characterised by particle rich and the particle deficient regions in the matrix of AZ91 alloy; X62.5	198
Fig. 6.11(a)	Microstructure of Squeeze cast hybrid composite based on AZ91 alloy, containing 16 vol % of alumina and ~ 0.4 vol% of graphite, showing dendritic solidification in particle areas; X250.	199
Fig. 6.11(b)	Microstructure of Squeeze cast hybrid composite based on AZ91 alloy, containing 16 vol % of alumina and ~ 0.4 vol% of graphite, showing the formation of relatively dark solute rich phase at the boundary between the primary of magnesium solid solution; X625.	199
Fig. 6.12	Microstructure of Squeeze cast hybrid composite based on AZ91 alloy, containing 17 vol % of alumina and ~0.4 vol% of graphite, showing inhomogeneous distribution of particles; X62.5.	201
Fig. 6.13	Microstructure of Squeeze cast hybrid composite based on AZ91 alloy containing 17 vol % of alumina and ~0.4 vol% of graphite, showing the lamellar eutectic formed in the last freezing liquid; X250.	201
Fig. 6.14	Microstructure of Squeeze cast hybrid composite based on AZ91 alloy containing 17 vol % of alumina and 0.4 vol% of graphite, showing the lamellar eutectic and irregular boundaries of alumina particles; X625.	202
Fig. 6.15 (a)	EPMA line scan between the boundaries of two alumina particles.	203
Fig. 6.15 (b)	EPMA line scan showing distribution of aluminium across grey areas, next to white area.	204
Fig. 6.15 (c)	EPMA line scan analysis of aluminium-magnesium-zinc in the grey area, form of network or particles.	205

Fig. 6.16	X-ray diffraction patterns of commercial and magnesium and AZ91 Alloy based Hybrid Composites containing alumina and graphite.1	207
Fig. 6.17	The variation of Brinell hardness with volume percent alumina particles in commercial magnesium based hybrid composites containing ~0.3 vol% of graphite.	209
Fig. 6.18	The variation of Brinell hardness with volume percent of alumina particles in AZ91 alloy based hybrid composites containing ~ 0.4 vol% of graphite.	209
Fig. 6.19	The variation of Vickers hardness with volume percent of alumina particles in commercial magnesium based hybrid composites containing ~ 0.3 vol% of graphite.	211
Fig. 6.20	The variation of Vickers hardness with volume percent of alumina particles in AZ91 alloy based hybrid composites containing ~0.4 vol% of graphite.	211
Fig. 6.21	The variation of cumulative volume loss with sliding distance in commercial magnesium based hybrid composite containing 13 vol% of alumina and ~0.3 vol% of graphite, during dry sliding under a constant sliding speed of 1.0 m/s against counterface of hardened steel.	213
Fig. 6.22	The variation of cumulative volume loss with sliding distance in commercial magnesium based hybrid composite containing 15 vol% of alumina and ~0.3 vol% of graphite, during dry sliding under a constant sliding speed of 1.0 m/s against counterface of hardened steel.	213
Fig. 6.23	The variation of cumulative volume loss with sliding distance in commercial magnesium based hybrid composite containing 18 vol% of alumina and ~0.3 vol% of graphite, during dry sliding under a constant sliding speed of 1.0 m/s against counterface of hardened steel.	214
Fig. 6.24	The variation of wear rate with normal loads in commercial magnesium based hybrid composite containing 13 vol% of alumina and ~ 0.3 vol% of graphite during dry sliding at a fixed sliding speed of 1.0 m/s against counterface of hardened steel.	214

- Fig. 6.25 The variation of wear rate with normal loads in commercial magnesium based hybrid composite containing 15 vol% of alumina and ~ 0.3 vol% of graphite during dry sliding at a fixed sliding speed of 1.0 m/s against counterface of hardened steel. 215
- Fig. 6.26 The variation of wear rate with normal loads in commercial magnesium based hybrid composite containing 18 vol% of alumina and ~ 0.3 vol% of graphite during dry sliding at a fixed sliding speed of 1.0 m/s against counterface of hardened steel. 215
- Fig. 6.27 The variation of coefficient of friction with sliding distance in commercial magnesium based hybrid composite containing 13 vol% of alumina and ~ 0.3 vol% of graphite, during dry sliding under a constant sliding speed of 1.0 m/s against counterface of hardened steel. 217
- Fig. 6.28 The variation of coefficient of friction with sliding distance in commercial magnesium based hybrid composite containing 15 vol% of alumina and ~ 0.3 vol% of graphite, during dry sliding under a constant sliding speed of 1.0 m/s against counterface of hardened steel. 217
- Fig. 6.29 The variation of coefficient of friction with sliding distance in magnesium based hybrid composite containing 18 vol% of alumina and ~0.3 vol% of graphite, during dry sliding under a constant sliding speed of 1.0 m/s against counterface of hardened steel. 218
- Fig. 6.30 The variation of coefficient of friction averaged over sliding distance, with normal loads in commercial magnesium based hybrid composite containing 13 vol% of alumina and ~ 0.3 vol% of graphite during dry sliding at a fixed sliding speed of 1.0 m/s against counterface of hardened steel. 218
- Fig. 6.31 The variation of coefficient of friction averaged over sliding distance, with normal loads in commercial magnesium based hybrid composite containing 15 vol% of alumina and ~ 0.3 vol% of graphite during dry sliding at a fixed sliding speed of 1.0 m/s against counterface of hardened steel. 219
- Fig. 6.32 The variation of coefficient of friction averaged over sliding distance, with normal loads in commercial magnesium based hybrid composite containing 18 vol% of alumina and about 0.3 vol% of graphite during dry sliding at a fixed sliding speed of 1.0 m/s against counterface of hardened steel. 219

- Fig. 6.33 The variation of cumulative volume loss with sliding distance in AZ91 alloy based hybrid composite containing 16 vol% of alumina and ~0.4 vol% of graphite, during dry sliding under a constant sliding speed of 1.0 m/s against counterface of hardened steel. 220
- Fig. 6.34 The variation of cumulative volume loss with sliding distance in AZ91 alloy based hybrid composite containing 17 vol% of alumina and ~0.4 vol% of graphite, during dry sliding under a constant sliding speed of 1.0 m/s against counterface of hardened steel. 220
- Fig. 6.35 The variation of cumulative volume loss with sliding distance in AZ91 alloy based hybrid composite containing 19 vol% of alumina and ~0.4 vol% of graphite, during dry sliding under a constant sliding speed of 1.0 m/s against counterface of hardened steel. 221
- Fig. 6.36 The variation of wear rate with normal loads in AZ91 alloy based hybrid composite containing 16 vol% of alumina and ~0.4 vol% of graphite, during dry sliding at a fixed sliding speed of 1.0 m/s against counterface of hardened steel. 221
- Fig. 6.37 The variation of wear rate with normal loads in AZ91 alloy based hybrid composite containing 17 vol% of alumina and ~ 0.4 vol% of graphite, during dry sliding at a fixed sliding speed of 1.0 m/s against counterface of hardened steel. 222
- Fig. 6.38 The variation of wear rate with normal loads in AZ91 alloy based hybrid composite containing 19 vol% of alumina and ~0.4 vol% of graphite, during dry sliding at a fixed sliding speed of 1.0 m/s against counterface of hardened steel. 222
- Fig. 6.39 The variation of coefficient of friction with sliding distance in AZ91 alloy based hybrid composite containing 16 vol% of alumina and ~ 0.4 vol% of graphite, during dry sliding under a constant sliding speed of 1.0 m/s against counterface of hardened steel. 224
- Fig. 6.40 The variation of coefficient of friction with sliding distance in AZ91 alloy based hybrid composite containing 17 vol% of alumina and ~0.4 vol% of graphite, during dry sliding under a constant sliding speed of 1.0 m/s against counterface of hardened steel. 224
- Fig. 6.41 The variation of coefficient of friction with sliding distance in AZ91 alloy based hybrid composite containing 19 vol% of alumina and ~ 0.4 vol% of graphite, during dry sliding under a constant sliding speed of 1.0 m/s against counterface of hardened steel. 225

- Fig. 6.42 The variation of coefficient of friction averaged over sliding distance, with normal loads in AZ91 alloy based hybrid composite containing 16 vol% of alumina and ~0.4 vol% of graphite during dry sliding at a fixed sliding speed of 1.0 m/s against counterface of hardened steel. 225
- Fig. 6.43 The variation of coefficient of friction averaged over sliding distance, with normal loads in AZ91 alloy based hybrid composite containing 17 vol% of alumina and ~0.4 vol% of graphite during dry sliding at a fixed sliding speed of 1.0 m/s against counterface of hardened steel. 226
- Fig. 6.44 The variation of coefficient of friction averaged over sliding distance, with normal loads in AZ91 alloy based hybrid composite containing 19 vol% of alumina and ~0.4 vol% of graphite during dry sliding at a fixed sliding speed of 1.0 m/s against counterface of hardened steel. 226
- Fig. 6.45 (a) SEM micrograph of the surface of commercial magnesium based hybrid composite containing 13 vol% alumina and ~0.3 vol% of graphite after dry sliding at a normal load of 2.5 kg, X77. 227
- Fig. 6.45 (b) SEM micrograph of the surface of commercial magnesium based hybrid composite containing 13 vol% alumina and ~0.3 vol% of graphite after dry sliding at a normal load of 2.5 kg, X200. 227
- Fig. 6.45 (c) SEM micrograph of the surface of commercial magnesium based hybrid composite containing 13 vol% alumina and ~0.3 vol% of graphite after dry sliding at a normal load of 2.5 kg, X400. 227
- Fig. 6.46 (a) SEM micrograph of the surface of commercial magnesium based hybrid composite containing 13 vol% alumina and ~0.3 vol% of graphite after dry sliding at a normal load of 5.5 kg, X77. 229
- Fig. 6.46 (b) SEM micrograph of the surface of commercial magnesium based hybrid composite containing 13 vol% alumina and ~0.3 vol% of graphite after dry sliding at a normal load of 5.5 kg, X200. 229
- Fig. 6.46 (c) SEM micrograph of the surface of commercial magnesium based hybrid composite containing 13 vol% alumina and ~0.3 vol% of graphite after dry sliding at a normal load of 5.5 kg, X400. 229
- Fig. 6.47 (a) Stereo microphotograph showing the wear debris of commercial magnesium based hybrid composite containing 13 vol% of alumina and ~0.3 vol% of graphite generated during dry sliding against steel disc at load of 2.5 kg; X16. 230

- Fig. 6.47 (b) Stereo microphotograph showing the wear debris of commercial magnesium based hybrid composite containing 13 vol% of alumina and ~ 0.3 vol% of graphite generated during dry sliding against steel disc at load of 5.5 kg; X16. 230
- Fig. 6.48 (a) SEM micrograph of the surface of AZ91 alloy based hybrid composite containing 16 vol% of alumina and ~0.4 vol% of graphite after dry sliding at a normal load of 2.5 kg; X200. 231
- Fig. 6.48 (b) SEM micrograph of the surface of AZ91 alloy based hybrid composite containing 16 vol% of alumina and ~0.4 vol% of graphite after dry sliding at a normal load of 2.5 kg; X400. 231
- Fig. 6.49 SEM micrograph of the surface of AZ91 alloy based hybrid composite containing 17 vol% of alumina and ~0.4 vol% of graphite after dry sliding at a normal load of 5.5 kg; X200. 231
- Fig. 6.50 (a) Stereo microphotograph showing the wear debris of AZ91 alloy based hybrid composite containing 16 vol% of alumina and ~ 0.4 vol% of graphite generated during dry sliding against steel disc at different load of 2.5 kg; X16. 232
- Fig. 6.50 (b) Stereo microphotograph showing the wear debris of AZ91 alloy based hybrid composite containing 16 vol% of alumina and ~ 0.4 vol% of graphite generated during dry sliding against steel disc at different load of 5.5 kg; X16. 232

LIST OF TABLES

		Page No.
Table No. 2.1	Average Power Requirements for Turning, Based on the Volume of Metal Removed Per Minute.	11
Table No. 2.2	Heat Treatment Parameters.	31
Table No. 2.3	Comparison of Mechanical Properties in Mg-Alloy-15% vol% SiC composition	35
Table No. 3.1	Chemical Composition of Magnesium and AZ91 Alloy wt%	51
Table No. 3.2	Processing Routes for Synthesis of Composites	56
Table No. 4.1	Chemical Composition of Magnesium-Steel Wool Composites	67
Table No. 4.2	Density of Magnesium Steel Wool Composites and Steel Wool content	68
Table No. 4.3 (a)	Brinell Hardness of the cast Commercial Magnesium and Magnesium-Steel Wool Composites	79
Table No. 4.3 (b)	Brinell Hardness of the AZ91 Alloy and Alloy-Steel Wool Composite	82
Table No. 4.4 (a)	Vickers Hardness of the Cast Commercial Magnesium and Magnesium-Steel Wool Composites	84
Table No. 4.4 (b)	Vickers Hardness of the AZ91 Alloy and AZ91 Alloy-Steel Wool Composites	84
Table No. 4.5 (a)	Ultimate Tensile Strength of the Cast Commercial Magnesium and Magnesium-Steel Wool Composites	86
Table No. 4.5 (b)	Ultimate Tensile Strength of the AZ91 and AZ91 Alloy-Steel-Wool Composites	86
Table No. 4.6 (a)	Average Wear Coefficient of Magnesium and Magnesium-Steel Wool Composites	96
Table No. 4.6 (b)	Average Wear Coefficient of AZ91 Alloy and AZ91 Alloy-Steel Wool Composites	108
Table No. 4.7 (a)	X-Ray Diffraction Analysis for Wear Debris Generated During Sliding of Magnesium	118

Table No. 4.7 (b)	X-Ray Diffraction Analysis for Wear Debris Generated During Sliding of Magnesium-4.5 vol% Steel Wool Composites	118
Table No. 4.7 (c)	X-Ray Diffraction Analysis for Wear Debris Generated During Sliding of Magnesium-6.5 vol% Steel Wool Composites	118
Table No. 5.1	Chemical Composition of Composites	141
Table No. 5.2	Densities and Alumina Content of Composites and Squeeze Cast Magnesium	142
Table No. 5.3 (a)	Composition of Solute Rich Phase at Particle Boundry	152
Table No. 5.3 (b)	Composition of Solute Rich Phase in Matrix	152
Table No. 5.4	Lattice Parameters for Magnesium Solid Solution in Composites	156
Table No. 5.5	Brinell Hardness of Composite and Squeeze Cast Magnesium	156
Table No. 5.6	Vickers Hardness of Composite and Squeeze Cast Magnesium	157
Table No. 6.1	Chemical Composition of Hybrid Composites Bearing Graphite and Alumina	191
Table No. 6.2	Density of Composites and Constituents and Estimated Particle Contents	192
Table No. 6.3	Composition of Solute Rich Phase at White Area	206
Table No. 6.4	Lattice Parameters for Magnesium Solid Solution in Hybrid Composites	208
Table No. 6.5	Brinell Hardness of the Mg-Alumina-Graphite Composites and AZ91-Alumina-Graphite Composites	210
Table No. 6.6	Vickers Hardness of the Mg-Alumina-Graphite Composites and AZ91-Alumina-Graphite Composites	210

NOTATION

PDN	Particulate Dispersion Number
H_0	Height of the Melt
Ω	Angular Velocity
r_i	Radius of the inner Cylinder
μ	Viscosity of the Slurry
d	Gap between the inner and outer Cylinder
V_t	Particle Settling Velocity
E_c	Young's Modulus of the Composite
E_f	Young's Modulus of the Reinforcement
V_f	Volume Fraction of the Reinforcement
V_m	Volume Fraction of the Matrix
s	Particle aspect ratio
σ_y	Yield Strength of Composite
G_m	Shear Moduli of the Matrix
G_p	Shear Moduli of the Particle
b	Burger's Vector
μ_1	Inter Particle Spacing
σ	Stress
ε_c	Strain
μ	Coefficient of Friction
S	Sliding Distance
ρ	Density, gm/cm ³
UTS	Ultimate Tensile Strength
μ	Coefficient of Friction
θ	Contact Angle
λ	Heat Coefficient
ρ_c	Density of Composite Containing Steel Wool

ρ_m	Density of Matrix
ρ_{st}	Density of Steel Wool
ρ_A	Density of Alumina
ρ_{gr}	Density of Graphite
N	Normal Contact Load
H₀	Microhardness of Magnesium Matrix
H_f	Microhardness of Steel wool
N₀	Normal Contact Load of the Matrix
N_f	Normal Contact Load of the Steel Wool
A_{ro}	Real Area of Contact in the Matrix
A_{rf}	Real Area of Contact in the Steel Wool
x	Volume Fraction of Particles of both Alumina and Graphite
f_A	Fraction Volume of Alumina in a Composite
f_{gr}	Fraction Volume of Graphite in a Composite

CHAPTER-1

INTRODUCTION

Development of cast metal matrix composites (MMC) is continuing for the last thirty years now because of active interest taken by automobile manufacturers, particularly in light weight composites. Toyota company, Japan, developed saffil fiber reinforced connecting rods made of aluminium in mid seventies and Honda Co., Japan, developed aluminium engine block reinforced by graphite and saffil fibers. Aluminium and its alloys have so far been the dominating choice as matrix material for the synthesis of MMC. The dispersoids have generally been ceramic particles, whiskers or fibers which also act as load bearing constituents in the composite. The composites containing hard dispersoids has superior strength and stiffness at ambient temperature and elevated temperatures compared to the matrix alloy. They may also have better resistance to abrasion wear. Honda company has developed valve seat from aluminium alloy reinforced with saffil fiber for enhanced life due to superior high temperature strength and wear resistance. Graphite particles and fibers have been incorporated in aluminium and its alloys to develop low friction material having higher resistance to wear even under dry sliding. The spectrum of properties that one can achieve in a composite, is the result of synergy between the constituents and these properties cannot be achieved in any of its constituents alone. Thus, the composite materials have extended the horizon of engineering materials and significant research efforts have been directed to develop different composites and determine their potential as future engineering material.

A major thrust in the development of composite technology has come from the efforts to substitute relatively heavier conventional components by those made of light weight composites. In these composites, lower density helps to reduce weight and superior stiffness results in reducing the dimensions of a component. About 200 composites with a high specific strength/weight ratio have so far been introduced in the recently manufactured aircraft (Dexter, 1980). However, depending on the quantum of economic

advantage, the premium on weight savings are different in the land, air and space transportation. For example, the automobile industries may be able to afford an additional expenditure of \$10 per kilogram of weight savings where as the missile industry may afford \$10,000 per kg (Ray, 1994). The quality and reliability of the components and the access to technologies for the manufacture of composite components are limited by the extent of economic advantage. The automobile industries are high volume user of materials compared to either space or aerospace industries but a lower premium on weight saving has limited their choice in metal matrix composites (MMC) primarily to composites synthesized by solidification processing (Ray, 1995).

Design of composite materials for a given application may address primary issues like the selection and distribution of constituent phases, the nature of interface and the need for interface tailoring to attain good bonding. The interface between the reinforcement and the matrix plays an important role in determining the characteristic properties in a composite. Normally in composites employed in static or dynamic structures, it is desirable to have a strong enough interface which could permit transfer and distribution of load from the matrix to the reinforcement. In the ideal case, the interface should be a continuum across the interface involving coherency of bonds at the atomic level but a chemical discontinuity requiring absence of any interdiffusion between the constituents. In magnesium alloys, wetting is generally not a problem with the reinforcements like alumina, SiC etc. that have been so far used to reinforce magnesium and its alloys. But interfacial reaction between the dispersed phase and the molten alloy has been a major problem.

The primary methods for solidification processing of metal matrix composites containing ceramic phase as established over recent years are: (1) melt stirring method of introducing and dispersing ceramic phase in molten alloy, (2) squeeze casting to force molten alloy under pressure into a preform or a bed of ceramic phase and finally, (3) pressure infiltration by the suction of molten alloy through ceramic preform or bed (Ray 1993, Rohatgi and Asthana 1988). All three methods as well as several variations of them have been used to make magnesium composites.

Largely overshadowed by aluminium alloys for the last three decades, magnesium alloys struggled to retain its share in light-weight castings during the forties and fifties and maintained a niche usage in certain machine housings, aerospace, automotive and nuclear applications. The development of magnesium alloys of enhanced strength has led to increasing use of magnesium alloys in components of automobiles. Currently about 10 kg of magnesium is used in components in every car and this amount is increasing every year. A number of components are being developed for application in aircraft and automobiles. Automotive pulley, cog tooth sprockets, oil pump cover, cylinder liner and aircraft engine castings made of magnesium and its alloys are already employed in service (Baker 1989 and Evans 1986).

From the pioneering investigation on stir casting of composites, alumina has been used as dispersoids because it is hard, abundantly available and cheap. Incorporating alumina in metals and alloys results in superior high temperature strength and creep resistance. However, alumina is not thermodynamically stable at the high temperatures of solidification processing of composites. There is a need to understand the reaction and assess the impact of the reaction products on the properties.

Steel has density around 7860 kg/m^3 compared to 1840 kg/m^3 in magnesium. It is possible to introduce different amounts of steel wool in magnesium and synthesize metal-metal composites retaining an extent of advantage in density. Since magnesium has negligible solubility for iron and is soft, it may be possible to use it as a matrix for bearing material if it is strengthened by a hard load bearing phase. Magnesium-steel wool metal-metal composite may prove to be an interesting tribological material.

Magnesium and its alloys require control of environment to prevent their burning during solidification processing. A number of fluxes have been developed to provide cover to the melt during processing. SF_6/CO_2 atmosphere over the melt is quite popular now-a-days. During squeeze casting the processing is done in an enclosed chamber where the control of environment or cover to prevent burning will not be necessary. The suction of molten magnesium in a chamber where packed steelwool could be infiltrated, is possible

by the evacuation of the chamber and under the low pressure conditions prevailing there may not be need for precaution to prevent burning.

In squeeze casting, a hydrostatic pressure is applied to the entire volume of liquid metal in a die cavity, so that a casting free from shrinkage and porosity, is produced. Squeeze casting is a process which involves the solidification of molten metal in a closed die under an imposed high pressure. The high applied pressure which is several orders of magnitude greater than the melt pressure developed in normal casting processes keeps entrapped gases in solution and squeezes molten metal from hot spots to incipient shrinkage pores. As a result, the porosity in a squeeze cast component is almost eliminated resulting in superior quality of composites. Further more, due to the elimination of the air gap at the liquid-mold interface by the applied high pressure, the heat transfer across die surface is enhanced, which increases solidification and cooling rates.

The hardness and the tensile strength needs to be improved in lightweight magnesium so that it may be employed in more engineering components. The present study aims to reinforce commercial magnesium and AZ91 alloy by reinforcing it with steelwool which is quite cheap. However, the advantages in density and corrosion resistance may get compromised to an extent in these composites containing steelwool but there will be no interfacial reaction or any significant dissolution of steelwool. These composites may also be applied in bearing as the soft matrix of magnesium or its alloys will be able to match the contour of the shaft to establish a uniform gap necessary for establishing the condition for hydrodynamic lubrication. The hard phase of steelwool will bear the load of the shaft. Thus, the magnesium-steelwool composite may have potential as bearing material and the present study investigates the dry sliding friction and wear behaviour of this metal-metal composite.

Ceramic particles generally do not make strong interfaces with the counterface. Hard ceramic particles in a composite increases its hardness and the real area of contact decreases during dynamic contact. Therefore, tribological materials showing low friction and wear have been developed by reinforcing metals or alloys by hard ceramic particles like alumina or silicon carbide (Rohatgi, Ray and Liu, 1992). Solidification processing of

composite containing hard particles like alumina will result in considerable reaction at the interface between the particle and the matrix (Kamado and Kojima, 1997). The present study aims to study the effect of the products of interfacial reaction in commercial magnesium and AZ91 alloy based composites containing alumina, on the friction and wear behaviour under dry sliding condition.

Soft particles like graphite are often incorporated in metals or alloys to develop tribological materials having low friction and wear. Graphite, being a layered solid with very weak bonds across the layers, slip easily over the layers and act as solid lubricant. In a composite, during dry sliding, graphite particles from below the sliding surface have been observed to squeeze out of its location on to the surface and smear over it. Thus, there is reduced contact of the metallic constituent of the composite with the counterface and the coefficient of friction decreases. However, a composite containing graphite has lower hardness compared to the matrix material and thus, the real area of contact during sliding increases. The present study, therefore, attempts to study the dry sliding friction behaviour of hybrid composites containing both hard particles of alumina and soft particles of graphite where alumina will help to reduce the real area of contact and graphite will reduce direct metal to metal contact between the matrix and the counterface.

In summary, the present study is an attempt to explore the possibilities of developing lightweight material based on magnesium with better friction and wear characteristics. In the three classes of composites investigated - metal-metal, metal-ceramic and hybrid, the effect of strengthening the matrix of a composite by alloying on the dry sliding friction and wear behaviour will be investigated by comparing the results observed in a class of composite when the matrix has been changed from commercial magnesium to AZ91 alloy. The impact of interfacial reaction between the matrix and the particles in metal-ceramic and hybrid composites on their friction and wear behaviour is another aspect of the present investigation. The knowledge base generated through this study is expected to offer a better understanding of these classes of composites and help to utilize their potential as tribological materials in future applications.

CHAPTER-2

✓LITERATURE REVIEW

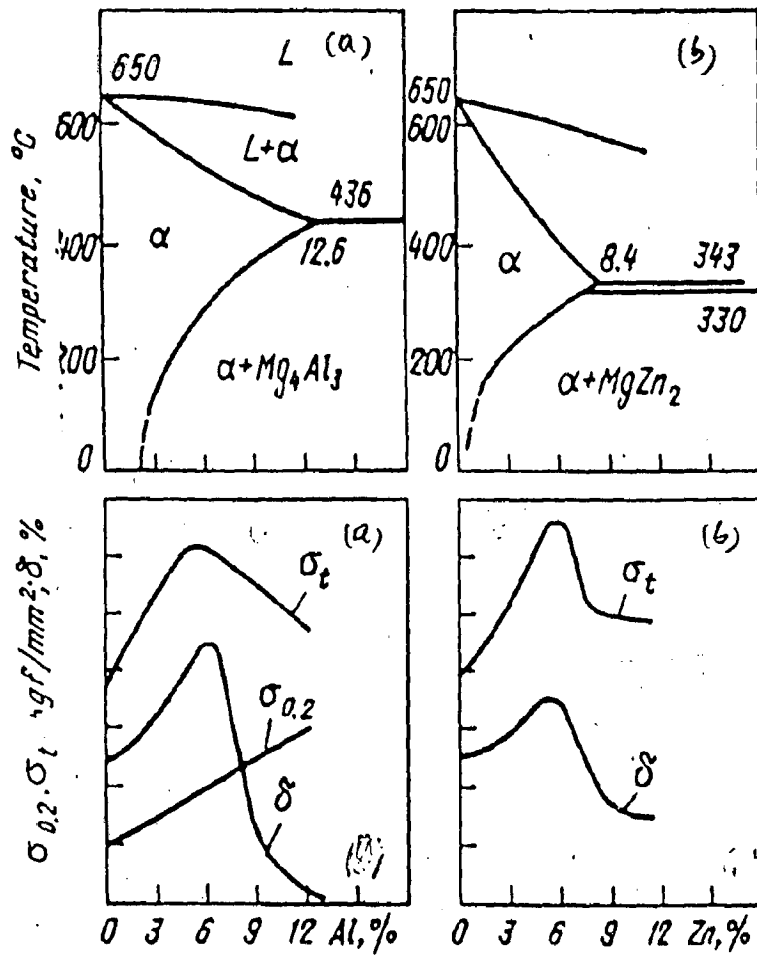
✓2.1 Magnesium and its Alloy

Magnesium is an alkaline-earth metal belonging to the second group of Mendeleev's periodic table of elements. Its atomic number is 12 and its atomic mass is 24.312. The color of magnesium is light - gray and its characteristic feature is its low density of 1.74 g/cm^3 . Magnesium has hexagonal close packed unite cell with lattice parameters of $a=3.203 \text{ \AA}$ and $c=5.2002 \text{ \AA}$. The c/a ratio is 1.62354 (Lakhtin, Yu., 1990) The thermal conductivity of magnesium is $0.3 \text{ cal/cm-s-}^\circ\text{C}$ which is considerably less than that of aluminium but their coefficients of linear expansion are about the same i.e., $26.1 \times 10^{-6} \text{ mm/(mm-}^\circ\text{C)}$ at 20°C to 100°C . Magnesium is lightweight and has excellent mechanical strength and proven corrosion resistance. All these properties have contributed to its increasing application particularly in automotive components.

The properties of magnesium can be substantially improved by alloying. The most widely used alloys are those containing aluminium up to 10 wt%, zinc up to 5 or 6 wt%, manganese up to 2.5 wt% and zirconium up to 1.5 wt%. The alloying elements form solid solution in magnesium and also, intermetallic compounds like $\text{Mg}_{17}\text{Al}_{12}$ and MgZn_2 etc. In alloys, generlly, 6 to 7 percent of these compounds are present, which enhance the mechanical properties of magnesium as shown in Fig. 2.1 (a) and (b).

✓2.1.1 Alloying in commercial cast magnesium Alloy

Several elements are alloyed with magnesium in commercial cast alloys. Other elements may be present as impurities and are controlled if they contribute



(a) Mg-Al Alloys (b) Mg-Zn Alloys (compound MgZn₂)

Fig.2.1 Equilibrium diagrams and the mechanical properties of magnesium alloys.

to excessive corrosion. The effects of several elements commonly found in cast magnesium alloys have been outlined below (Daniel, 1994).

Aluminium is a common alloying element in cast magnesium alloys and it has several beneficial effects on magnesium alloys. As it has been pointed out in the beginning of section 2.1, aluminium increases room temperature strength of cast magnesium alloys. Aluminium also improves the fluidity of the alloys. However, increasing amounts of aluminium may cause the ductility to decrease through formation of brittle intermetallic phase and elevated temperature strength may also decrease.

Zinc is added in the Mg-Al-Zn alloys system. Zinc addition improves the fluidity of an alloy. In general, zinc also improves the room temperature strength of an alloy through solid solution strengthening. However, high levels of zinc greater than 2% may cause hot cracking.

Manganese addition to magnesium alloy does not affect the mechanical properties of the alloy significantly but produce beneficial results in the control of corrosion. Manganese levels have been established in die cast magnesium alloys through careful research into the interactions between iron, manganese and aluminium.

Silicon may be present in small amounts in all the magnesium alloys. Silicon is used in magnesium alloys to result in Mg_2Si phase which improves creep strength at elevated temperatures.

Beryllium may be used in magnesium alloys at levels equal to or lower than 10 ppm. Beryllium addition does not affect mechanical properties of the alloys but are useful in minimizing the oxidation of the molten alloys.

Iron, nickel and copper are carefully controlled at parts per million (ppm) level particularly in die cast magnesium alloys. Each of the three elements has a

negligible effect on mechanical properties at this low level. The effect of any of these elements exceeding the specified level may lead to a loss in corrosion resistance. As with manganese, a great deal of research has been conducted to determine the permissible levels of each of these elements in common magnesium alloys.

✓ 2.1.2 Properties of Magnesium and its Alloys

Magnesium, is a very active structural metal in the electromotive series and it has a very high tendency to corrode substantially during storage even in laboratory environment. Therefore, magnesium and its alloys may be employed in applications where there is little or no moisture (e.g. space) or with protective coating.

At pH levels greater than about 8.5, magnesium passivates by the formation of an $Mg(OH)_2$ film and is, therefore, resistant to alkalis. Corrosion rate can be high in acidic or neutral solutions where of magnesium does not passivate. Magnesium is attacked by pitting corrosion in solutions containing chlorides. The corrosion rate of magnesium is highly dependent on its purity. In sea water, ultrapure magnesium (i.e. distilled Mg) corrodes at a rate of 0.25 mm/year, which is about twice the rate of iron. Commercial magnesium, however, corrodes about 100-500 times faster. In mildly corrosive environment like marine environment, magnesium corrodes rapidly but corrosion becomes much worse in salt water. The higher corrosion rate of commercial magnesium is primarily caused by noble impurity elements that have low hydrogen overvoltages, such as iron, nickel, cobalt, and copper. These elements serve as efficient cathodic sites, which accelerate the corrosion rate of magnesium by the formation of local galvanic couples. Residual particles from processing that are left on the surface of magnesium also serve as efficient cathodes.

Magnesium and its alloys are easily machinable amongst structural metals and permit machining operation at very high speeds. Their excellent machinability

is characterized by low power requirements, long tool life, excellent surface evenness and small fragmented chips. Commonly dry machining of magnesium is carried out. Table-2.1 compares average power requirements for machining of magnesium alloys with other metals and alloys.

Table 2.1
Average Power Requirements for Removing a given Volume of Metal per Minute by Turning

Material	Power Requirements kW/dm³/min	Power Requirements Relative to Magnesium
Magnesium alloys	7	1.0
Aluminium alloys	11	1.6
Brass	29	4.1
Cast iron	32	4.6
Mild steel	50	7.1
Nickel alloys	91	13.0

Tool wear during machining of magnesium is generally very low. For carbide tools, the tool life is five to ten times higher for machining magnesium compared to that observed during machining of aluminium alloys. Relatively higher tool life while machining magnesium has also been observed for tools made of high speed steel. The machined surface is generally very good and excellent surface specifications can be achieved without supplementary grinding.

2.1.3 The Physical Properties of Dispersoids

(a) Mild Steel

Mild steel is used in large tonnage's for structural purposes and it contains 0.15-0.25% carbon. It is not heat treated, but used in the as- rolled and air- cooled condition. The microstructure consists of relatively smaller amount of fine pearlite

interspersed in a ferrite matrix. Due to higher carbon contents, the strengths of mild steel are higher as compared to the low carbon steels but the ductility is lower (Rangachary et al., 1996).

(b) Alumina

Al_2O_3 is chemically inert and has a high melting point, high electrical resistance and high hardness. Changes in the calcination conditions of $\text{Al}(\text{OH})_3$ may result in products that contain the so called transition aluminas or pure alpha-alumina $\alpha\text{-Al}_2\text{O}_3$ or Corundum is prepared by heating aluminium hydroxide above 1100°C . The compound exists as rhombohedral crystals with melting point of 2050°C . $\beta\text{-Al}_2\text{O}_3$ crystallizes from molten aluminium oxide containing 5% of an Alkali oxide. The transition takes place at a temperature not much below the melting point of cryolite (1020°C) when a mixture of cryolite and $\alpha\text{-Al}_2\text{O}_3$ is annealed. The α form is converted into $\beta\text{-Al}_2\text{O}_3$ after annealing a mixture of alumina and 15-20% cryolite for 20 hours. This compound exists as hexagonal crystals and it is occasionally considered to be a very aluminium rich, alkali aluminate. $\gamma\text{-Al}_2\text{O}_3$ is obtained by annealing of aluminium hydroxides at temperatures between 400°C and 1000°C along with a series of various phases.

Aluminium oxide crystals are normally hexagonal, and are minute in size. Alumina ceramics are the most widely used oxide type ceramic, chiefly because alumina is plentiful, relatively low in cost, and equal to or better than most oxides in mechanical properties. Alumina ceramics are the hardest, the strongest and the stiffest of the oxides and exhibit outstanding electrical resistivity and dielectric strength. Alumina is resistant to a wide variety of chemicals and are unaffected by air, water vapour and sulphurous atmospheres.

(c) Graphite

In the crystalline form of graphite, carbon is a material with low thermal expansion (about 1/4th that of steel). Thermal conductivity of the higher conductivity grades is comparable to that of aluminium. The material is very stable dimensionally during thermal excursions and is not susceptible to thermal shock. Graphite is a material with low modulus about one tenth to one fifteenth of that in steel. It is brittle and requires careful handling to minimize impact loads and tensile stresses when used in machine elements.

Graphite is a self lubricating material with a high resistance to corrosion by most aggressive media except strongly oxidizing acids. It will retain its strength at very high temperatures. The temperature limitations of graphite are related to oxidation inhibitor additives, the upper limit can be pushed to 500⁰C to 650⁰C.

2 1.4 Solidification Processing of Magnesium Composites

2.1.4.1 Vacuum Infiltration

In this method, the melt is kept in a crucible placed inside a furnace, and a pipe is immersed in liquid metal at one end, while the other end is vented to either a neutral atmosphere or a vacuum (Ray., 1995). A preform or bed of particles is placed in the pipe blocking the passage. These particles in the pipe are either preheated by immersion in liquid metal or by a separate heater around the segment of the pipe containing the preform or bed. The liquid metal will infiltrate due to the pressure difference between the liquid metal and the preform connected to vacuum pump. This infiltration process is called vacuum infiltration.

2.1.4.2 Squeeze Casting

Squeeze casting has been developed based on the principle of pressurized solidification, in which finished castings can be produced in a single process from molten metal to solid components inside reusable dies (Hu, 1998). The process which is schematically shown in Fig.2.2. Involves several steps.

(1) A suitable die set is preheated to the required working temperature. During the heating-up period, the die set is usually sprayed with a commercial graphite lubricant.

(2) A metered quantity of molten metal is poured into an open female die cavity. Then, an upper male die or punch is lowered, coming into contact with the molten metal.

(3) The pressure is applied after molten metal begins to solidify and is maintained until all the molten metal has solidified.

(4.) The upper punch returns to its original position and the casting is ejected.

In general, two different kinds of squeeze-casting techniques, known as “direct” and “indirect”, have been developed based on different approaches of metal metering and metal movement. The direct squeeze-casting technique is characterized by a direct pressure imposed on to the casting without any gating system as illustrated in Fig.2.2. Because the pressure is directly applied to the entire surface of the molten metal during solidification, this technique gives fully densified components and extremely fast heat transfer which yields fine grain structure and also higher mechanical properties are attained (Hu, 1998). In the indirect technique, as shown in Fig. 2.3, however, the pressure is exerted on a gate which transmits the load to the component (Hu, 1998). Owing to the fact that the pressure is imposed at a distance from the component, it is difficult to maintain a high pressure on the component throughout its solidification and cooling periods. This indicates that it is difficult to cast long freezing range alloys with the indirect

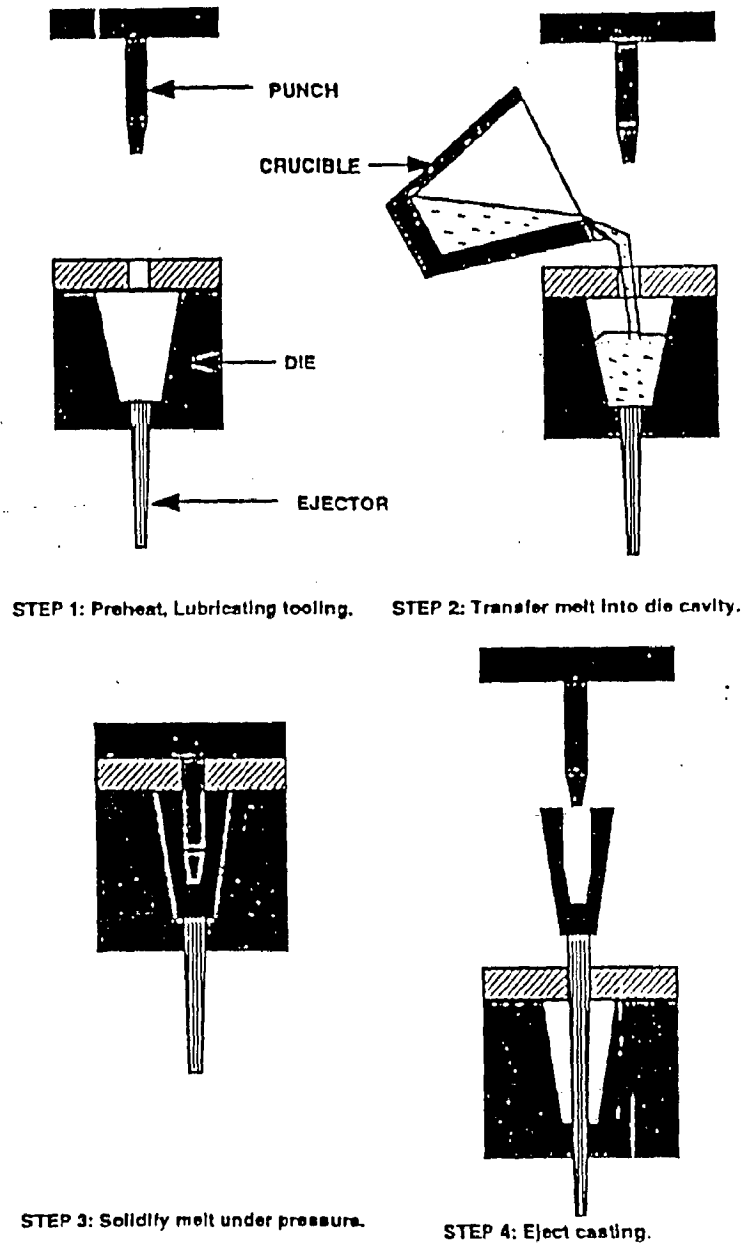


Fig.2.2 Schematic diagram of the direct squeeze casting process.

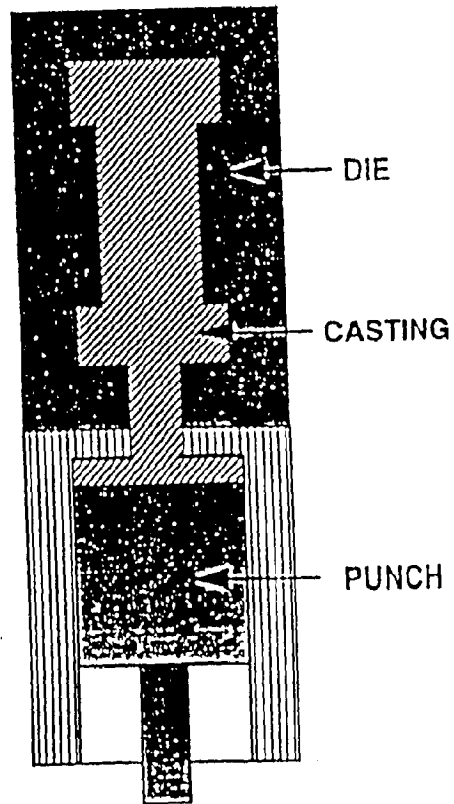


Fig.2.3 Schematic diagram of the indirect casting method.

technique. Also, metal yield is much lower than that achievable with direct squeeze casting.

Squeeze casting or similar processes are often described by other names like liquid metal forging, extrusion casting and pressure crystallization. The high applied pressure, which is several orders of magnitude greater than the melt pressure developed in normal casting processes, keeps entrapped gases in solution and squeezes molten metal from hot spots to incipient shrinkage pores. As a result, the porosity in a squeeze-cast component is almost eliminated. Furthermore, due to the elimination of air gap at the liquid-mould interface by the applied high pressure, the heat transfer across die surface is enhanced and it increases solidification and cooling rates. Thus, superior mechanical properties of the casting resulting from the pore-free fine microstructure are achieved in squeeze casting processes.

In recent years, there is increasing attention on reinforced magnesium composites which have high technological potential for use in aerospace and automotive applications. This is due to their high specific strength, high specific stiffness even at elevated temperatures and high damping capacity. However, there are restrictions of fabricating methods which could be employed for the synthesis of these composites. Owing to economic considerations, the selection of the reinforcement is often limited to those which are inexpensive and readily available. SiC, Al₂O₃ and graphite are most frequently used as reinforcement being added to a magnesium matrix.

Y.Kagawa and E.Nakata (1992), developed a composite by squeeze casting, reinforcing high- strength carbon fiber in commercially pure magnesium (99.5 wt%) matrix. Before casting, the carbon fibers were undirectionally packed into a stainless steel holder and fixed with a stainless mesh. The holder with carbon fiber was preheated at 327⁰ C in an argon gas atmosphere. The holder was then placed into the die and the magnesium melt was poured into the die. Immediately after pouring the magnesium melt, a pressure of 49 MPa was applied

through the action of press and the pressure was applied for 120s until after solidification of the magnesium melt. The magnesium melt was completely solidified under the applied pressure.

Institute of Magnesium Technology (Referred to as ITM) has carried out extensive research work on squeeze casting of magnesium alloys motivated by the development of components for automotive applications such as pistons and wheels. For squeeze casting of AZ91D alloy, a pressure of 87 MPa and a die temperature of 450°C have been used.

2.1.4.3 Stir Casting

Stir casting provides the cheapest route for the synthesis of composite and for this reason, it has engaged attention of automobile industries looking for cheaper light weight composites. Stirring is employed to help in two ways: (i) to transfer particles into the liquid metal and (ii) to maintain the particles in the state of suspension. While remelting the composite ingots, only the latter aspect is relevant. For transferring particles into liquid metals, the development of vortex during stirring is observed to be helpful. The dispersoids added to the top of the stirred liquid is drawn towards the center of the vortex and a larger velocity of rotation at a smaller radial distance from the center may impart sufficient centrifugal velocity to the dispersoids for their entry into liquid metal. Also, a pressure difference between the inner and outer surfaces of the melt sucks the dispersoids into the liquid (Ghosh and Ray 1988a, b). Injection of particles with inert gas directly in to the molten alloy may also contribute to porosity apart from an increase in cost. It has been possible to reduce the extent of porosity considerably by use of vacuum at the stage of ingot production but use of vacuum during remelting, is strongly discouraged by user industries. Therefore, during remelting the ingot manufacturers are recommending use of some special design of stirrer which maintains a quiet surface at the top. Some research efforts should be directed to device new methods for incorporation of dispersoids without the

associated problem of porosity which compels one to use vacuum during synthesis, adding to the cost of manufacture.

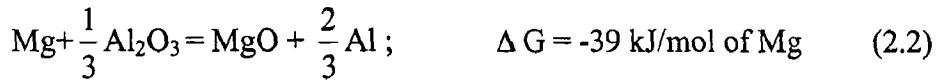
To create homogeneous distribution of dispersoids in molten metal/ally, stirring the slurry helps to maintain a high shear rate which gives a fairly uniform distribution in the radial direction and also prevents particle agglomeration (El-Kaddah and Chang, 1991). However, distribution in the axial direction will depend on the ability of an impeller to lift dispersoids denser than the molten alloy, by the rotating flow created by stirring. One defines a particulate dispersion number (PDN) as the ratio of the axial velocity of flow to the terminal settling velocity. For flow in coaxial rotating cylinder, PDN is given by

$$PDN = [H_o(\mu\Omega)^{\frac{1}{2}}] / [r_i^{1/4} d^{3/4} V_t], \quad (2.1)$$

where, H_o is the height of the melt, Ω the angular velocity of the container, r_i the radius of the inner cylinder, d the gap between the inner and outer cylinders, V_t the particle settling velocity and μ the viscosity of the slurry. If PDN is much greater than one, the settling velocity is smaller than the axial velocity of flow and the particles will be carried to the top of the melt. On the other hand if PDN is smaller than one, the particles will remain at the bottom. El-Kaddah and Chang (1991) recommended that PDN should be greater than 4 for homogeneous dispersion.

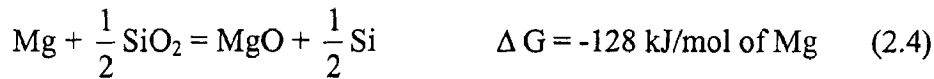
2.1.4.4 Chemical Reaction During Solidification Processing

During solidification processing of alumina in molten magnesium it has been widely observed that there is chemical reaction. These reactions between alumina and magnesium matrix in metal matrix composites at 1000 K have been investigated theoretically and experimentally by Hallstedt et-al (1990). The following reaction may take place.



The ternary phase diagram of Mg-Al-O system at 1000 K indicates that at magnesium rich end there is only one stable phase and that is MgO. But kinetic analysis of reaction between a particle and its surrounding molten magnesium shows that there may be an inner layer of spinel i.e., MgAl_2O_4 , next to unreacted alumina and over the spinel layer the phase of MgO, that is in equilibrium with molten magnesium, may form. Wilks, King and Wardlow (1997) have claimed that alumina reaction is sluggish at normal melt temperatures.

Often the composites are made by infiltrating fiber preforms containing alumina which are bonded by siliceous compounds, resulting into silica on heating. There is a strong tendency of reaction between magnesium and silica following reactions given below.



In preform infiltrated composites Hallstedt et al (1990) attributed MgO formed to SiO_2 and not to interfacial reaction between magnesium and alumina. Further, they found that the liquid infiltration process was comparatively slow process requiring long time to achieve a homogeneous silicon content in the molten metal and hence, Mg_2Si precipitated homogeneously in the matrix. This process seems to be different in the squeeze casting because of more rapid cooling. As a result the molten metal does not achieve homogeneous composition and hence, Mg_2Si form along alumina leading to deterioration of the mechanical properties.

2.1.5 Magnesium-Aluminium and Magnesium-Zinc Alloys

(a) Microstructure and Phase Diagram of Mg-Al Alloys

Aluminium has been one of the primary alloying element used in magnesium alloys for many years. At the magnesium end, the aluminium-magnesium equilibrium phase diagram shows a eutectic reaction at 437°C and 32.3 wt% aluminium where liquid transforms into a mixture of (i) terminal solid solution of aluminium in magnesium containing 12.7 wt% of aluminium and (ii) intermetallic compound of $\text{Mg}_{17}\text{Al}_{12}$. The solid solubility of aluminium in magnesium reduces rapidly with temperature to about 1.5 wt% aluminium at 100°C as shown in Fig 2.4. Because of rapidly decreasing solid solubility of aluminium in magnesium it is possible to have age hardenable alloys. The precipitation of $\text{Mg}_{17}\text{Al}_{12}$ from solid solution can be either continuous or discontinuous. At aging temperatures above about 204°C , it appears in a continuous widmannstatten pattern. Discontinuous precipitation, which starts at grain boundaries and has a lamellar form, is favored at lower aging temperatures and aluminum contents above 8 wt%. At about 290°C , the lamellar precipitate begins to coalesce, and at about 370°C , it redissolves in the matrix (ASM Hand Book, Vol, 9).

(b) Microstructure and Phase Diagram of Mg-Zn Alloys

Zinc is another important alloying element in magnesium and the equilibrium phase diagram magnesium-zinc system is shown in Fig 2.5(Hansen, 1958). Apart from two terminal solid solutions, the system has five intermediate phases of Mg_7Zn_3 , MgZn , Mg_2Zn_3 , MgZn_2 and $\text{Mg}_2\text{Zn}_{11}$. In the composition range between 0 to 64.32 wt% Zn which corresponds to the composition of MgZn_2 , it is observed that MgZn_2 reacts peritectically with liquid at $416 \pm 2^{\circ}\text{C}$ to form Mg_2Zn_3 which in turn reacts with liquid to form MgZn at $347 \pm 1^{\circ}\text{C}$. This phase MgZn again reacts with the liquid peritectically to form Mg_7Zn_3 at $342 \pm 1^{\circ}\text{C}$. Apart from these peritectic reactions there is one eutectic and one eutectoid reaction in this

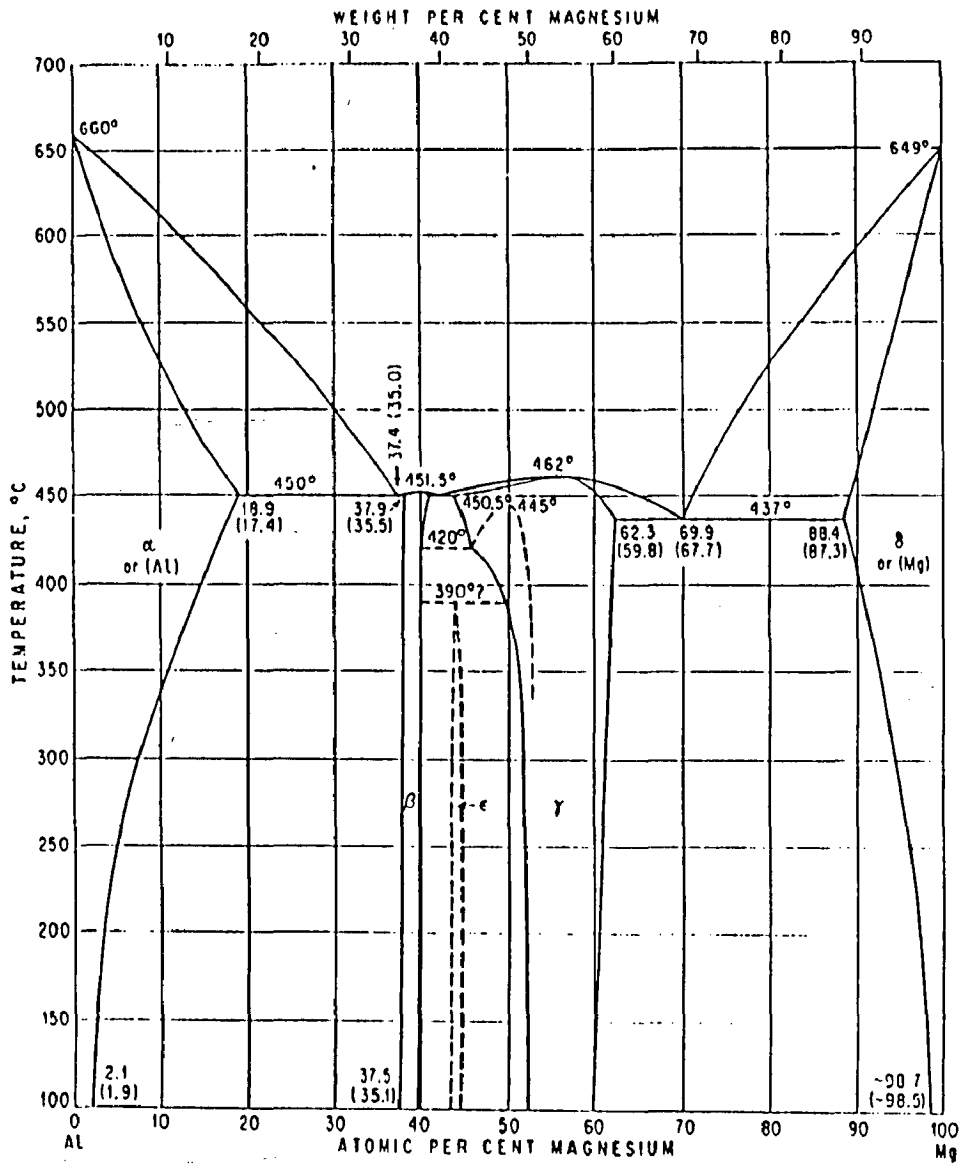


Fig.2.4 Equilibrium phase diagram of Mg-Al alloy system

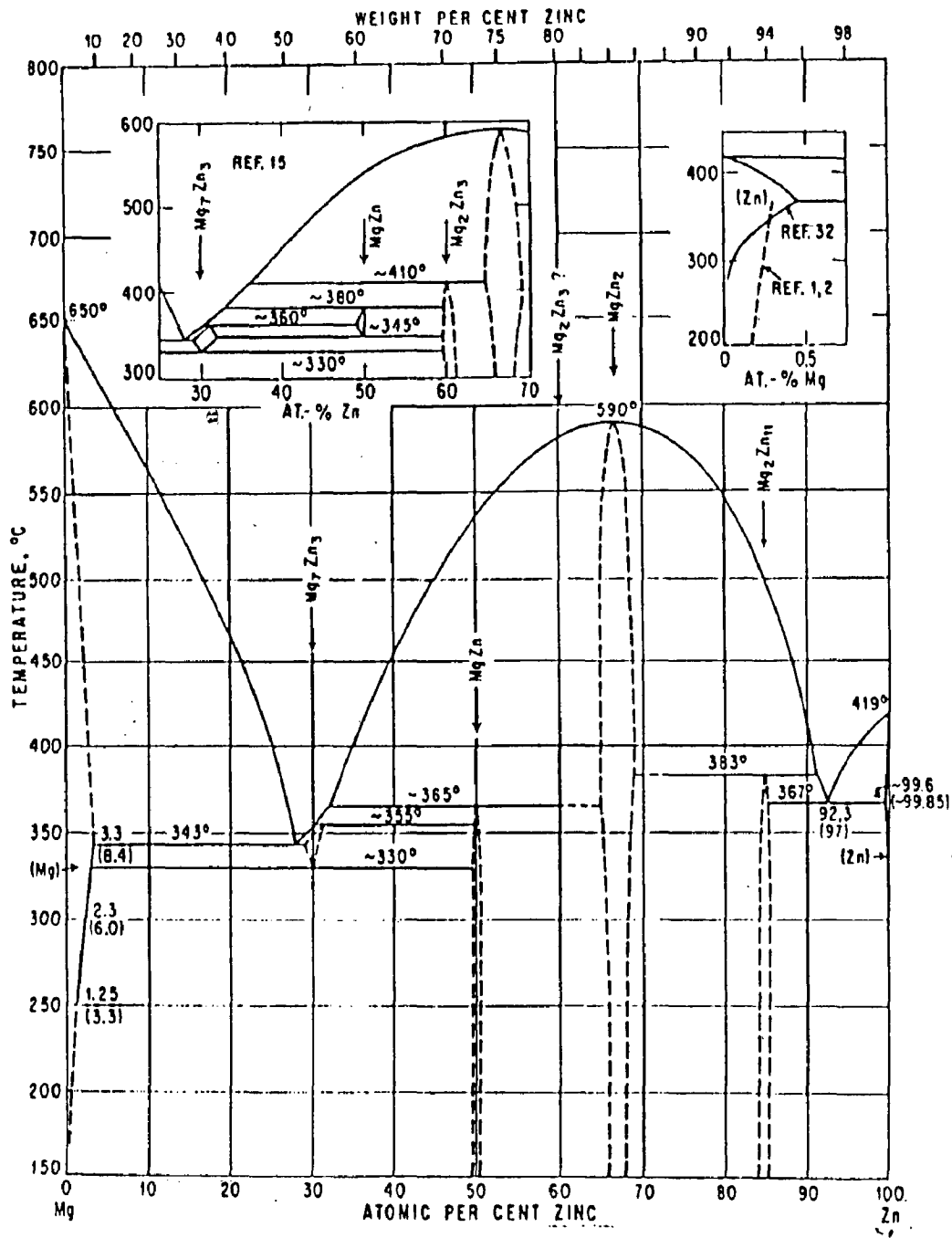


Fig.2.5 Equilibrium phase diagram of Mg-Zn alloy system

composition range - (a) liquid containing 28.1 at% of zinc transforms eutectically into terminal solid solution of zinc in magnesium and the compound Mg_7Zn_3 at $340 \pm 1^\circ C$ and (b) Mg_7Zn_3 transforms eutectoidally to terminal solid solution of zinc in magnesium and Mg Zn compound at $312 \pm 2^\circ C$. Magnesium has a solid solubility for 8 wt% Zn at $312 \pm 2^\circ C$ but it reduces to 3.3 wt% at about $250^\circ C$. The solubility decreases further to about 1.7 wt% Zn at room temperature. When an alloy with higher zinc soluble in magnesium at elevated temperature is cooled, there is general precipitation of Mg-Zn compound and the particles of this compound are not clearly resolvable even by an electron microscope until the alloy is overaged (ASM Hand Book, vol. 9).

(c) Microstructure and Phase Diagram of Ternary Magnesium Alloys

The ternary phase diagrams of Mg-Al-Zn alloys are shown in Figs.2.6 indicating the intersection of solvus surface at different temperatures. When zinc is added to magnesium-aluminum alloys, the Mg-Al eutectic takes a completely divorced form, in which massive particles of $Mg_{17}Al_{12}$ compound are surrounded by magnesium solid solution. When the ratio of zinc to aluminum exceeds 1/3 the compound changes to $Mg_{32}(Al,Zn)_{49}$ as shown in Fig.2.6. Addition of zinc to magnesium-rare earth metal alloys similarly helps to form divorced Mg-R eutectic and increases the amount and continuity of the compound at the grain boundaries. By the addition of about 2% zinc to magnesium alloys containing at least 2% thorium, an acicular or platelet form of compound develops. The acicular form entirely replaces the massive form when the zinc content is increased to about 3%, but it again disappears when the zinc content is further increased to above 5%.

2.1.6 Mechanical Properties of Magnesium Alloys and Composites

The mechanical properties of the particulate composites are relevant when one employs such composites in static and dynamic structures. The mechanical properties obtained in a composite depends not only on the type of dispersoid used but also on their size and distribution in the matrix of the composite. Besides these

Mg-Al-Zn

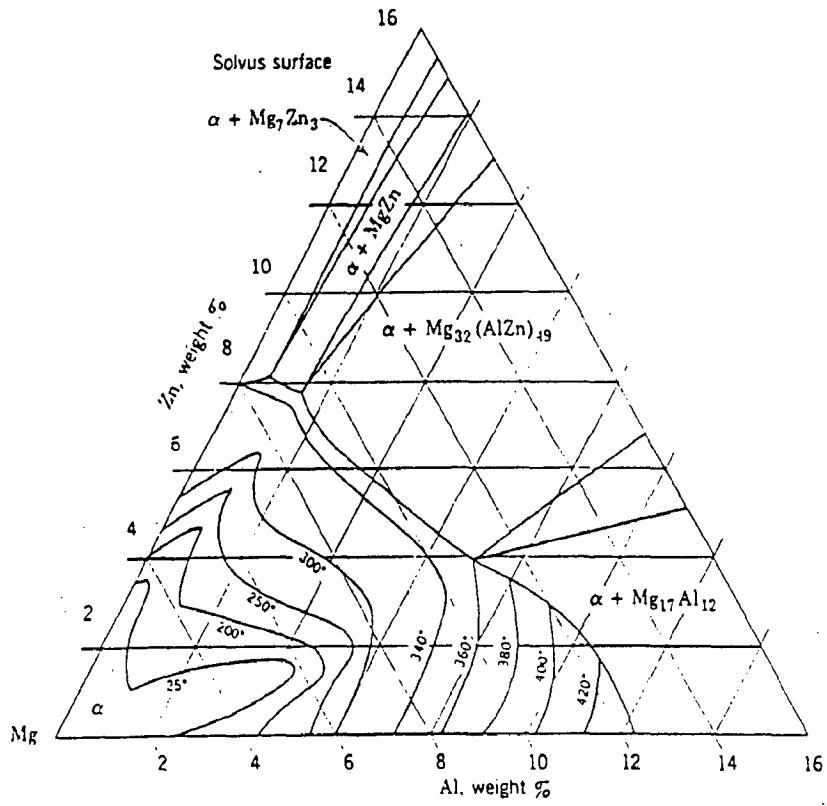


Fig.2.6 The solvus surfaces in magnesium alloys with aluminium and zinc.

but also on their size and distribution in the matrix of the composite. Besides these factors, bonding at the particle-matrix interface is also an important factor determining the mechanical properties of the composites. When one develops low friction or low wear composites for tribological applications, the tensile strength of the composites becomes important also in this context(Lloyd, 1994).

In particle reinforced metal matrix composites, both the matrix and the dispersoid particles are load bearing constituents. Many factors contribute to the strength of a particulate composite - (a) the deformation characteristics of the matrix, the particle and their interface (b) shape, size, amount and distribution of particles in the matrix and (c) the interaction between the particles and the flaws like porosity and voids in the matrix. The tensile properties manifested in a composite depend on the mechanical behaviour of its constituents. At the initial stage of loading of a composite containing two constituents, the matrix and the dispersoid, both the constituents are elastically deformed. The limits of elastic properties of such a composite could be estimated following two simple models resulting in two rules of mixtures (Broutman and Krock, 1967). The first one represents the iso-strain condition of the two constituent phases and predicts the upper limit estimate of the Young's modulus of the composite, E_c , which is written as,

$$E_c = E_f V_f + E_m V_m \quad (2.6)$$

where, E_f and E_m are respectively the Young's moduli of the reinforcement and the matrix. V_f and V_m are respectively the volume fraction of the reinforcement and the matrix. The other limiting model represents the iso-stress condition of the two constituent phases and predicts the lower limit estimate of the Young's modulus of the composite, E_c which is written as,

$$\frac{1}{E_c} = \frac{V_m}{E_m} + \frac{V_f}{E_f} \quad (2.7)$$

The rule of mixture expression has been found most appropriate for the composites with continuous reinforcement. However, it has been modified for the composites with discontinuous reinforcement by as given below.

$$E_c = \frac{E_m(1 + 2sqV_f)}{1 - qV_f} \quad (2.8)$$

where, s is the particle aspect ratio and q is estimated as,

$$q = \frac{(E_f / E_m - 1)}{(E_f / E_m + 2s)} \quad (2.9)$$

Beyond the elastic limit, the strain in a composite increases nonlinearly with stress and it is generally contributed by the plastic deformation of the matrix while the strong and stiff particles may still deform elastically. Higher strain of plastic deformation may introduce high shear stress across the matrix-particle interface. If the bonds at the interface are not strong, there will be debonding and serrations will appear in the load-elongation curve (Ghosh and Ray, 1986). In presence of deformable particles the composite may undergo an extensive plastic deformation. The yield stress of a composite, under a matrix constraint sufficient to develop stresses to deform the particles is expressed (Broutman and Krock, 1967) as follows.

$$\sigma_y = [(G_m G_p b) / C]^{1/2} \quad (2.10)$$

where, G_m and G_p are the shear moduli of the matrix and the particle respectively. b is the Burger's vector of the dislocation pile up against the particle and C is a constant. The yield strength of a composite, σ_y containing non-deformable particles can be expressed as follows.

$$\sigma_y = [(G_m G_p b / c'' \mu_1)]^{1/2} \quad (2.11)$$

where, μ_1 is the inter-particle spacing, expressed (LeRoy, 1981) as follows.

$$\mu_1 = d [\sqrt{(2\pi / 3V_p) - (8 / 3)}] / 2 \quad (2.12)$$

and

$$d = \sqrt{(3 / 2)l} \quad (2.13)$$

where, l is the mean linear intercept of a random- particle distribution.

The hard particles normally used in strengthening metals are often dislocation free. The share of load which can be carried by the particle depends on its aspect ratio and so, it is limited for nearly equiaxed particles in a composite. Further, the stresses in the hard particles are transmitted through the particle/matrix interface. For, an interface with strong bonding the transmitted stress tends to deform the metal matrix which has generally a lower yield strength than that of the particle. These particles are often brittle materials such as oxides, carbides and inter-metallic phases. Lloyd (1994) argues that the strengthening of these composites containing oxide particles should depend on the ability of the interface to transfer stresses from the matrix to the stronger reinforcing particles. This, in turn, is dependent on achieving a strong interfacial bond between the matrix and the reinforcement. If the interfacial bond is weak the interface fails before transfer of any significant load to the particle and there will be no

strengthening of the composite over and above that of the matrix. The composite may in fact appear to be weaker than the unreinforced matrix because of the reduced effective area supporting the load.

Milleiko (1969) has developed a theory of mechanical properties of fiber reinforced composites of two ductile phases loaded in tension parallel to the fiber axis. It is based upon the application of plastic instability criteria to the composite under the following assumptions:

- (i) The bond between the Fiber and the matrix is ideal, so that there exists equal strain in both the phases.
- (ii) The flow stress of the composite can be estimated by the law of mixture, and,
- (iii) The relationship between the stress and strain of both the composite and the components follows a power law of the form.

$$\sigma = k_f \varepsilon_c^n \quad (2.14)$$

where, σ is the stress, ε_c is the strain, and k_f and n are constants.

(a) Hardness of Magnesium Alloys and Composites

The hardness of cast magnesium has been reported to be 30 HB. In sand cast AZ63A magnesium alloy, the hardness increases to 50 HB due to alloying (Lakhtin, 1990). When this alloy is solution treated and aged under T_4 and T_5 conditions (as explained in Table-2.2), the hardness increases further to 55 HB. The natural ageing of T_4 and short artificial ageing of T_5 show similar hardness results. However, the hardnesses observed under T_6 and T_7 conditions i.e., hardening followed by full artificial ageing and hardening followed by stabilization, are 73 HB and 64 HB respectively. When aluminium is increased but zinc is

reduced keeping the level of alloying similar as in AZ81A, the hardness under T_4 condition remains more or less the same at 55 HB. But in AZ91A and AZ91B, where the level of alloying has been increased by further addition of aluminium compared to AZ81, the hardness of the as cast alloys are 63 HB and 60 HB respectively. The AZ91C alloy, under T_4 condition shows a hardness of 55 HB, similar to that observed in AZ63A or AZ81A alloy but under T_6 temper, the hardness of AZ91C alloy increases to 70 HB, lower than that observed in AZ63A. When the level of zinc is increased as in AZ92A alloy compared to that in AZ91 alloy, the hardness in the as cast alloy increases to 65 HB, higher than those observed either in AZ91A or AZ91B alloy. For T_4 temper, the hardness of AZ92A alloy decreases slightly to 63 HB but under T_5 temper, the hardness increases to 69 HB. Under T_6 temper, the hardness of AZ92A alloy increases further to 81 HB. The hardness of the cast magnesium alloys vary in the range between 50 to 80 HB. Zinc appears to be relatively more potent in increasing the hardness of aged alloys as compared to aluminium (Lakhtin, 1990).

Table-2.2
Heat- Treatment Parameters

Tempering (Designation)	Treatment	Temperature (°C)	Time in hours
T ₁	Artificial ageing	175 ⁰ ± 5 ⁰ C	5 to 20
T ₂	Annealing	about 300 ⁰ C	5 to 10
T ₃	Hardening	510 ⁰ - 520 ⁰ C	quenched in hot water (40 ⁰ -100 ⁰ C)
T ₄	Hardening and Natural ageing	535 ⁰ -545 ⁰ C	quenched in hot water
T ₅	Hardening and a short ageing operation	175 ⁰ C	2 to 3
T ₆	Hardening and full artificial ageing	200 ⁰ C	3 to 5
T ₇	Hardening and stabilization	230 ⁰ C or at 250 ⁰ C	3 to 10
T _{8v}	Hardening and softening	240 ⁰ -260 ⁰ C	3 to 5

(b) Tensile Properties of Magnesium Alloys and Composites

(Cast magnesium has shown the yield strength of 24.52 MPa and the tensile strength of 112.81 MPa. In magnesium based cast alloys, the yield strength increases to a value in the range between 83 and 207 MPa and tensile strength increases between 152 to 310 MPa. Videm and Hansen used self generated Vacuum technique to cast AZ91 alloy and obtained an yield strength of 160 MPa, tensile strength of 230 MPa and elongation of 3%. Suman observed that the mechanical properties of as cast alloy depend also on section thickness. For as cast AZ91D, when section thickness increased from 3.2 to 10 mm, the ultimate tensile strength was around 234 MPa but the yield strength decreased from 186 to 152 Mpa and % elongation also decreased from 6 to 4. Hillis and Shook (1989) studied mechanical properties of die cast AZ91D alloy at room temperature and elevated temperature. At room temperature the tensile strength was 230 MPa while at 175⁰C it was 140 MPa. The room temperature yield strength was 150 MPa but at 175⁰ C it was 100 MPa. The room temperature elongation was 3%)

The tensile properties of extruded AZ91D alloy and AZ91D-15 vol% SiC composites have been investigated by Laurent et al (1992). Both reinforced and unreinforced alloys were stirred in the semi- solid temperature range between of 581 to 587⁰C prior to extrusion. The tensile properties were compared with the room-temperature tensile test results published by the Dow chemical company for AZ91D alloys. Laurent et al (1992) found that in composites containing 15 vol% SiC particles of size 54 μm , the room-temperature yield strength was 257 MPa, a value 20% higher than the yield strength of 215 MPa observed in unreinforced AZ91D alloy. The ultimate tensile strength observed in the same composite was 289MPa, a value close to 296 MPa, observed in the unreinforced alloys. A significant improvement in elastic modulus of up to 46% was observed compared to elastic modulus of 45 GPa observed in the AZ91D alloy but the total elongation of the composite decreased drastically to 0.7% compared to 10.2% measured in the unreinforced alloy for die cast AZ91-15 vol% SiC particle reinforced composites. These authors used similar test conditions to those used by Dow

chemicals for the tensile test of the alloys. However, Mikucki et al have observed elastic modulus of 60 GPa, yield strength of 205 MPa and ultimate tensile strength of 233 MPa in AZ91D-15 vol% SiC composites, which are lower than those observed by Laurent et al (1992). But the corresponding total elongation observed is 1.1% which is higher than the value observed by Laurent et al (1992). From these results it appears that reinforcement of AZ91D alloy by 15 vol% SiC resulted in lowering of tensile strength and the elongation but there is improvement of elastic modulus. But no such clear trend for the yield strength was observed as the values reported by Mikucki et al (1990) and Laurent et al (1992) are respectively lower and higher than that of the alloy.

Lloyd reported typical properties of some commercially available magnesium alloy based composites and unreinforced base alloys as provided by Dow Co. For AZ91 alloy reinforced with 9.4% and 15.1% SiC particles, the yield strengths were observed to be 191 and 208 MPa respectively but the ultimate tensile strengths were 236 MPa for both these composites. In these composites, the elastic modulus were 47.5 to 54 GPa in the composites containing 9.4% and 15.1% SiC particles respectively but the elongation observed were 2 and 1% respectively. When the base alloy has been changed to AZ61 containing lower amount of aluminium but reinforced with 20 vol% of SiC, it was observed that the yield strength of the unreinforced alloy, 157 MPa, increased to 260 MPa in the composite. The tensile strength of the unreinforced alloy, 198 MPa also increased to 328 MPa in the composite. There was very little reduction of % elongation with reinforcement from 3.0 to 2.5. The elastic modulus increased considerably from 38 GPa to 80 GPa on reinforcement. Thus, it appears that one may get relatively better tensile strength, elastic modulus and % elongation in lower aluminium alloys.

Luo et al (1994) has shown the influence of casting process on the strength of cast products. While the die cast AZ91D alloy shows the yield strength of 150 MPa but the squeeze cast alloy shows 96 MPa. Tissier observed an yield strength of 215 MPa in compocast and extruded AZ91D alloy. But the tensile strengths of

the die cast alloy and the compocast and extruded alloy are 230 and 296 MPa respectively but in squeeze cast alloy it came down to 179 MPa. MercerII and Hillis observed both yield and tensile strengths of die cast AZ91D as 150 and 230 MPa which are similar to those obtained by Luo et al (1994). But these authors reported higher values of yield and tensile strengths of 160 and 230 MPa for squeeze cast AZ91D alloy which are considerably higher than those reported by Luo et al (1994). Luo made AZ91 alloy by liquid mixing and casting process developed at the Institute of magnesium technology and obtained a lower yield strength of 86.7 MPa but a tensile strength of 203 MPa. These results cited above clearly demonstrates the importance of casting route in determining the mechanical properties of the alloy product (Vijaymohan & Gopalakrishan, 1996).

Some of the results discussed above have been compared in Table-2.3 to examine the effect of processing and matrix alloy composition on the mechanical properties observed in Mg-alloy-15 vol% SiC composites. Laurent et al (1992) observed better mechanical properties through compocasting and extrusion than those obtained by Mikucki et al (1990) by die casting when the matrix alloy is AZ91D. But Lloyd reported a lower yield strength and a similar tensile strength to die cast AZ91, when the composite has been prepared by Dow. Jones process with the matrix alloy of AZ91. Vijaimohan and Gopalakrishnan have observed a much lower yield and tensile strength of 100-120 MPa 160 MPa respectively in and composite when they used magnesium as their matrix to reinforce it with 5-15 vol% of silicon carbide. But in Mg-Al alloy based composite containing 5-15 vol% SiC the yield strength and tensile strength increased respectively to 280 to 290 and 225 to 250 MPa respectively. It is interesting to note that both these composites based on magnesium and Mg-Al alloy, the strength, both yield and tensile, does not get significantly affected by the amount of silicon carbide in the range between 5 to 15% (Vijaymohan & Gopalakrishan, 1996).

Table 2.3**Comparison of mechanical properties in Mg-Alloy-15 vol% SiC composites**

Alloy	SiC content	Casting method	Yield strength (Mpa)	Ultimate Tensile strength (Mpa)	Elongation %	Investigators
AZ91D	15 Vol.%	Compocasting	257	289	0.7	V. Laurent et al
AZ91D	15 Vol%	Die casting	205	233	1.1	B.A. Milkucki et al
Mg	15 Vol%	Liquid metal	100	150	1.0	V. Vijay Mohan and Gopalkrishna
AZ91	15.1 Vol%	Commercially available MMC	208	236	1.0	D.J. Lloyd and Dow

2.1.7 Friction and Dry Sliding Wear

(a) Friction and its Origin

Friction is the resisting force tangential to the common boundary between two bodies when, under the action of an external force, one body moves or tends to move relative to the surface of the other (Suh, 1973).

The Frictional behaviour of materials is important in tribology not only because the Frictional force between sliding surfaces is of interest, but also because it generally affects the wear behaviour (Rabinowicz, 1977; Suh and Sin, 1981). Frictional force is generated as a consequence of three basic mechanisms of asperity deformation, plowing, and adhesion, are responsible for the generation of the friction force in metals. The asperity deformation determines the static coefficient of friction and also affects the dynamic coefficient of friction, as the asperities are continuously generated due to delamination of the sliding surface (Suh, 1973). However, the contribution of asperity deformation to the dynamic coefficient of friction is not large relative to those by plowing and adhesion. New asperities are generated only with the formation of delaminated wear particles, which often requires a large number of cyclic loading by the asperities of the opposing surface. The contribution of the asperity deformation to friction is expected to be the largest when two identical metals slid against each other since the surfaces always remain rough. In a dynamic situation where the surfaces become smooth, most of the normal load is carried by the entrapped wear particles and the flat contacts. Therefore, the actual contribution of the asperity deformation to the frictional force is expected to be a small fraction of the estimated value in a dynamic situation. A frictional force can arise also due to the adhesion of two nearly flat surfaces. Unlike the deformation of asperities this frictional force is a function of the adhesion between the two opposing surfaces. The adhesion force arises due to the welding of two nearly flat portion of the surface or when the atoms are brought together in close proximity for interatomic interactions but without welding. The adhesion can also arise at the slopes of the interacting

asperities. The plowing component of the frictional force can be due to the penetration of hard asperities or due to the penetration of wear particles. When two surfaces are of equal hardness, the particle can penetrate both surfaces. As the surfaces move with respect to each other, grooves will be formed in one or both of the surfaces. When one of the surface is very hard and smooth, the wear particle will simply slide along the hard surface and no plowing can occur. However, when the hard surface is very rough wear particles can anchor in the hard surface and plow the soft surface. The friction due to plowing was investigated by Sin et al (1979), who showed that the contribution of plowing to the friction coefficient is very sensitive to the ratio of the radius of curvature of the particle to the depth of penetration.

To clarify the time-dependent friction behavior of the materials tested, the plot of friction versus distance slid may be subdivided into the following stages (Fig. 2.7) and each stage is discussed below qualitatively (Suh, 1973).

Stage I In this early stage the frictional force is largely a result of plowing of the surface by asperities. Adhesion does not play any significant role in this stage, due to the contaminated nature of the surface. The deformation of asperities does take place at the onset of sliding which affects the static coefficient of friction. However, in stage I, asperity deformation is not a major factor that determines the coefficient of friction, since the asperities in contact deform as soon as sliding commences and the surface is easily polished. Consequently, the coefficient of friction in this initial stage, μ_i , is largely independent of material combinations, the surface conditions and the environmental conditions.

Stage II The friction force begins to rise slowly due to increase in adhesion. When the interface is lubricated, stage I persists for a long time and stage II may not be present. The slope in stage II can be steeper if the wear particles generated by the asperity deformation and fracture are entrapped between the sliding surfaces and contribute to plowing of the surfaces.

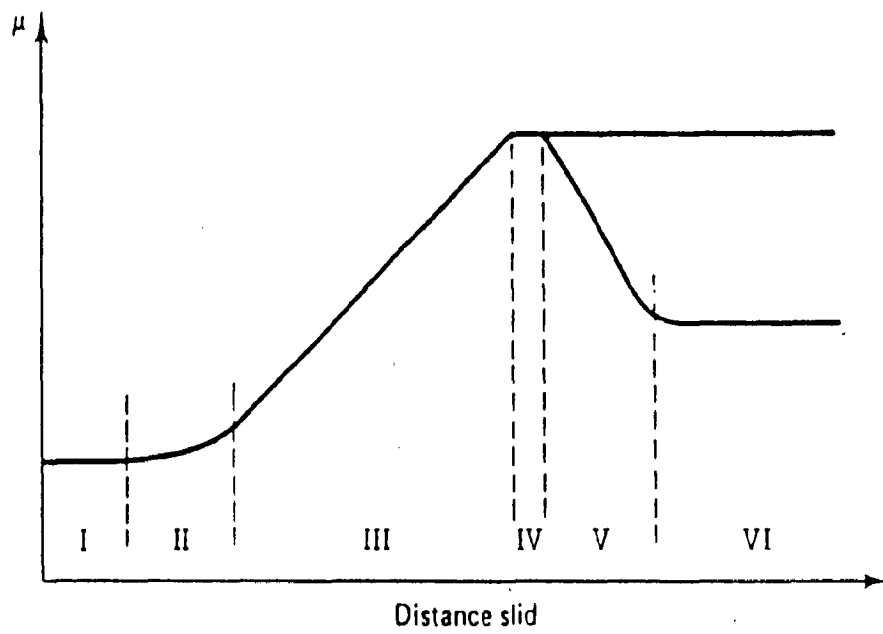


Fig.2.7 The six stages in coefficient of friction versus distance slid relationship

Stage III This stage is characterized by a steep increase in slope due to a rapid increase in the number of wear particles entrapped between the sliding surfaces as a consequence of higher wear rates. The slope is also affected by the increase in adhesion due to the increase in clean interfacial areas. The force required to deform the asperities will continue to contribute to the frictional force in this stage as long as the surface asperities are present. The wear particles are generated when the process of wear particles formation by subsurface deformation, crack nucleation and crack propagation postulated by the delamination theory of wear is completed (Suh, 1973). Some of the wear particles get entrapped between the surfaces, causing plowing. The plowing will be the greatest when the wear particles are entrapped between metals equal hardness, because they will penetrate into both surfaces, preventing any slippage between the particle and the surface.

Stage IV This stage is reached when the number of wear particles entrapped between the interface remains constant. This occurs when the number of the newly entrapped particles equal the number of entrapped particles leaving the interface. The adhesion contribution to friction also remains constant in stage IV.

Stage V In some cases, such as when a very hard stationary slider is slid against a soft specimen, the asperities of the hard surface are gradually removed, creating a mirror finish. In this case the frictional force decreases, due to the decrease in plowing and asperity deformation. Plowing decreases since wear particles cannot anchor to a polished hard surface.

Stage VI Eventually, when the hard surface becomes mirror smooth to a maximum extent, the softer surface also acquires the same mirror finish and the frictional force levels off. The surfaces are never completely smooth since there are always “potholes” due to the creation of delamination wear particles. These craters provide anchoring points for wear particles. When the hard surface is not stationary but moving against the softer surface, the hard surface remains

rough, because the number of wear particles entrapped at the interface is large due to the more rapid rate of the stationary soft slider.

Peter (1983) reported that the friction at the initial stage rises and then settle to an almost steady value. They suggested that the friction force results from adhesion interlocking of asperities in his friction model, where he introduced most of the variables that affected the friction force like, the environment, temperature, normal load, and so on. Liu et al (1992) described the source of the friction force due to interaction between the asperities as (a) adhesion at the contacting points and (b) deformation either elastic or plastic of the asperities by load. The force required to overcome friction will consist of the force required to shear the adhesion bond F_a and the force required to deform elastically or plastically F_d , the obstructing asperities of the relatively softer material in the path of the asperities of the relatively harder material. The coefficient of friction μ is expressed as

$$\mu = F_a + F_d / L = \mu_a + \mu_d \quad (2.15)$$

where, L , is the applied normal load on the contacting surface, μ_a , and μ_d are the friction coefficient due to adhesion and deformation respectively.

Bengisue and Akay (1997), focused on the friction force resulting from elastic and plastic deformation of the asperities and local friction due to adhesion between asperities of sliding pair in absence of lubricants. Yen (1997) has recently observed over the effect of humidity on the friction and wear of Al-Si eutectic alloy. It has been shown that the moisture content has a significant effect on the friction and wear of Al-Si alloy. The wear rate decreases by two orders of magnitude as the relative humidity increases from 3% to 100%, while the friction coefficient has a higher value at those humidity.

(b) Dry Sliding Wear

The progressive loss of substance from the operating surface of a body occurring as a consequence of the interfacial rubbing process is called wear (Ramesh et al., 1991). Based on the nature of movement or the media involved in an interaction under load, different types of wear have been classified as follows: (1) Adhesive wear, (2) Abrasive wear, (3) Corrosive wear, (4) Erosive wear and (5) Surface fatigue wear.

Adhesion is the phenomenon resulting in attractive force between two surfaces in close contact. The adhesive wear of metals and alloys occurs through the formation and destruction of adhesive junctions followed by transfer, oxidation and diffusion between sliding surfaces. **Adhesive wear** is associated with low sliding velocity, small load and smooth surfaces. This is an universal type of wear that can occur with every machine and is hard to be eliminated but can only be reduced. **Abrasive wear** occurs when two surfaces, one of which is harder and rougher than the other, are in sliding contact. This type of wear is dangerous because it can occur suddenly with introduction of a contaminant and leads to high wear rates and extensive damage to the surfaces. In a corrosive environment sliding surface experience **corrosive wear**. When there is no sliding, the surfaces are subjected to corrosive attack which forms a film wearing away during sliding resulting in continuous removal of metal. **Erosive wear** is a combined process of repeated deformation and cutting. This type of wear is often caused by the impact of solids, liquids, gases or a combination of these. Due to cyclic and repeated loading and unloading the sliding or rolling surfaces develop subsurface cracks. These cracks will eventually break-up making the surface to have large pits. This is known as **surface fatigue wear**.

Sliding wear of materials depends on the constitutive relationship of materials, contact geometry, and the ambient conditions. When a blunt asperity contact is sliding over an elastic glassy material, semicircular ring cracks can form behind the moving asperity. The cracks can propagate from the asperity tip

radially and laterally as well as axially when the contact geometry is very sharp. Since there are many asperity contact points in a given contact area, there are many sources for cracks. When these cracks emanating from various different locations intersect, loose wear particles are generated.

In contrast to the sliding wear of brittle material as described above, the wear of elasto-plastic materials is largely caused by the accumulation of deformation induced damages. Wear particles in elasto-plastic solids are generated during sliding by one or more of the following three mechanisms: (i) asperity deformation and fracture, which generate wear particles by the removal of original surface asperities in a single asperity interaction or in multiple, repeated interactions, (ii) plowing, which generates wear particles by plowing action involving cutting and formation of ridges which deform and fracture due to subsequent asperity interactions, (iii) delamination, which results in large wear particles by the process of plastic deformation of the surface layer, subsurface crack nucleation and crack propagation.

The wear particles resulted by these processes can either transfer to the counterface by mechanical interlocking and by adhesion. They may also leave the interface in the form of loose wear particles called wear debris as seen in most sliding situation.

(i) Asperity Deformation and Fracture

When two surfaces come in contact, their surface asperities accommodate the stresses and therefore undergo elastic and plastic deformation (ASM Handbook, vol, 18). A large part of surface is covered with films of oxides, adsorbates, and only a few of the highest asperities are able to penetrate these films to form metal-to-metal contact which may result in adhesion. There is a large, elastically deformed region below plastically stressed, adhering volume associated with the few spots of intimate contact. As there is sliding, the elastic strain release dominates over the energy of the adhesive bond which ruptures.

Bowden and Tabor noted that no adhesion is observed if the surfaces are pulled apart without sliding. It was, therefore, suggested that the friction is caused by the growth of junction under horizontal force during sliding and adhesion does not contribute a clearly separate component to friction. Adhesion is thought to be a consequence of the plastic deformation of asperities and is strongly influenced by the amount and the nature of the deformation. Archard challenged this concept that the contacts are exclusively plastic. He argued that even if for the first few traversals of one body over another plastic flow may be assumed to occur, the surface must reach a steady state where the load is supported elastically. For very rough surfaces, initial plastic flow occurs but for the very smooth surfaces, the contact may be mostly elastic.

A model for the condition of changeover from elastic to plastic has been developed by Greenwood and Williamson. This is multiasperity model which assumed that the asperities have a Gaussian height distribution and the same tip radius. The model also assumed that the elastic deformation and stresses can be calculated from the Hertzian equations. A plastic index ψ defined as

$$\psi = \frac{E^1}{H} \sqrt{\frac{\sigma}{\beta}} \quad (2.16)$$

is introduced where E^1 is the effective elastic modulus and is obtained by Hertzian equation given by

$$E^1 = \left(\frac{1 - \nu_1^2}{E_1} + \frac{1 - \nu_2^2}{E_2} \right) \quad (2.17)$$

Here E_1 and E_2 are the elastic moduli and ν_1 and ν_2 are the poisson ratios of the two materials. A plane stress modulus is taken when one material is considerably harder than the other.

$$E_1 = \frac{E}{1 - \nu^2} \quad (2.18)$$

If the two materials are identical E^1 is half of that given by Eqn. (2.17).

In equation (2.16), H is the indentation hardness in (N/m^2), σ is the standard deviation of the asperity height distribution, and β is the radius of the asperity tips. The plasticity index combines mechanical properties (E^1 and H) and topographical properties (σ and β) of the solids in contact. Greenwood and Williamson (GW) have found that ψ may vary from 0.1 to 100 for real surfaces. But in practice, it falls in a narrow range. When $\psi > 1$ there is significant plastic flow and if $\psi < 0.6$, plastic flow is unlikely. In the intermediate range when $0.6 < \psi < 1$, there is significant extent of both elastic and plastic deformation.

It may be noted that in Eqn.(2.16) the load term is absent. From this it is clear that the surface properties and surface topography are the important parameters to determine the extent of plastic deformation. If the surface topography helps plastic deformation initially the surface interactions in the repeated passes may smoothen the surface during run-in until the standard deviation of the asperity height distribution (σ) decreases and / or the radius of curvature of the asperities (β) increases. The plasticity index eventually falls into the elastic range of contact. In the GW model the real area of contact is almost proportional to load, also in the case when the contact is entirely elastic. The plastic deformation is of great importance even when the total area of plastic contact is small. For an oxide covered contact, the plastic contact will be the points where electrical and thermal conduction takes place. However, many surfaces probably have no plastic contacts at all or have primarily elastic contacts rather than plastic contacts in each pass.

The effect of friction on the deformation process has been described by Johnson for a single asperity contact. This is an idealized theory of a two dimensional asperity which involves slip-line-field analysis. For large friction, a

cap of restrained material which does not flow plastically, will form below the tip of wedge. If the friction is zero, no such restrained material develops and metal deformation takes place in narrower zone around the indentation. If the wedge is made to move across the metal surface, it will initially dig deeper into the counterface because the load will have to be supported on one side only. This causes junction growth. The wedge will return to the surface level pushing a prow of plastically deformed material before it. When the interface friction is high and the adhesion is perfect, the overall coefficient of friction becomes unity. If the adhesion is zero, pure plowing takes place.

(ii) Plowing

When a relatively hard asperity or wear particle penetrates into a sliding surface, grooves are formed in the surface. Under this circumstance if one of the surfaces is very hard and smooth the wear particle will simply slid along the hard surface and hence no plowing can occur. If the hard surface is very rough the wear particles stick to hard surface and plow the soft surface (Halling). Plowing creates small wear particles which affect the subsequent wear of sliding surfaces. The plowing action forms ridges along the slides of grooves formed by plowing. Due to repeated loading, these ridges get deformed and some of them become loose wear particles with continued sliding. The surface ridges due to plowing are formed by plastic deformation. The plowing leads to the formation of small thin layer of wear particles. The plowing process also causes subsurface plastic deformation and therefore helps generation and propagation of subsurface cracks.

(iii) Delamination

Whenever there is contact between two surfaces normal and tangential loads are transmitted through the contact points. As a consequence of such a loading the asperities of the softer surface get deformed and fractured (Suh, 1973). Due to repeated loading action small wear particles are formed. During the process hard asperities are also removed but at slower rates. As a result of the above

process, relatively smooth surface is generated initially, either when these asperities are deformed or when they are removed as described earlier. The pressure exerted by harder asperities at the contact points induces incremental plastic deformation during each loading cycle. This is accumulated with repeated loading. The subsurface gets deformed continuously, cracks are nucleated below the surface. Once cracks are originated either by crack nucleation or from pre-existing voids and cracks, with further loading and deformation, the cracks start to extend and propagate parallel to the surface at a depth which depends upon the material properties and the state of loading. Finally as the cracks reaches the surface, long and thin wear sheets delaminate. The thickness of the wear sheet depends upon the location of subsurface crack growth which is affected by the normal and tangential loads acting at the surface. The wear rate is controlled by either the crack nucleation rate or the crack propagation rate, whichever is slower.

(c) Friction and Dry Sliding Wear in Hard Particle Reinforced Composites

The friction coefficient of various composites containing hard particles show higher coefficient of friction which may be attributed to higher deformation during asperity-asperity interaction (Rohatgi, Liu and Ray, 1992) despite reduced contribution of adhesion. Rana and stefanescu (1989) have observed a substantial decrease in coefficient of friction with increasing volume fraction of SiC particles. However, they observed that increasing the size of SiC particles for a given volume fraction, has hardly much effect on coefficient of friction. Similarly, Roy et al (1992) have observed lowering of coefficient of friction in the composite reinforced by hard particles but particle size does not affect the coefficient of friction. But Jokinen and Andresson (1990) observed that coefficient of friction depend moderately on particle size. Sato and Mehrabian (1976) have observed that by reinforcing Al-4Cu-0.75Mg alloy reinforced by a wide range of particles like alumina, TiC, SiC, silica and silicon carbide, results in higher coefficient of friction in the composites.

The wear rate of the composite may decrease significantly due to the presence of hard particles. Sato and Mehrabian (1976) have observed that there is reduction of wear rate by a factor of four when Al-4Cu-0.75Mg alloy is reinforced by a wide range of particles like alumina, TiC, SiC, silica and silicon carbide. Surappa et al (1982) have observed that when reinforced with 5 wt% alumina, both Al and Al-Si alloy show improved wear resistance. Anand and Kishore (1983) have also observed a similar effect of continuous decrease in wear rate with increasing corundum content in Al-Zn alloy upto 30 wt% of corundum. Zamzam (1989) has observed that there is an improved wear resistance in composites reinforced by hard particle of SiC only upto a critical volume fraction and beyond it the wear resistance deteriorates. This critical volume fraction depends on the applied load. But Alpas and Embury (1990) observed a marginal decrease in wear rate when 2024 Al alloy was reinforced by 20 wt% of 14 μm SiC particles although the hardness almost doubled. Jokinen and Andresson (1990) have observed that in Al 6061 alloy reinforced with 20 vol% of SiC particles, the wear rates reduced in the composites at low loads resulting in contact stress of 3.2 MPa but not under heavy loads corresponding to contact stress of 12.7 MPa. Roy et al (1992) observes that the wear rate in composites reinforced with hard particles decreases but it depends only on volume fraction but not on the type and size of particles. Iwai et al (1995) have observed that the wear rate in SiC whisker reinforced composite decreases with increasing volume fraction of reinforcement under mild wear. It has been attributed to smaller wear particles owing to the increase in hardness.

From the results on wear rate and coefficient of friction summarized above it is apparent that there are divergence. It may be due to processing which may decide the state of interfacial bonding. If the hard particles are not well bonded, there might be easy debonding of the particles resulting in increased contribution to wear rate more than compensating the decrease in the real area of contact due to increased hardness.

The results on wear should be rationalized on the basis of its variation proposed by Archard (1980). He assumed that all the engineering surfaces are rough and the asperities of the relatively hard material are indented in the soft material during contact. Thus, the contact between two surfaces are limited to local contacts at the asperities and the true area of contact may be significantly lower than the apparent area of contact. The entire load at the contact is thus shared by these relatively small local contacting areas and the resulting stress there may be very high. Under this high stress there may be adhesive welding in the contact region and relative motion between the contacting surfaces break these contacts. If the adhesive welding leads to strong bonds it does not break along the original interface but through the weaker material which may cause transfer of material from the weaker to the stronger material leading to adhesive wear. The volume of material lost due to adhesion wear, V , has been estimated by Archard as follows:

$$V = k \frac{NS}{H} \quad (2.19)$$

Where, S is the sliding distance, N is the normal load at the sliding contact, H is the hardness of the soft material and k is called the wear coefficient.

The wear coefficient, k , represents the properties of the friction couple and only has real meaning provided the wear mechanisms does not change. i.e there is no change from mild to sever wear.

Suh, (1977) has proposed a mechanism of delamination wear due to continuous deformation of subsurfaces through sliding of two surfaces in contact under a load. The normal and tangential loads are transmitted through the contactpoints when two surfaces are under sliding contact. The asperities of the softersurface get progressively deformed under repeated loading and get fractured generating small wear particles. However, the asperities of harder surfaces gets removed only at a slower rate. The accumulated incremental plastic deformation

per cycle of loading results in generation of cracks below the surface. On the surface the triaxial state of compressive stress below the asperity contact does not allow crack to nucleate upto a depth below the surface. Sarkar and Clarke (1980), in their investigation on the friction and wear of Al-Si alloys, state that the nucleation sites for wear debris are probably created below the sliding surfaces as a result of Hertzian stresses. Once the cracks are formed a further loading and deformation causes the cracks to extend and propagate, eventually joining neighbouring cracks. These cracks propagate parallel to the surface and finally shear to the surfaces, delaminating long and thin wear sheets. The wear rate is controlled by crack nucleation or crack propagation rate whichever is slower. In spite of the different mechanisms proposed to explain wear during dry sliding, the proposed behaviour for wear by Archard is obeyed under a variety of situation although the mechanism assumed by him may not always hold.

CHAPTER-3

EXPERIMENTAL WORK

This chapter describes the experimental procedures used in the present investigation in respect of solidification processing and characterisation of properties of the different composites investigated.

3.1 Selection of Matrix Alloy

Magnesium based alloys are attractive matrices because of their low density, 35 % lighter than aluminium, and consequently, high strength to weight ratios. Magnesium and its alloys are potential matrix materials for developing composites for applications in reciprocating components in motors, pistons, gudgeon pins, spring caps etc. It is also attractive in aerospace due to its low coefficient of thermal expansion and high -stiffness properties combined with low density .Magnesium has a greater vapour pressure than aluminum and sublimates more strongly under vacuum conditions. On the basis of strength to weight ratio, magnesium casting alloys are superior to aluminum casting alloys. These properties indicate the potential of magnesium and its alloys as a matrix, leading to their selection for the solidification processing of metal-metal and metal-ceramic composites which have been investigated in the current study.

The chemical composition of the matrix magnesium alloys in weight percent used in different composites are given in Table-3.1.

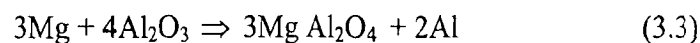
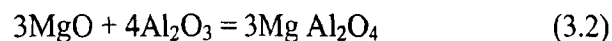
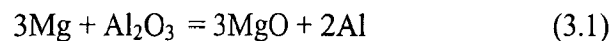
Table 3.1
Chemical Composition of Magnesium and AZ91 Alloy wt%

Alloys	Al	Zn	Fe	Mn
Pure mg	0.018	0.004	0.036	0.002
AZ91	8.79	0.51	0.003	0.18

3.2 Selection of Dispersoids

The matrix alloys selected have been reinforced with steel wool fibers and particles of alumina and graphite. Steel wool is a relatively cheaper dispersoid which could be used to strengthen magnesium by sacrificing the lower density to an extent. The magnesium end of the phase diagram of binary Mg-Fe system as given in Fig.3.1, shows that iron has very limited solubility of less than 0.1 wt% in molten magnesium at the processing temperatures used and the solid solubility of iron in magnesium is negligible i.e., 0.0010 ± 0.0001 wt% at the eutectic temperature close to the melting point of 650°C . The eutectic composition is 0.0060 ± 0.0007 wt% of iron. The small solubility of iron in magnesium may be ideally suited to impart enough wettability for a good interface in magnesium reinforced with steel wool. Further, steel wool fibers have also been reinforced in AZ91 alloys which contains aluminium and zinc. Zinc has a significant solid solubility in iron and aluminium has a number of intermetallic compound with iron which may promote reaction wetting.

The aluminium oxide (Al_2O_3) has been found to react with many divalent transition metal oxides and forms aluminates having a crystal structure similar to mineral spinels. Fig 3.2 shows standard free energies of formation of various oxides from the elements as a function of temperature. It is evident that magnesium may reduce alumina to result in MgO in the range of processing temperatures to be used for the synthesis of Mg- Al_2O_3 composites. The equilibrium phase diagram of the system MgO- Al_2O_3 as shown in Fig 3.3, reveals that MgO produced by the reduction of alumina by magnesium, may combine with the remaining alumina to coat it with a layer of spinel $\text{MgO}.\text{Al}_2\text{O}_3$ and protect alumina particles from further reaction. These reactions have been described in terms of chemical reactions as



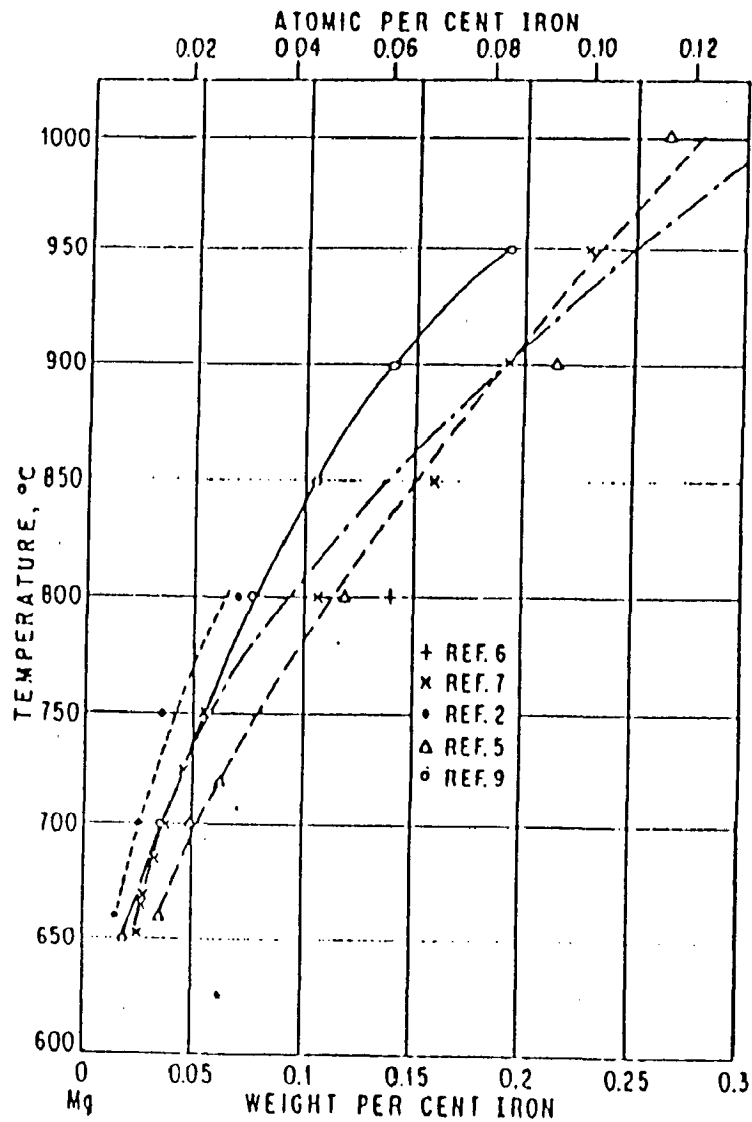


Fig.3.1 Part of equilibrium phases diagram of Mg-Fe alloy system showing solubility of Fe in liquid Mg.

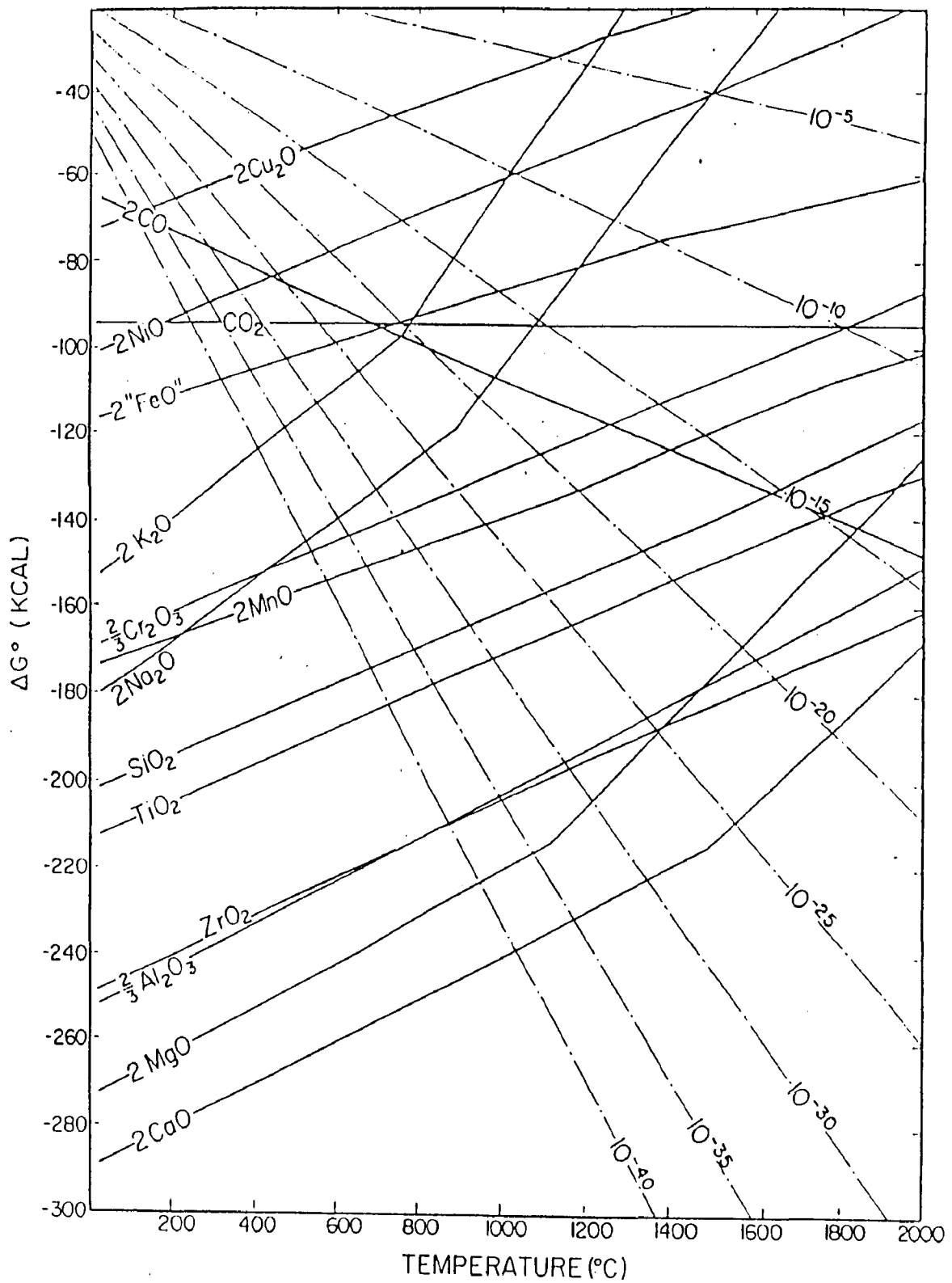


Fig.3.2 The standard free energies formation of various oxides, as a function of temperature.

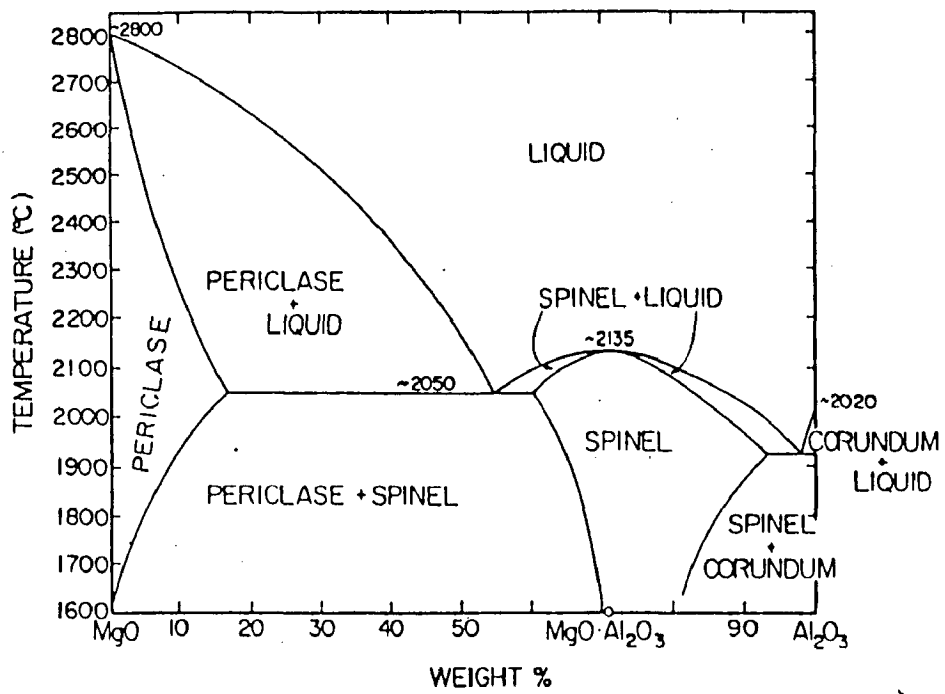


Fig.3.3 Phase diagram for the system MgO-Al₂O₃

The choice of alumina as a dispersoid in magnesium has been made in the context of these chemical reactions. The role and extent of chemical reactions during processing will be investigated in order to understand its impact on the properties.

3.3 Solidification Processing of Composites

For the present study, two types of metal matrix composites namely, metal-metal and metal ceramic, have been processed by solidification synthesis. Table-3.2 gives the processing routes for the synthesis of different types of composites

Table 3.2
Processing Routes for Synthesis of Composites

Types of Composite	Composite System	Processing Routes
Metal-Metal	Magnesium-Steel wool	Vacuum Casting
Metal-Metal	AZ91-Steel wool	Vacuum Casting
Metal-Ceramic	Magnesium-Alumina	Squeeze Casting
Metal-Ceramic	AZ91-Alumina	Squeeze Casting
Hybrid	Magnesium-Alumina-Graphite	Squeeze Casting
Hybrid	AZ91-Alumina-Graphite	Squeeze Casting

3.3.1 Vacuum Casting

Vacuum casting was carried out in a set-up shown in Fig.3.4. About 250 gms of commercially pure magnesium was taken in the mild steel crucible inside a resistance wound - muffle furnace and heated upto 800⁰C. The melting was carried out under a fluid-type of flux such as Dow 230 which contains 55 wt% potassium chloride, 34 wt% magnesium chloride, 9 wt% calcium chloride and 2 wt% calcium fluoride, and it was added from time to time to retain a flux cover continuously in order to prevent oxidation and burning of the molten magnesium. After melting, the alloying elements, if any, were added to the melt. The furnace was switched off and the temperature of the melt was allowed to come down to 730⁰C. The surface of the melt was skimmed to remove the flux

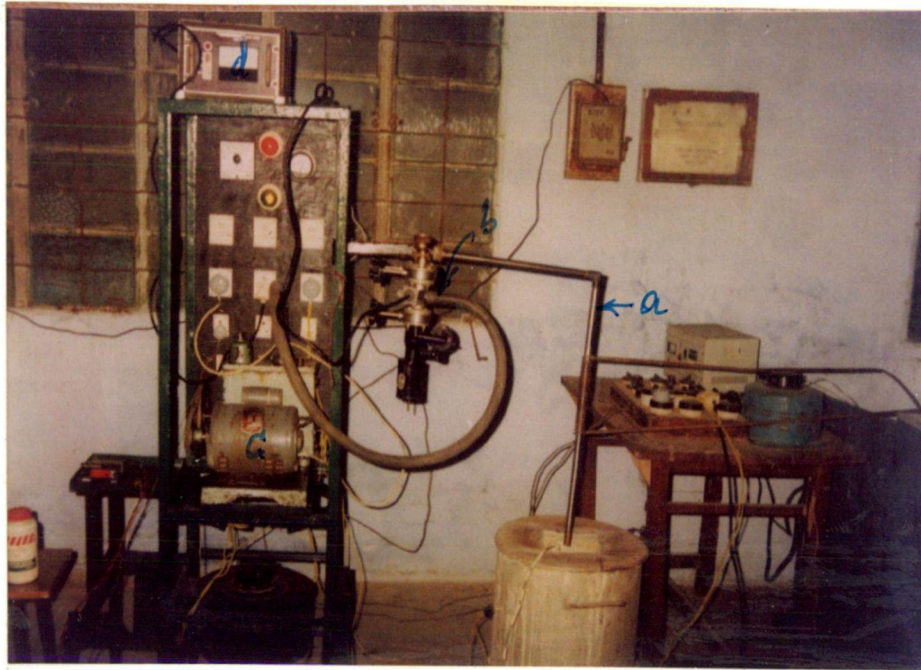


Fig.3.4 Vacuum casting setup used in present study
(a) Steel pipe (b) Vacuum system (c) Rotary Pump (d) Pirani guage.

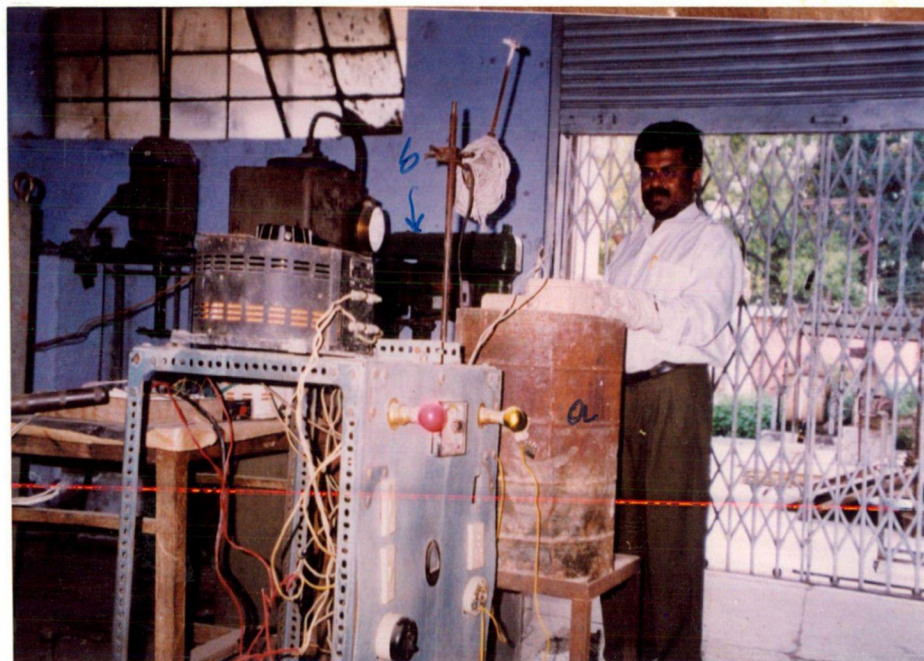


Fig.3.5 Squeeze casting set-up in present study
(a) Resistance wound muffle furnace (b) Hydraulic press

cover and the dross with the help of a heated mild steel spoon. A pipe of 18 mm diameter containing cylindrical steel wool preform of the same diameter was immersed into molten magnesium or its alloy and the other end of the pipe was connected to a vacuum system. The melt surface was then sprinkled with sulphur powder to prevent oxidation. The vacuum system consisted of a rotary pump which was switched on to suck the melt through the preform of steel wool. The level of vacuum was measured using a pirani gauge.

3.3.2 Squeeze Casting

Squeeze casting was carried out using a set-up shown in Fig 3.5. About 250gms of commercially pure magnesium was taken in a mild steel crucible inside a resistance wound muffle furnace following the same procedure as described in 3.3.1. A cylindrical die of diameter of 120 mm and height of 120 mm with a cavity of diameter 40 mm and wall thickness of 40 mm was used for squeeze casting as shown in Fig.3.5. The stopper or ejector pin, the inner cavity of the die and the punch was sprayed with graphite dispersed in water and dried at 100⁰C. 20 to 40 gms of dispersoid particles of alumina or alumina and graphite were placed in the die cavity before preheating the die to a temperature in the range of 600⁰C to 700⁰C. The die was taken out from the preheating furnace and a metered quantity of molten metal with a certain degree of superheat was poured onto the bed of dispersoid particles inside the cylindrical cavity. The pouring temperature of the metal was in the range of 730⁰C to 800⁰C. The die was placed on a steel plate and the punch was lowered. The pressure was applied on the punch with the help of the plunger of a 60 Ton hydraulic press made in England. A pressure of 100 MPa was applied and molten metal begins to solidify. The time application of pressure was kept below 5 seconds. The casting was ejected with the help of ejector pin.

3.4 Determination of Chemical Composition and Densities

The chemical compositions of the alloys and the composites were carried out by wet chemical analysis. The density of the composites was determined by weight loss method. The volume of the composite, V_c , is equal to the total of the volume of the matrix

alloy, V_m , that of the particles, V_r , and that of the voids, V_p . But the weight of the composite, W_c , is equal to the total weight of the matrix alloy, W_m , and that of the particles, W_r . Therefore, the density of the composite, ρ_c , may be written as,

$$\rho_c = \frac{W_c}{V_c} = \frac{W_m + W_r}{V_m + V_r + V_p} \quad (3.4)$$

3.5 Metallography

The scheme of sectioning of the cast ingot for making the specimens for various metallographic studies has been shown schematically in Fig. 3.6. The cast ingot was used for metallographic examination after preparing the specimens by standard metallographic procedure. The final polishing was carried out on a polishing cloth using polishing grade alumina suspension. After polishing the specimens were cleaned thoroughly with water, dried and etched for 20 to 30 seconds with oxalic acid solution containing 2% of oxalic acid in water, followed by washing and drying again. Etched specimens and sometimes, polished specimens were examined under optical microscope.

3.6 Estimation of Dispersoid Content

The steel wool and alumina particles present in magnesium based composites were observed as relatively darker areas under optical microscope. The area fraction of the steel wool and alumina particles were measured by 'point counting method'. The magnification in the microscope was so adjusted that a maximum resolution could be obtained and at the same time the condition of not more than one grid-point in one dark spot could be satisfied. For each sample, 10 such observations were made at random locations. The area fraction of dark spots on the matrix was evaluated dividing the average value of the number of grid points in dark spots by the total number of grid points.

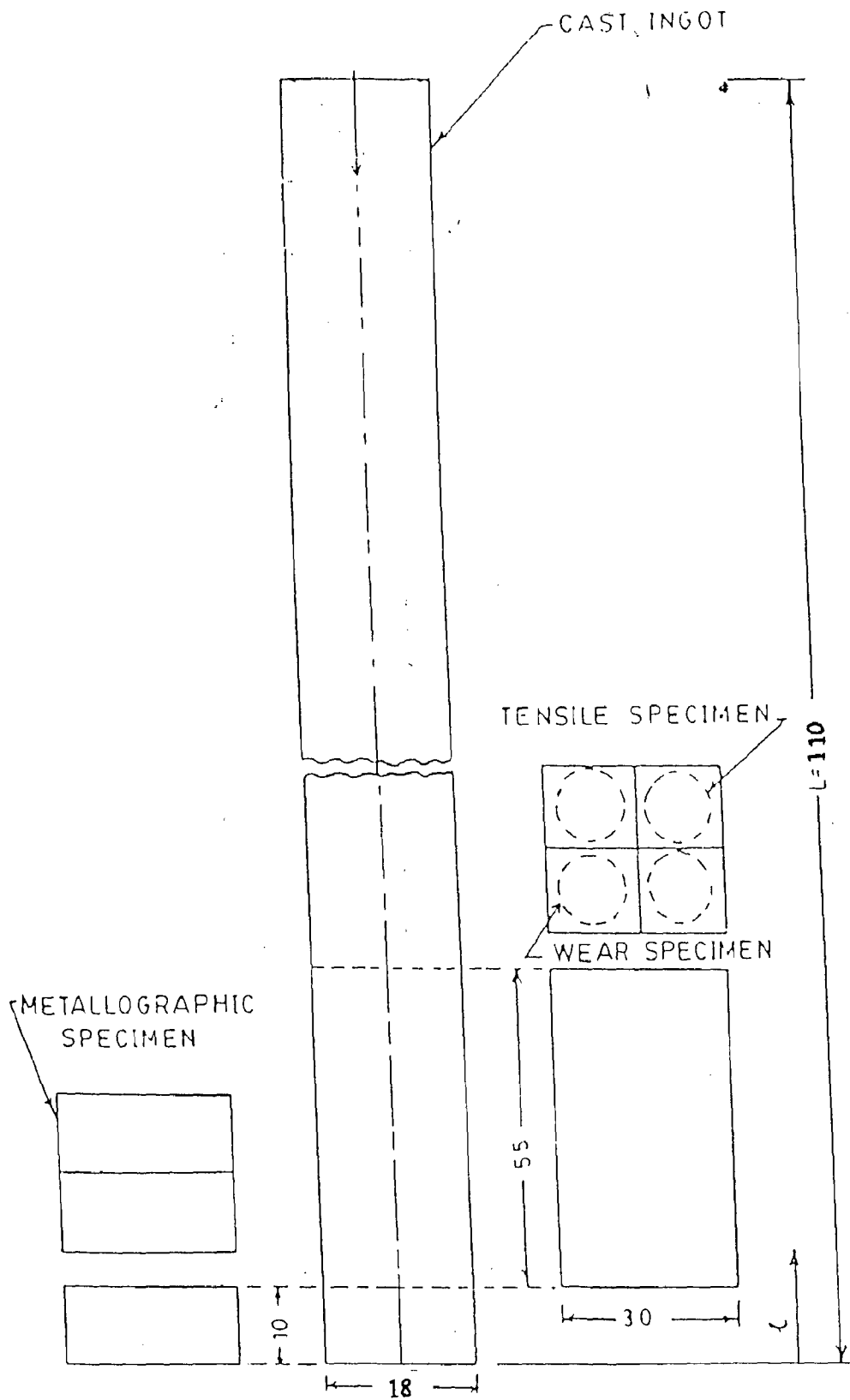


Fig.3.6 The test specimens machined out from the cast ingots.

3.7 X-Ray Diffraction Electron Probe Micro-Analysis (EPMA)

The X-ray diffraction study was carried out by using powder samples of cast composite in a Philips X-ray diffractometer, to identify the various phases formed in the cast composites of magnesium-alumina, magnesium alloy AZ91-alumina. The hybrid composites of magnesium-alumina-graphite and alloy AZ91-alumina-graphite were also examined to detect any major chemical reaction taking place during processing. The powder of the sample to be examined by X-ray diffraction was prepared and the size of the powder was in the range of 0.15-0.25 mm. The diffraction study was carried out by using copper target, nickel filter, 20 mA current, 35 kV voltage. The diffraction pattern was automatically scanned under a X-ray diffractometer model PW 1140/90 made in Holland, for an angle of diffraction 2θ from 5° to 120° . The intensity of diffracted beam against 2θ was plotted on a graphical chart where the chart speed and Goniometer speed were maintained at 1 cm/min and $1^\circ / \text{cm}$ respectively. For all the intensity peaks and corresponding values of 2θ , the interplanar spacing, d , was

$$\lambda = 2d\sin\theta \quad (3.5)$$

where, λ , is the wave length of CuK_α radiation used for diffraction and was taken as 1.5405 \AA for estimating the d values which was finally used for identification of various phases with the help of inorganic ASTM X-ray diffraction data cards.

The polished and etched metallographic samples of squeeze cast magnesium-alumina, hybrid magnesium-alumina-graphite and hybrid AZ91 alloy-alumina-graphite composites were examined under JEOL superprobe micro analyser model JXA 8600 M. The quantitative and line analysis of this specimen were carried out with respect to elements like Al and Mg. An acceleration voltage of 20 kV was employed for these studies.

3.8 Hardness and Tensile Testing

(a) Hardness Testing

The Brinell test is a simple indentation test for determining the hardness of a wide variety of materials and it is particularly preferred for composites as it could provide a better average hardness over a larger area containing several dispersoids in the matrix. The measurements were carried out in a Brinell cum Vickers hardness tester (WPM) made in the German Democratic Republic. Generally, five separate indentations at different locations were taken. The test consists of applying load was 15.625 kg (force), for a specified time of 10 to 30 seconds using a 2.5 mm-diameter hardened steel ball on the flat surface of the workpiece. The time of application of load should be such as to ensure that the plastic flow of the metal in the area under indentation has ceased. The load is removed to allow elastic recovery and the round impression was measured in millimeters to the nearest 0.01 mm using a low-power microscope. To eliminate any error in the measurements due to deviation from sphericity, measurements were taken along two diameters at 90° to each other. Hardness was determined by taking the mean diameter of the indentation. The Brinell hardness number has been estimated from the diameter of indentation at the applied load.

Microhardness were carried out in a Vickers indenter made in the Germany Leitz wetzlar. Generally, five separate indentations at matrix and fiber, particles of different locations were taken. The test consists of applying load was 5gm and 50gms, for a specified time of 30 seconds by using a square diamond pyramid indenter with an angle of 136° . The diagonals of the square indentation was measured under optical microscope at a magnification of X500 provided with the microhardness Leitz Wetzler 721464 tester and the average of the two diagonals was used to find out the corresponding microhardness. At least five readings were taken on the matrix of each composite by choosing the indentation spots away from the voids and the particles. Average of these readings for each samples is reported as the microhardness of a matrix in a composite. The microhardness number has been estimated from the diameter of indentation at the applied load.

(b) Tensile Testing

The tensile tests were carried out at ambient temperature for the base alloy and the composites. The specimens were machined from each castings. The dimension of the tensile specimens, conforming to ASTM specification, is shown schematically in Fig. 3.7. The tensile tests were performed in a motor driven Monsanto Tensometer type W, having an arrangement for tracing the load vs extension curve. All the tests were carried out on a load scale of 0-500 kg. The diameter and the gauge length of each specimen was measured prior to and after the test. The tensile tests were carried out on the specimens of the base alloys and also, the composites. The ultimate tensile strength of the specimens was evaluated by dividing the maximum tensile force by the initial cross-sectional area of the specimens in units of MN/m^2 or MPa. After fracture of the specimen, the increase in gauge length was measured and the engineering fracture strain, e_f was estimated as a change in gauge length per unit initial gauge length of 25mm.

3.9 Dry Sliding Wear Tests

Dry sliding wear tests for the matrix magnesium and magnesium alloy AZ91 were carried out using pin-on-disc machine, apart from the tests on composites containing steel wool, alumina or hybrid of alumina and graphite. The test material was taken in the form of a pin of diameter 6 mm and length 30 mm and held against the counterface of a 100 mm diameter rotating disc made of EN - 32 steel hardened to HRC 58 to 62. The pins were polished up to 4/0 grade emery paper and both the disc and the pin were cleaned by acetone and dried before carrying out the test. The pin was loaded against the disc through a dead weight loading system. Five different normal loads of 0.5, 1.0, 1.5, 2.0, and 2.5 kg were applied on pins of each test material. The track radius of the pin was kept at 50 mm and the linear speed at this track radius was 1 m/s. Each wear test was carried out for a total sliding distance of about 2199.12m. Tangential force was monitored continuously during the wear test. The cumulative weight loss of the test pin due to wear, was measured by interrupting the wear test at regular intervals of five minutes and weighing the pin by an electronic balance having an accuracy of 0.01 mg. Each test was replicated three times under the same load and sliding velocity to check the reproducibility of cumulative weight

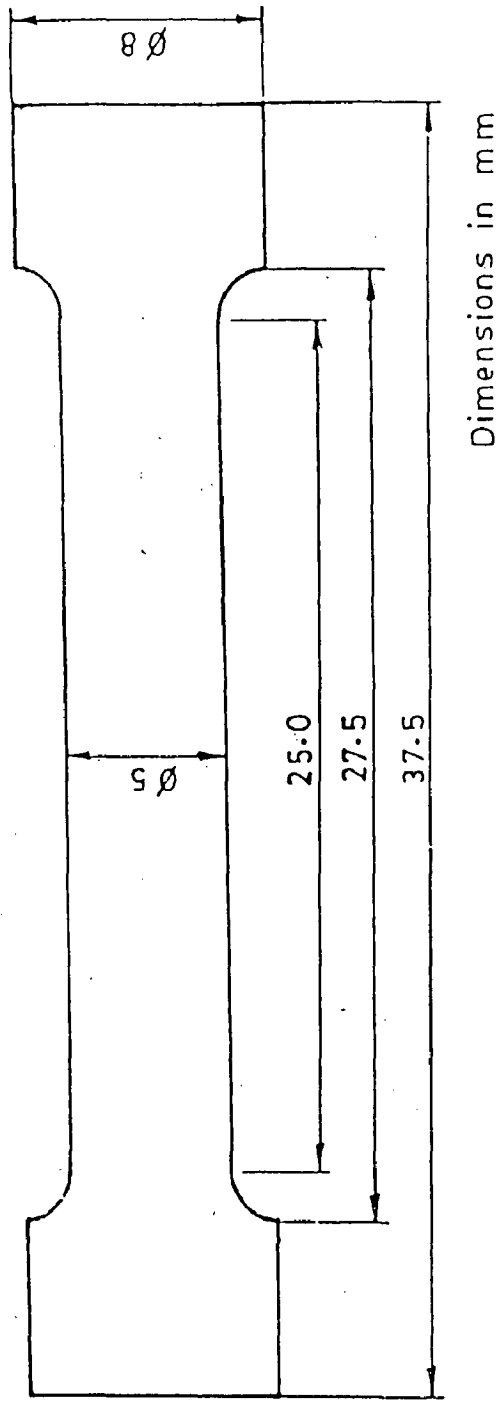


Fig.3.7 Dimensions of the tensile specimens

loss. The cumulative weight loss was taken as the average of the three tests and the cumulative volume loss was estimated by dividing the weight loss by the density of the test pin. The variation of cumulative volume loss with sliding distance was plotted as the basic data for a test. In view of their superior wear resistance, the squeeze cast composites were tested under higher normal loads of 2.5, 3.5, 4.5, and 5.5 kg.

3.10 Microscopic Examinations

3.10.1 Examination of Sliding Surface

The sliding surfaces of commercial magnesium, AZ91 alloy and different composites based on these materials were examined under a LEO, 435 VP scanning electron microscope (SEEM) and photographed.

3.10.2 Examination of Wear Debris

Examination of the nature of wear debris provides basic information regarding the degree of work hardening or the composition of the transferred layer. The debris material generated during wear experiments was carefully collected during dry sliding wear of commercial magnesium, magnesium-steel wool, AZ91 alloy-steel wool composites, magnesium-alumina, AZ91 alloy-alumina, hybrid magnesium-alumina-graphite and hybrid AZ91 alloy-alumina-graphite. These samples of wear debris were examined under Zeus stereo-microscope and photographed.

CHAPTER-4

MAGNESIUM BASED METAL-METAL COMPOSITES

This chapter describes the results on processing of steel wool reinforced magnesium and AZ91 alloy matrix composites and their mechanical and tribological properties. In the end, the results have been discussed to develop a coherent understanding of the phenomena involved.

4.1 Results

4.1.1 Chemical Composition

The chemical composition of the matrix alloys in the composite has been determined in wt% in respect of the weight of composite and the result are reported in Table-4.1.

Table 4.1
Chemical Composition of Magnesium Steel wool Composites

Composite	Chemical Composition wt%			
	Al	Zn	Mn	Mg & Impurities
1.Mg-Steel wool composite	0.017	0.005	0.003	balance
2.AZ91-steel wool composite	8.45	0.49	0.16	balance

4.1.2 Density of composites and steel wool content

The densities of the composites containing different amount of steel wool are reported in Table-4.2. The steel wool content of the composites has been determined from density and not by quantitative microscopy technique of point counting because of clustering of steel wool observed in the microstructure. When ρ_c is the density of a composite containing steel wool, ρ_m is the density of the matrix and ρ_{st} is the density of steel wool, the volume fraction of steel wool in the matrix, V_f , is estimated as,

$$V_f = \frac{\rho_c - \rho_m}{\rho_{st} - \rho_m} \quad (4.1)$$

The steel wool contents in different composites estimated using Eq.(4.1) are reported in the last column of Table-4.2.

Table 4.2
Density of Steel wool Composites and Steel wool Content

Sample number	Sample designation	Matrix	Density (kg/m ³ x10 ³)	Steel wool content Vol%
1	Pmg	Mg	1.73	0.0
2	MS3	Mg	2.00	4.5
3	MS4	Mg	2.07	5.5
4	MS5	Mg	2.09	6.0
5	MS2	Mg	2.12	6.5
6	MA	AZ91	1.82	0.0
7	MAS3	AZ91	2.12	5.0
8	MAS2	AZ91	2.19	6.0
9	MAS5	AZ91	2.24	7.0
10	MAS4	AZ91	2.31	8.0

4.1.3 Microstructure of the composites

The microstructures of steel wool reinforced composites based on commercial magnesium and AZ91 alloy have been examined under optical microscope to find the amount and distribution of phases in the matrix alloy, in the context of phase diagram and also the volume fraction of reinforcements as determined from density given in Table 4.2.

(a) Magnesium based composite

Fig 4.1 shows the microstructure of a composite containing 4.5 volume percent of steel wool and the strands of steel wool are clustered which may be due to pushing by liquid metal during infiltration. Fig 4.2 shows a location in the same composite where the strands have solidified leaving shrinkage cavity between the strand near and away from steel wool strands. The marked A, B and C could be three streams of infiltration which solidified from the side to the centre resulting in shrinkage cavity at the boundary.

Fig.4.3 shows the microstructure of cast commercial magnesium taken at a magnification of X250 for comparison with the matrix microstructure of the composite. The bright areas in this figure show primary magnesium dendrites separated by interdendritic area containing dark precipitates which could be intermetallic phases containing Al, Zn and Mn which are there as impurities as indicated in Table 4.1. Fig. 4.4 shows the precipitates along with at a higher magnification of X250 One could also observe twins and grain boundaries in both Figs.4.3 and 4.4. It is interesting to note that there is no significant trend for dendritic solidification in the streams of infiltrated composite and the impurity segregation is relatively less in the matrix of the composite as shown in Figs. 4.1 and 4.2 compared to that in cast commercial magnesium as indicated in Figs 4.3 and 4.4.

Fig 4.5 shows the microstructure of the composite when the steel wool content increased to 5.5 volume percent. The steel wool strands are transverse to the plane of the microstructure and one observes relatively better distribution of steel wool although there is some clustering of the strands. Fig 4.6 shows an area of the same composite where the shrinkage cavities at the boundary of infiltration streams could be clearly observed. Fig 4.7 shows another area of the same composite where it appears that a different phase has formed. Fig.4.8 shows the microstructure of steel wool at a magnification of X625 embedded in the matrix of the same composite containing 5.5 vol% of steel wool. The matrix region around the strand could not be focused along with the strands as the surrounding matrix, being soft, has worn out more during polishing compared to the steel strands. The steel wool contains about 0.14 wt% of carbon and the microstructure shows

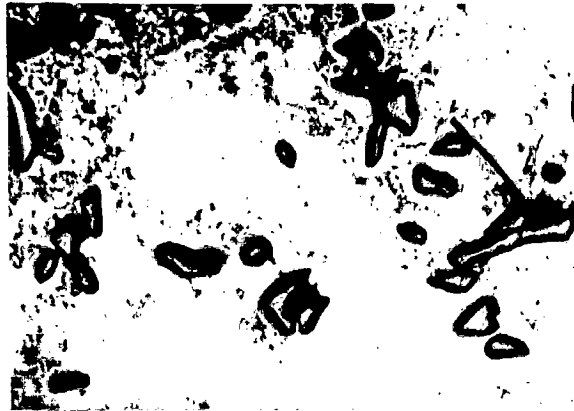


Fig.4.1 Microstructure of vacuum infiltrated commercial magnesium based composite containing 4.5 vol% of steel wool , showing transverse section of steel wool strands in the matrix of commercial magnesium; X125.



Fig.4.2 Microstructure of vacuum infiltrated commercial magnesium based composite containing 4.5 vol% of steel wool , showing shrinkage cavity at the boundary of infiltrating streams; X250.



Fig.4.3 Microstructure of commercial magnesium cast by vacuum infiltration showing bright primary phase and relatively dark interdendritic areas; X250.



Fig.4.4 Microstructure of commercial magnesium cast by vacuum infiltration showing solute rich interdendritic area containing dark precipitates; X250.

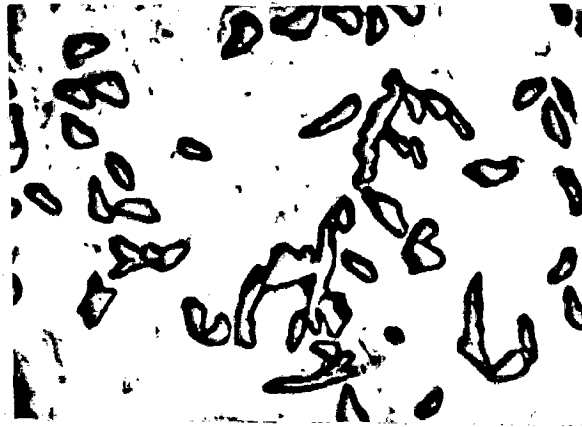


Fig.4.5 Microstructure of vacuum infiltrated commercial magnesium based composite containing 5.5 vol% of steel wool , showing steel wool strands in the matrix of commercial magnesium; X125.



Fig.4.6 Microstructure of vacuum infiltrated commercial magnesium based composite containing 5.5 vol% of steel wool , showing shrinkage cavities at the boundary of infiltration streams; X125.



Fig.4.7 Microstructure of vacuum infiltrated commercial magnesium based composite containing 5.5 vol% of steel wool , showing relatively dark solute rich area; X125.

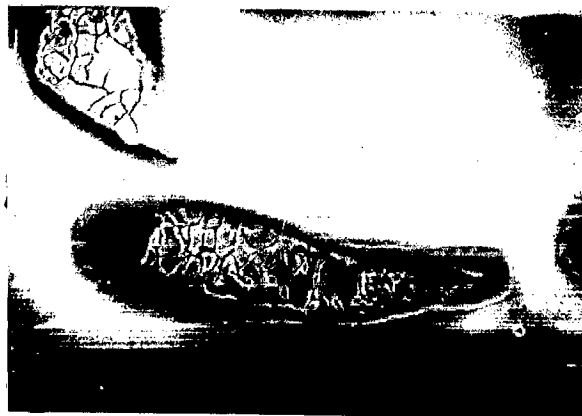


Fig.4.8 Microstructure of vacuum infiltrated commercial magnesium based composite containing 5.5 vol% of steel wool, showing steel wool in focus, containing ferrite and a little pearlite; X625.

primarily the bright phase of ferrite with very little dark areas of pearlite, consistent with its carbon content.

Fig.4.9 shows the microstructure of the magnesium based composite at a magnification of X62.5 when the steel wool content increased to 6 volume percent. The strands of steel wool are reasonably well distributed and there are strands lying on the plane of microstructure as well as transverse to it. The relatively dark areas near the steel strands indicates segregation of impurities near the steel strands. Fig.4.10 shows the microstructure of the same composite at a higher magnification of X250. It is observed how the different strands touch each other surrounding the stream of liquid metal which solidified.

Fig 4.11 shows the microstructure of a composite containing the highest volume percent of 6.5 volume percent of steel wool in a matrix of commercial magnesium. Here also the steel wool strands are touching each other at phases and the matrix has got some marks which were examined at the higher magnification of X250 as shown in Fig 4.12. The liquid streams have solidified from different locations and the last freezing liquid containing more solute has etched dark giving the granular appearance of the matrix.

(b) Magnesium AZ91 alloy based composite

Fig.4.13 shows the microstructure of the composite containing of steel wool in a matrix of AZ91 alloy. It is clearly observed that the steel strands are quite clustered. At a higher magnification of X250 the microstructure shows that the matrix has solidified dendritically and the primary phase is surrounded by network of precipitates of $Mg_{17}Al_{12}$ in the interdendritic region as observed in Fig 4.14. It is further observed that the precipitates of $Mg_{17}Al_{12}$ and the primary phase has also formed on steel strands in certain regions. When one compares this microstructure with that of AZ91 alloy cast by pressure infiltration, as shown in Fig.4.15, it is observed that the primary phase here is significantly more dendritic than that in the matrix of composite as seen on Fig.4.14 but the interdendritic region has similar network of precipitated $Mg_{17}Al_{12}$.



Fig.4.9 Microstructure of vacuum infiltrated commercial magnesium based composite containing 6.0 vol% of steel wool , showing both transverse and longitudinal sections of steel wool strands in the matrix of commercial magnesium; X625.



Fig.4.10 Microstructure of vacuum infiltrated commercial magnesium based composite containing 6.0 vol% of steel wool , showing steel wool strands surrounding a location in the matrix of commercial magnesium; X250.



Fig.4.11 Microstructure of vacuum infiltrated commercial magnesium based composite containing 6.5 vol% of steel wool , showing different sections of steel wool strands in the matrix of commercial magnesium; X125.



Fig.4.12 Microstructure of vacuum infiltrated commercial magnesium based composite containing 6.5 vol% of steel wool , showing streams relatively darker marks in the last freezing area of the boundary of commercial magnesium; X250.



Fig.4.13 Microstructure of vacuum infiltrated AZ91 alloy based composite containing 5.0 vol% of steel wool , showing clustering of steel wool strands in the matrix of dendritically solidified AZ91 alloy; X250.



Fig.4.14 Microstructure of vacuum infiltrated AZ91 alloy based composite containing 5.0 vol% of steel wool , showing steel wool strands in the matrix of AZ91 alloy, where the last freezing liquid shows divorced eutectic; X625.

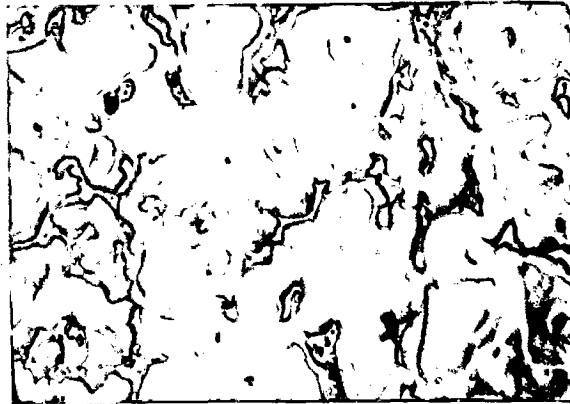


Fig.4.15 Microstructure of AZ91 alloy cast by vacuum infiltration showing primary phase dendrites and interdendritic area of divorced eutectic; X250.

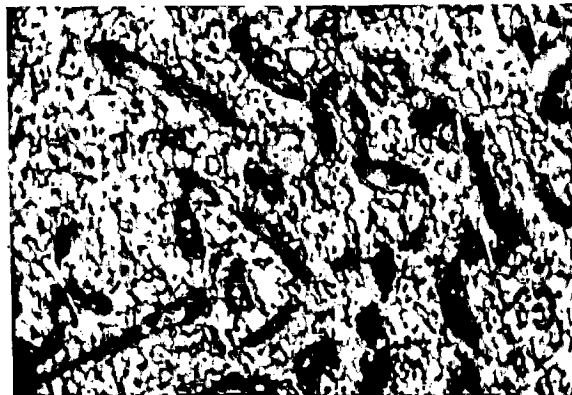


Fig.4.16 Microstructure of vacuum infiltrated AZ91 alloy based composite containing 6.0 vol% of steel wool, showing steel wool strands well distributed in the matrix of AZ91 alloy; X125.

Fig 4.16 shows the microstructure of a composite when the volume fraction of steel wool increases to 6.2 volume percent. The steel wool strands are fairly well distributed in the microstructure as shown in Fig 4.16 but there is coarsening of interdendritic region as observed at a higher magnification X625 in Figs.4.17 and 4.18. There are thicker network of $Mg_{17}Al_{12}$ in comparison to that observed in the composite containing 5.1 volume percent of steel wool in Fig.4.14. Figs 4.19 and 4.20 show the microstructure of the composites containing 7.1 and 8.2 volume percent of steel wool respectively and the microstructures are similar to that in Fig.4.16 for composite containing 6.2 volume percent steel wool.

4.1.4 Hardness of the composites

The macro- and micro- hardnesses have been measured and expressed in terms of Brinell and Vickers hardness for commercial magnesium, Mg-steel wool composite, AZ91 alloy and AZ91-steel wool composites.

The Brinell hardness of the as cast commercial magnesium, Mg-steel wool composite, AZ91 alloy and AZ91-steel wool composites containing different volume percent of steel wool contents are given in Table-4.3 (a) and 4.3 (b).

Table-4.3.(a)

Brinell Hardness of the Cast Commercial Magnesium and Magnesium-steel wool Composites

Sample number	Sample designation	Matrix	Steel wool content Vol %	Brinell hardness HB
1	Pmg	Mg	0.0	20.38
2	MS3	Mg	4.5	21.92
3	MS4	Mg	5.5	22.80
4	MS5	Mg	6.0	23.88
5	MS2	Mg	6.5	24.30



Fig.4.17 Microstructure of vacuum infiltrated AZ91 alloy based composite containing 6.0 vol% of steel wool , showing a thick network of solute rich phase touching steel wool strands in the matrix of AZ91 alloy; X625.

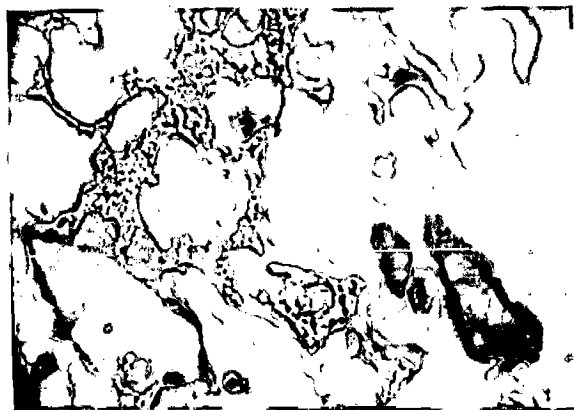


Fig.4.18 Microstructure of vacuum infiltrated AZ91 alloy based composite containing 6.0 vol% of steel wool , showing steel wool strands in the matrix of AZ91 alloy where there is a thick network of solute rich phase; X625.



Fig.4.19 Microstructure of vacuum infiltrated AZ91 alloy based composite containing 7.0 vol% of steel wool , showing steel wool strands in the matrix of AZ91 alloy; X125.



Fig.4.20 Microstructure of vacuum infiltrated AZ91 alloy based composite containing 8.0 vol% of steel wool , showing steel wool strands in the matrix of AZ91 alloy; X125.

Table 4.3 (b)

Brinell Hardness of the AZ91 alloy and AZ91 alloy-Steel wool Composites

Sample number	Sample designation	Matrix	Steel wool content Vol %	Brinell hardness HB
1	MA	AZ91	0.0	34.06
2	MAS3	AZ91	5.0	36.66
3	MAS2	AZ91	6.0	37.74
4	MAS5	AZ91	7.0	38.50
5	MAS4	AZ91	8.0	39.18

Fig. 4.21 shows the variation in the Brinell hardness with volume percent of steel wool in the composites based on commercial magnesium also those based on AZ91 alloy. It has been found that for both the composites, the hardness increases with the steel wool content. But for AZ91 alloy based composite the Brinell hardness is significantly higher compared to the composites based on commercial magnesium. The variation of hardness with steel wool content is almost linear with relatively less of scatter for the AZ91 alloy based composites but for the softer matrix of commercial magnesium, there is more scatter and possibly a non linear variation.

The Vickers microhardnesses for as cast commercial magnesium, Mg-steel wool composite, AZ91 alloy and AZ91-steel wool composites have been measured and expressed in terms of Vickers hardness numbers (VHN) The Vickers hardness of the below mentioned casting materials containing different steel wool contents are given in Table-4.4(a) and 4.4(b).

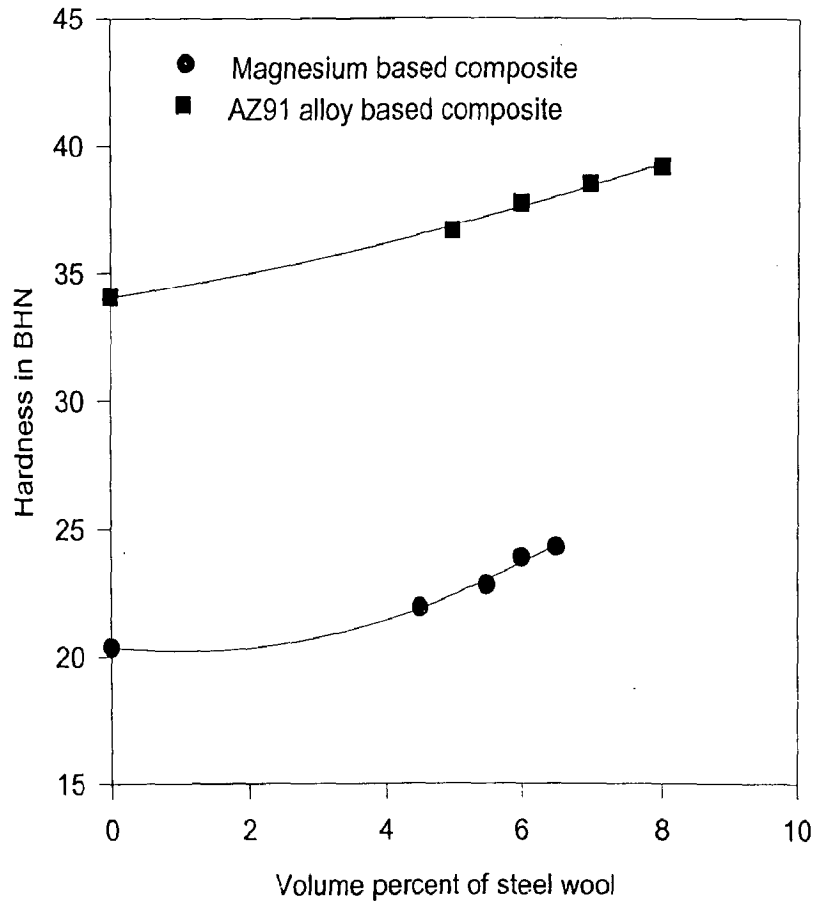


Fig. 4.21 The variation of Brinell hardness with volume percent of steelwool in commercial magnesium and AZ91 alloy based composites containing steel wool.

Table-4.4.(a)

Vickers Hardness of the Cast Commercial Magnesium and Magnesium Steel wool Composite

Sample number	Sample designation	Matrix	Steel wool content Vol %	Vickers microhardness HV		
				Bright Area	Fiber	Dark Area
1	Mg	Mg	0.0	52.40	-----	66.56
2	MS3	Mg	4.5	69.56	200.00	79.22
3	MS4	Mg	5.5	68.80	246.00	81.90
4	MS5	Mg	6.0	58.90	279.00	84.40
5	MS2	Mg	6.5	58.22	348.00	77.57

Table-4.4.(b)

Vickers Hardness of the AZ91 alloy and AZ91-Steel wool Composites

Sample number	Sample designation	Matrix	Steel wool content Vol %	Vickers microhardness HV	
				Bright Area	Fibre
1	MA	AZ91	0.0	120.00	-----
2	MAS3	AZ91	5.0	123.00	279.00
3	MAS2	AZ91	6.0	119.00	340.00
4	MAS5	AZ91	7.0	117.00	377.00
5	MAS4	AZ91	8.0	109.00	401.00

Fig. 4.22 shows the variation of microhardness in VHN with volume percent of steel wool in composites based on commercial magnesium. It is observed that the microhardness of the bright area of primary phase is a little lower than the dark area in the interdendritic region. It may be interesting to note that the hardness of the steel wool strand increases rather rapidly with steel wool content.

Fig. 4.23 shows the variation of microhardness in VHN with volume percent of steel wool in the composite based on AZ91 alloy. The bright area has a significantly higher hardness than that in magnesium-steel wool composite. But it may be noted that this bright

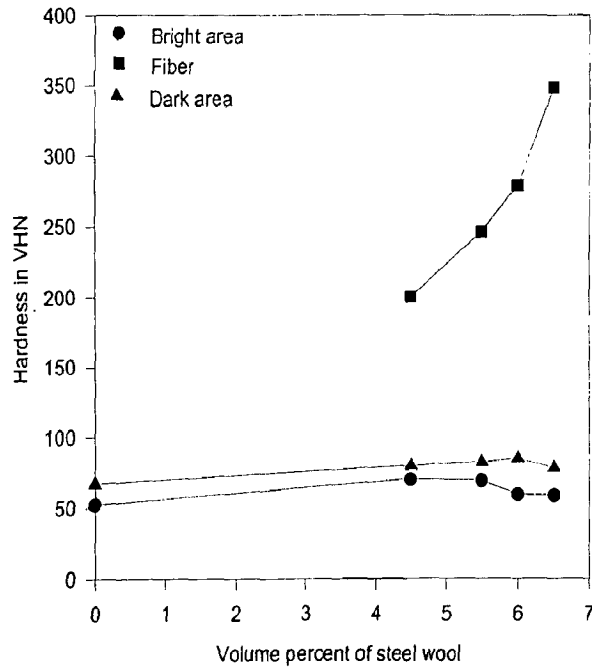


Fig.4.22 The variation of Vickers hardness with volume percent of steel wool in composites based on commercial magnesium.

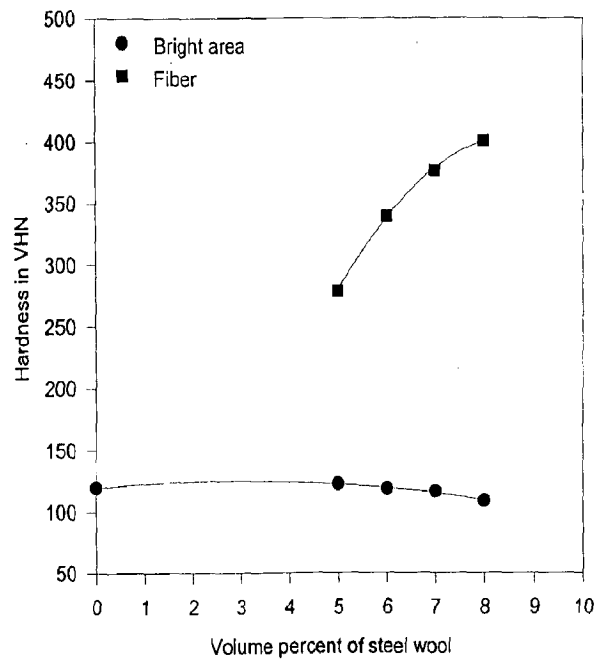


Fig.4.23 The variation of Vicker hardness with volume percent of steel wool in composites based on AZ91 alloy.

area is the magnesium solid solution phase of the divorced eutectic. The dendrite of the primary phase is relatively darker in the microstructures of the alloy and the composites based on AZ91 alloy. The dark strands of steel wool has hardness increasing with steel wool content in the composite as it has been observed for magnesium-steel wool composites.

4.1.5 Tensile properties

The ultimate tensile strength (UTS) in cast commercial magnesium, Mg-steel wool composite, AZ91 alloy and AZ91-steel wool composites with different steel wool contents have been carried out and the results are tabulated in Table-4.5(a) and 4.5(b).

Table-4.5.(a)

Ultimate Tensile Strength of the Cast Commercial Magnesium and Magnesium -Steel wool Composites

Sample number	Sample designation	Matrix	Steel wool content Vol %	Ultimate tensile strength (UTS) MPa	Elongation %
1	Mg	Mg	0.0	100.94	4.09
2	MS3	Mg	4.5	107.12	0.80
3	MS4	Mg	5.5	114.18	2.16
4	MS5	Mg	6.0	118.11	2.49
5	MS2	Mg	6.5	132.04	2.94

Table 4.5 (b)

Ultimate Tensile Strength of the AZ91 alloy and AZ91-Steel wool Composites

Sample number	Sample designation	Matrix	Steel wool content Vol %	Ultimate tensile strength (UTS) MPa	Elongation %
1	MA	AZ91	0.0	112.22	2.52
2	MAS3	AZ91	5.0	132.83	6.77
3	MAS2	AZ91	6.0	141.95	2.71
4	MAS5	AZ91	7.0	148.03	1.62
5	MAS4	AZ91	8.0	153.43	3.93

Fig. 4.24 shows the variation of the ultimate tensile strength (UTS) of the composites based on commercial magnesium and those based on AZ91 alloy. It is observed that the UTS increases rather rapidly with steel wool content in the range between 4.5 to 6.5 vol% for magnesium based composite and it could be indicative of the importance steel wool distribute in the composite. But in the composites based on AZ91 alloy, the variation of UTS with steel wool content as shown in Fig. 4.24, is almost linear as it has been observed for Brinell hardness. For similar steel wool content, the UTS values of AZ91 alloy based composites are higher than those based on commercial magnesium.

4.1.6 Dry Sliding Friction and Wear

(a) Magnesium-Steel wool Composites

Figs. 4.25 to 4.29 show the variation of cumulative volume loss with sliding distance for the composites having steel wool contents of 0.0, 4.5, 5.5, 6.0 and 6.5 vol% respectively in the matrix of commercial magnesium, tested at different normal loads of 0.5, 1, 1.5, 2.0 and 2.5 kg under a sliding speed of 1.0 m/s. The cumulative volume loss increases linearly with sliding distance at a given load and the least square fit for this variation at different loads are indicated by the lines drawn in these figures. However, these lines at different loads sometimes converge at low sliding distances where the difference in wear volumes at different loads are relatively small. One may also observe that many of these linear least square fit lines do not pass through the origin and the lines corresponding to those tested at higher loads have negative intercepts. The negative intercepts may have been contributed by the run-in period and also by the transfer of iron oxides from the counterface to the sliding surface of the test pin. The red layer of oxide is often visible with the naked eye on the sliding surface of the test pin particularly at lower loads. The average volume loss due to wear is plotted as a function of sliding distance at a given load and the variation was observed to be linear with a coefficient of correlation mostly exceeding 0.99 but 0.98 in certain cases. The wear rate i.e., volume wear per unit sliding distance at a given load is determined from the slope of the linear least square fit lines at different loads.

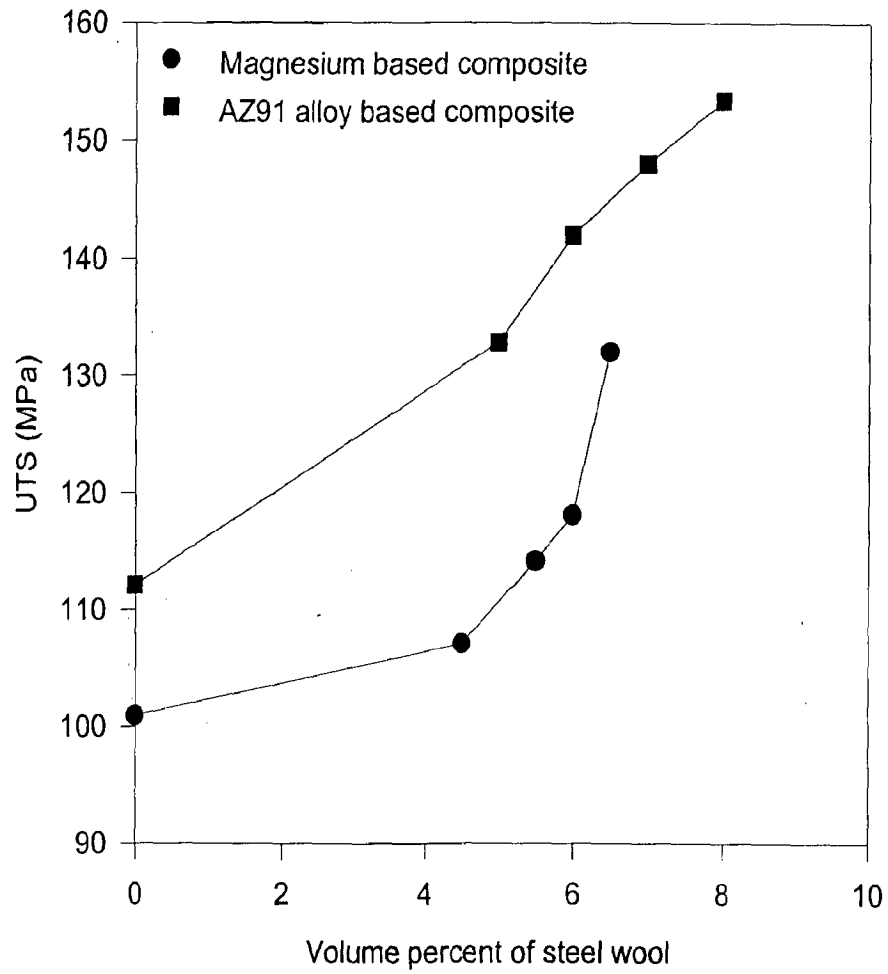


Fig. 4.24 The variation of Ultimate tensile strength (UTS) with volume percent of steel wool in magnesium and AZ91 alloy based composites containing steel wool.

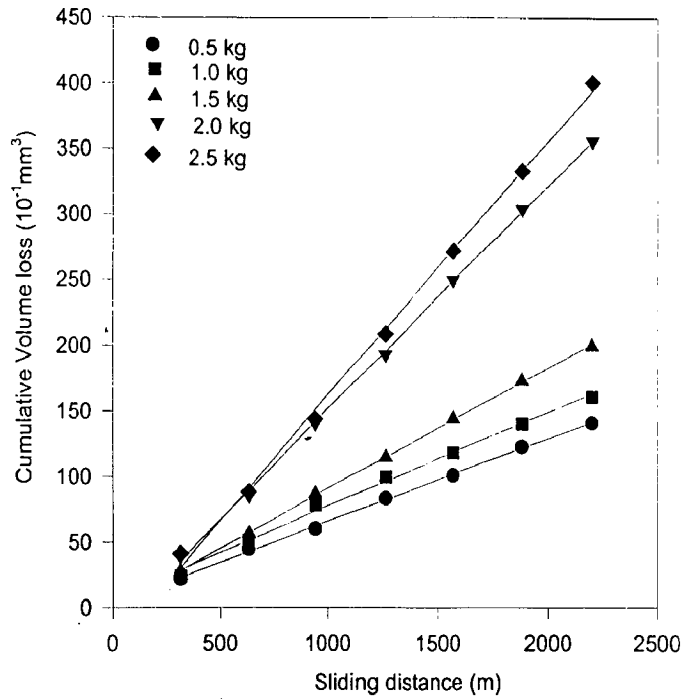


Fig.4.25 The variation of cumulative volume loss with sliding distance in commercial magnesium during dry sliding under a constant sliding speed of 1.0 m/s against counterface of hardened steel.

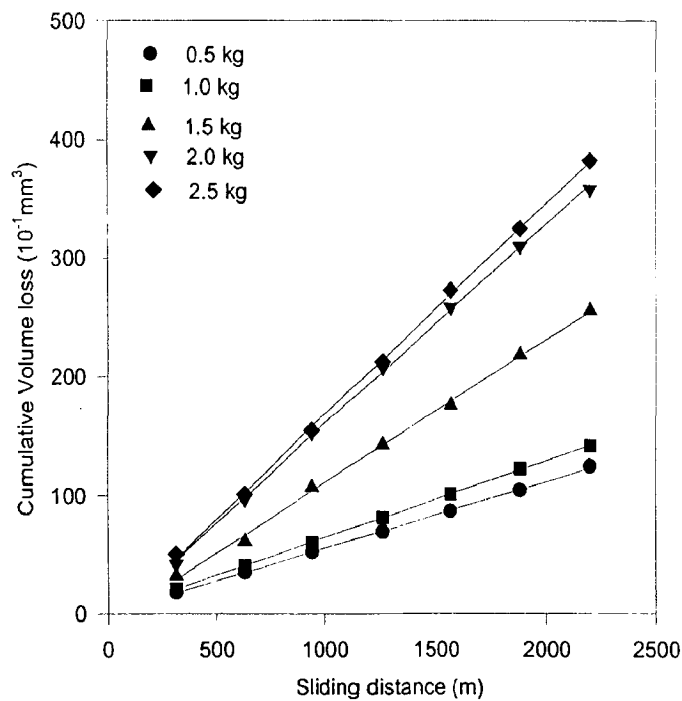


Fig.4.26 The variation of cumulative volume loss with sliding distance in commercial magnesium based composite containing 4.5 vol.% of steel wool, during dry sliding under a fixed sliding speed of 1.0 m/s against counterface of hardened steel.

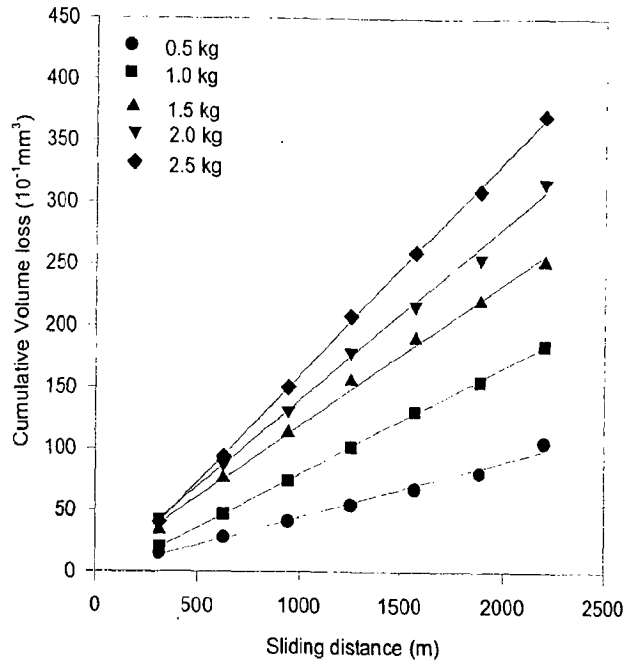


Fig.4.27 The variation of cumulative volume loss with sliding distance in commercial magnesium based composite containing 5.5 vol.% of steel wool, during dry sliding under a fixed sliding speed of 1.0 m/s against counterface of hardened steel.

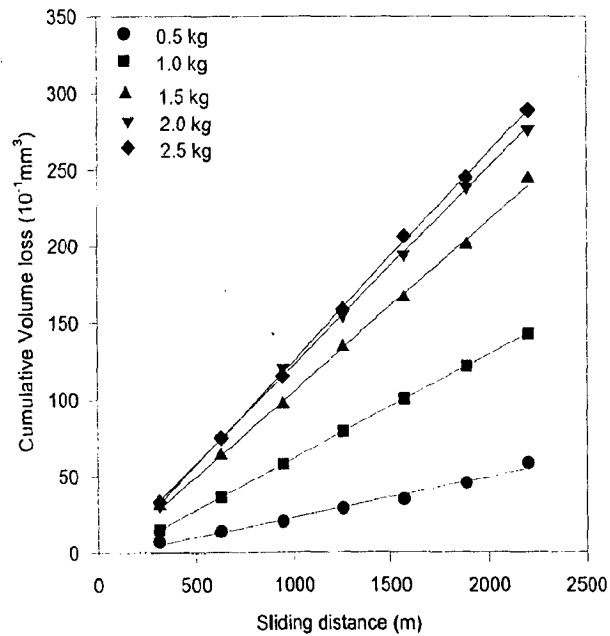


Fig.4.28 The variation of cumulative volume loss with sliding distance in commercial magnesium based composite containing 6.0 vol.% steel wool, during dry sliding under a fixed sliding speed of 1.0 m/s against counterface of hardened steel.

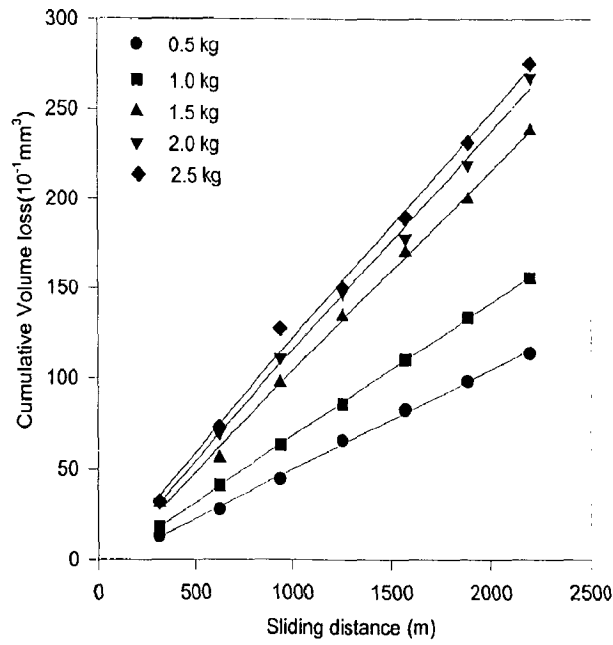


Fig.4.29 The variation of cumulative volume loss with sliding distance in commercial magnesium based composite containing 6.5 vol.% of steel wool, during dry sliding under a fixed sliding speed of 1.0 m/s against counterface of hardened steel.

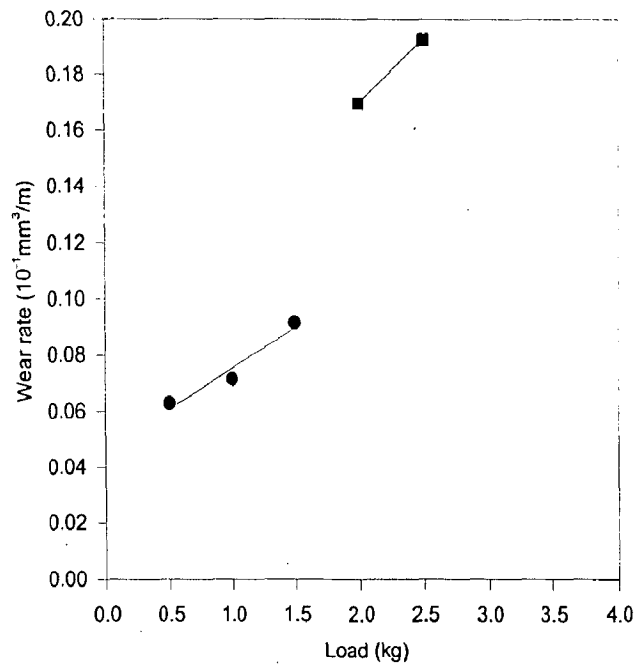


Fig.4.30 The variation of wear rate with normal load for commercial magnesium, during dry sliding at a fixed sliding speed of 1.0 m/s against counterface of hardened steel.

The variations of the wear rate with normal load are shown in Figs. 4.30 to 4.34 for the composites containing 0.0, 4.5, 5.5, 6.0, and 6.5 vol% steel wool respectively, reinforced in commercial magnesium. It is observed that for the commercial magnesium the wear rate increases more or less linearly in the range of load between 0.5 to 1.5 kg, and beyond this load, there is a discontinuity and the wear rate becomes almost double at 2.0 kg compared that at 1.5 kg as shown in Fig. 4.30 may be indicative of a transition in mechanism. When magnesium is reinforced with steel wool the wear rate at lower load of 0.5 kg reduces with increasing steel wool content. But at a load of 1.5 kg the wear rate increases with steel wool content. In the second segment at loads of 2.0 kg and 2.5 kg, the wear rate reduces with steel wool content. As a result the discontinuity disappears in a composite containing 5.5 vol % steel wool and the wear rate varies as shown in Fig. 4.32. But at higher steel wool content, the slope in the second segment reduces making the variation of wear rate with load non linear in the entire range of load as shown in Figs. 4.33 and 4.34. The wear coefficients of the composites have been determined at each load for commercial magnesium and the composites reinforced with steel wool. The average wear coefficient of commercial magnesium is 1.7×10^{-4} and that for composites containing 4.5 to 6.5 vol% of steel wool is in the range between 1.5 to 1.80×10^{-4} in the load interval between 0.5 to 2.5 kg. There is no significant trend of variation of wear coefficient with steel wool content.

Fig. 4.35. shows the variation of coefficient of friction with sliding distance in as cast commercial magnesium for different applied loads ranging between 0.5 kg to 2.5 kg in steps of 0.5 kg. It is observed that at the lower load of 0.5 kg, there is maximum friction compared to that at other applied loads. In Fig. 4.36, the variation of coefficient of friction with sliding distance is observed for a commercial magnesium based composite containing 4.5 vol% steel wool. The coefficient of friction appears to decrease with load similar to that observed in commercial magnesium in Fig. 4.35. At the lower load of 0.5 kg, the coefficient of friction appears to have remained similar to that of commercial magnesium or might have decreased a little. But at higher loads above 0.5 kg, the composite shows a definite increase in coefficient of friction compared to that in commercial magnesium at corresponding loads. At higher loads above 1.5 kg, the coefficient of friction in the composite appears to have become relatively insensitive to variation of load.

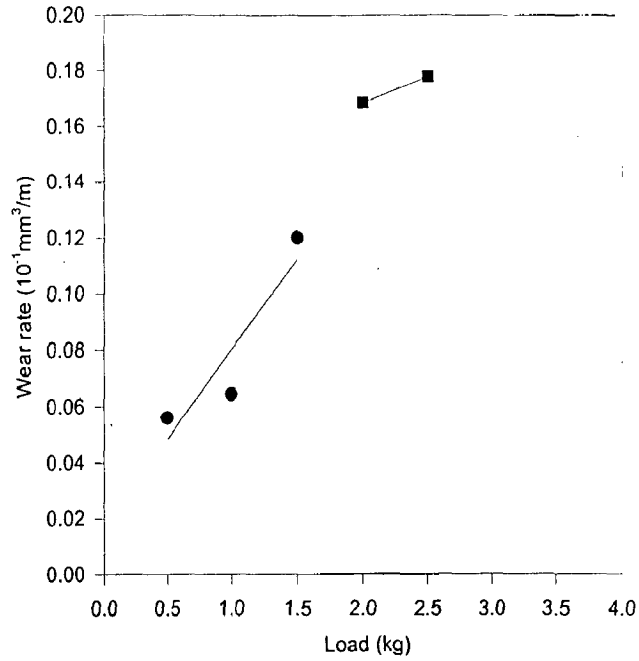


Fig.4.31 The variation of wear rate with normal load in commercial magnesium based composite containing 4.5 vol.% steel wool, during dry sliding at a fixed sliding speed of 1.0 m/s against counterface of hardened steel.

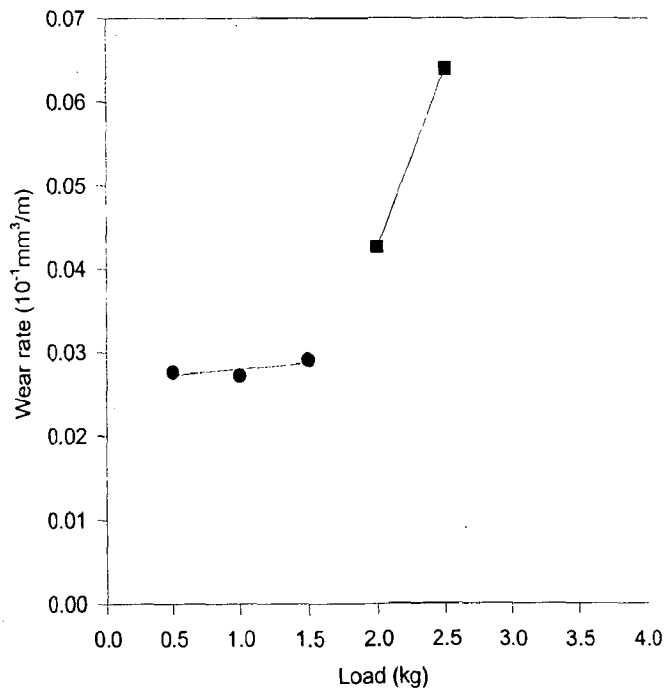


Fig.4.32 The variation of wear rate with normal load in commercial magnesium based composite containing 5.5 vol.% of steel wool, during dry sliding at a fixed sliding speed of 1.0 m/s against counterface of hardened steel.

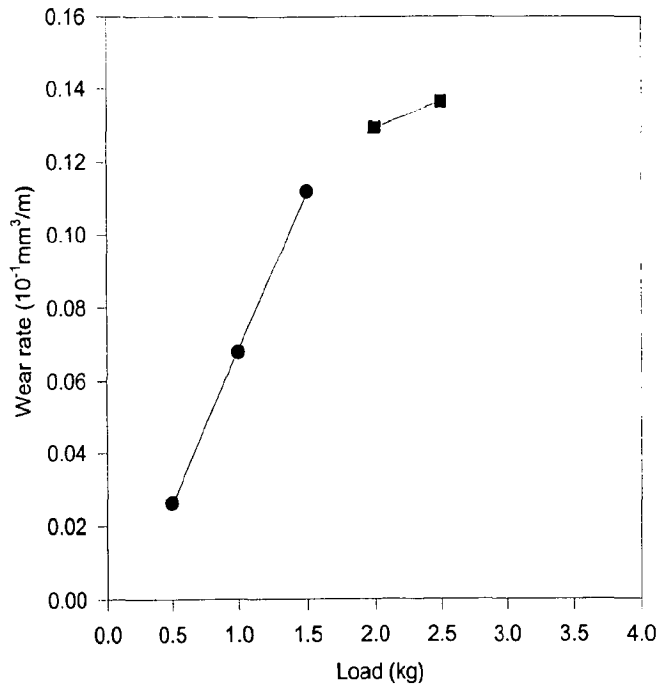


Fig.4.33 The variation of wear rate with normal load in commercial magnesium based composite containing 6.0 vol.% steel wool, during dry sliding at a fixed sliding speed of 1.0 m/s against counterface of hardened steel.

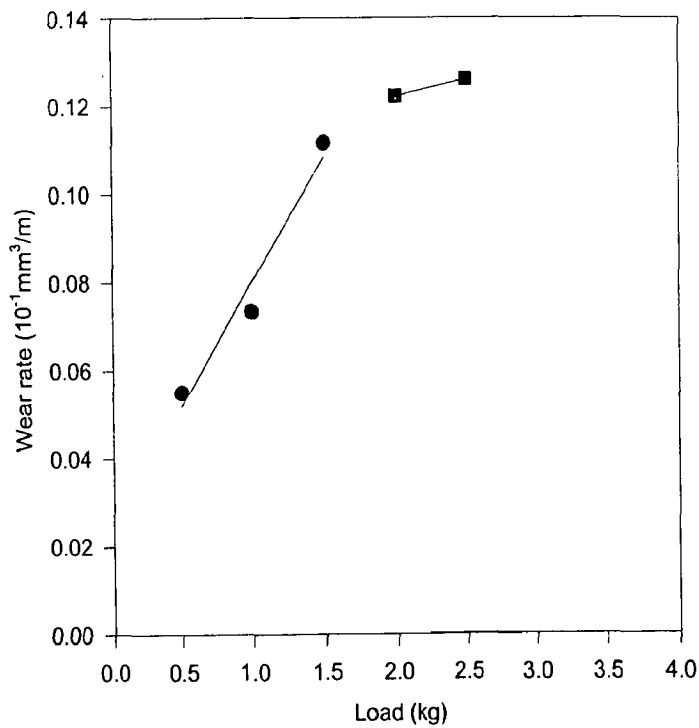


Fig.4.34 The variation of wear rate with normal load in commercial magnesium based composite containing 6.5 vol.% of steel wool, during dry sliding at a fixed sliding speed of 1.0 m/s against counterface of hardened steel.

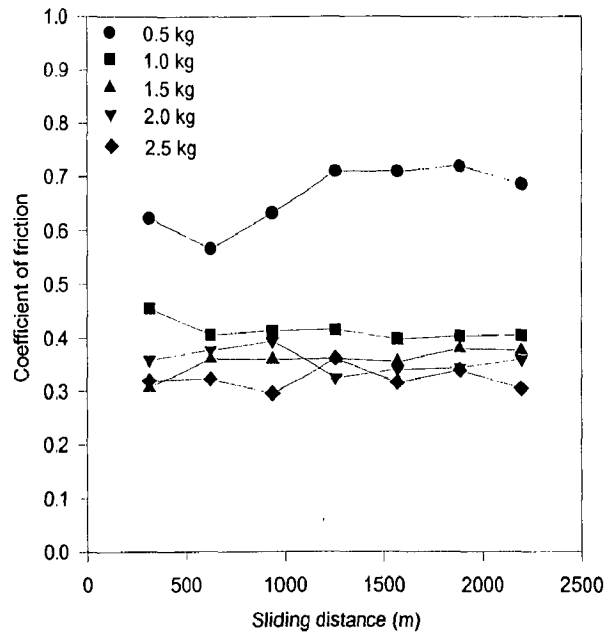


Fig.4.35 The variation of coefficient of friction with sliding distance in commercial magnesium, during dry sliding under a constant sliding speed of 1.0 m/s against counterface of hardened steel.

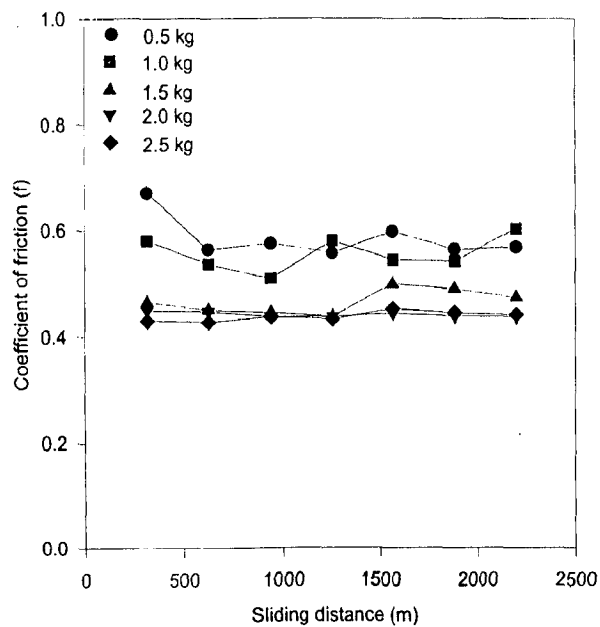


Fig.4.36 The variation of coefficient of friction with sliding in commercial magnesium composite containing 4.5 vol.% of steel wool, during dry sliding under a fixed sliding speed of 1.0 m/s against counterface of hardened steel.

Fig. 4.37. shows the variation of coefficient of friction with sliding distance for the composite containing 5.5 vol% of steel wool. In this figure the curves corresponding to different loads are relatively well spaced and there is no overlapping of curves corresponding to higher loads except those corresponding to loads of 1.5 and 2.0 kg. In addition to increased coefficient of friction at higher loads in the composite compared to that in commercial magnesium the general trend of decreasing coefficient of friction with increasing load is observed. Fig.4.38 and Fig.4.39 show the trend in variation of coefficient of friction with sliding distance for composites containing 6.0 and 6.5 vol% of steel wool respectively. At higher steel wool content the coefficient of friction has increased further at lower loads but at higher load of 2.5 kg, the coefficient of friction appears to lie around 0.4 in the composite irrespective of steel wool content. Fig.4.40(a) to (e) show the variation of coefficient of friction averaged over sliding distance, with load for commercial magnesium and composites based on it but containing different amount of steel wool. When load increases from 0.5 kg, there is a sharp drop in coefficient of friction in all these materials.

Table-4.6(a)

Average Wear Coefficient of Magnesium and Magnesium-Steel wool Composites

Sample number	Sample designation	Matrix	Volume percent of steel wool	Average wear coefficient $k(10^{-4})$
1	Mg	Mg	0.0	0.7621
2	MS3	Mg	4.5	0.9085
3	MS4	Mg	5.5	1.5583
4	MS5	Mg	6.0	1.1903
5	MS2	Mg	6.5	0.7836

(b) Magnesium AZ91 Alloy-Steel wool Composites

Figs. 4.41 to 4.45 show the variation of cumulative volume loss with sliding distance for the AZ91 magnesium alloy based composites having steel wool contents of 0.0, 5.0, 6.0, 7.0 and 8.0 vol% respectively, tested at different normal loads of 0.5, 1, 1.5, 2.0 and 2.5 kg under a sliding speed of 1.0 m/s. The cumulative volume loss increases linearly with sliding distance at a given load as indicated by the least square fit lines drawn

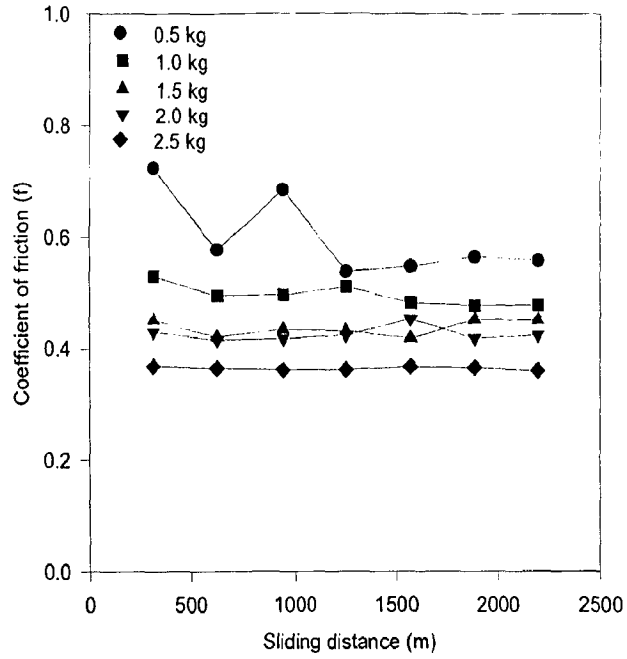


Fig.4.37 The variation of coefficient of friction with sliding distance in commercial magnesium based composite containing 5.5 vol.% steel wool, during dry sliding under a fixed sliding speed of 1.0 m/s against counterface of hardened steel.

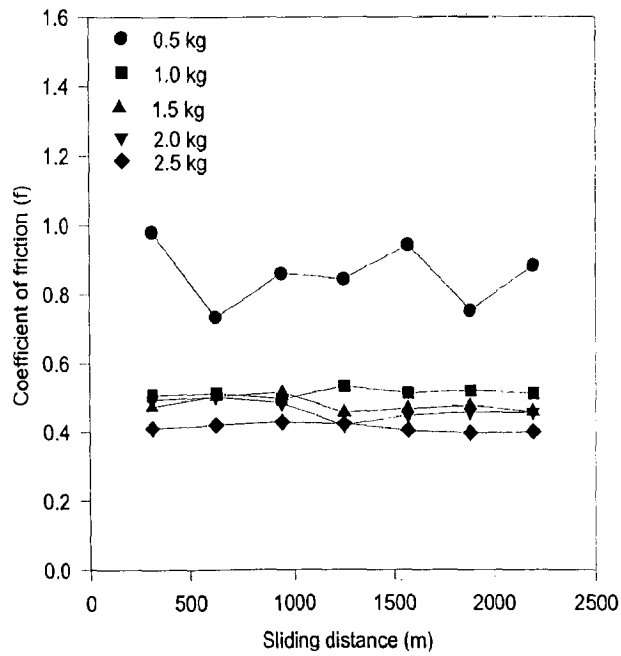


Fig.4.38 The variation of average coefficient of friction with sliding distance in commercial magnesium based composite containing 6.0 vol.% steel wool, during dry sliding under a fixed sliding speed of 1.0 m/s against counterface of hardened steel.

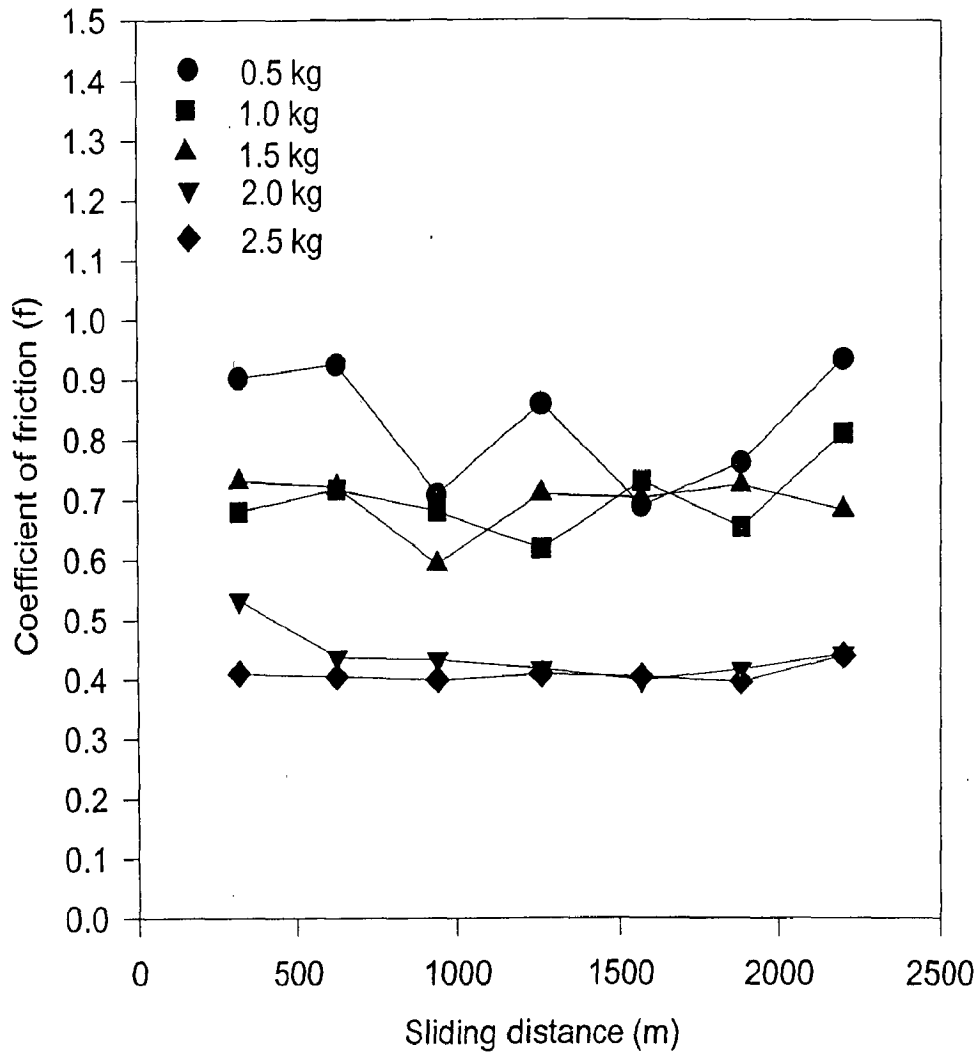


Fig.4.39 The variation of average coefficient of friction with sliding distance in commercial magnesium based composite containing 6.5 vol.% steel wool, during dry sliding under a fixed sliding speed of 1.0 m/s against counterface of hardened steel.

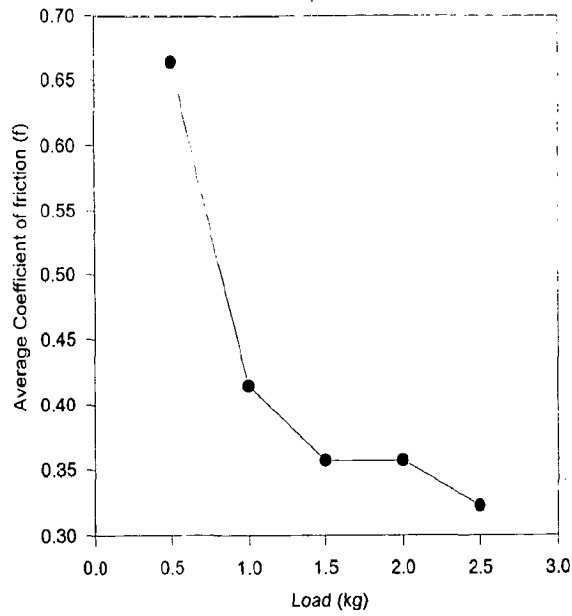


Fig.4.40(a) The variation of coefficient of friction averaged over sliding distance, with normal load for commercial magnesium, during dry sliding at a fixed sliding speed of 1.0 m/s against counterface of hardened steel.

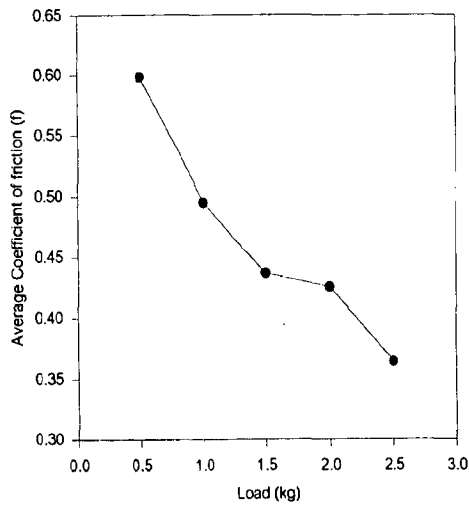


Fig.4.40(b) The variation of coefficient of friction averaged over sliding distance with normal load in commercial magnesium based composite containing 4.5 vol.% of steel wool, during dry sliding at a fixed sliding speed of 1.0 m/s against counterface of hardened steel.

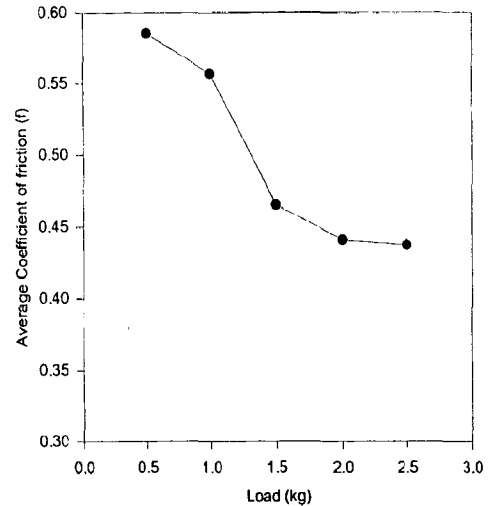


Fig.4.40(c) The variation of coefficient of friction averaged over sliding distance with normal load in commercial magnesium based composite containing 5.5 vol.% of steel wool, during dry sliding at a fixed sliding speed of 1.0 m/s against counterface of hardened steel.

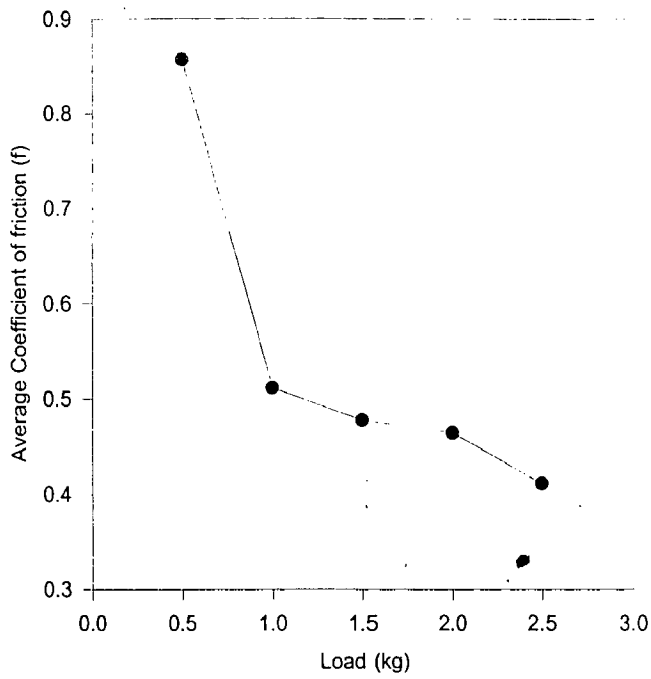


Fig.4.40(d) The variation of coefficient of friction averaged over sliding distance with normal load in magnesium based composite containing 6.0 vol.% steel wool, during dry sliding at a fixed sliding speed of 1.0 m/s against counterface of hardened steel.

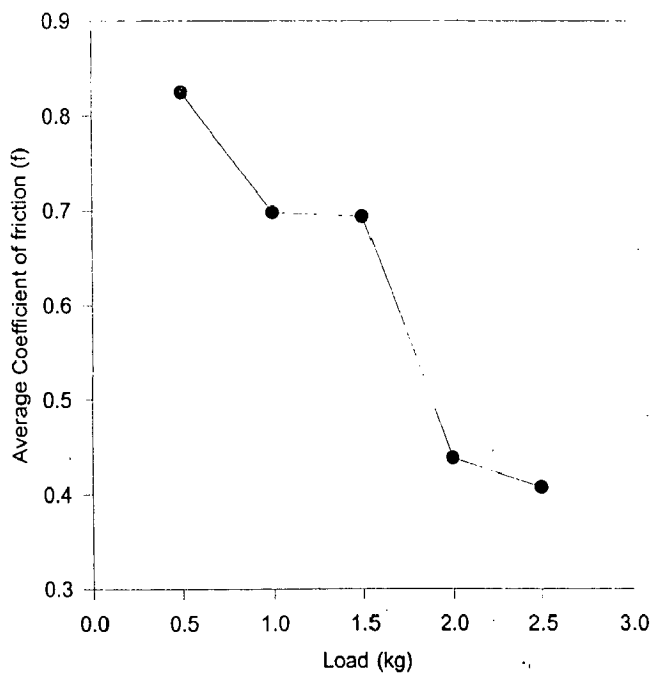


Fig.4.40(e) The variation of coefficient of friction averaged over sliding distance with normal load in commercial magnesium based composite containing 6.5 vol.% steel wool, during dry sliding at a fixed sliding speed of 1.0 m/s against counterface of hardened steel.

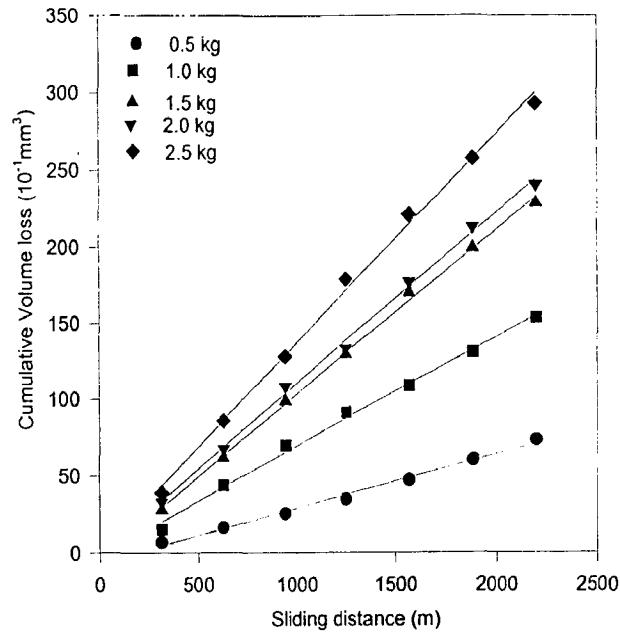


Fig.4.41 The variation of cumulative volume loss with sliding distance in AZ91 alloy, during dry sliding under a constant sliding speed of 1.0 m/s against counterface of hardened steel.

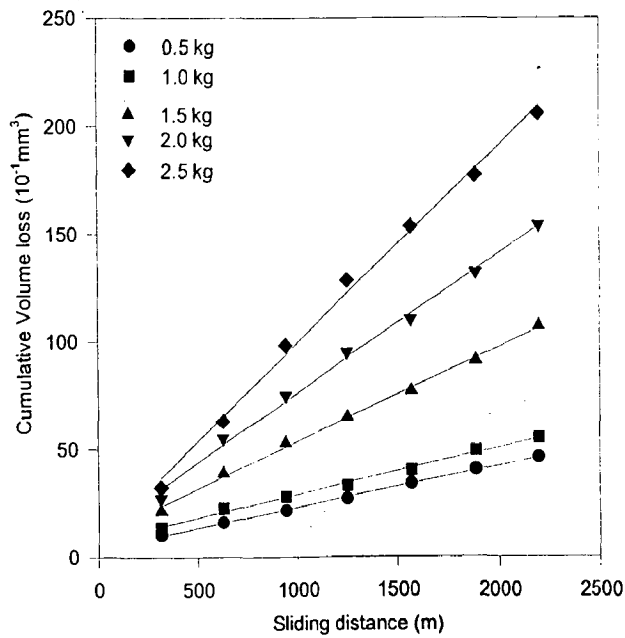


Fig.4.42 The variation of cumulative volume loss with sliding distance in AZ91 alloy based composite containing 5.0 vol.% of steel wool, during dry sliding under a fixed sliding speed of 1.0 m/s against counterface of hardened steel.

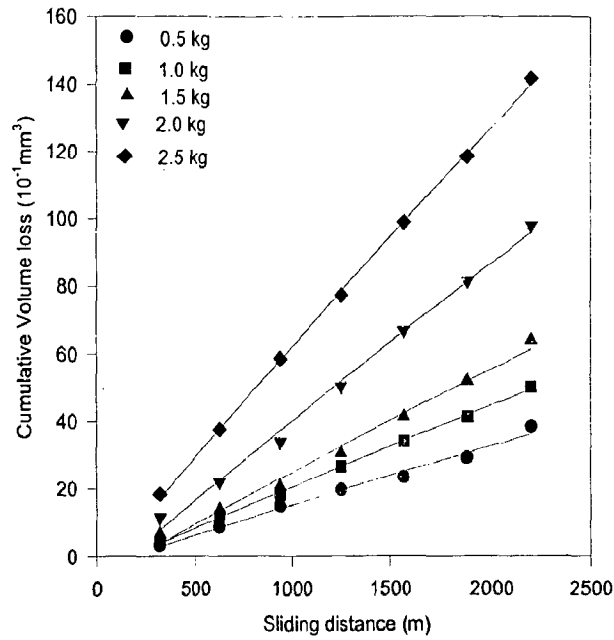


Fig.4.43 The variation of cumulative volume loss with sliding distance in AZ91 alloy based composite containing 6.0 vol.% of steel wool, during dry sliding under a fixed sliding speed of 1.0 m/s against counterface of hardened steel.

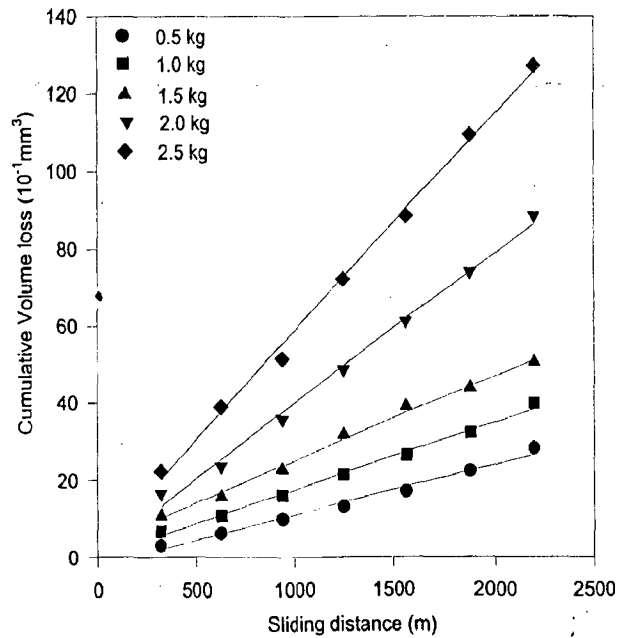


Fig.4.44 The variation of cumulative volume loss with sliding distance in AZ91 alloy based composite containing 7.0 vol.% of steel wool, during dry sliding under a fixed sliding speed of 1.0 m/s against counterface of hardened steel.

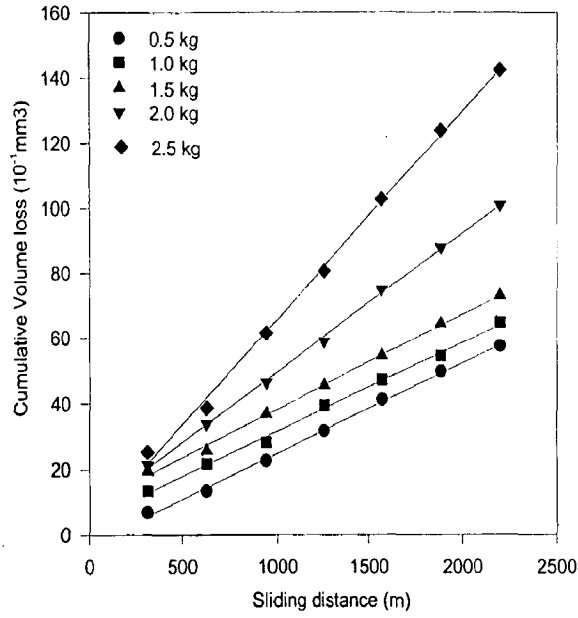


Fig.4.45 The variation of cumulative volume loss with sliding distance in AZ91 alloy based composite containing 8.0 vol.% of steel wool, during dry sliding under a fixed sliding speed of 1.0 m/s against counterface of hardened steel.

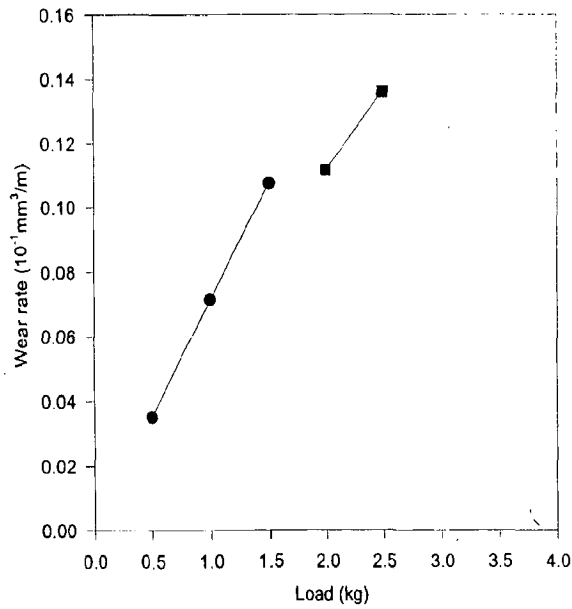


Fig.4.46 The variation of wear rate with normal load in AZ91 alloy, during dry sliding at a fixed sliding speed of 1.0 m/s against counterface of hardened steel.

in these figures for different loads. These lines at different loads for a given material appear to converge at low sliding distances similarly as it has been observed in cases of commercial magnesium based composites shown in Figs. 4.25 to 4.29 where the difference in wear volumes at different loads are relatively small. Also, these linear least square fit lines do not pass through the origin as shown Figs. 4.41 to 4.45 and those corresponding to higher loads have negative intercepts.

The wear rates have been calculated from the slope of least square fit lines in Figs. 4.41 to 4.45. The variations of wear rate with normal load are shown in Figs. 4.46 to 4.50 for AZ91 alloy and composites based on it containing 5.0, 6.0, 7.0 and 8.0 vol% steel wool respectively. If one compares Fig. 4.46 and Fig. 4.30 it is apparent that alloying decreases the wear rates in both the segments of the variation of wear rate with load. At low load of 0.5 kg the alloying has reduced wear rate but at intermediate load of 1.5 kg the wear rate has increased. The defects in cast alloys are also important in deciding wear behaviour particularly at higher loads. The wear rates at still higher loads have come down in the alloy compared to that in commercial magnesium. By reinforcing AZ91 alloy with steel wool the wear rate of the entire segment before transition reduces and also its rate of change with load decreases as shown in Figs. 4.47 to 4.50. The wear rates in the segment after transition also reduces in magnitude but the slope of the lines do not appear to change much with the extent of steel wool reinforcement. We have only two experimental points in the second segment and so it may not be fair to draw any serious inference about the rate of change of wear rate with load particularly in this segment.

Fig. 4.51. shows the variation of coefficient of friction with sliding distance in as cast AZ91 alloy for different applied loads ranging between 0.5 kg to 2.5 kg in steps of 0.5 kg. It is observed that at the lower load of 0.5 kg, there is maximum friction and it decreases in general with increasing load. In Fig. 4.52, the variation of coefficient of friction with sliding distance is observed for AZ91 alloy based composite containing 5.0 vol% steel wool. The coefficient of friction increases significantly with the introduction of steel wool but it decreases with increasing load. In this figure the curves corresponding to loads of 0.5 kg and 1.0 kg are relatively well spaced and at higher loads of 1.5 to 2.5 kg the curves have almost merged around the coefficient of friction of 0.4.

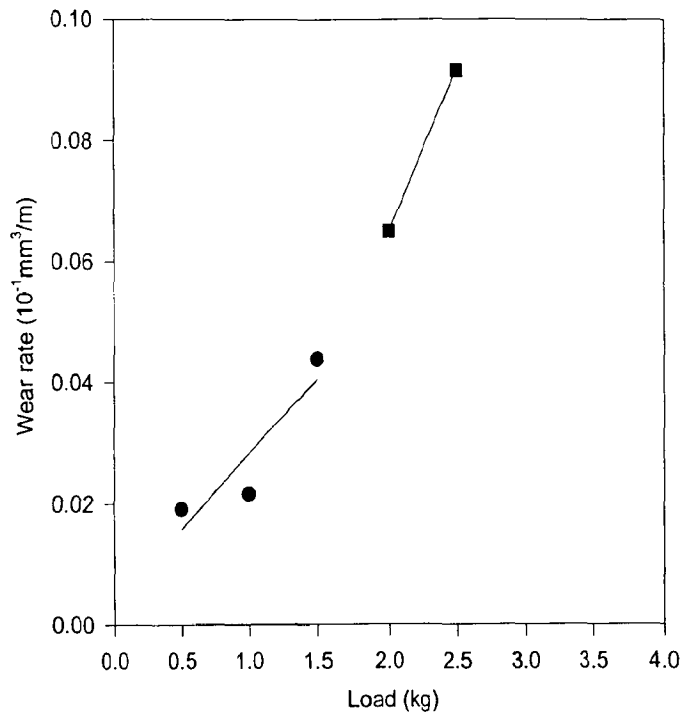


Fig.4.47 The variation of wear rate with normal load in AZ91 alloy based composite containing 5.0 vol.% of steel wool, during dry sliding at a fixed sliding speed of 1.0 m/s against counterface of hardened steel.

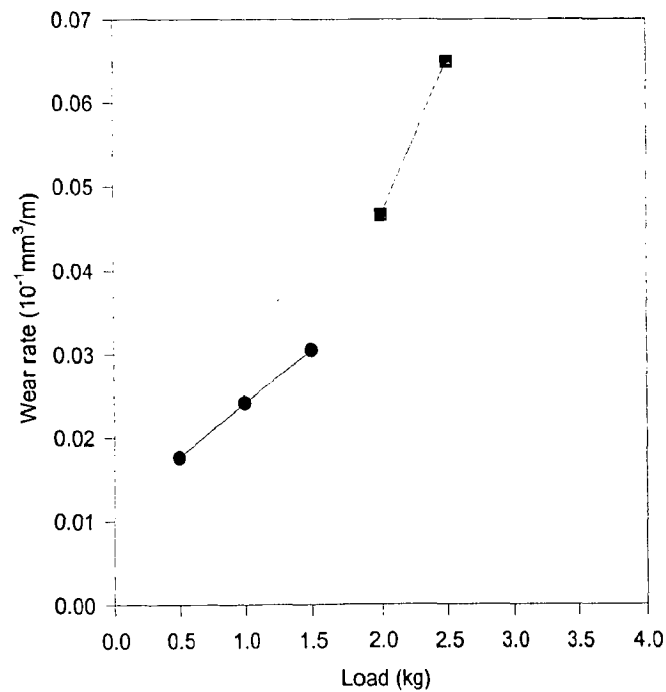


Fig.4.48 The variation of wear rate with normal load in AZ91 alloy based composite containing 6.0 vol.% steel wool, during dry sliding at a fixed sliding speed of 1.0 m/s against counterface of hardened steel.

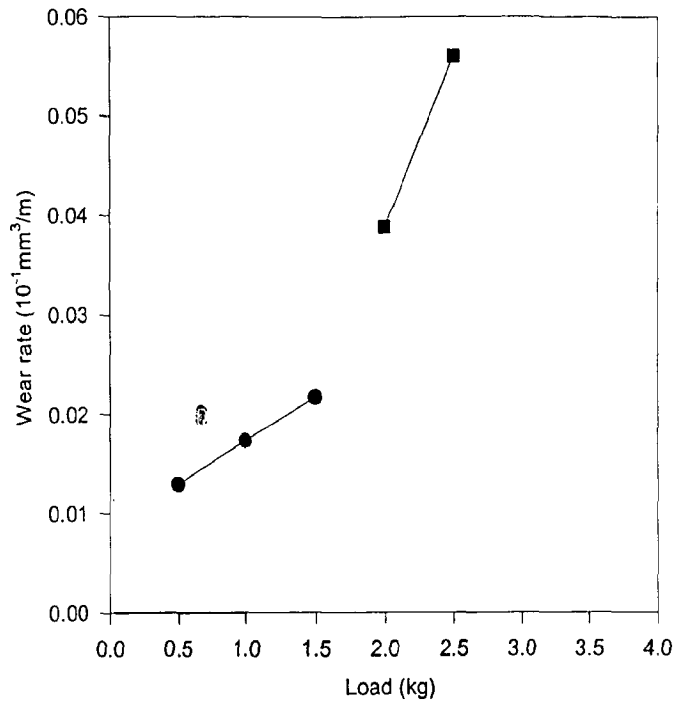


Fig.4.49 The variation of wear rate with normal load in AZ91 alloy based composite containing 7.0 vol.% of steel wool, during dry sliding at a fixed sliding speed of 1.0 m/s against counterface of hardened steel.

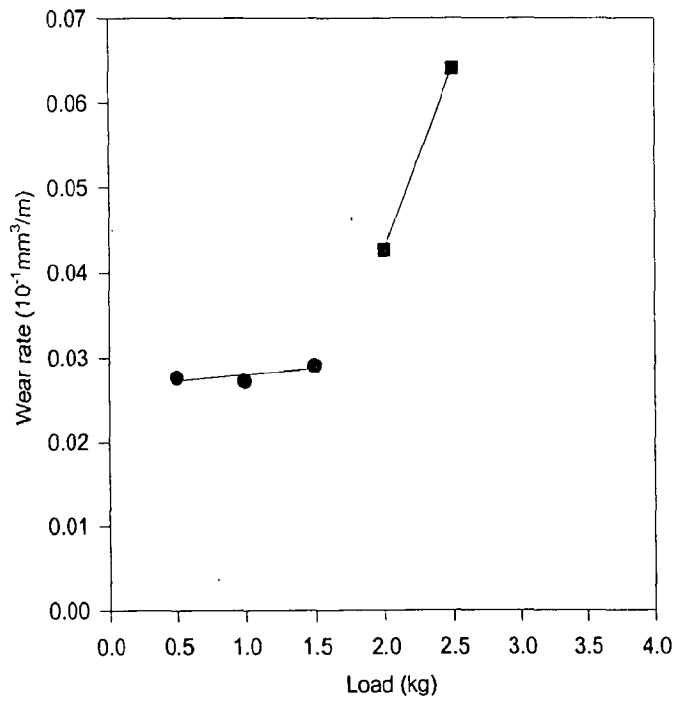


Fig.4.50 The variation of wear rate with normal load in AZ91 alloy base composite containing 8.0 vol.% steel wool, during dry sliding at a fixed sliding speed of 1.0 m/s against counterface of hardened steel.

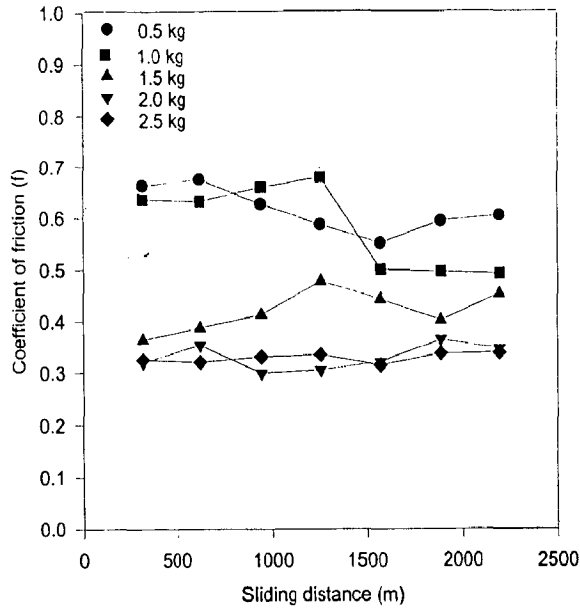


Fig.4.51 The variation of coefficient of friction with sliding distance in AZ91 alloy, During dry sliding under a constant sliding speed of 1.0 m/s against counterface of hardened steel.

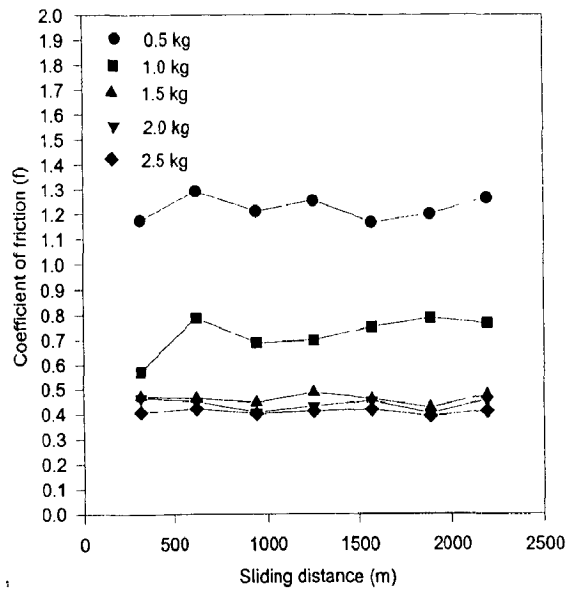


Fig.4.52 The variation coefficient of friction with sliding distance in AZ91 alloy based composite containing 5.0 vol.% of steel wool, during dry sliding under a fixed sliding speed of 1.0 m/s against counterface of hardened steel.

Fig. 4.53. shows the variation of coefficient of friction with sliding distance for the composite containing 6.0 vol% steel wool. In this figure it is observed that at the lower load of 0.5 kg, there is maximum friction and overlapping of curves at intermediate loads between 1.0 kg to 2.0 kg. But at higher load of 2.5 kg the coefficient of friction has lowered to around 0.4. Fig.4.54 shows the trend of variation in coefficient of friction with sliding distance for composites containing 7.0 vol% of steel wool. In this figure the curves corresponding to different loads are relatively well spaced and there is no overlapping between the curves. Fig.4.55 show the trend in variation of coefficient of friction with sliding distance for composites containing 8.0 vol% of steel wool. At higher steel wool content the coefficient of friction has increased further at lower loads but at higher load of 2.5 kg, the coefficient of friction appears to lie around 0.4 in the composite irrespective of steel wool content. Fig.4.56(a) to (e) show the variation of coefficient of friction averaged over sliding distance, with load for AZ91 alloy and composites based on it but containing different amount of steel wool. When load increases from 0.5 kg, there is a sharp drop in coefficient of friction in all these composites but at higher load the coefficient of friction attains a similar value of around 0.4 irrespective of the steel wool content and their distribution.

Table-4.6(b)

Average Wear Coefficient of AZ91 Alloy and AZ91 Alloy -Steel wool Composites

Sample number	Sample designation	Matrix	Volume percent of steel wool	Average wear coefficient $k(10^{-4})$
1	AZ91	AZ91	0.0	2.0708
2	MAS3	AZ91	5.0	1.4279
3	MAS2	AZ91	6.0	0.9340
4	MAS5	AZ91	7.0	0.8316
5	MAS4	AZ91	8.0	0.8638

4.1.7 Examination of sliding surface and wear debris

(a) Commercial Magnesium and Steel wool Composite

Figs. 4.57(a) and (b) shows the micrographs of surfaces of commercial magnesium after sliding under contact loads of 0.5 kg and 2.5 kg at sliding speed of 1 m/s, as examined

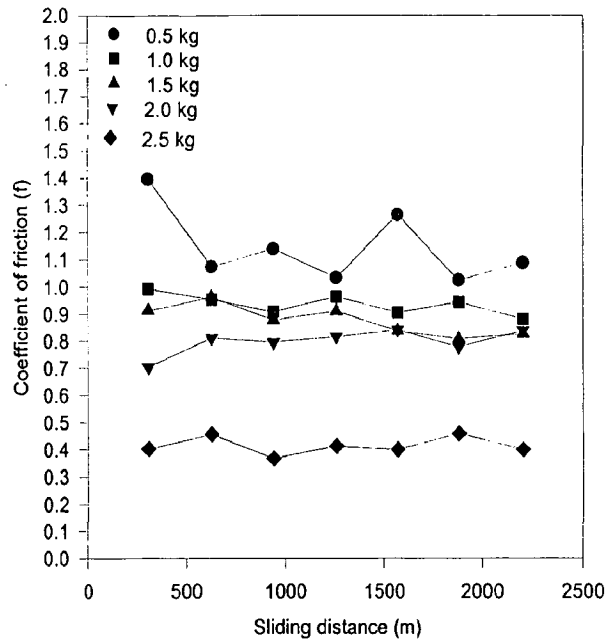


Fig.4.53 The variation of coefficient of friction with sliding distance in AZ91 alloy based composite containing 6.0 vol.% of steel wool, during dry sliding under a fixed sliding speed of 1.0 m/s against counterface of hardened steel.

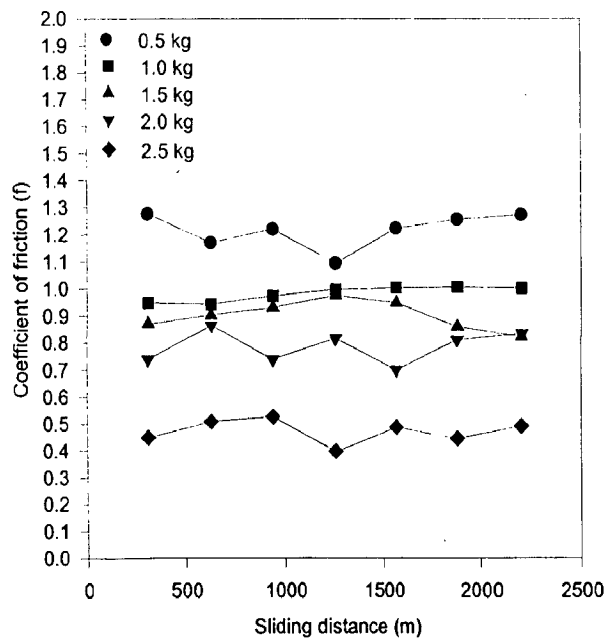


Fig.4.54 The variation of coefficient of friction with sliding distance in AZ91 alloy based composite containing 7.0 vol.% of steel wool, during dry sliding under a fixed sliding speed of 1.0 m/s against counterface of hardened steel.

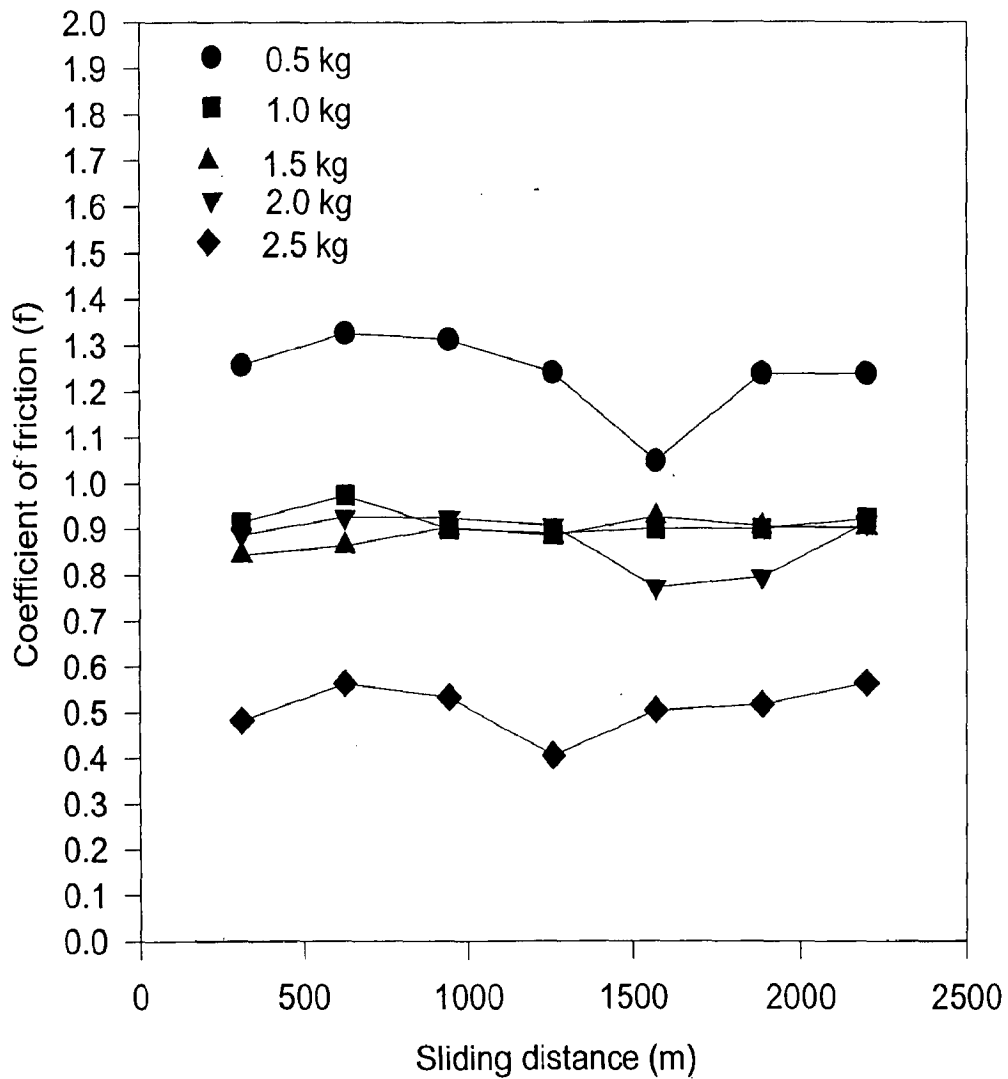


Fig.4.55 The variation of coefficient of friction with sliding distance in AZ91 alloy based composite containing 8.0 vol.% of steel wool, during dry sliding under a fixed sliding speed of 1.0 m/s against counterface of hardened steel.

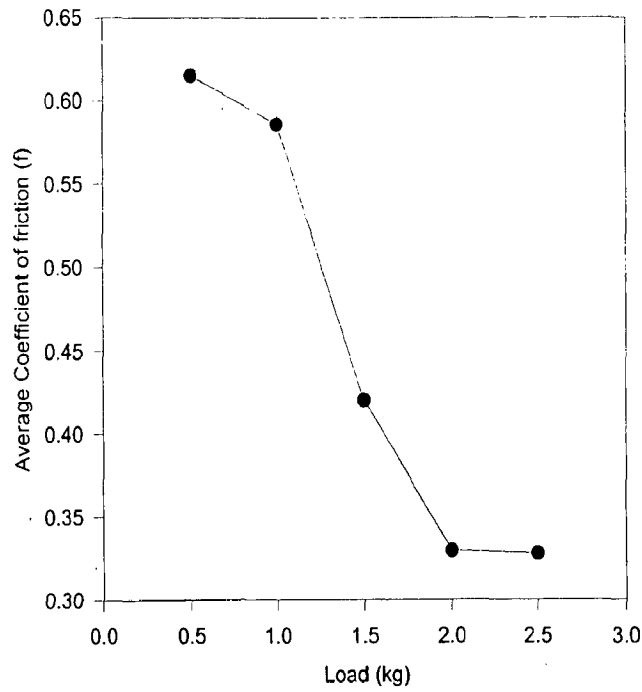


Fig.4.56(a) The variation of coefficient of friction averaged over sliding distance, with normal load for AZ91 alloy, during dry sliding at a fixed sliding speed of 1.0 m/s against counterface of hardened steel.

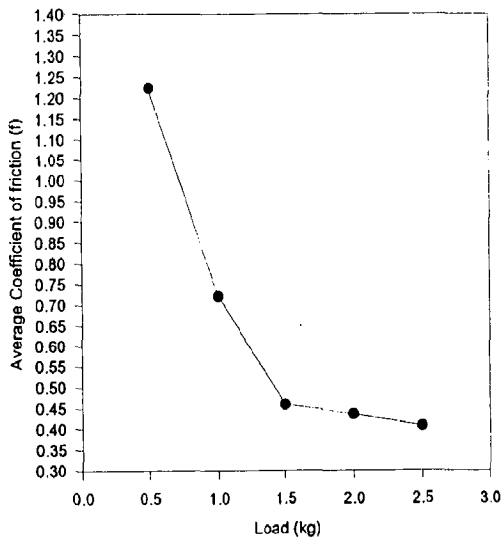


Fig.4.56(b) The variation of coefficient of friction averaged over sliding distance, with normal load in AZ91 alloy based composite containing 5.0 vol.% of steel wool, during dry sliding at a fixed sliding speed of 1.0 m/s against counterface of hardened steel.

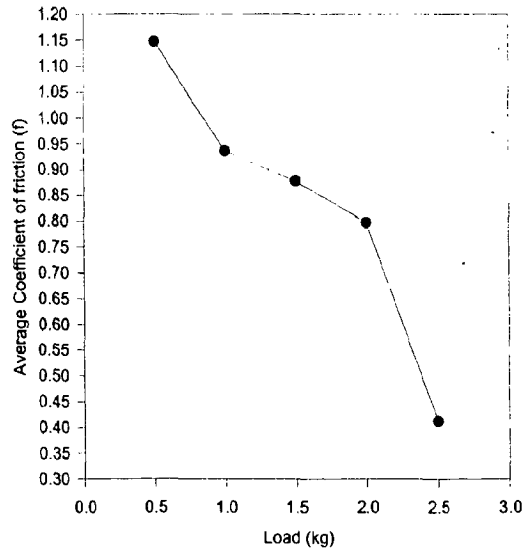


Fig.4.56(c) The variation of coefficient of friction averaged over sliding distance, with normal load in AZ91 alloy based composite containing 6.0 vol.% of steel wool, during dry sliding at a fixed sliding speed of 1.0 m/s against counterface of hardened steel.

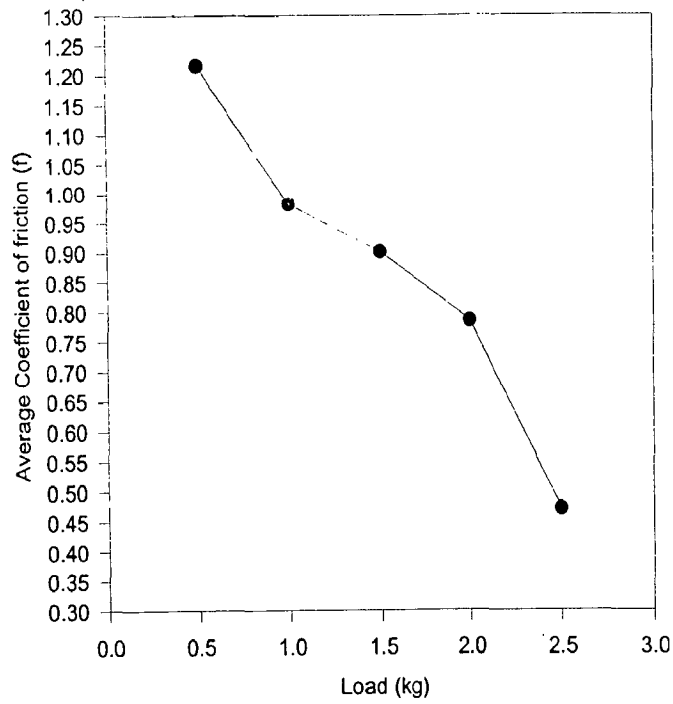


Fig.4.56(d) The variation of coefficient of friction averaged over sliding distance with normal load in AZ91 alloy 7.0 vol.% steel wool, during dry sliding at a fixed sliding speed of 1.0 m/s against counterface of hardened steel.

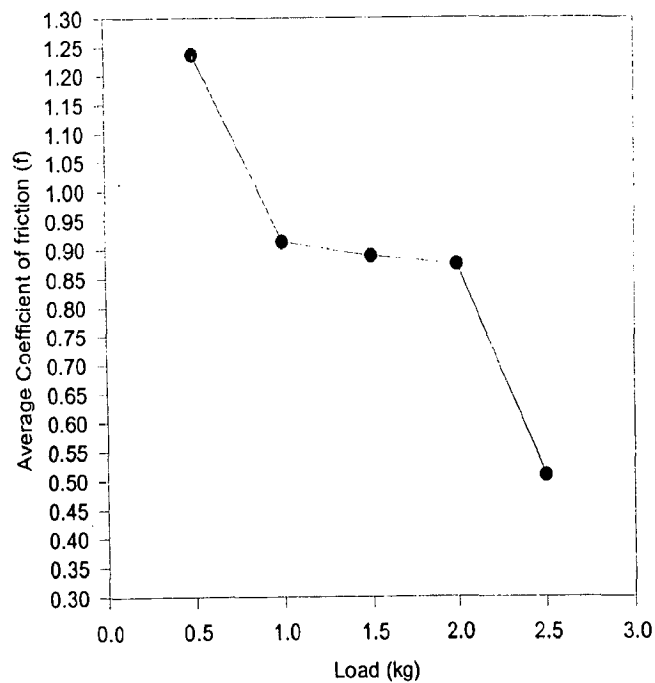


Fig.4.56(e) The variation of coefficient of friction averaged over sliding distance with normal load in AZ91 alloy 8 vol.% steel wool, during dry sliding at fixed sliding speed of 1.0 m/s against counterface of hardened steel.

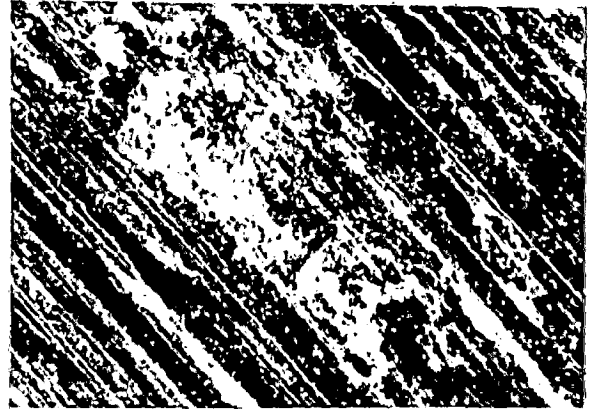
under scanning electron microscope. In Fig.4.57(a), it is observed that the surface is almost covered with transfer layer of oxide debris which is very smooth. The soft nature of the metal magnesium may have helped in the formation of such smooth layer on the surface. But at higher loads it is observed that transfer layer has broken at places where there is excessive oxide as shown in Figs 4.57(b). This area has been examined at higher magnifications as shown in Figs.4.57(c) and (d). The local cracking of transfer layer is visible in Fig.4.57(d) and it could be due to frictional heating under higher load in the local area of contact.

Figs. 4.58(a) and (b) shows the surface of commercial magnesium based composite containing 4.5 vol% steel wool after sliding under contact loads of 0.5 and 2.5 kg at a sliding speed of 1 m/s. At low load of 0.5 kg, the steel wool reinforcements are visible particularly at higher magnification as shown in Fig.4.58(c). The steel wool strands are often standing high and the magnesium area becomes recessed around it. It is observed that there are certain dark voids visible in Fig.4.58(a). These voids may have resulted due to debonding and fatigue failure of some of the raised strands. At higher loads one does not observe any raised strands or recessed regions. The softer magnesium flows over the steel wool to cover it completely as shown in Fig.4.58(b) and in 4.58(d) at higher magnification. The transfer layer of oxides are there uniformly without giving any indication of underlying steel wool strands. At higher loads of 2.5 kg one observes weakening of transfer layer at places and its flaking off due to cracking as shown in Fig.4.58(d). The features of sliding surfaces of other composites are very similar to those observed in Fig.4.58.

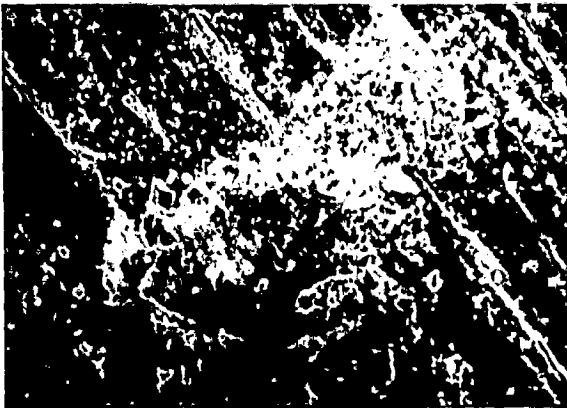
Figs 4.59(a) and (b) show the wear debris collected during sliding of commercial magnesium under contact loads of 0.5 and 2.5 kg respectively. The debris shows fine oxide particles and flaked off transfer layers. Figs.4.60(a) and (b) show the wear debris of a typical composite containing steel wool at loads of 0.5 and 2.5 kg respectively. At lower load there is relatively lower extent of flaking of the transfer layers compared to that at higher load. The wear debris was tested with magnet and it was observed that there are more magnetic particles at higher load compared to that at lower load. A few bright metallic particles could also be observed in the wear debris.



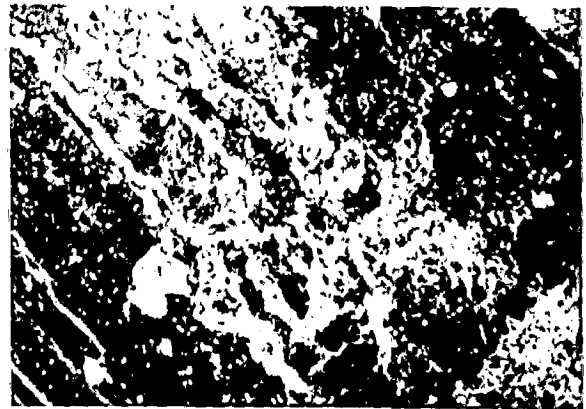
(a)



(b)

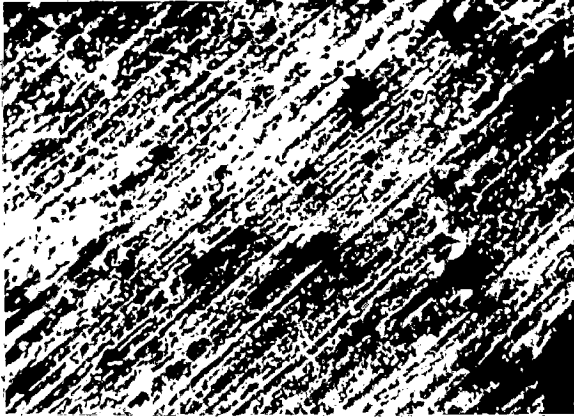


(c)

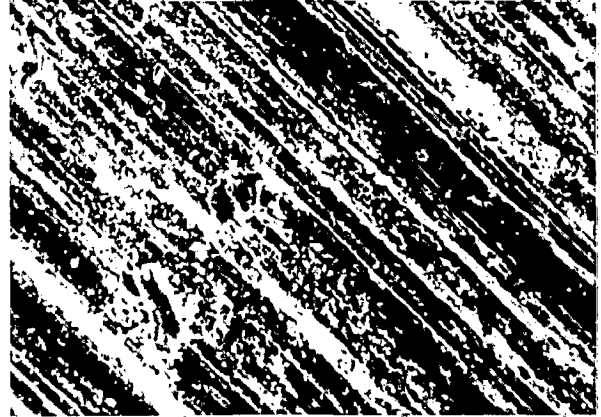


(d)

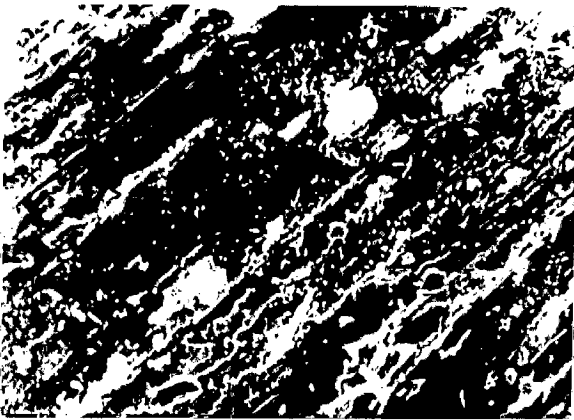
Fig 4.57 SEM micrographs of the surfaces of commercial magnesium after sliding at normal loads of (a) 0.5 kg; X77 (b) 2.5 kg; X77 (c) 2.5 kg, X200 and (d) 2.5 kg; X400.



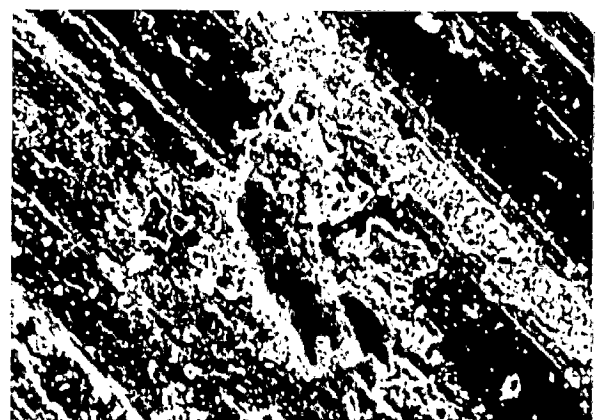
(a)



(b)



(c)



(d)

Fig 4.58 SEM micrographs of the surfaces of commercial magnesium based composite containing 4.5 vol% of steel wool after sliding at normal loads of (a) 0.5 kg; X77 (b) 2.5 kg; X77 (c) 0.5 kg; X300 and (d) 2.5; X400.

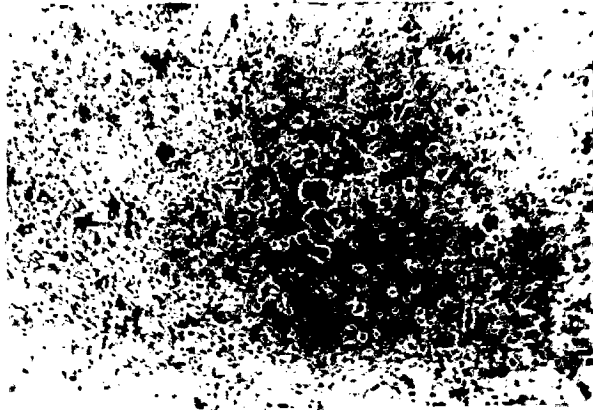


Fig 4.59(a) Stereo microphotograph showing the wear debris of commercial magnesium, generated during dry sliding against steel disc at a normal load of 0.5 kg, X16.

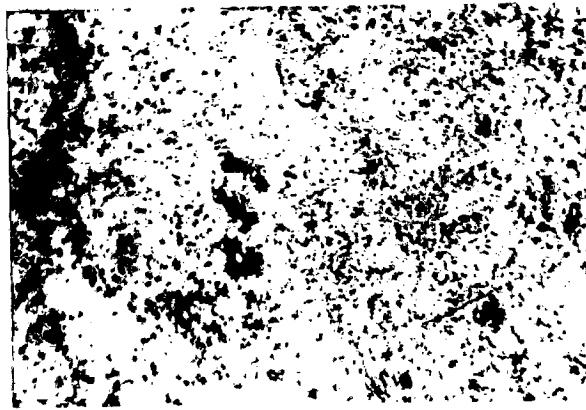


Fig 4.59 (b) Stereo microphotograph showing the wear debris of commercial magnesium, generated during dry sliding against steel disc at a normal load of 2.5 kg, X16.



Fig 4.60 (a) Stereo microphotograph showing the wear debris of commercial magnesium based composite containing 4.5 vol% of steel wool, generated during dry sliding against steel disc at a normal load of 0.5 kg, X16.

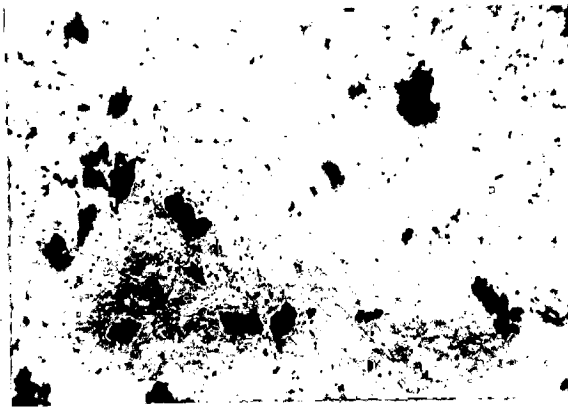


Fig 4.60 (b) Stereo microphotograph showing the wear debris of commercial magnesium based composite containing 4.5 vol% of steel wool, generated during dry sliding against steel disc at a normal load of 2.5 kg, X16.

Table 4.7(a)

X-Ray Diffraction Analysis for Wear Debris Generated During Sliding of Magnesium

$\sin\theta$	I/I_0	D	Phase	I/I_0 as in ASTM Chart
0.1633	85.68	4.7167	$Mg(Al,Fe)_2O_4$	20
0.3156	71.40	2.4405	$Mg(Al,Fe)_2O_4$	100
0.3272	100	2.3540	Mg-Al-O, Fe	70
0.3810	42.84	2.0213	$Mg(Al,Fe)_2O_4$	45

Table 4.7(b)

X-Ray Diffraction Analysis for Wear Debris Generated During Sliding of Magnesium-4.5 vol% Steel wool Composite

$\sin\theta$	I/I_0	d	Phase	I/I_0 as in ASTM Chart
0.1624	75	4.7414	$Mg(Al,Fe)_2O_4$	20
0.3156	50	2.4405	$Mg(Al,Fe)_2O_4$	100
0.3255	100	2.3659	Mg-Al-O, Fe	70
0.3810	62.5	2.0213	$Mg(Al,Fe)_2O_4$	45

Table 4.7(c)

X-Ray Diffraction Analysis for Wear Debris Generated During Sliding of Magnesium-6.5 vol% Steel wool Composite

$\sin\theta$	I/I_0	d	Phase	I/I_0 as in ASTM Chart
0.1633	80	4.7414	$Mg(Al,Fe)_2O_4$	20
0.3156	50	2.4405	$Mg(Al,Fe)_2O_4$	100
0.3272	100	2.3540	Mg-Al-O, Fe	70
0.3810	62.5	2.0213	$Mg(Al,Fe)_2O_4$	45

X-ray diffraction analysis of the wear debris generated during sliding of the composite containing steel wool in a matrix of commercial magnesium, against

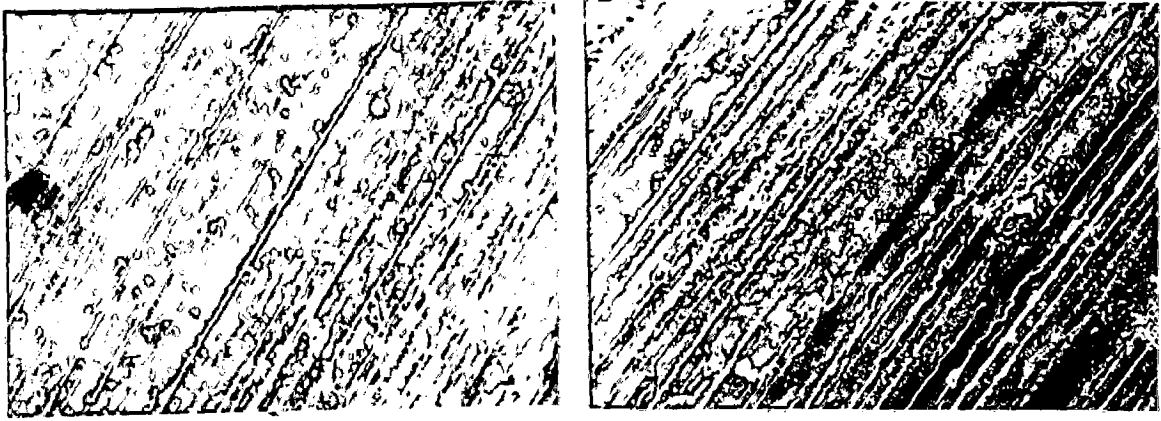
counterface of hardened steel disc, show a broad amorphous peak at 2θ values of around 10 degrees. In addition there are a few diffraction peaks belonging to crystalline compound as shown in Table 4.7(a) to 4.7(c). The d-values match with mixed oxide of magnesium and aluminium and with mixed oxides of magnesium, aluminium and iron. One of the diffraction peaks matches with that of iron.

(b) AZ91 Magnesium Alloy and Steel wool Composite

Figs. 4.61(a) and (b) show the sliding surface of AZ91 alloy at contact loads of 0.5 and 2.5 kg respectively as observed under scanning electron microscope at a lower magnification. Both the surfaces appear to be covered by transfer layers of oxide debris. At lower load the layer is relatively sound as shown in Fig.4.61(c) but at higher loads of 2.5 kg the transfer layer appear to get broken at places as seen at higher magnification in Fig.4.61(d).

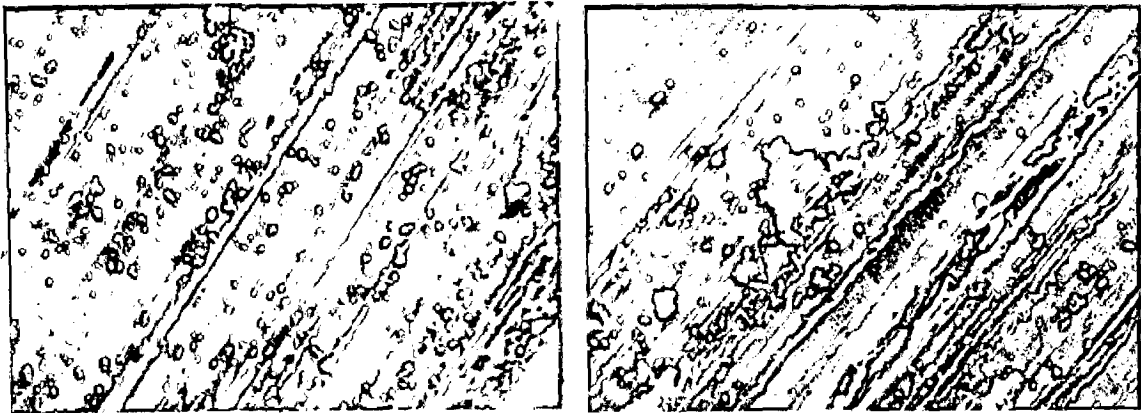
Figs.4.62(a) and (b) show the sliding surface in the AZ91 alloy base composite containing 6 vol% of steel wool under contact loads of 0.5 and 2.5 kg. It is observed that steel wool strands are standing out and oxide debris are collecting around it at lower load of 0.5 kg as shown at higher magnification in Fig.4.62(c). At higher loads the steel wool strand are getting covered by the flow of alloy but the transfer layers are getting broken at places as shown in Fig.4.62(d).

Figs.4.63(a) and (b) show the wear debris obtained during sliding of AZ91 alloy at loads of 0.5 and 2.5 kg. Both the photographs show significant extent of flaking of the transfer layer which may be due to lack of softening in the alloy. But in a composite containing steel wool one observes that flaked off transfer layer along with a large number of bright metallic particles as shown in Figs.4.64(a) and (b) corresponding to loads of 0.5 and 2.5 kg respectively.



(a)

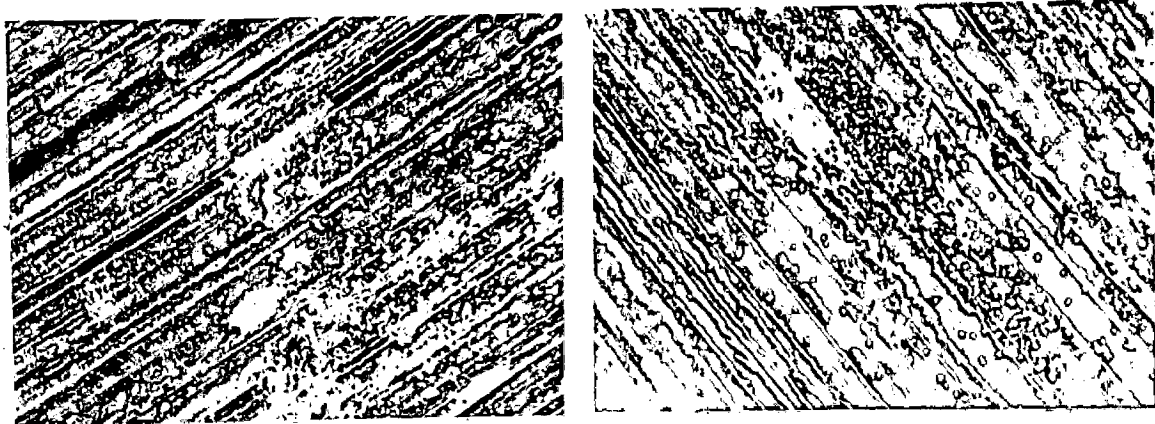
(b)



(c)

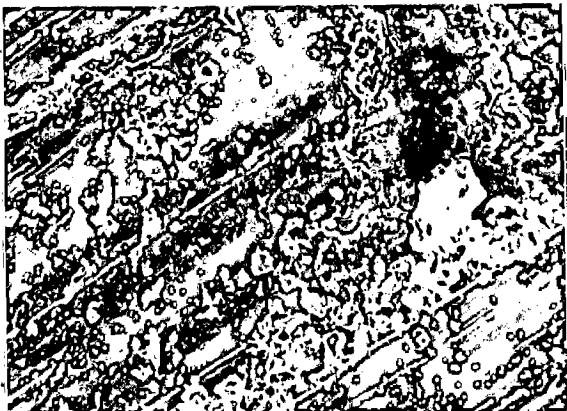
(d)

Fig 4.61 SEM micrographs of the surfaces of AZ91 alloy after sliding at normal loads of (a) 0.5 kg; X77, (b) 2.5 kg; X77, (c) 0.5 kg; X200 and (d) 2.5 kg, X200.

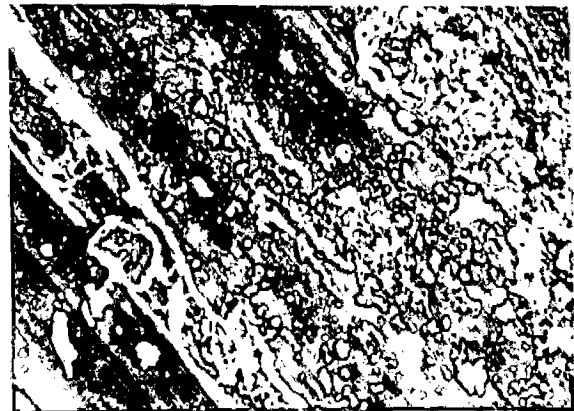


(a)

(b)



(c)



(d)

Fig 4.62 SEM micrographs of the surfaces of AZ91 alloy based composite containing 6.0 vol% of steel wool after sliding at normal loads of (a) 0.5 kg; X77 (b) 2.5 kg; X77 (c) 0.5 kg; X400 and (d) 2.5 kg; X400.

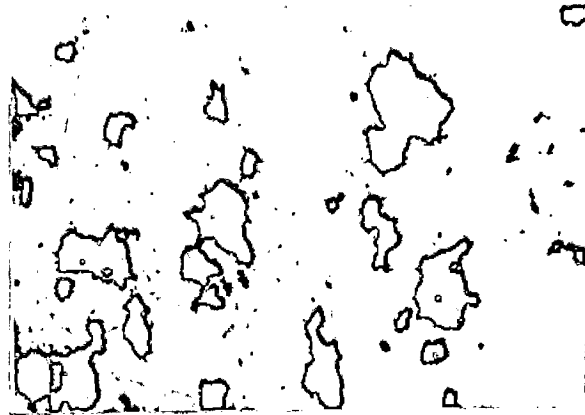


Fig 4.63 (a) Stereo microphotograph showing the wear debris of AZ91 alloy based composite, generated during dry sliding against steel disc at a normal load of 0.5 kg, X16.



Fig 4.63 (b) Stereo microphotograph showing the wear debris of AZ91 alloy based composite, generated during dry sliding against steel disc at a normal load of 2.5 kg, X16.

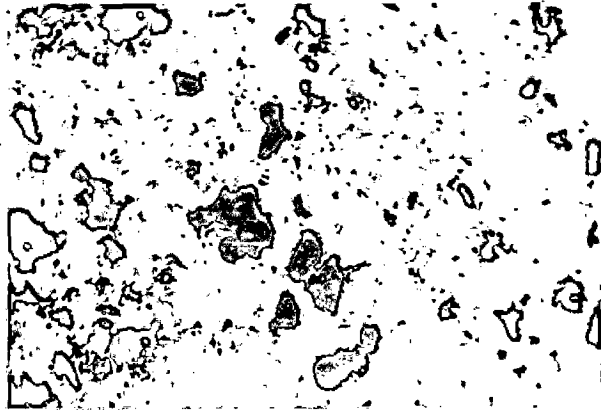


Fig 4.64 (a) Stereo microphotograph showing the wear debris of AZ91 alloy based composite containing 5.0 vol% of steel wool, generated during dry sliding against steel disc at a normal load of 0.5 kg, X 16.

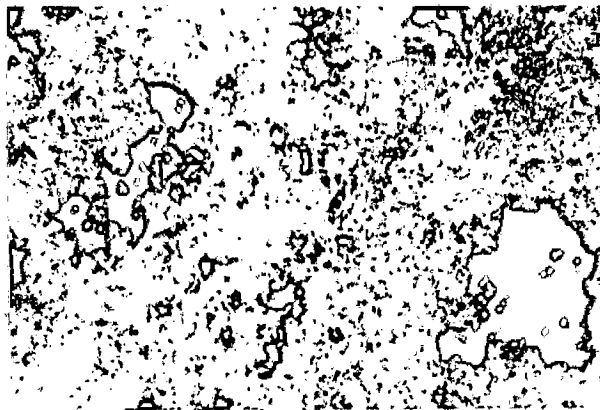


Fig 4.64 (b) Stereo microphotograph showing the wear debris of AZ91 alloy based composite containing 5.0 vol% of steel wool, generated during dry sliding against steel disc at a normal load of 2.5 kg, X16.

4.1.8 Estimation of Wear Rate

In this subsection the possibility of estimating wear rate in composites in terms of wear behaviour of the constituents has been explored in the framework of Archard's law given in Eqn.(2.15) in chapter 2. The volume loss in wear is directly proportional to sliding distance and normal load but indirectly proportional to hardness of the material. This law has been proposed for single phase material but it works fairly well for multiphase alloys. The Archard's law may also be written as

$$\frac{V}{S} = k \frac{N}{H} \quad (4.2)$$

Where, V is the volume loss in wear after the test material of hardness H has undergone dry sliding against counterface under normal contact load of N through a distance of S . k is a constant known as wear coefficient. Since N/H is an estimate of real area of contact and V/S is the wear rate one may rephrase the Archard's law to state that wear rate is proportional to the real area of contact. For a composite one may assume that the wear rate is the sum of wear rates of its constituents and write,

$$\left(\frac{V}{S}\right)_{com} = k_0 \frac{N_0}{H_0} + k_{st} \frac{N_f}{H_f} \quad (4.3)$$

Where, V is the volume loss of the composite in wear after sliding through a distance of S and $(V/S)_{com}$ is the wear rate of composite. k_0 is the wear coefficient of commercial magnesium, k_{st} is the wear coefficient of steel wool, H_0 is the microhardness of magnesium matrix and H_f is the microhardness of the steel wool in the composite. N_0 and N_f are the normal contact loads shared by the matrix and the steel wool respectively.

The contact loads of N_0 and N_f may be estimated as follows. If total normal load applied to the composite is N , then

$$N = N_0 + N_f \quad (4.4)$$

From the definition of hardness one may write that

$$H_0 = \frac{N_0}{A_{r_0}} \quad (4.5)$$

$$H_f = \frac{N_f}{A_{r_f}} \quad (4.6)$$

Where A_{r_0} and A_{r_f} are the real areas of contact in the matrix and the steel wool respectively. Substituting the values of N_0 and N_f from Eqns.(4.5) and (4.6) in Eqn.(4.4), one gets,

$$N = A_{r_0}H_0 + A_{r_f}H_f \quad (4.7)$$

It is reasonable to assume that the counterface has uniform distribution of asperities and the ratio of the real area of contact in matrix and dispersed phase i.e., A_{r_0} / A_{r_f} , will be in proportion to their relative area on the surface of the composite, one may write that,

$$\frac{A_{r_0}}{A_{r_f}} = \frac{1 - V_f}{V_f} \quad (4.8)$$

where, V_f , the volume fraction of dispersed phase in the composite, is assumed to be equal to the area fraction on the surface. This assumption is strictly valid if the distribution of the dispersed phase is random. Substituting Eqn.(4.8) in Eqn.(4.7) one gets,

$$N = A_{r_f} \frac{H_0(1 - V_f) + H_f V_f}{V_f} \quad (4.9)$$

Thus, one may estimate A_{r_0} and A_{r_f} as

$$A_{r_f} = \frac{NV_f}{H_o(1-V_f) + H_fV_f} \quad (4.10)$$

$$A_{r_0} = \frac{N(1-V_f)}{H_o(1-V_f) + H_fV_f} \quad (4.11)$$

Using Eqns. (4.5) and (4.6) one may arrive at the estimates of loads shared by the matrix and the dispersed steel wool as

$$N_0 = \frac{N(1-V_f)H_o}{H_o(1-V_f) + H_fV_f} \quad (4.12)$$

$$N_f = \frac{NV_fH_f}{H_o(1-V_f) + H_fV_f} \quad (4.13)$$

The values of H_o and H_f are experimentally determined. The volume fraction of steel wool, V_f , is estimated using Eqn.(4.1) from the experimentally determined density of the composite and constituents. The wear rate in the composite may thus be estimated using Eqn.(4.3) by putting the values of wear coefficients of the constituents known a priori.

The estimated and observed variations of wear rate with normal load in composites based on commercial magnesium containing 4.5, 5.5, 6.0 and 6.5 vol% steel wool respectively are shown in Figs.4.65 to 4.68. When magnesium is reinforced with steel wool the estimated wear rate varies linearly with load but the observed wear rate deviates significantly compared to the estimated values. The estimated values are significantly higher and the discontinuities in the observed values reported in Figs.4.31 to 4.34 have been obliterated in Figs.4.65 to 4.68. The wear rate in composite has been estimated by superposition of wear rates in the matrix and dispersoid area. However, increase in

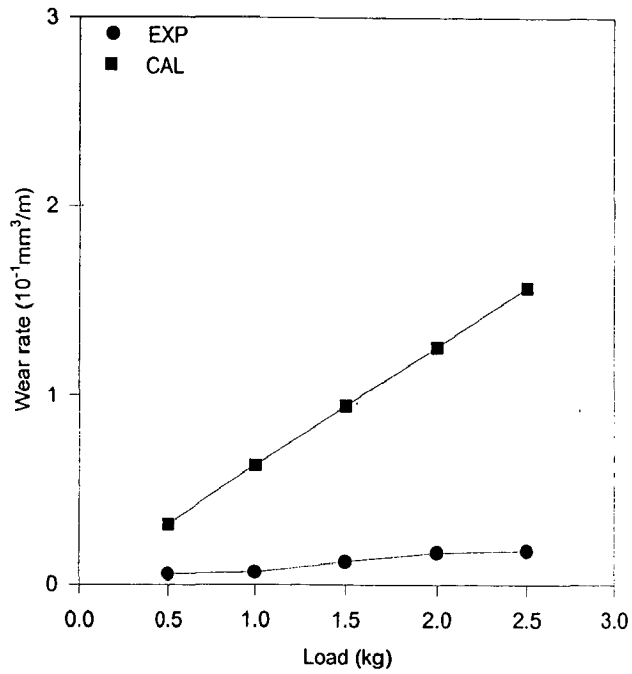


Fig.4.65 The calculated and experimental variation of wear rate with normal load in commercial magnesium based composite containing 4.5 vol.% of steel wool, during dry sliding at a fixed sliding speed of 1.0 m/s against counterface of hardened steel.

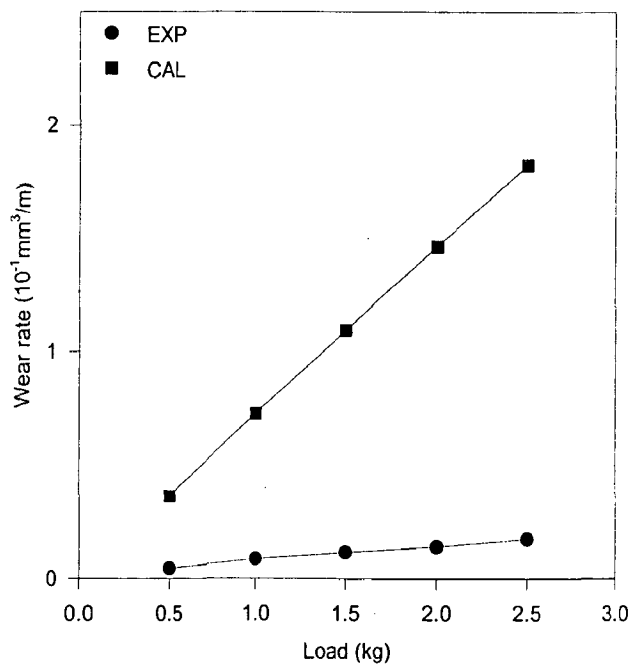


Fig. 4.66 The calculated and experimental variation of wear rate with normal load in commercial magnesium based composite containing 5.5 vol.% steel wool, during dry sliding at a fixed sliding speed of 1.0 m/s against counterface of hardened steel.

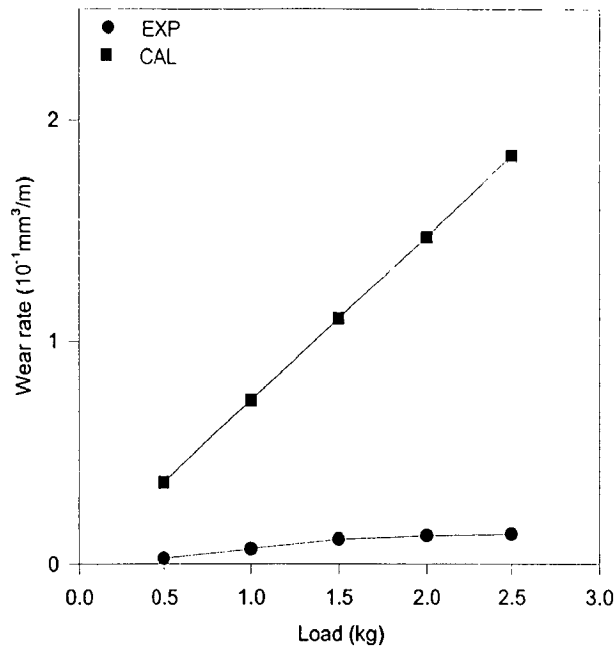


Fig. 4.67 The calculated and experimental variation of wear rate with normal load in commercial magnesium based composite containing 6.0 vol.% of steel wool, during dry sliding at a fixed sliding speed of 1.0 m/s against counterface of hardened steel.

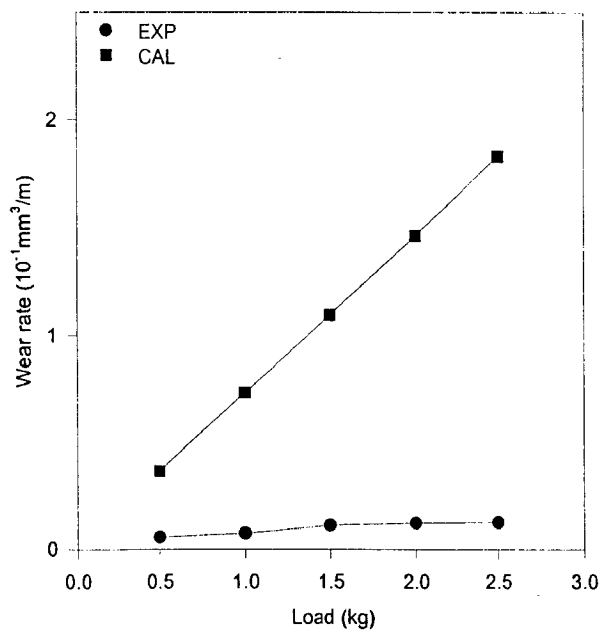


Fig. 4.68 The calculated and experimental variation of wear rate with normal load in commercial magnesium based composite containing 6.5 vol.% of steel wool, during dry sliding at a fixed sliding speed of 1.0 m/s against counterface of hardened steel.

temperature due to frictional heating has not been included in the estimate. No interaction or synergy between the matrix and the dispersed steel wool has been taken into account. Since the observed wear rate for the limiting case of unreinforced commercial magnesium or the material of steel wool has been correctly incorporated in superposition the estimated values should not be 4.4 to 6.4 times higher than the observed wear rates, when averaged over load, unless one attributes this difference primarily to the synergy between the matrix and the dispersed phase.

The variations of wear rate with normal load in AZ91 alloy based composites containing 5.0, 6.0, 7.0 and 8.0 vol% steel wool respectively, are shown in Figs.4.69 to 4.72. Both the estimated and the observed wear rate increases almost linearly with load and their ratio averaged over load is larger in the case of alloy based composite ranging from 5.1 to 8.2.

4.2 Discussion

The infiltration of packed bed of steel wool is expected to divide the molten magnesium stream sucked under vacuum. In absence of steel wool, a single stream is sucked in and its solidification takes place dendritically similar to that in normal castings, as observed in Fig. 4.6. But in case of composite these sucked streams may push the steel wool strands away from its path leading to inhomogeneous distribution of steel wool in the composite. Thus, there are steel wool rich and steel wool deficient areas as it has been observed in almost all the composites as shown in Figs. 4.5, 4.9 and 4.11 and its extent possibly depends on the packing density of the steel wool and the pressure gradient under which suction takes place. Since the streams become divided, the solidification may start at different times in different streams. It is possible that some late infiltrating stream may solidify when its surrounding has already solidified. A shrinkage cavity may thus be created at the boundary of this stream as observed in Fig.4.6. When one compares Fig.4.3 and Fig.4.5 the solute rich interdendritic area in cast commercial magnesium is relatively more than that observed in composites based on commercial magnesium. This may be an indication of the fact that solidification has taken place at a relatively lower temperature in presence of steel wool. The primary phase of magnesium solid solution has more solute in it than the equilibrium value. The last freezing liquid has relatively less solute and,

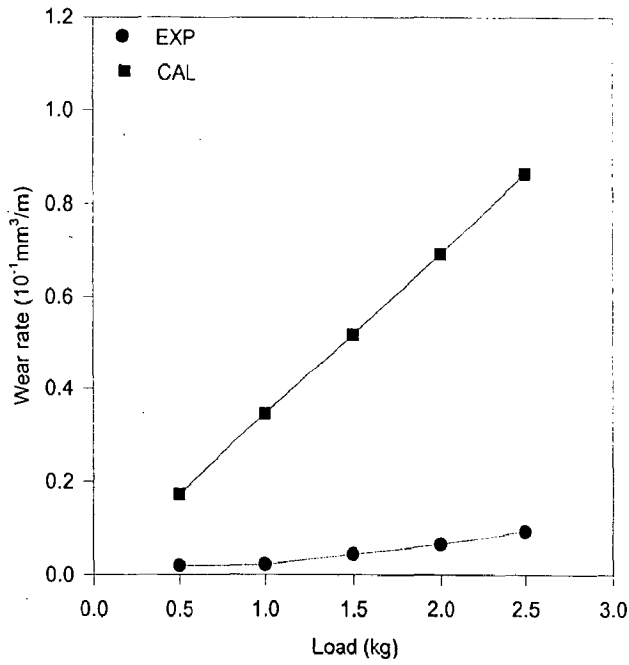


Fig. 4.69 The calculated and experimental variation of wear rate with normal load in AZ91 alloy based composite containing 5.0 vol.% of steel wool, during dry sliding at a fixed sliding speed of 1.0 m/s against counterface of hardened steel.

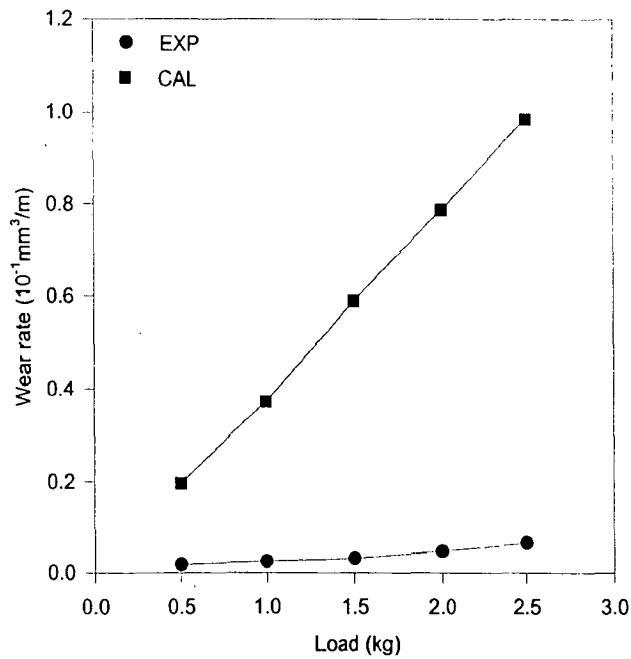


Fig. 4.70 The calculate and experimental variation of wear rate with normal load in AZ91 alloy based composite containing 6.0 vol.% of steel wool, during dry sliding at a fixed sliding speed of 1.0 m/s against counterface of hardened steel.

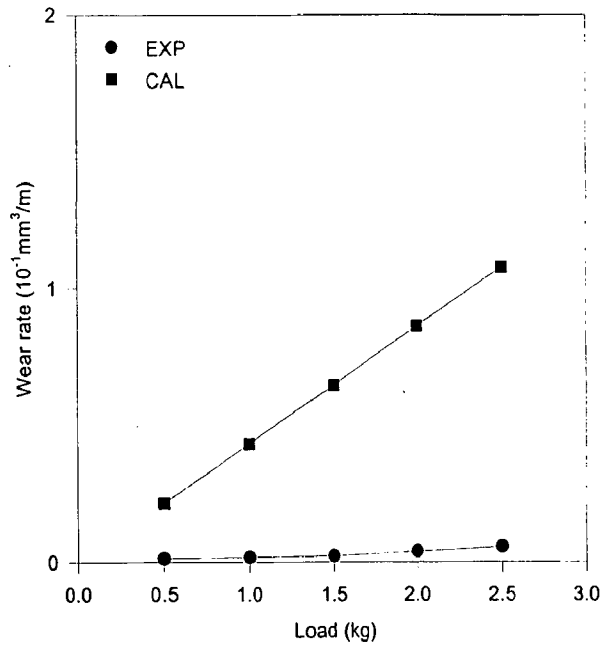


Fig. 4.71 The calculated and experimental variation of wear rate with normal load in AZ91 alloy based composite containing 7.0 vol.% of steel wool, during dry sliding at a fixed sliding speed of 1.0 m/s against counterface of hardened steel.

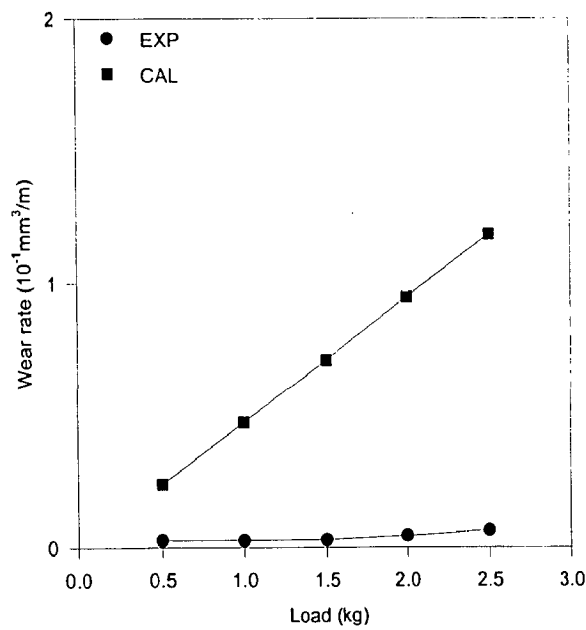


Fig. 4.72 The calculated and experimental variation of wear rate with normal load in AZ91 alloy based composite containing 8.0 vol.% of steel wool, during dry sliding at a fixed sliding speed of 1.0 m/s against counterface of hardened steel.

therefore, there are very small dark solute rich interdendritic area in the matrix of the composites.

The Brinell hardness of commercial magnesium based composite containing steel wool increases with steel wool content as shown Fig.4.21. However, the increase in hardness is not as much as one may estimate by the rule of mixture. This may be attributed to steel wool being pushed under indentation load because of yielding of soft matrix of magnesium surrounding steel wool. This effect is further evident in the measurement of microhardness as shown Fig.4.22. The hardness of the same steel wool increases with volume percent of steel wool in a composite. The flow in magnesium adjacent to the steel wool strands whose microhardness is being measured, may get more restrained due to higher steel wool content. Thus, steel wool strand shows higher microhardness with increasing steel wool content in the composite. Further, the commercial magnesium has relatively smaller amount of impurity and thus, the microhardness in the interdendritic area is only a little higher than the primary phase dendrites. The ultimate tensile strength in a composite is also observed to increase particularly when the steel wool content is beyond 4.5 volume percent as shown in Fig. 4.24. The ultimate tensile strength increases by about 30% between 4.5 and 6.5 vol% of steel wool in composites. But the vacuum cast strength of AZ91 alloy is significantly lower than squeeze cast AZ91 alloy (Weastengen, Albright and Nygaard, 1990). Such rapid increase in strength with steel wool content may not be due to the effect of steel wool alone as a constituent. The entanglement between steel wool strands may result in higher frictional and mechanical restraint which may also contribute to enhanced strength. The increase in elongation with steel wool content from 4.5 to 6.5 as shown in Table 4.5 (a) may be an indication of this effect. The mechanical properties reported here are based on the best result obtained out of three samples tested from a composite. This procedure has been adopted in view of inhomogeneity observed in the steel wool distribution.

The dry sliding friction and wear are known to be relatively insensitive to inhomogeneous distribution of phases. Further, a hard phase like steel wool embedded in a soft matrix like magnesium may satisfy textbook prescription for a good bearing material. The soft phase adjusts to the contour of shaft and the hard phase bears the load. The

matching of contour between shaft and bearing helps to maintain a constant gap to establish hydrodynamic condition for lubrication. The cumulative volume loss in the commercial magnesium based composite containing steel wool increases linearly with sliding distance at different loads following Archard's law predicting linear variation of cumulative volume loss in wear with load, as shown in Fig. 4.25 to 4.29. However, the wear rate has not varied linearly with load although linear variation is predicted by Archard's law. The observed variation of wear rate with load may be represented by two linear segments with a discontinuity as shown in Figs 4.30 to 4.34. But, such representation may have limited validity in view of limited number of experimental points.

The examination of test surface after sliding reveals that the transfer layer starts flaking off at higher loads as shown in Figs.4.58. This is further confirmed by the wear debris shown in Figs. 4.59 and 4.60. The discontinuity of wear rate at a load between 1.5 Kg to 2 kg as observed in all the composites investigated, may, therefore, be attributed to softening of magnesium below the transfer layer caused by frictional heating. The transfer layer appears to contain amorphous oxide and some crystalline mixed oxides involving magnesium, aluminium and iron as shown in Table 4.7(a) to 4.7(c). Although commercial magnesium does not have so much of aluminium, it could be a mixed oxide of similar structure where other impurities may have substituted aluminium atoms. The oxides sometimes contain small amounts of bright metallic particles which has not been detected by X-ray because of its smaller amount. The wear debris generated during sliding has magnetic particles which may be due to mixed oxides bearing iron or due to iron particles in it.

The discontinuous increase in wear rate attributed to softening of magnesium at a higher load exceeding 1.5 kg, may have a lubricating effect which may reduce frictional force as evident from Figs 4.40 (b) to 4.40 (e). Decreasing friction with increasing load starts from 0.5 kg itself in commercial magnesium and the maximum decrease in coefficient of friction takes place when the load is between 0.5 kg and 1.0 kg. This may be contributed by increased cover of transfer layer with load at the lower range of load. Since transfer layer contains amorphous and mixed oxides it will have lower adhesion with the counterface and thus, the coefficient of friction may decrease. But it has not been

confirmed by the observation under SEM. A perusal of Figs 4.30 and 4.40 (a) indicates that the decrease in coefficient of friction due to softening and the corresponding discontinuous increase in wear rate is not as large as it is between 0.5 and 1.0 kg. The discontinuous increase in wear is associated with flaking of the transfer layer as explained earlier. In composites the steel wool is helping to hold the transfer layer by strengthening the magnesium below it and the wear rate decreases significantly compared to commercial magnesium even after its discontinuous increase as observed in Figs. 4.40 (a) to 4.40 (e).

The wear rate in the composites has been calculated at different loads on the basis of estimated sharing of load and superposition of wear rates in the constituent phases. But the calculated values are much higher compared to those observed experimentally as shown in Figs. 4.67 to 4.70. Since the superposition has been made on the basis of experimentally determined wear behaviour for the constituent phases of commercial magnesium and steel wool, such a large deviation in calculated wear rate from the observed one, increasing with increasing load, could only be explained on the basis of the observed synergy between the constituent phases during dry sliding. At higher loads, the sliding surface has not revealed the presence of steel wool strands as shown in Figs. 4.58(b) and (d). The transfer layer and the flow of softer magnesium has covered the steel wool strands which has helped to reduce the overall friction. The real area of contact should decrease because of higher hardness due to the presence of steel wool underlying the surface layer. The extent of wear has decreased because of (a) low shear strength of the layer at the surface and (b) low real area of contact. The higher the load, the magnesium becomes softer due to frictional heating and contributes to lowering of shear strength contributing to lower friction and wear but the lowering of hardness due to softening may increase contact area and thus increases wear. The balance between these two factors should decide the overall friction and wear behaviour observed in the composites of magnesium containing steel wool. The synergy between steel wool and commercial magnesium in these composite is of immense importance in decreasing the observed wear rates compared to the calculated ones.

The wear coefficient which may be interpreted as wear rate per unit real area of contact, does not change significantly as observed in Table 4.6 (a). But the composites

because of increased hardness is expected to result in a significant reduction in real area of contact which provides the major advantage in this composites. The measure of wear coefficient is not satisfactory as it cannot reflect this fact. The observed wear rate has decreased in the composite but the real area of contact has also decreased. The wear coefficient, thus, is not sensitive to reflect the change in wear behaviour in a composite.

The microstructure of AZ91 alloy shows primary dendrite and massive $Mg_{17}Al_{12}$ in the interdendritic area as shown Fig. 4.15. When a bed of steel wool is infiltrated by AZ91 alloy the cast structure of the infiltrated composite as shown in Fig. 4.14, does not show well developed dendrites as observed in the case of unreinforced alloy shown in Fig. 4.15. The clustering of steel wool is clearly visible in Figs. 4.13, 4.19 and 4.20 which has been attributed to pushing of steel wool by infiltrating streams resulting in steel wool rich areas and steel wool deficient areas as it has also been observed in magnesium-steel wool composites. In the steel wool deficient area, the dendrites are well formed as shown Fig. 4.13. The massive $Mg_{17}Al_{12}$ phase has formed on the surface of the steel wool and also, away from it, in the form of network as shown in Fig. 4.14 and 4.18. A higher amount of steel wool, however, has changed the morphology of $Mg_{17}Al_{12}$ from network to smaller numerous precipitates as shown Figs. 4.19 and 4.20. This change in morphology of $Mg_{17}Al_{12}$ with higher steel wool content does not appear to emerge from the nucleation potency of steel wool as one observes $Mg_{17}Al_{12}$ nucleating away from steel wool also. This change in morphology could be due to lowering of transformation temperature which may have affected nucleation. On the basis of microstructure, AZ91 alloy-steel wool composites are distinct from magnesium-steel wool composites in respect of its higher solute content in the primary phase which makes it relatively darker after etching and the network or individual precipitates of $Mg_{17}Al_{12}$.

The Brinell hardness of cast AZ91 alloy is HB 34 compared to HB 20 observed in cast commercial magnesium which could be attributed to enhanced solid solution strengthening of the primary phase and also to the presence of $Mg_{17}Al_{12}$ precipitates in cast AZ91 alloy. But the hardness of both vacuum cast commercial magnesium and AZ91 alloy are lower than those reported (Mikuki, Shook, Mercedes and Green, 1986). In the composite, the hardness increases further to HB 39 when the alloy is reinforced with 8.0 vol% of steel

wool. The hardness observed in the composite is lower than the estimated rule of mixture hardness as it has been observed in magnesium-steel wool composites. The relatively soft magnesium alloy surrounding the steel wool could give way during indentation lowering its contribution to overall hardness. The Vickers microhardness of the cast AZ91 alloy shows two distinct areas - the primary phase dendrite and the interdendritic area which often contains divorced eutectic. The dendrite etches relatively darker as compared to the bright magnesium solid solution which is a constituent of the divorced eutectic in the interdendritic area. This may indicate the magnesium solid solution in the divorced eutectic has lower amounts of solute in it compared to the primary phase of dendrites which has a little higher microhardness. The steel wool has increasingly higher microhardness when the steel wool component in the composite increases as shown in Table 4.4 (b). This observation is similar to that of observed in commercial magnesium based composite and it has been attributed to the restraint imposed by neighbouring steel wool on the deformation of softer magnesium surrounding the steel wool fiber whose microhardness is being measured.

The ultimate tensile strength (UTS) of AZ91 alloy based composite containing steel wool is higher than that of a magnesium-steel wool composite of similar steel wool content. as shown in Fig. 4.24. The increase in UTS with steel wool content in the case of AZ91 alloy based composite than that for magnesium based composite. The UTS of vacuum cast magnesium is similar to that observed in cast magnesium (Videm, Hansen, Tomac and Tennessen, 1994). But the UTS of AZ91 alloy obtained in this investigation is significantly lower than reported for vacuum cast alloy (Videm, Hansen, Tomac and Tennessen, 1994). It appears that the level of vacuum used has not been enough to eliminate casting defects. The percent elongation are similar in both these types of composites. The presence of alloying elements and the relatively harder phase of $Mg_{17}Al_{12}$ may have contributed to higher matrix strength resulting in a higher tensile strength in the AZ91 alloy based composites compared to that in commercial magnesium-steel wool composites at similar steel wool content. The change in morphology $Mg_{17}Al_{12}$ from network to small precipitates at higher steel wool content does not appear to have any significant impact on either strength or ductility.

The variation of cumulative volume loss in wear with sliding distance is linear as observed in Figs. 4.41 to 4.45, during sliding of the composites containing steel wool in a matrix of AZ91 alloy, against the counterface of hardened steel. This linear variation is in agreement with Archard's law in the range of load and sliding distance chosen for this study. The wear rate increases with increasing load as shown in Fig. 4.46 to 4.50 for AZ91 alloy based composites. A number of investigators have found similar behaviour for wear rates in composites (Rohatgi, Liu and Ray, 1992). But the variation of wear rate with load are not linear as predicted by Archard's law. The experimental results have been presented as two

linear segments with a discontinuity in between as it has been observed in magnesium-steel wool composites. It is interesting to note that the results on the variation of wear rate with load in the AZ91 alloy based composite could be represented by two linear segment with a discontinuity. The second linear segment has shown a more rapid rate of variation of wear rate compared to the first segment as shown in Fig. 4.47 to 4.50 contrary to that observed in magnesium-steel wool composite. The examination of test surface after sliding and the wear debris of AZ91 alloy as shown in Figs.4.61 and 4.63, indicates that even at low load of 0.5 kg, there is flaking of the transfer layer while the test surface appears smooth. At the same time one may compare the wear rates of the composites based on magnesium and AZ91 alloy containing 6 vol% steel wool as shown in Figs. 4.33 and 4.48. The alloy based composite has relatively lower wear rates in the first segment. Thus it appears that even at lower loads, the hard surface of the alloy results in better compacting and build up of transfer layer which flakes off when the thickness reaches above a critical limit. In magnesium based composites a lot of oxide particles come out as such at lower loads, before getting compacted in a transfer layer. The wear rate in the second segment may be interpreted on the basis of loss of strength in the matrix and the formation of transfer layer. In magnesium based composite, frictional heating may result in local melting which may embed wear debris at local hot spots to help in the formation of transfer layer there. The build up of transfer layer results in its flaking off as observed in the wear debris in Fig. 4.60(b). But in the case of alloy, the loss in matrix strength may remove its advantage of hard surface for compacting but at the same time may not soften it enough for embedding the wear debris. These reasons may provide a plausible explanation

of the rapid increase in wear rate in the second segment as observed in alloy based composites.

The coefficient of friction in the alloy based composite decreases rapidly with load as shown in Fig. 4.56(a) to 4.56(e). The lowering of friction with load has been explained on the basis of the extent of cover provided by the transfer layer at lower loads and the softening of the matrix at higher loads. These results on friction are similar to those observed in magnesium based composites and so, could be explained similarly.

Figs. 4.57 to 4.64 show the composition of observed wear rate with the ones calculated on the basis of estimated load sharing between the constituents and the superposition of wear rates in these areas as it has been done in magnesium based composites. It is observed that at a given load, there is significant difference between the calculated and the observed wear rates which increases with increasing load for different composites as shown in Figs. 4.65 to 4.72. This difference has been attributed to increasing synergy between hard steel wool and soft magnesium during sliding wear at higher loads the relatively softer matrix alloy flows during sliding over the steel wool and provides a low shear strength cover which reduces the frictional force while at the same time, the underlying steel wool is providing a higher hardness for the material which counteracts the growth of real area of contact due to softening. This is the reason which causes a reduction in observed wear rate by a factor 5 to 8 as compared to the estimated wear rate which does not consider this kind of interaction.

The average wear coefficient shows a reduction compared to that observed in the alloy as shown in Table 4.6 (b). It is interesting to note that commercial magnesium has a lower wear coefficient compared to AZ91 alloy. The wear rate in the alloy is lower at lower load compared to that in commercial magnesium but increases rather rapidly with load, particularly in the second segment. In commercial magnesium, the second segment shows much higher wear rates than that in the alloy. In spite of a relatively lower overall wear rate the wear coefficient, i.e., the wear rate per unit real area of contact, is higher in the alloy because of its lower area of contact due to higher hardness. But in composites

based on AZ91 alloy, the wear coefficients are similar or even lower than that observed in commercial magnesium based composites.

The results reported in this chapter indicates that the variation of average coefficient of friction is similar in both commercial magnesium and AZ91 alloy. For both the base materials and the composites the average coefficient of friction decreases with increasing load. A decrease in coefficient of friction with increasing load has been reported earlier (Yang and chung, 1989). But the extent of decrease appears to be affected by the nature of steelwool distribution in a composite. Irregular variation of average coefficient of friction with load may indicate also in homogeneous distribution of steelwool in the matrix. A higher coefficient of friction at a given load may be an indication of better distribution of steelwool because it is able to delay the effect of softening of the matrix. The wear volume of commercial magnesium based composite decreases when it is reinforced with increasing amount of steelwool. Similarly, the wear rate also decreases with increasing steelwool content in the composites. Similar decrease of wear rate with reinforcement in a composite has also been observed by other workers (Roy, Venkatraman, Bhanuprasad, Mahajan and Sundararajan, 1992). But Alpas and Embury (1990) have observed marginal decrease in wear rate with reinforcement but Zamzam (1989) has observed decrease in wear rate upto a critical volume fraction of reinforcement. Since increasing amount of ceramic dispersoid decreases the extent of strong junctions, the wear rate should decrease. When the amount of ceramic in a composite is so large as to make the composite very brittle the wear rate should increase. Thus, existence of a critical volume fraction upto which the wear rate should decrease appears likely. But in case of metallic dispersoid such critical volume fraction may not exist and the present study has not varied the steelwool content extensively to decide on that point. If one observes the difference in the variation of wear rate with load as shown in Figs.4.32 and compares it with any of the other Figs.4.31 to 4.34, it appears that the composite containing 5.5 vol% steelwool has better distribution of steelwool in the matrix of commercial magnesium which has delayed the softening of the matrix, as compared to that in the other composites based on commercial magnesium where magnesium could soften as in commercial magnesium shown in Fig.4.30, in the area where there is very little steelwool.

The volume loss in wear in AZ91 alloy is lower than that in commercial magnesium. Similarly, the the volume loss in wear in AZ91 alloy based composites are significantly lower than those composites based on commercial magnesium. When the steelwool content is similar as in 6 vol% steelwool reinforced composites the effect of different matrices could be easily seen by comparing Fig..4.28 and 4.43. The variation of wear rate in commercial magnesium and AZ91 alloy show that the latter has lower wear rates at similar loads. But there is discontinuity in wear rates between the loads of 1.5 kg and 2.0 kg for the composites based on either commercial magnesium and AZ91 alloy. However, in the second segment the slope in the variation of wear rate with load is not lower than that in the first segment as it has been observed in commercial magnesium based composites. It may be because the alloy does not flow as easily on softening as commercial magnesium to provide a lubricating layer during dry sliding. Thus, it is clear from the above discussion that reinforcing both commercial magnesium and AZ91 alloy with steelwool provides composites with lower volume loss and wear rate when compared those observed in the corresponding matrix material at similar loads. However, the alloy matrix provides relatively lower wear rates in the composite compared to a matrix of commercial magnesium.

CHAPTER-5

MAGNESIUM BASED METAL CERAMIC COMPOSITE

This chapter describes the results on chemical composition and microstructure of squeeze cast alumina reinforced composites based on commercial magnesium and AZ91 alloy. The results on the mechanical and tribological properties of these composites are also included in this chapter. In the end, the results have been discussed to develop a coherent understanding of these materials in terms of their properties as it has emerged from this study.

5.1.1 Chemical Composition

The chemical composition of the matrix alloys in the composite based on AZ91 alloy has been determined in wt% in respect of weight of composite and the results are reported in Table-5.1.

Table 5.1
Chemical Composition of AZ91-Alumina Composites

Material	Chemical Composition wt%			
	Al	Zn	Fe	Mn
1. AZ91 alloy based composite	8.58	0.47	0.042	0.17

5.1.2 Density of Composites and Alumina Content

The densities of the composites containing different amounts of alumina are reported in Table-5.2. The alumina content of the composites has been determined from the measured density as the porosity content in these squeeze cast composites is negligible. Point counting technique has not been followed since the clustering of alumina particles observed in the microstructure may lead to erroneous results. When ρ_c is the density of a

composite containing alumina, ρ_{mg} is the density of the matrix and $\rho_{Al_2O_3}$ is the density of alumina, the volume fraction of alumina in the matrix, f_s , is estimated as,

$$f_s = \frac{\rho_c - \rho_{mg}}{\rho_{Al_2O_3} - \rho_{mg}} \quad (5.1)$$

The alumina contents in different composites estimated using Eq.(5.1) are reported in the last column of Table-5.2.

Table.5.2

Densities and Alumina Content of Composites and Squeeze Cast Magnesium

Sample number	Sample designation	Matrix	Density X10 ³ kg/m ³	Alumina (Vol%)
1	Pmg	Mg	1.75	00
2	Sq1A	Mg	2.22	23
3	Sq1B	Mg	2.19	21
4	Sq11A	AZ91	2.04	14
5	Sq11B	AZ91	2.07	16
6	Sq11C	AZ91	2.24	24

5.1.3 Microstructure of the Composites

The microstructures of alumina reinforced composites based on commercial magnesium and AZ91 alloy have been examined under optical microscope to find the amount and distribution of phases in the matrix alloy, in the context of phase diagram and also the volume fraction of reinforcements as determined from density given in Table 5.2.

(a) Magnesium- Alumina Composite

Figure 5.1 shows the microstructures of composites based on commercial magnesium containing an average of 23 vol% of alumina. There are more particles in

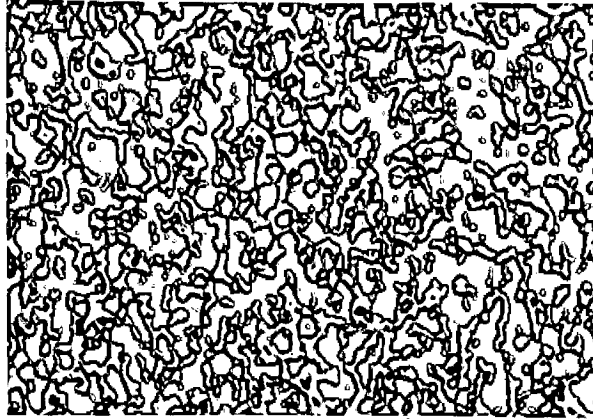


Fig.5.1 Microstructure of Squeeze cast composite based on commercial magnesium containing 23 vol % of alumina, showing fairly uniform distribution of alumina particles in the matrix of commercial magnesium; X62.5.

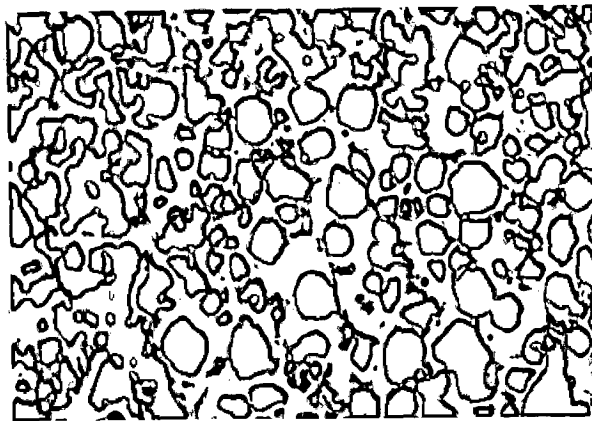


Fig.5.2 Microstructure of Squeeze cast composite based on commercial magnesium containing 23 vol % of alumina, showing fairly uniform distribution of alumina particles of different sizes in the matrix of commercial magnesium; X125.

certain areas but relatively lower volume fraction in other areas that is often the result of particle pushing by infiltrating liquid stream during squeeze casting. In the area containing larger concentration of particles the microstructure shows fairly uniform distribution of particles as observed at a lower magnification of X62.5 in Fig.5.1. Figures 5.2 and 5.3 show the same microstructures at higher magnifications of X125 and X250 respectively. Both these microstructures show alumina particles of size varying over a range and the particles are generally much coarser than the thickness of a relatively darker phase which is in the form of a network within the brighter phase of magnesium solid solution. Because of the presence of so many particles, there is no evidence of dendritic solidification, but the last freezing liquid, rich in solute, may have resulted in the network of solute rich phase by eutectic reaction that is divorced as shown at still higher magnification of X625 in Fig 5.4. A phase similar to that in the network appears to have formed also at the boundary of the alumina particles and it could be $MgAl_2O_4$. It is observed that the particle boundaries are highly irregular which may indicate matrix-particle reaction during processing.

Figure 5.5 shows the microstructure of composite containing an average of 21 vol% alumina, slightly lower than that in the composite whose microstructures has been described in Fig 5.1 to 5.4. Fig 5.5 clearly shows the particle rich and the particle deficient regions which is typical of these squeeze cast composites. At a higher magnification in Fig.5.6, the microstructures have shown semicircular patterns similar to that observed in Fig 4.6 for magnesium based steel wool reinforced composite. This pattern could be the boundary of streams of liquid which has infiltrated later during processing and solidified last when the surrounding streams have already solidified. The last freezing boundary is therefore marked by either shrinkage cavity and/or solute rich phases. But such patterns are not commonly observed. There extent of matrix-particle reaction is relatively less as evident from more regular particle boundaries as shown in Fig.5.6, but there is a phase at the particle boundary. This phase could be product of matrix-particle reaction or could be an alloy phase that has used the particle as site for heterogeneous nucleation.

(b) AZ91 Alloy-Alumina Composite

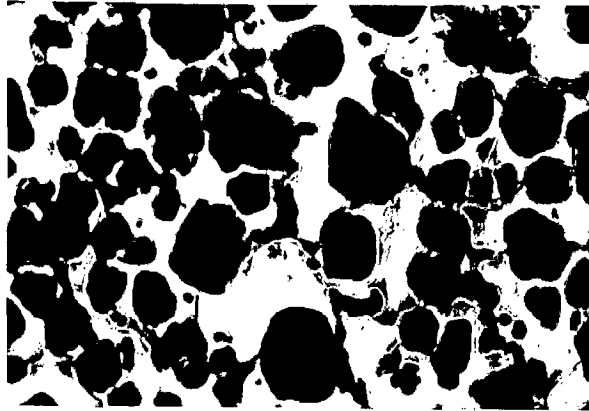


Fig.5.3 Microstructure of Squeeze cast composite based on commercial magnesium containing 23 vol % of alumina, showing network solute rich phase at the boundary of particles and in the matrix; X250.



Fig.5.4 Microstructure of Squeeze cast composite based on commercial magnesium containing 23 vol % of alumina, a network of a phase in the matrix of commercial magnesium and irregular surface of the alumina particles; X625.

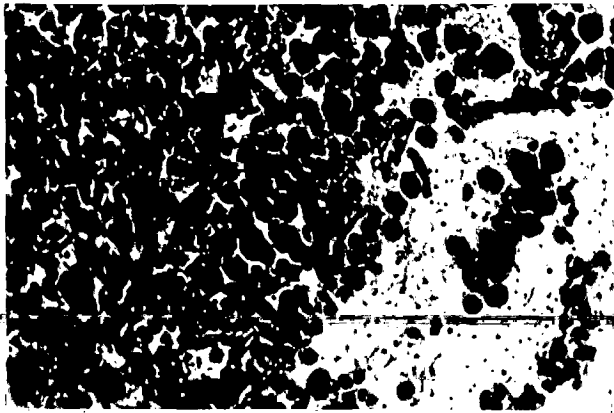


Fig.5.5 Microstructure of Squeeze cast composite based on commercial magnesium containing 21 vol % of alumina, showing the particles rich and the particle deficient regions in the matrix of commercial magnesium; X62.5



Fig.5.6 Microstructure of Squeeze cast composite based on commercial magnesium containing 21 vol % of alumina, boundaries of stream and relatively darker phases at the boundary of particles that is relatively more regular; X625.

Figure 5.7 shows the microstructures of AZ91 alloy based composite containing an average alumina content of 16 vol%. The microstructure shows inhomogeneous particle distribution characterised by particle rich and particle deficient region. One could observe dendritic solidification particularly in particle deficient regions where interference by particles during solidification is relatively less as given in Figs 5.8 and 5.9 at higher magnifications of X250 and X625 respectively. The alloy appears to contain another phase that is marked A and B which could be $Mg_{32}(Al,Zn)_{49}$ as shown Fig. 5.9. In the particle-deficient area one could observe dendrites of magnesium solid solution and lamellar eutectic containing lamella of $Mg_{17}Al_{12}$ in the matrix of magnesium solid solution. It is interesting to note that in the microstructure of vacuum infiltrated AZ91 alloy as shown in Fig. 4.15, the eutectic in the interdendritic region is divorced resulting in a network of $Mg_{17}Al_{12}$.

5.1.4 Electron Probe Microanalysis

EPMA of commercial magnesium based composite containing alumina particles has been carried out to assess the extent of reaction between alumina particles and molten magnesium during processing of composites at higher temperature as indicated in the microstructure. Since the commercial magnesium used has very small amount of aluminium as impurity as given in Table 4.1, estimation of aluminium content in different phases in the matrix alloy will be an indirect measure of the extent of matrix particle reaction. In a typical composite of this category containing 23 vol% alumina, EPMA line scan for aluminium, shown in Fig.5.10 (a), has been taken between two alumina particles along the matrix where it contains primary magnesium solid solution. The scan shows that the magnesium content decreases near alumina particles. However, one could detect solute rich phase between some particles and at the particle boundaries. The EPMA analysis of magnesium based composite containing 21 vol% as shown that there is a phase which contains aluminium to magnesium ratio of about 11:8. Which is higher than the ratio of aluminium : magnesium in $Mg_{17}Al_{12}$, but same ratio in $MgAl_2O_4$. The line scan in Figure 5.10 (b) show increase in aluminium concentration over that of the matrix indicating the presence of aluminium rich phase.



Fig.5.7 Microstructure of Squeeze cast composite based on AZ91 alloy containing 16 vol % of alumina, showing the inhomogeneous particle distribution characterised by particle rich and the particle deficient regions in the matrix of AZ91 alloy; X62.5

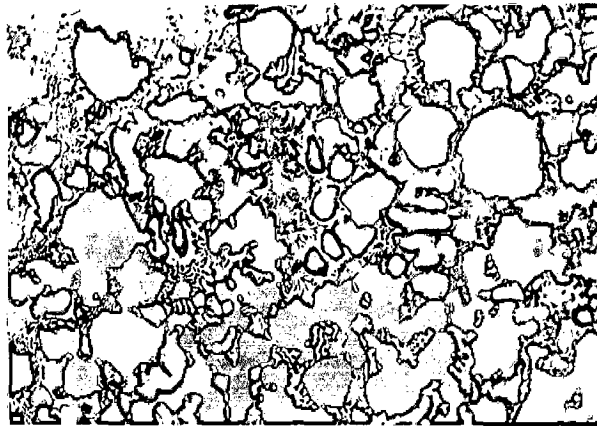


Fig.5.8 Microstructure of Squeeze cast composite based on AZ91 alloy containing 16 vol % of alumina, showing dendrites in the particle deficient regions in the matrix of AZ91 alloy and lamellar eutectic in the last freezing liquid; X250.



Fig.5.9 Microstructure of Squeeze cast composite based on AZ91 alloy containing 16 vol % of alumina, showing irregular surface of the particles and lamellar eutectic rich and the particle deficient regions in the matrix of AZ91 alloy; X625.

LINE ANALYSIS

22-AUG-98

INTENSITY
(Counts)

File no. : 45
Comment : 1-MG

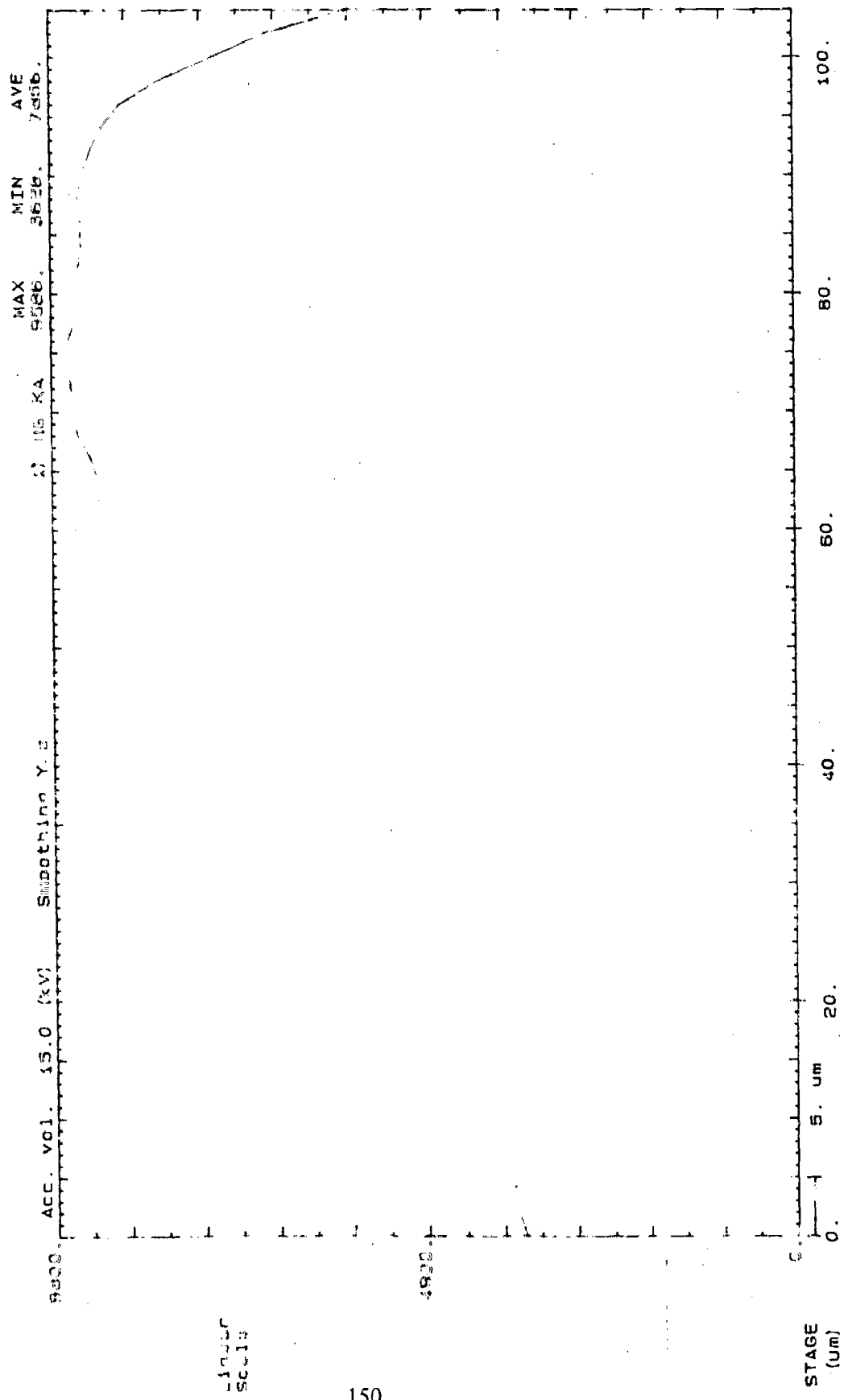


Fig.5.10(a) EPMA line scan for aluminium between two alumina particles in commercial magnesium based composite containing 23 vol% of alumina.

LINE ANALYSIS

22-AUG-98

File no. : 46
Comment : 1-AL

INTENSITY
(Counts)

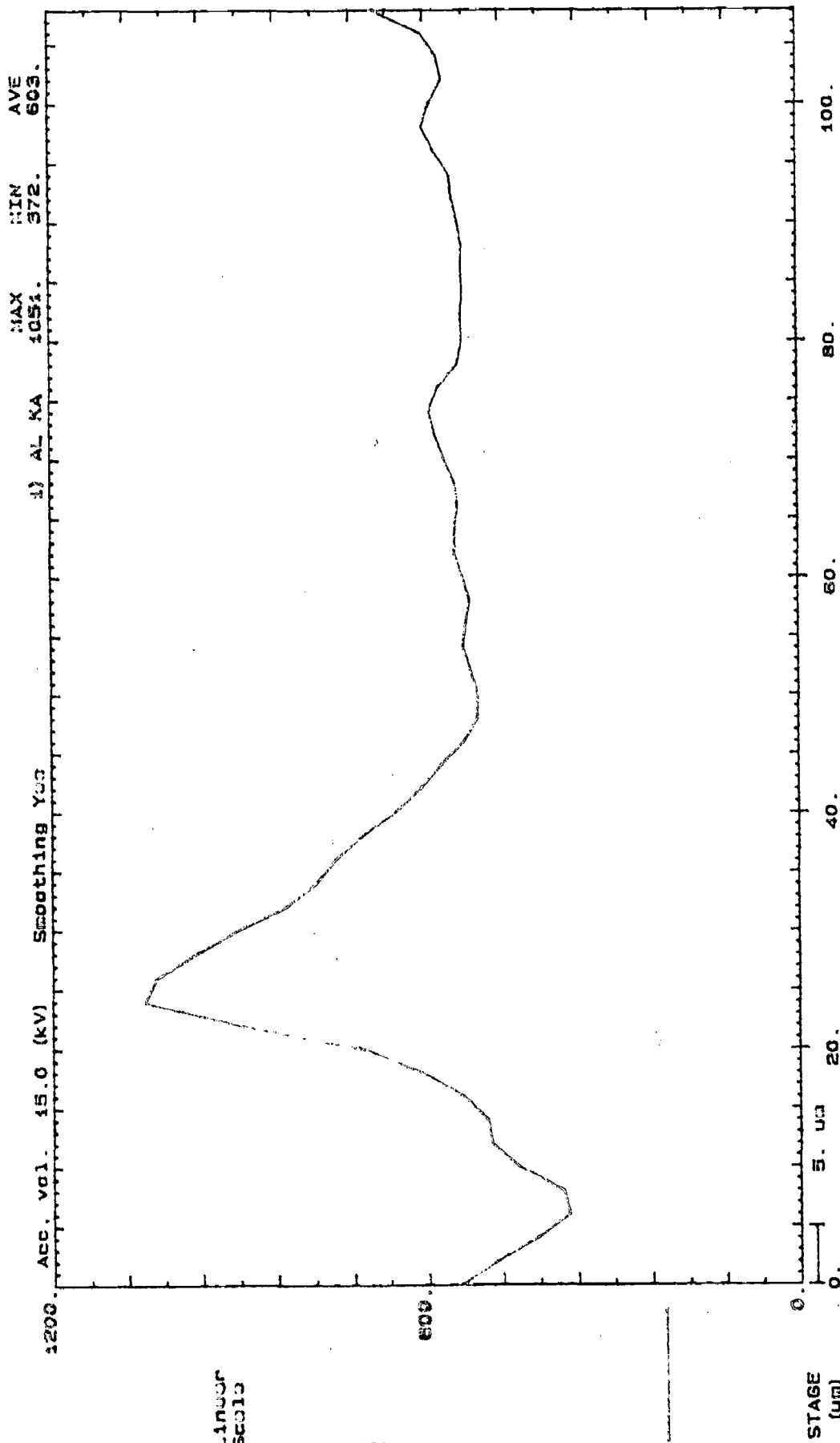


Fig.5.10(b) EPMA line scan for aluminium between two alumina particles in commercial magnesium based composite containing 21 vol% of alumina.

The chemical analysis of the solute rich phase at the boundary of particles and that present as network in the matrix is given in Table 5.3 (a) and (b). The tables show that the

Table 5.3 (a)

Composition of Solute Rich Phase at Particle Boundary

Element	Wt (%)	Wt% Normalized to 100%
Al	13.737	58.373
Mg	09.796	41.627
Total	23.534	100.000

Table 5.3 (b)

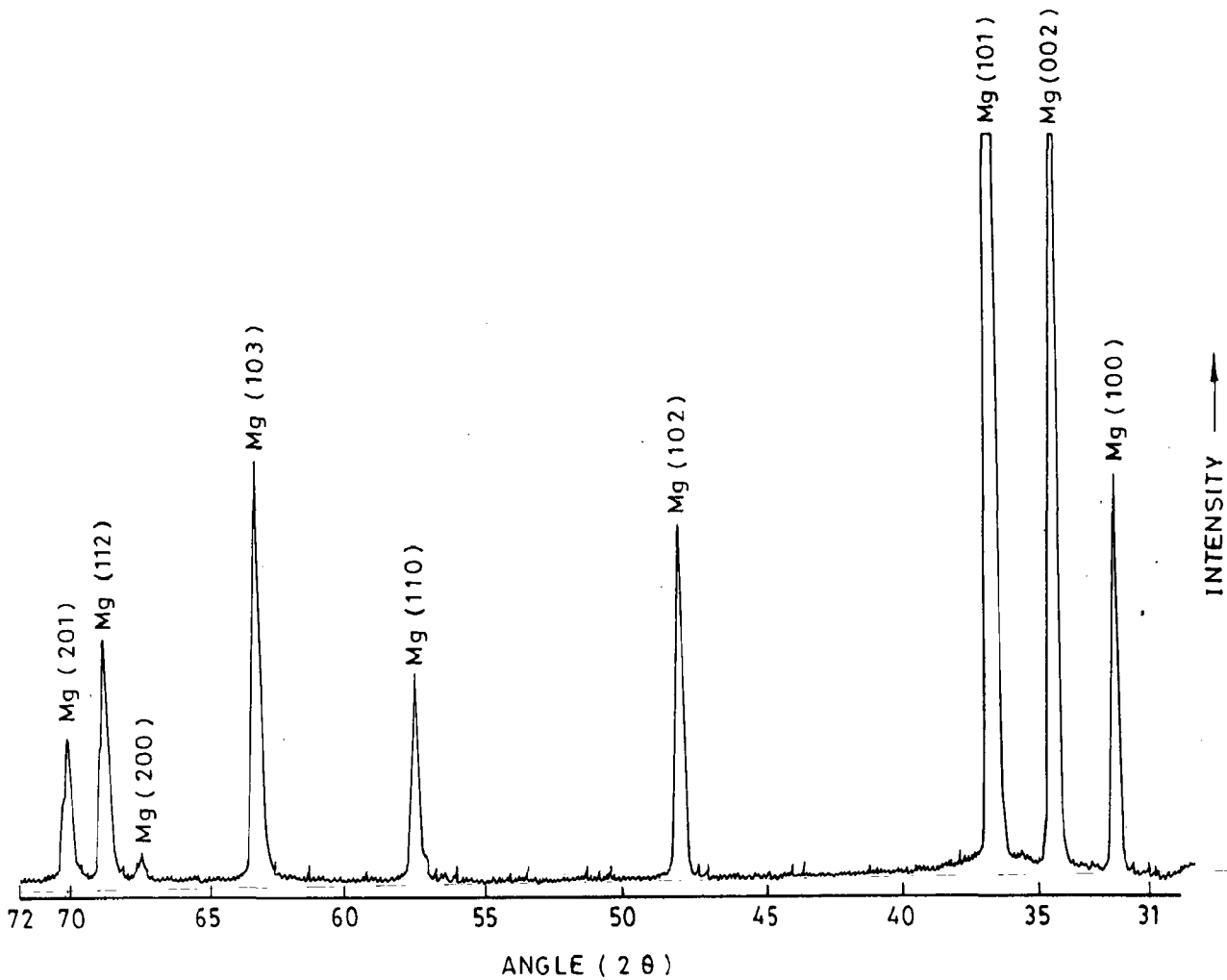
Composition of Solute Rich Phase in Matrix

Element	Wt (%)	Wt% Normalized to 100%
Al	13.716	59.670
Mg	09.270	40.330
Total	22.986	100.000

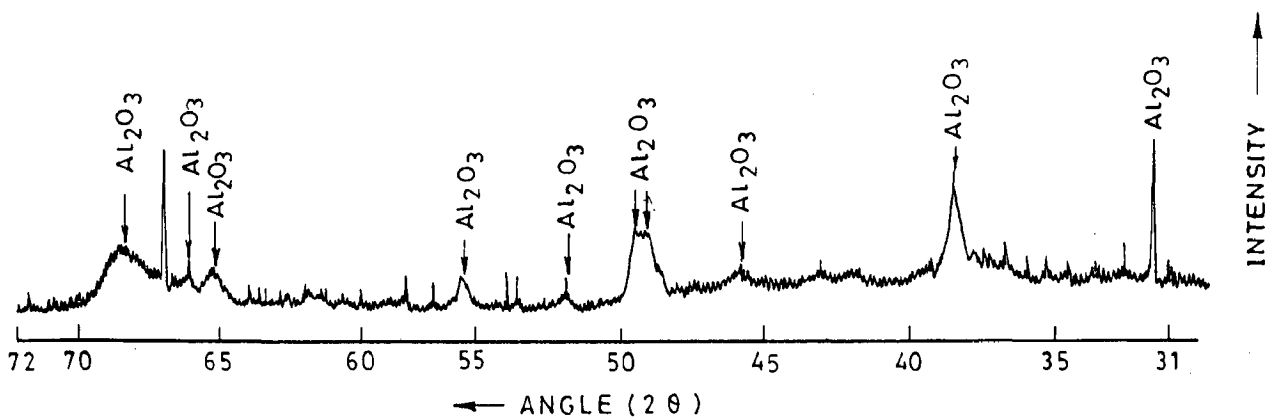
composition of solute aluminium rich phases at the particle boundary and in the network are similar phases are same and it contains aluminium and magnesium. The ratio of wt% in aluminium and magnesium varies from 1.42 to 1.5 which may be identified as $Mg_{17}Al_{12}$ which has a weight ratio of magnesium to aluminium of around 1.3.

5.1.5 X-ray Diffraction Studies

The X-ray diffraction peaks in the interval between 2θ values of 31 and 71 degrees for the sample of commercial magnesium are shown in Fig.5.11 (a). The lattice parameters of magnesium are shown in Table 5.4. All the peaks with I/I_0 values of 9 and higher have been observed. The diffraction peaks obtained from alumina and the magnesium based composites containing 21 and 23 vol% alumina are also shown in Fig.5.11 (b). It is noticed that the 2θ values corresponding to magnesium have shifted slightly in these composites compared to those observed for commercial magnesium. This shift indicates that

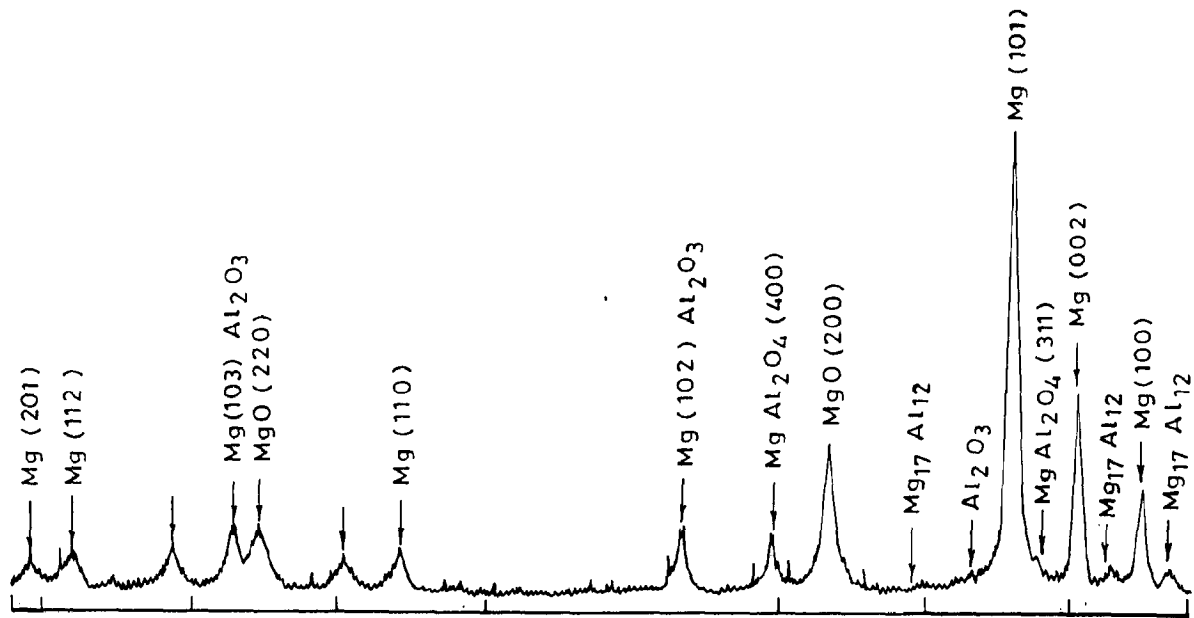


(a) COMMERCIAL MAGNESIUM

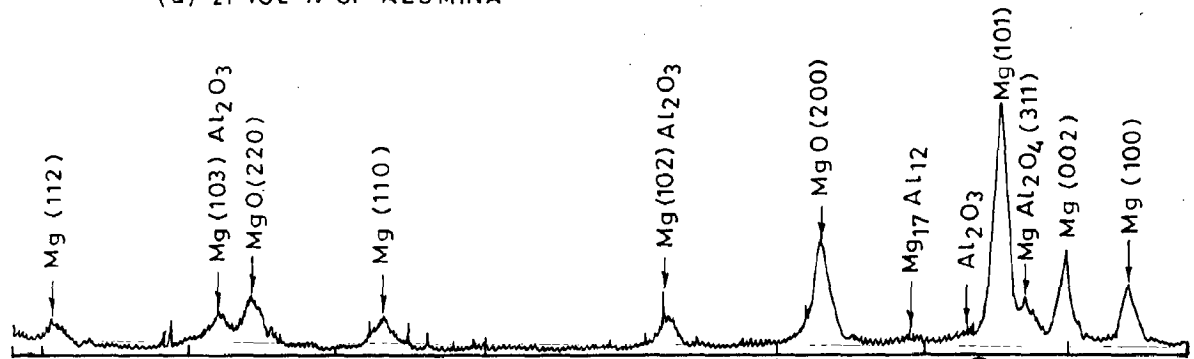


(b) ALUMINA PARTICLES USED FOR THE SYNTHESIS OF COMPOSITES

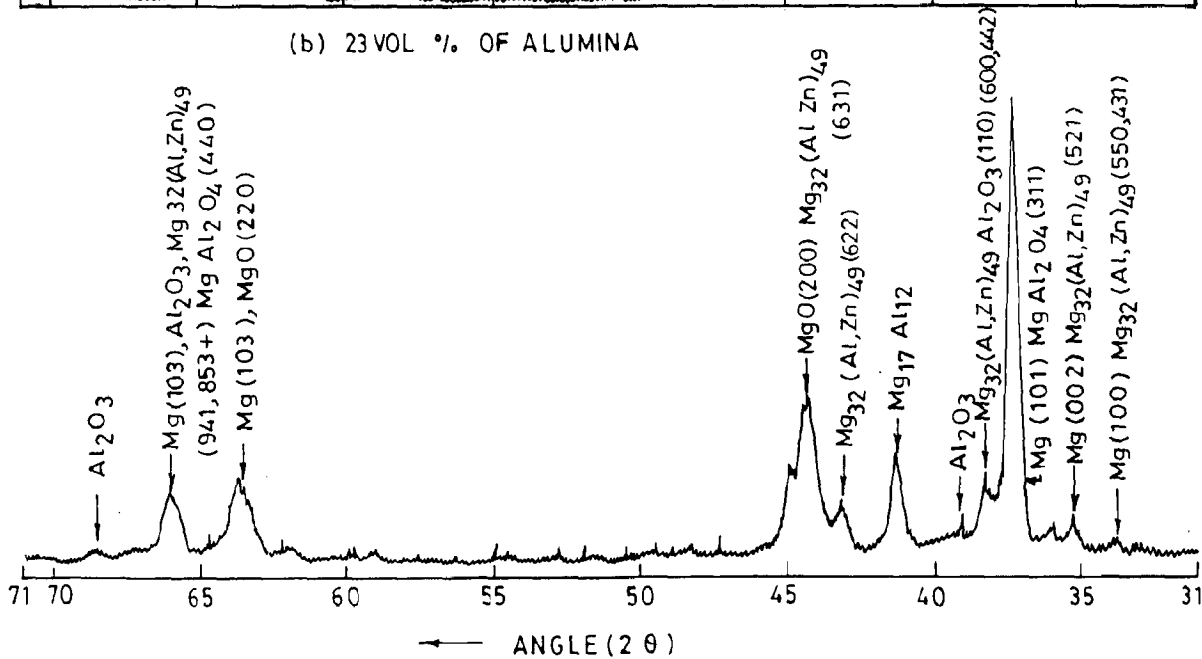
FIG. 5.11(a) X-RAY DIFFRACTION PATTERNS



(a) 21 VOL % OF ALUMINA



(b) 23 VOL % OF ALUMINA



(c) AZ 91 ALLOY BASED COMPOSITE CONTAINING 14 VOL % ALUMINA

FIG. 5.11 (b) X-RAY DIFFRACTION PATTERNS OF COMMERCIAL MAGNESIUM BASED COMPOSITES CONTAINING

magnesium has taken some solute in its lattice to become magnesium solid solution and there is change in lattice parameters which are reported in Table 5.4 for the composites. The peaks from alumina in the composites have been identified by comparing the diffraction pattern of alumina with those of the composites. The strongest peak of $MgAl_2O_4$ is from (311) which falls at 2θ , just before (101) peak of magnesium solid solution. The presence of this peak in the composite containing 23 vol% of alumina as shown in Fig. 5.11(b) has been taken as definite indication of significant amount of $MgAl_2O_4$ in this composite. In the composite containing 21 vol% alumina this peak is absent and so it may be inferred that it does not contain significant amount of alumina. There is a peak at $2\theta = 62.3$ which could be from (220) of go which has intensity I/I_0 of 52 and the only other stronger peak of this compound is at $2\theta = 42.9$ from (200) where the peak of (113) from alumina is also there as given in ASST. chart. Thus, the composites containing alumina have magnesium solid solution, alumina and MgO . But the composite containing 23 vol% alumina has, in addition, significant presence of $MgAl_2O_4$. The peak at $2\theta = 65.5$ degrees does not belong to any of the compounds mentioned. However, the presence of $Mg_{17}Al_{12}$ could be seen in the microstructure as expected from the phase diagram but the diffraction pattern for this phase is not available. In addition, these may be FeMnAl intermetallic phase in AZ91 alloys as it has been processed in ferrous anvil and die.

The X-ray diffraction peaks as observed in the AZ91 alloy based composite containing 14 vol% alumina have been compared with the peaks obtained from commercial magnesium shown in Fig. 5.11(a) and the lattice parameter of magnesium solid solution in the AZ91 alloy based composite containing 14 vol% alumina has been observed as $a=3.226 \text{ \AA}$ $c=5.2476 \text{ \AA}$. The position of the peaks from magnesium solid solution has been identified and those peaks resulting from alumina have been identified, as shown in Fig. 5.11(b). The major peak from (311) of $MgAl_2O_4$ has not merged with the peak from (101) of solid solution. The other peaks being relatively weak a positive identification of $MgAl_2O_4$ phase is not possible in AZ91 alloy based composite. The peak that has been observed at 2θ values of 42.2 degrees could not be identified and the other peaks may belong to either magnesium solid solution, alumina, $MgAl_2O_4$ or MgO . The composite may have in addition $Mg_{32}(Al, Zn)_{49}$ but it could not be positively identified as its major peaks

have occurred at 2θ of other constituents. Further, the peaks at $2\theta = 32.2$ degrees and the unidentified peaks could also belong to $Mg_{17}Al_{12}$ which is present as indicated in the microstructure.

Table 5.4
Lattice Parameters for Magnesium Solid Solution in Composites

Material	Alumina content Vol%	a	c
Magnesium	00	3.208	5.1073
Magnesium-Alumina	21	3.176	5.1580
Magnesium-Alumina	23	3.146	5.1080
AZ91Alloy-Alumina	14	3.226	5.2476

5.1.6 Hardness of the Composites

The macro-and microhardnesses have been measured by Brinell and Vickers hardness for commercial magnesium and magnesium based and AZ91 based composites containing alumina. The Brinell hardness of the as cast commercial magnesium, magnesium-alumina composites and AZ91 alloy-alumina composites containing different volume percent of alumina are given in Table-5.2.

Table-5.5
Brinell Hardness of Composites and Squeeze Cast Magnesium

Sample number	Sample designation	Matrix	Alumina content Vol %	Brinell hardness HB
1	Mg	Mg	00	25.4
2	Sq1B	Mg	21	91.0
3	Sq1A	Mg	23	109.14
4	Sq11A	AZ91	14	103.5
5	Sq11B	AZ91	16	113.8
6	Sq11C	AZ91	24	132.2

The Vickers microhardnesses for as cast commercial magnesium, Mg-alumina composite and AZ91-alumina composites have been measured and are given in Table-5.6.

Table-5.6
Vickers Hardness of Composites and Squeeze Cast Magnesium

Sample number	Sample designation	Matrix	Alumina content Vol %	Vickers microhardness (HV) Primary phase/Alumina	
1	Mg	Mg	00	54.20	****
2	Sq1B	Mg	21	105.26	597.0
3	Sq1A	Mg	23	111.00	569.0
4	Sq11A	AZ91	14	94.00	683.4
5	Sq11B	AZ91	16	96.46	537.2
6	Sq11C	AZ91	24	108.6	407.0

Fig.5.12 shows the variation in the Brinell hardness with volume percent of alumina in the composites based on commercial magnesium and also, those based on AZ91 alloy. It has been found that for both these types of composites, the hardness appears to increase generally with the alumina content. But for AZ91 alloy based composite, the Brinell hardness is significantly higher compared to the composites based on commercial magnesium. The variation of hardness with alumina content could not be ascertained with some confidence because of limited data.

Table 5.6 shows the variation of microhardness in VHN with volume percent of alumina in squeeze cast commercial magnesium. It is observed that the hardness of primary phase increases by a little with alumina content which could be due to alumina restraining the flow under indentation. Fig. 5.13 shows the variation of microhardness in VHN with volume percent of alumina in the composite based on AZ91 alloy. It is observed that the microhardness of the primary phase increases from 94 to 108.6 VHN when volume percent of alumina increases from 14 to 24 vol% in the composite. The alumina particles

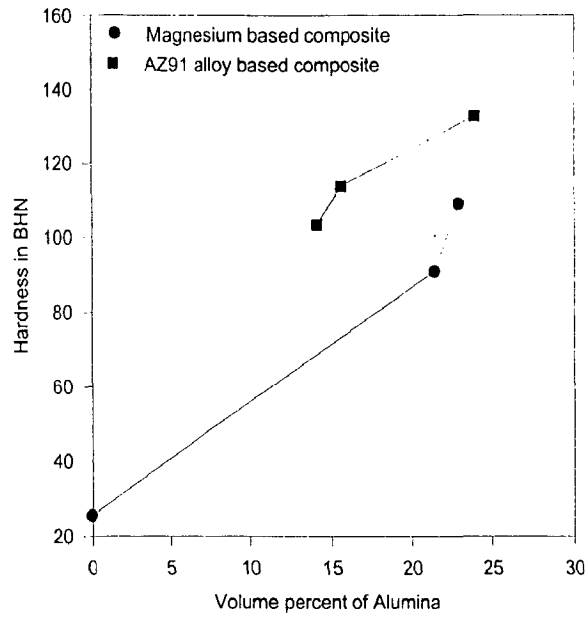


Fig.5.12 The variation of Brinell hardness with volume percent of alumina in commercial magnesium based composites and AZ91 alloy based composites.

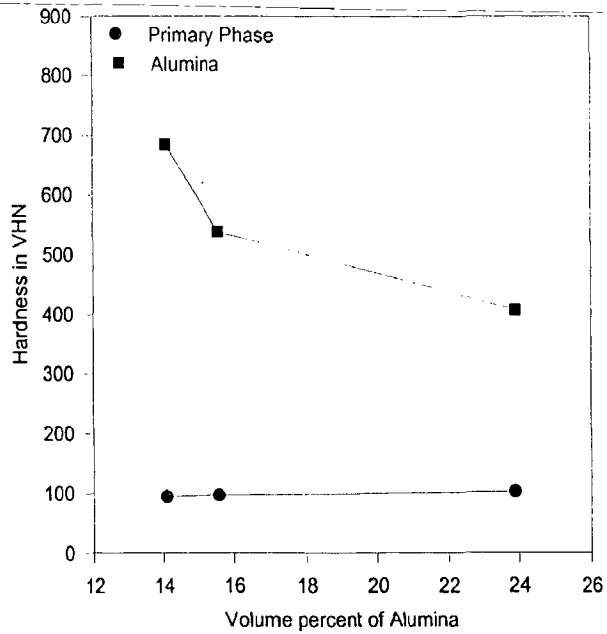


Fig. 5.13 The variation of Vickers hardness with volume percent of alumina in AZ91 alloy based composites.

region has hardness of 683.4 VHN at 14 vol% alumina and it decreases to 407 VHN when alumina content increases to 24 vol%.

5.1.7 Dry Sliding Friction and Wear

(a) Magnesium- Alumina Composite

Figs. 5.14 to 5.16 show the variation of cumulative volume loss with sliding distance for commercial magnesium and the composites based on it containing 21 and 23 vol% respectively, tested under normal loads of 2.5, 3.5, 4.5 and 5.5 kg at contact and at a sliding speed of 1.0 m/s. The cumulative volume loss increases more or less linearly with sliding distance at a given load and the least square fit for this variation at different loads are indicated by the lines drawn in these figures. The coefficient of correlation for the fit mostly exceeds 0.99 but in certain cases it is 0.98. It is observed that the volume loss in the composite containing 21 vol% of alumina shown in Fig. 5.15 is spread over a relatively narrower range compared to that in commercial magnesium or the composite containing 23 vol% alumina as shown in Figs.5.14 and 5.16 respectively. At lower loads, the volume loss in magnesium-21 vol% alumina composites is significantly less compared to that in commercial magnesium but at higher loads the volume loss increases as shown in Fig. 5.16, but still it is significantly lower than that in commercial magnesium. It may be noted that the difference in alumina content in the composites investigated here are relatively small but there is a significant difference in volume loss as shown in Figs.5.15 and 5.16.

The wear rate, i.e., volume loss in wear per unit sliding distance at a given load, has been determined from the slope of the linear least square fit lines at different loads in Figs.5.14 to 5.16. The variation of wear rate with normal load for commercial magnesium and the composites based on it and having alumina contents of 21 and 23 vol% are shown respectively in Figs.5.17 to 5.19. It is observed that the wear rate increases more or less linearly with contact load for the composite containing 21 vol% alumina but for the other composites the variation is nonlinear and the wear rates are also similarly high.

Fig. 5.20 to 5.22 shows the variation of coefficient of friction with sliding distance in squeeze cast commercial magnesium and the composites based on it, containing 21 and

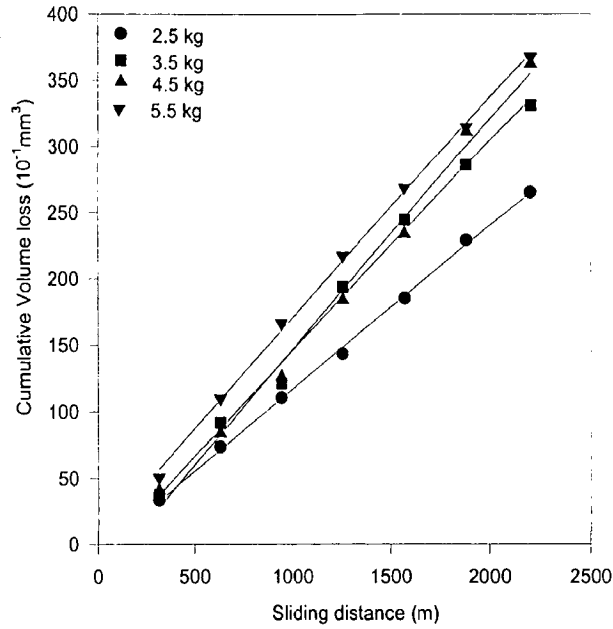


Fig.5.14 The variation of cumulative volume loss with sliding distance in commercial Magnesium, during dry sliding under a constant sliding speed of 1 m/s against counterface of hardened steel.

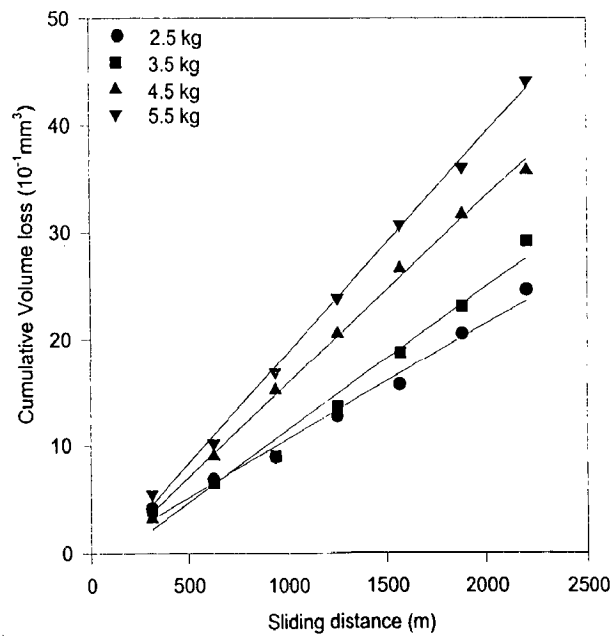


Fig.5.15 The variation of cumulative volume loss with sliding distance in commercial magnesium based composite containing 21 vol.% of alumina, during dry sliding under a constant sliding speed of 1.0 m/s against counterface of hardened steel.

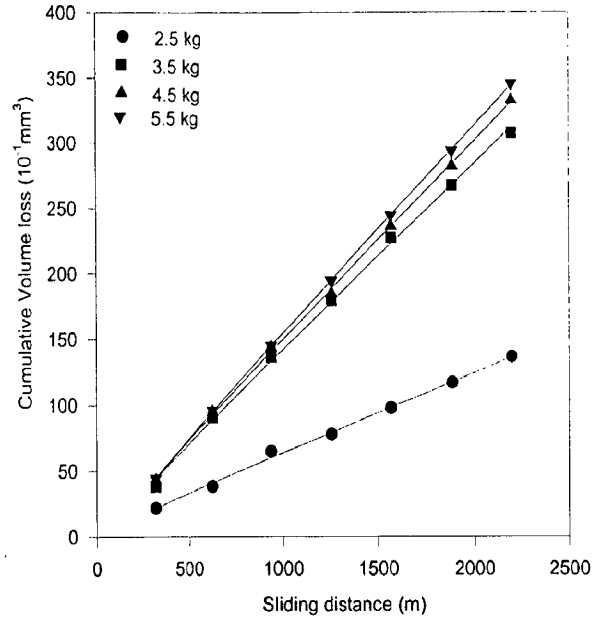


Fig.5.16 The variation of cumulative volume loss with distance in commercial magnesium based composite containing 23 vol.% of alumina, during dry sliding under a constant sliding speed of 1 m/s against counterface of hardened steel

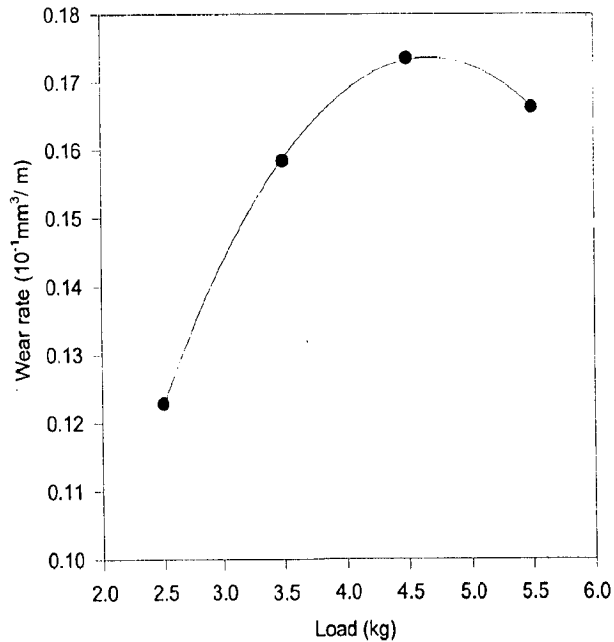


Fig.5.17 The variation of wear rate with normal loads for commercial magnesium, during dry sliding at a fixed sliding speed of 1.0 m/s against counterface of hardened steel.

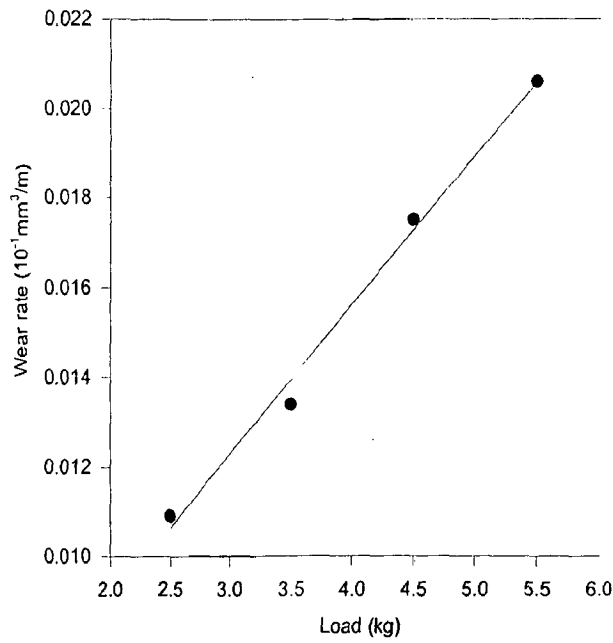


Fig.5.18 The variation of wear rate with normal load in commercial magnesium based composite containing 21 vol.% of alumina, during dry sliding at fixed sliding speed of 1 m/s against counterface of hardened steel.

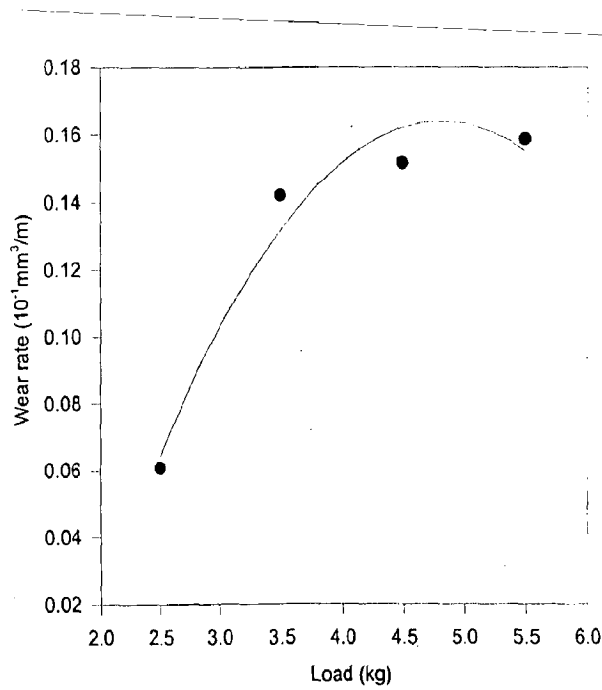


Fig.5.19 The variation of wear rate with normal load in commercial magnesium based composite containing 23 vol.% of alumina, during dry sliding at a fixed sliding speed of 1m/s against counterface of hardened steel.

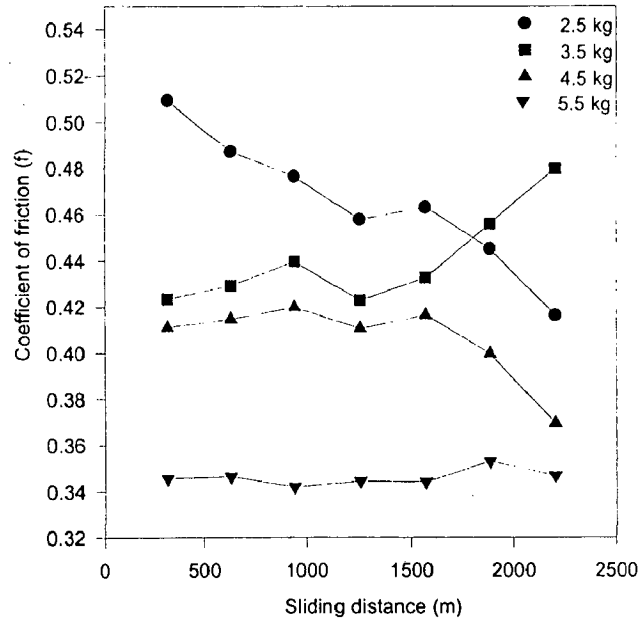


Fig.5.20 The variation of coefficient of friction with sliding distance in commercial Magnesium, during dry sliding under a constant sliding speed of 1 m/s against counterface of hardened steel

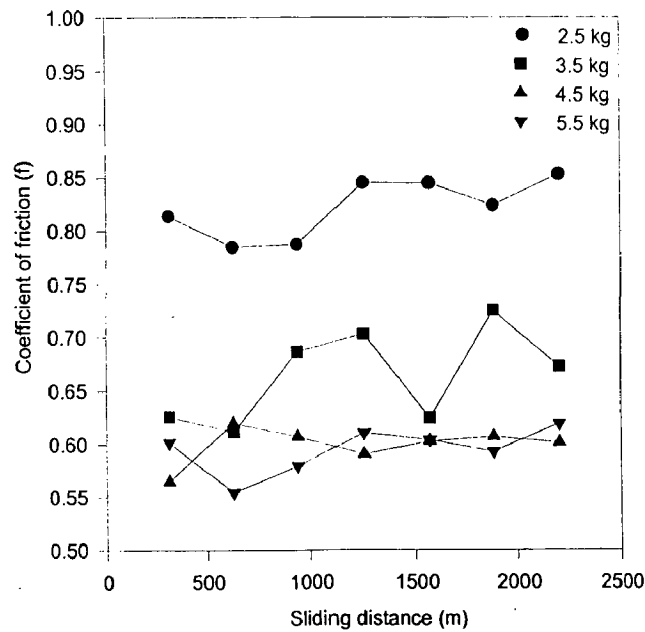


Fig.5.21 The variation of coefficient of friction with sliding distance in commercial Magnesium, based composite containing 21 vol.% of alumina, during dry sliding under a constant sliding speed of 1 m/s against counterface of hardened steel.

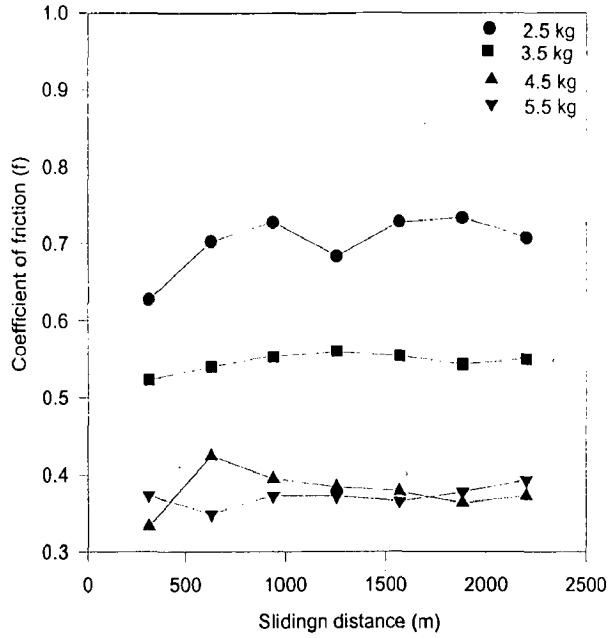


Fig.5.22 The variation of coefficient of friction with sliding distance in commercial Magnesium based composite containing 23 vol.% of alumina, during dry sliding under a constant sliding speed of 1 m/s against counterface of hardened steel.

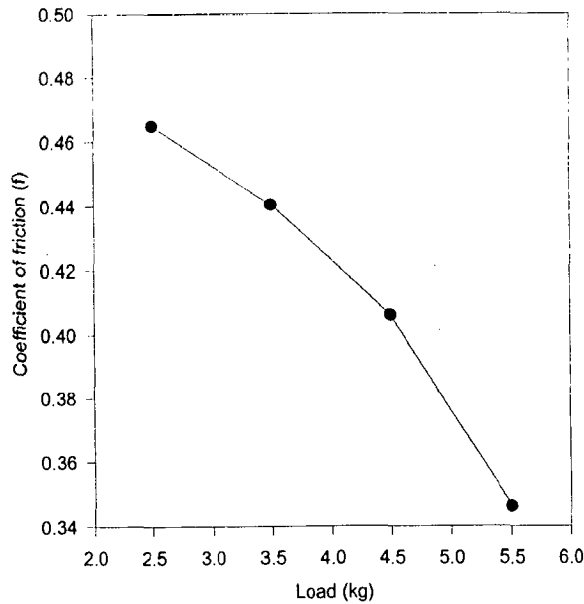


Fig.5.23 The variation of coefficient of friction average over sliding distance, with normal load for commercial magnesium, during dry sliding at a fixed sliding speed of 1 m/s against counterface of hardened steel.

23 vol% respectively, for different applied loads ranging between 2.5 kg to 5.5 kg in steps of 1.0 kg. It is observed that at the lower load of 2.5 kg, the coefficient of friction is higher and it decreases with increasing load. In commercial magnesium and the composite containing 23 vol% alumina the coefficient of friction decreases to a value of about 0.35 but in the composite containing 21 vol% alumina the coefficient of friction retains a high value between 0.55 and 0.6 when the applied loads increases to 5.5 kg. Figures.5.23 to 5.25 show the variation of the coefficient of friction, averaged over sliding distance, with load for commercial magnesium and composites based on it but containing different amounts of alumina. When load increases from 2.5 kg, there is more rapid drop in coefficient of friction in the composites compared to that in commercial magnesium.

The wear coefficient of commercial magnesium has been observed to be 0.36×10^{-4} which is very similar to that in composite containing 21 vol% of alumina i.e., 0.30×10^{-4} . However, the wear coefficient in the composite containing 23 vol% of alumina is considerably higher at 3.31×10^{-4} .

(b) AZ91 Alloy-Alumina Composite

Figs. 5.26 to 5.28 show the variation of cumulative volume loss with sliding distance for AZ91 alloy based composites having alumina contents of 14, 16 and 24 vol% of alumina respectively, tested at different normal loads of 2.5, 3.5, 4.5 and 5.5 kg under a sliding speed of 1.0 m/s. The cumulative volume loss increases more or less linearly with sliding distance at a given load and the least square fit for this variation at a given load is indicated by the lines drawn in these figures. It is observed that the volume loss in the composite containing 16 vol% alumina is significantly lower than the other two composites.

The wear rate has been calculated from the slope of the linear least square fit lines at different loads as outlined earlier. Figs. 5.29 to 5.31 show the variation of the wear rate with normal load for AZ91 alloy based composites having alumina contents of 14, 16 and 24 vol% respectively, it is observed that the wear rate increases more or less linearly but

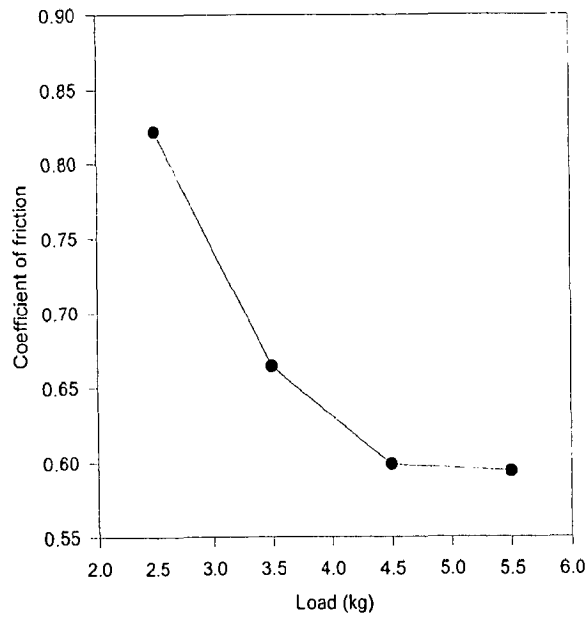


Fig.5.24 The variation of coefficient of friction average over sliding distance, with normal load in commercial magnesium based composite containing 21 vol.% of alumina, during dry sliding at a fixed sliding speed of 1 m/s against counterface of hardened steel.

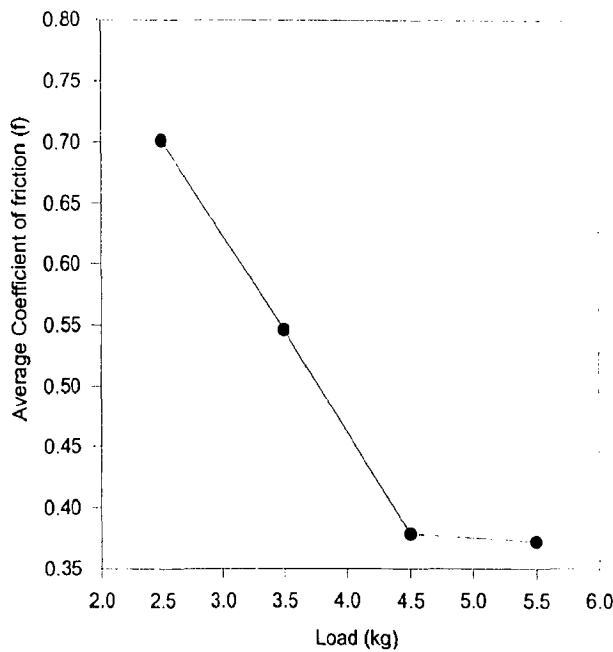


Fig.5.25 The variation of coefficient of friction averaged over sliding distance, with normal load in commercial magnesium based composite containing 23 vol.% of alumina, during dry sliding at a fixed sliding speed of 1 m/s against counterface of hardened steel.

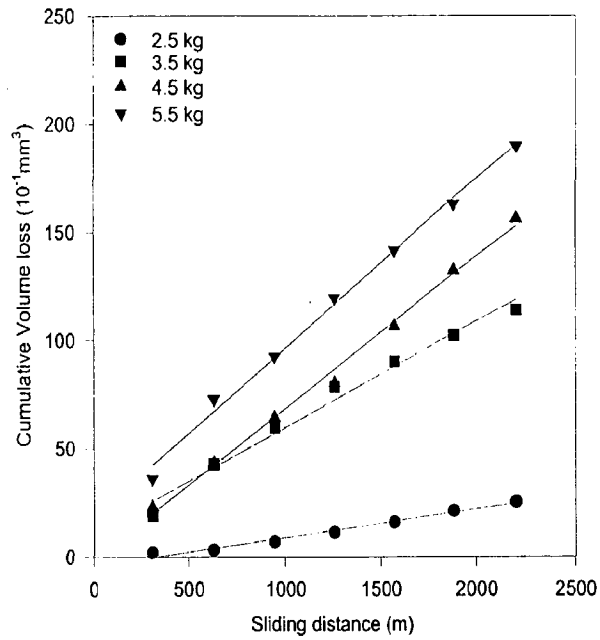


Fig.5.26 The variation of cumulative volume loss with sliding distance in AZ91 alloy based composite containing 14 vol.% of alumina, during dry sliding under a constant sliding speed of 1 m/s against counterface of hardened steel

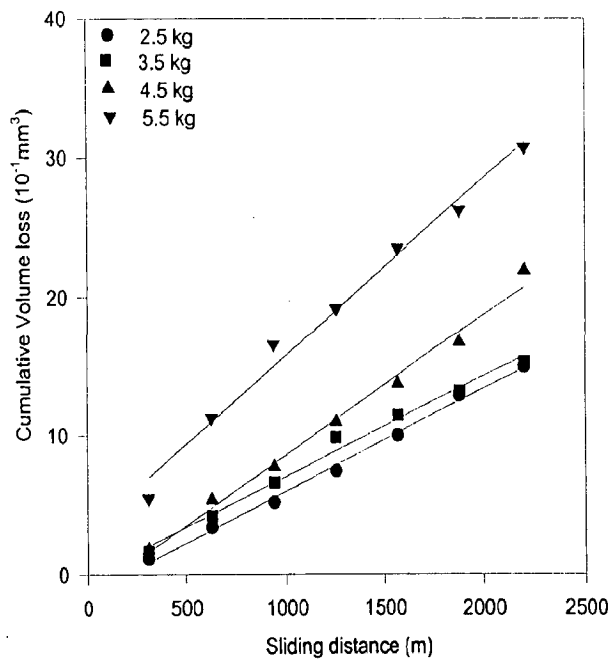


Fig.5.27 The variation of cumulative volume loss with sliding distance in AZ91 alloy based composite containing 16 vol.% of alumina, during dry sliding under a constant sliding speed of 1 m/s against counterface of hardened steel

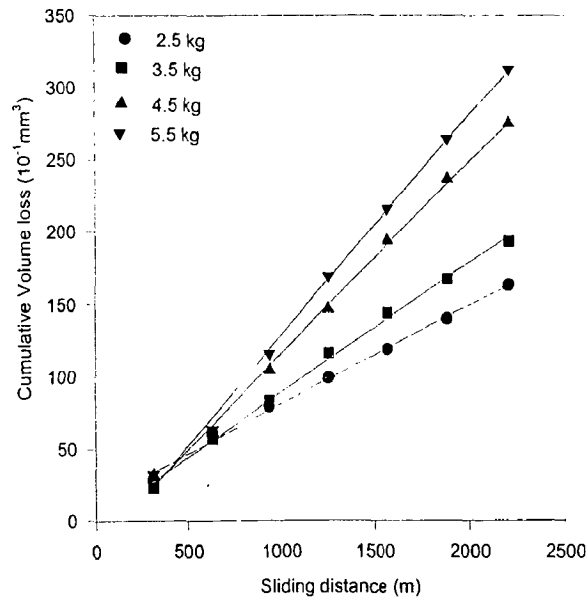


Fig.5.28 The variation of cumulative volume loss with sliding distance in AZ91 alloy based composite containing 24 vol.% of alumina, during dry sliding under a constant sliding speed of 1 m/s against counterface of hardened steel

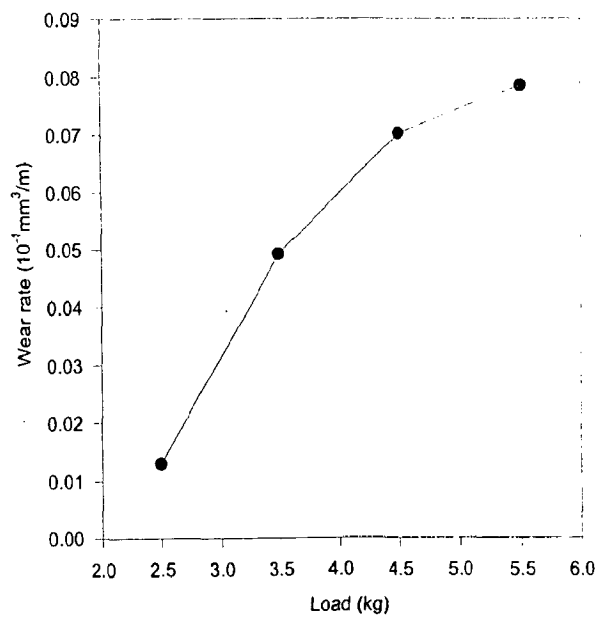


Fig.5.29 The variation of wear rate with normal load for AZ91 alloy based composite containing 14 vol.% of alumina, during dry sliding at a fixed sliding speed of 1 m/s against counterface of hardened steel

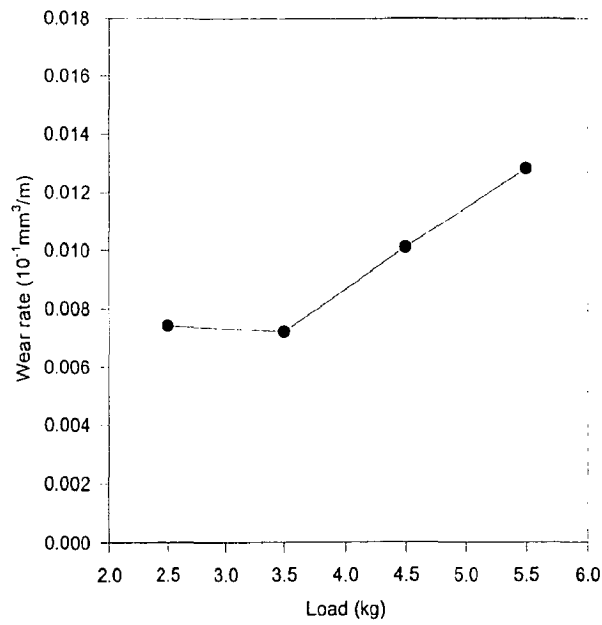


Fig.5.30 The variation of wear rate with normal load for AZ91 alloy based composite containing 16 vol.% of alumina, during dry sliding at a fixed sliding speed of 1 m/s against counterface of hardened steel

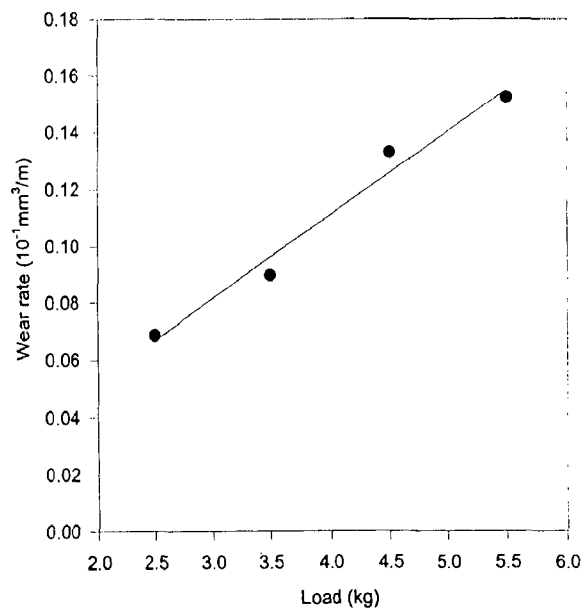


Fig.5.31 The variation of wear rate with normal load for AZ91 alloy based composite containing 24 vol.% of alumina, during dry sliding at a fixed sliding speed of 1 m/s against counterface of hardened steel.

the wear rate observed in the composite containing 16 vol% alumina is considerably lower than the other two composites at similar loads.

Fig. 5.32 to 5.34 shows the variation of coefficient of friction with sliding distance for different applied loads ranging between 2.5 kg to 5.5 kg in steps of 1.0 kg, in AZ91 alloy based composites containing 14, 16 and 24 vol% respectively. It is observed that at a lower load of 2.5 kg, the coefficient of friction is relatively more and it decreases with increasing load at contact. It may be noted that for the composites containing 14 and 16 vol% of alumina the coefficient of friction varies in the range between 0.55 to 0.9 but the composite containing higher alumina of 24 vol%, the coefficient of friction remains in the range between 0.31 and 0.50. Figures.5.35 to 5.37 show the variation of coefficient of friction averaged over sliding distance, with load for AZ91 alloy based composites. When load increases from 2.5 kg, there is a drop in coefficient of friction in all these composites.

The wear coefficient of AZ91 alloy based composite containing 14 vol% of alumina is 2.25×10^{-4} but the composite containing 16 vol% of alumina has wear coefficient which is an order of magnitude lower, i.e., 0.21×10^{-4} . But the composite containing higher alumina of 24 vol% has considerably higher wear coefficient of 3.89×10^{-4} .

5.1.8 Examination of Sliding Surface and Wear Debris

(a) Magnesium- Alumina Composite

The composite containing Al_2O_3 particles in a matrix of commercial magnesium have been tested at a higher load range between 2.5 kg to 5.5 kg as the volume loss in wear at lower loads below 2.5 kg is observed to be very small. The wear surface of the composite tested under the load of 2.5 kg has shown the transfer layer covering the sliding surface as shown in Fig 5.38 (a). At high magnification, it is observed that the wear debris are sticking to the surface and getting compacted to increase the thickness and extent of coverage of the transfer layer as shown in Fig 5.38 (b) and 5.38 (c). At a high load of 5.5 kg the transfer layer appears to have flaked off exposing the underlying particles or voids as shown in Fig 5.39 (a). At higher magnification one may observe the area where the

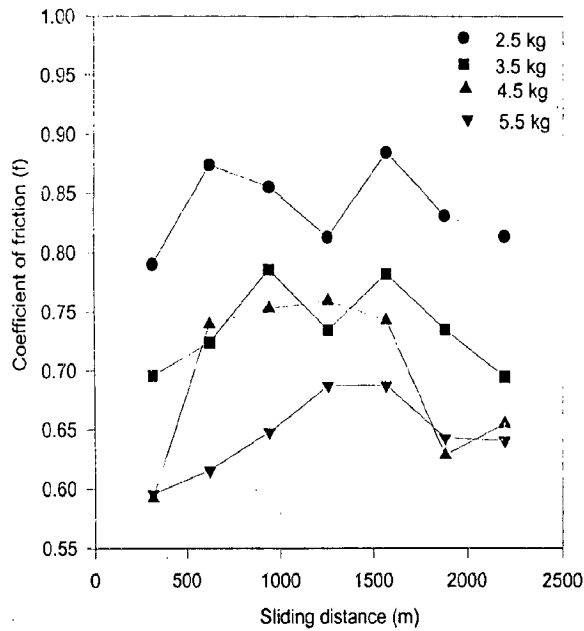


Fig.5.32 The variation of coefficient of friction with sliding distance for AZ91 alloy based composite containing 14 vol.% of alumina, during dry sliding under constant sliding speed of 1 m/s against counterface of hardened steel

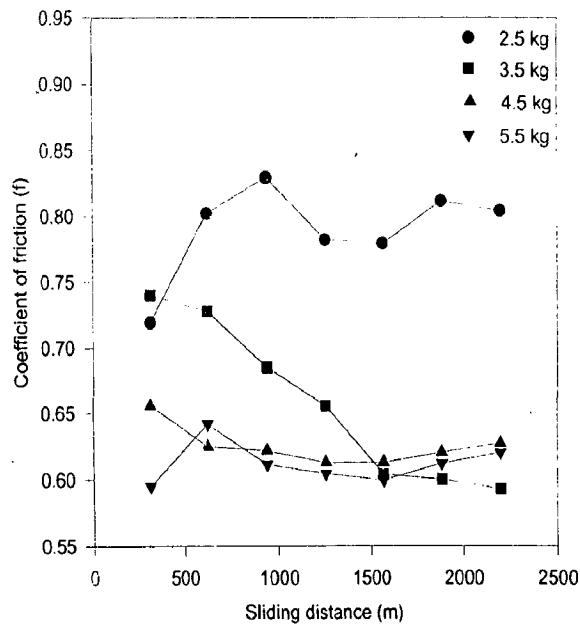


Fig.5.33 The variation of coefficient of friction with sliding distance for AZ91 alloy based Composite containing 16 vol.% of alumina, during dry sliding under a constant sliding speed of 1 m/s against counterface of hardened steel

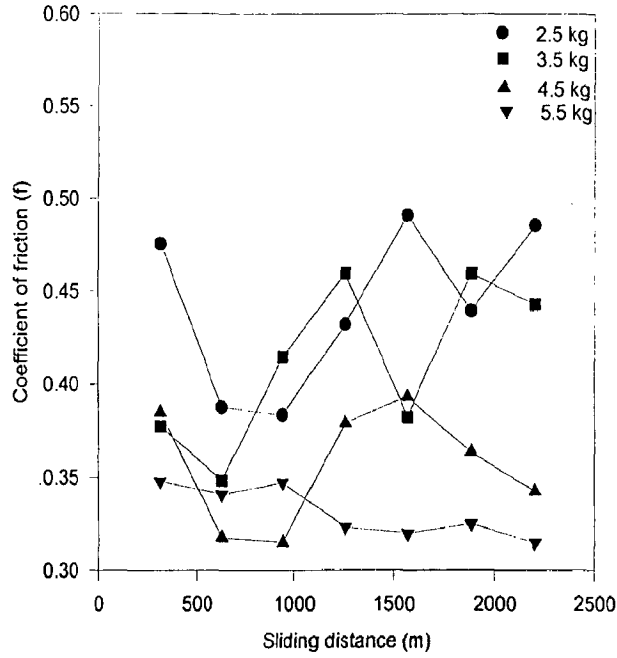


Fig.5.34 The variation of coefficient of friction with sliding distance in AZ91 alloy based composite containing 24 vol.% of alumina, during dry sliding under a constant sliding speed of 1 m/s against counterface of hardened steel

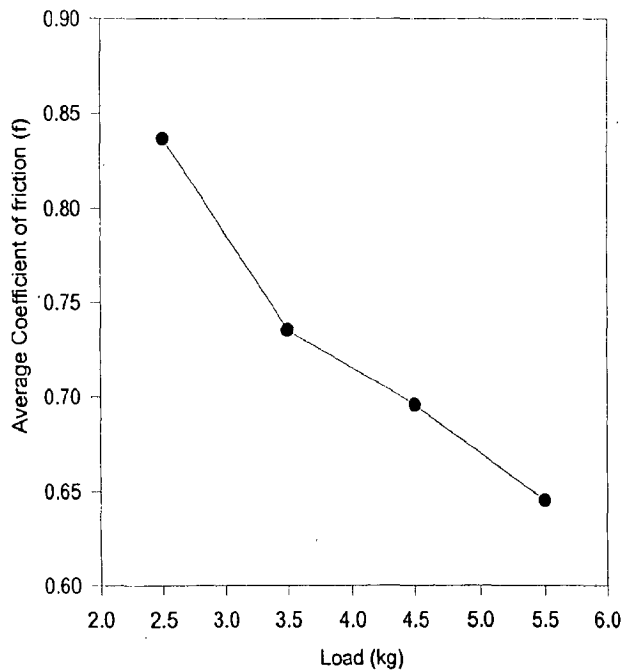


Fig.5.35 The variation of coefficient of friction averaged over sliding distance, with normal load in AZ91 alloy based composite containing 14 vol.% of alumina, during dry sliding at a fixed sliding speed of 1 m/s against counterface of hardened steel.

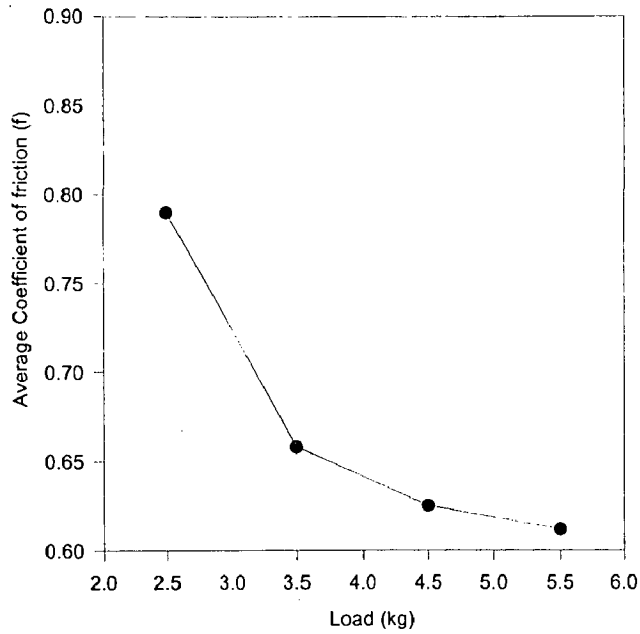


Fig.5.36 The variation of coefficient of friction averaged over sliding distance, with normal load in AZ91 alloy based composite containing 16 vol.% of alumina, during dry sliding at a fixed sliding speed of 1 m/s against counterface of hardened steel

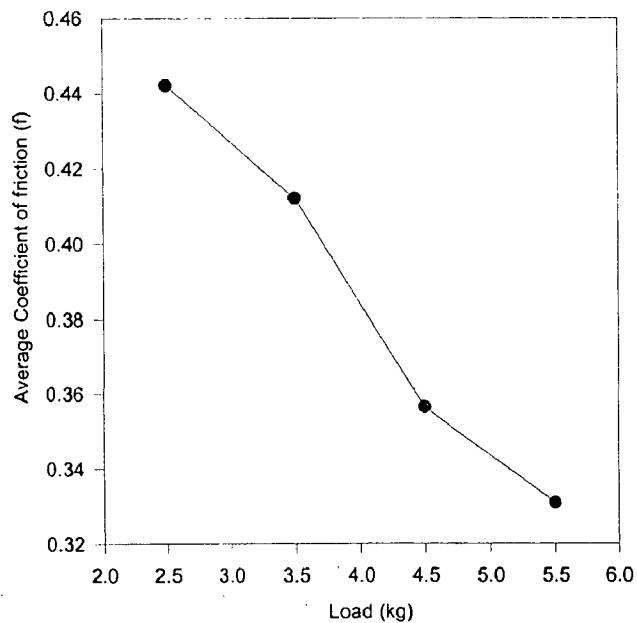
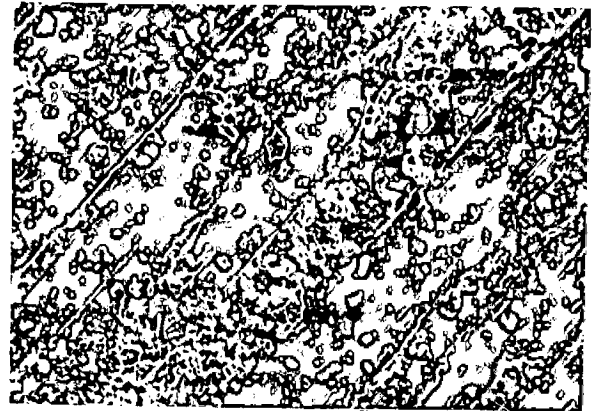


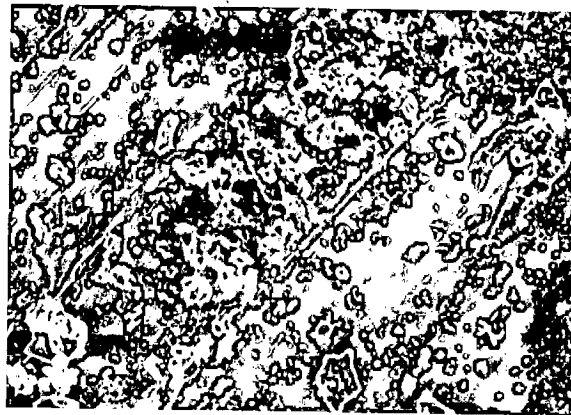
Fig.5.37 The variation of coefficient of friction averaged over sliding distance, with normal load in AZ91 alloy based composite containing 24 vol.% of alumina, during dry sliding at a fixed sliding speed of 1 m/s against counterface of hardened steel.



(a)

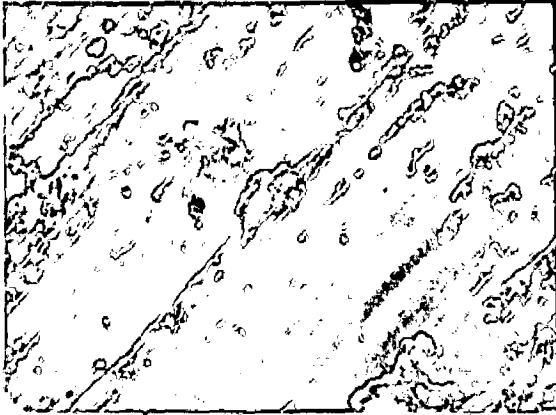


(b)



(c)

Fig.5.38 SEM micrograph of the surface of commercial magnesium based composite containing 21 vol% of alumina, after dry sliding at a normal load of 2.5 kg, (a) X77 (b) X200 and (c) X400.



(a)



(b)



(c)

Fig.5.39

SEM micrograph of the surface of commercial magnesium based composite containing 21 vol% of alumina, after dry sliding at a normal load of 5.5 kg, (a) X77 (b) X200 and (c) X400.

transfer layer has flaked off and fresh debris have accumulated in the recessed region as shown in Fig 5.39 (b) and (c).

The wear debris formed during sliding of magnesium-alumina composite under a load of 2.5 kg, shows the fine particles of oxide along with some flakes of transfer layer as shown Fig. 5.40(a). There are some very small bright metallic particles also. But at a high load of 5.5 kg the extent of flakes present in the wear debris increases as compared to that at lower load of 2.5 kg as shown in Fig 5.40(b).

(b) AZ91 Alloy-Alumina Composite

In the composite containing alumina particles in the matrix of AZ91 alloy the test surface after sliding under a load of 2.5 kg, shows large number of voids which could be due to debonding of alumina particles during sliding as shown in Fig 5.41(a). At a higher magnification, one may observe plowing tracks where debris has accumulated as shown in Fig 5.41(b) and 5.41(c). These debris may eventually get compacted to form transfer layer protecting the metal underneath. At a high load, the flow of magnesium may have covered the alumina particles before their debonding during sliding and thus, there are very few voids as shown Fig 5.42(a) and (b). There are some evidence of plowing as shown in Fig 5.42(c) at a higher magnification. The long voids which are being termed as plowing marks, may not have originated during plowing but could be due to voids created by debonding, getting extended during sliding.

In Fig 5.43 (a), one observes the wear debris generated during sliding of the composites containing alumina particles in the matrix of AZ91 alloy. It is observed that even at the low load of 2.5 kg, there is significant flaking of the transfer layer. But at a high load of 5.5 kg the fragments are relatively small as shown in Fig 5.43 (b).

5.2 Discussion

The results of X-ray diffraction clearly shows that in commercial magnesium based composites containing alumina there is reaction between the alumina particles and the

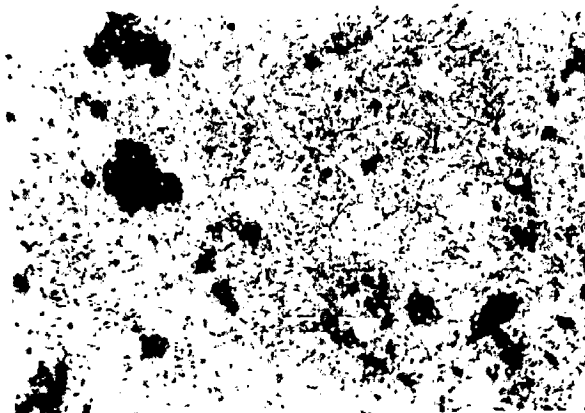
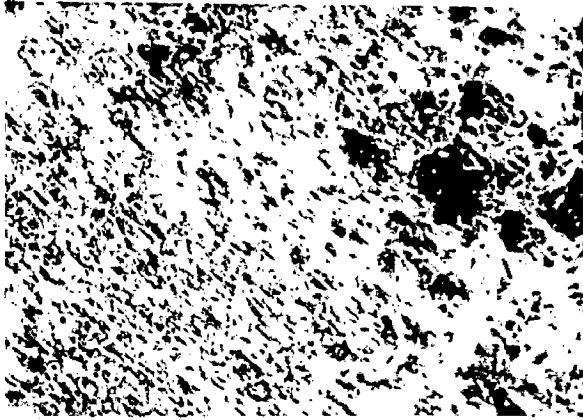


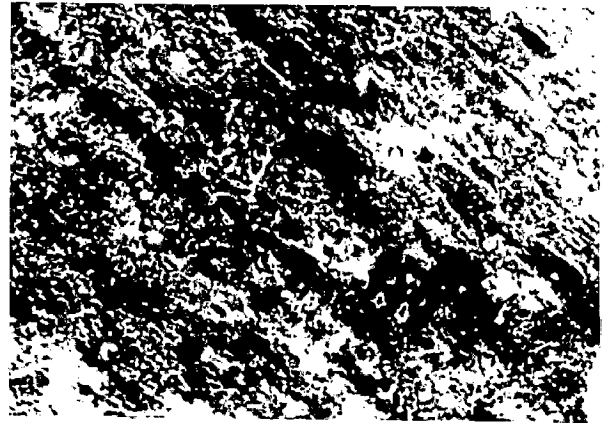
Fig.5.40(a) Stereo microphotograph showing the wear debris of commercial magnesium based composite containing 21 vol% of alumina, generated during dry sliding against steel disc at load of 2.5 kg; X16.



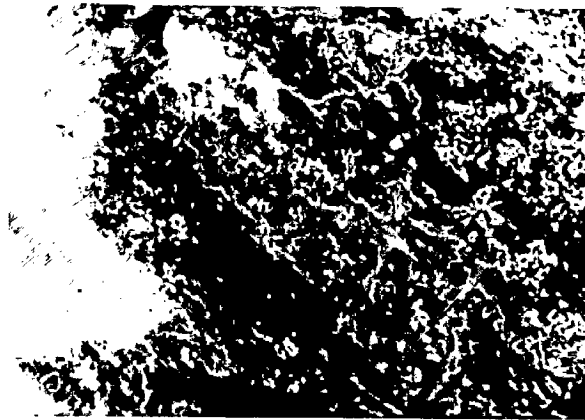
Fig.5.40(b) Sterec microphotograph showing the wear debris of magnesium based composite containing 21 vol% of alumina, generated dry sliding against steel disc at load of 5.5 kg; X16.



(a)

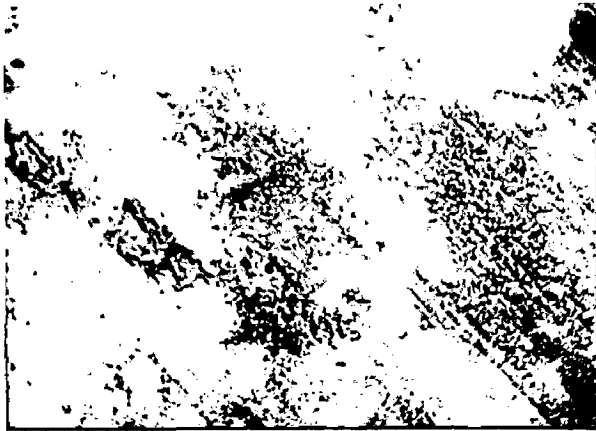


(b)

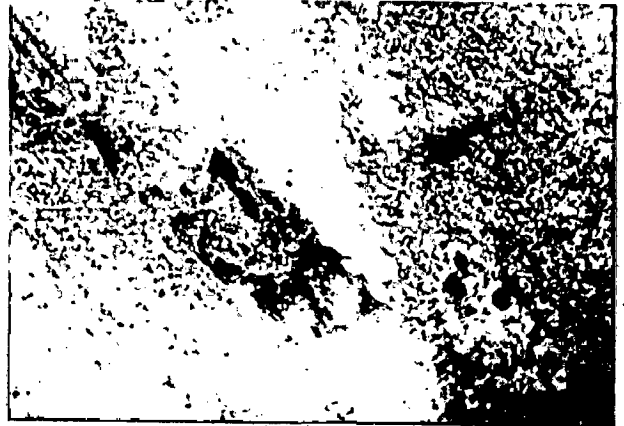


(c)

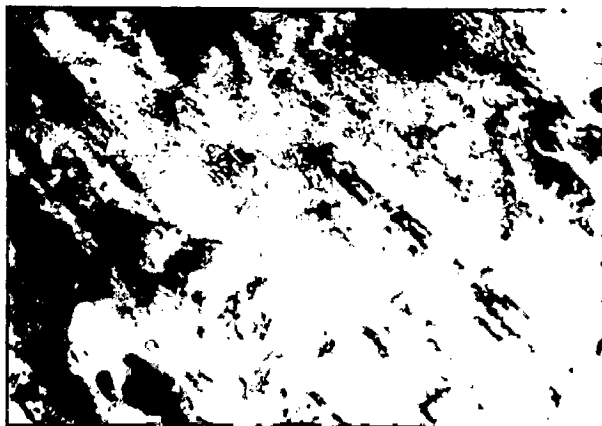
Fig.5.41 SEM micrograph of the surface of AZ91 alloy based composite containing 16 vol% of alumina, after dry sliding at a normal load of 2.5 kg, (a) X77 (b) X200 and (c) X400.



(a)



(b)



(c)

Fig.5.42 SEM micrograph of the surface of AZ91 alloy based composite containing 16 vol% of alumina, after dry sliding at a normal load of 5.5 kg, (a) X77 (b) X200 and (c) X400

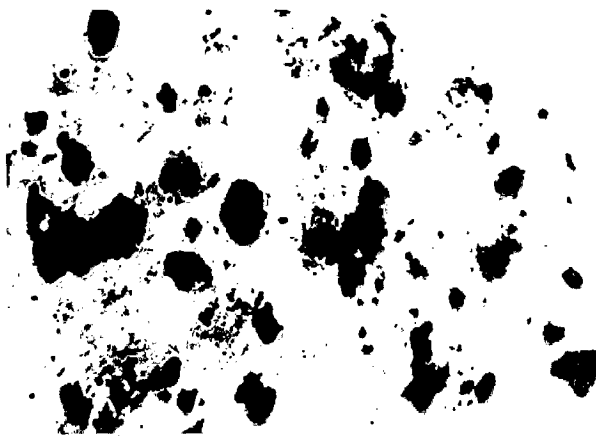


Fig.5.43(a) Stereo microphotograph showing the wear debris of AZ91 alloy based composite containing 16 vol% of alumina, generated during dry sliding against steel disc at different load of 2.5 kg; X16.

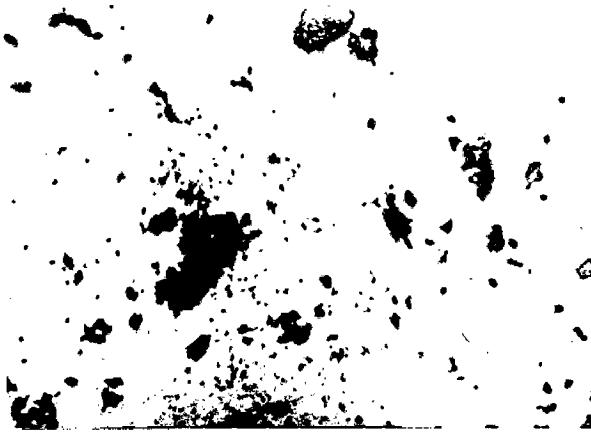
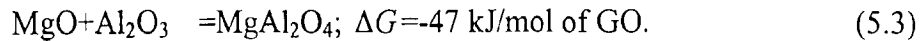
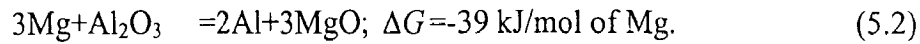


Fig.5.43(b) Stereo microphotograph showing the wear debris of AZ91 alloy based composite containing 16 vol% of alumina, generated during dry sliding against steel disc at different load of 5.5 kg; X16.

molten commercial magnesium during processing following the chemical reactions given below (Hallstedt, Liu and Agren, 1990).



It has been claimed that the above reactions are sluggish at normal melt temperatures (Wilks, King and Wardlow, 1997). The aluminium released due to reduction of alumina by molten magnesium following Eqn.(5.2), may dissolve in magnesium and on solidification, should also go into the lattice of magnesium. Thus, the lattice parameters of the matrix magnesium may change in the composite as shown in Table 5.4. The X-ray diffraction also reveals the formation of MgAl_2O_4 which may have formed also around the alumina particles as shown in microstructures given in Figs.5.4. Isothermal section of Al-Mg-O system at 1000 K clearly indicates that MgO is the only stable product at magnesium rich corner and MgAl_2O_4 should not form. But one may observe MgAl_2O_4 at the interface between alumina and MgO which has formed by reaction of magnesium with alumina. (Hallstedt, Liu and Agren, 1990). The network of relatively darker phase within the bright phase of magnesium solid solution as shown Fig. 5.3 to 5.4 for the composite containing 23 vol% of alumina, appears very similar to the phase at the boundary of alumina particle as shown Fig. 5.4. The results of EPMA from the same composite as given in Tables 5.3 (a) and (b) confirm it. This phase may either be MgAl_2O_4 or $\text{Mg}_{17}\text{Al}_{12}$. The ratio of aluminium to magnesium by weight are respectively 18:8 or 13:8.5 for MgAl_2O_4 and $\text{Mg}_{17}\text{Al}_{12}$. But the ratio observed under EPMA is 13.7:19.3. Thus, it is likely that the phase could also be a mixture of MgAl_2O_4 and $\text{Mg}_{17}\text{Al}_{12}$ as the appearance of this is spotted. It is possible that significant amount of aluminium is released due to reduction of Al_2O_3 by magnesium and it is dissolved in molten magnesium which may result in eutectic solidification in the last freezing liquid. The phase constituents of the eutectic -namely magnesium solid solution and $\text{Mg}_{17}\text{Al}_{12}$, may become divorced as the magnesium solid solution may form over the same phase separating before eutectic solidification. The other phase of the eutectic mixture, $\text{Mg}_{17}\text{Al}_{12}$, may nucleate on the aluminate which may have separated from the alumina particle due to fluid flow during infiltration and form a network.

The extent of reaction between the matrix and the particles could be controlled by controlling the processing time. The composite containing 21 vol% alumina has relatively much less aluminate which is apparent from the absence of (311) peak of MgAl_2O_4 in the diffraction pattern shown in Fig. 5.11.

The hardness of the composites based on commercial magnesium is significantly more than the hardness of commercial magnesium as shown in Fig. 5.4. The microhardness in the matrix of these composites show that the matrix magnesium has strengthened significantly in both the composites containing 21 and 23 vol% alumina, thereby confirming significant solid solution strengthening by aluminium resulting from matrix-particle reaction. The extent of this reaction is more in the composite containing 23 vol% alumina as the microhardness of magnesium solid solution in this composite is higher than that observed in the composite containing 21 vol% alumina. In the composite containing 23 vol% of alumina the measurement of microhardness could not be carried out on the phase or phase mixture observed in the network. The hardness of Al_2O_3 particles in these composite are significantly higher than the microhardness of the magnesium solid solution.

It is interesting to note that the volume loss of composite containing 21 vol% of alumina as shown in Fig. 5.14, varies over a relatively narrow range compared to that in composite containing 23 vol% of alumina as shown in Fig. 5.15. It should be noted that the difference in alumina content between these two composites based on commercial magnesium is estimated to be only 2% but there is a significant difference in the volume loss observed during dry sliding wear in these two composites. The composite containing 21 vol% of alumina has relatively lower amount of MgAl_2O_4 below the limit that could be indicated by X-ray diffraction, but it has shown relatively lower wear rate compared to the composites containing 23 vol% of alumina in the entire load range between 2.5 to 5.5 kg. Thus it appears that the amount of MgAl_2O_4 in a composite containing alumina may play a critical role in determining the wear behaviour of a composite. The variation of wear rate in the composite containing 21 vol% alumina with load is linear following Archard's law. In commercial magnesium the wear rate is an order of magnitude higher than that observed

in the composite containing 21 vol% alumina. The composite containing 23 vol% of alumina has shown a lower wear rate in the composite at the lower load of 2.5 kg, about half of that observed in commercial magnesium. But at loads of 3.5 kg and higher, there is hardly any difference in wear rate of the composite from that in commercial magnesium. Both the material - the commercial magnesium and the composite containing 23 vol% of alumina, show nonlinear variation of wear rate with load in violation of Archard's law. In commercial magnesium the wear rate increases with load but at higher load of 5.5 kg the wear rate may taper off or even reduce slightly. At higher loads frictional heating may result in slight melting or softening of magnesium on the sliding surface and it acts as a lubricant. Bulging of the pin at the sliding surface has been observed in commercial magnesium and it may confirm softening of magnesium at such high load. The observed friction coefficient also indicate the possibility of local melting and softening. At lower load of 2.5 kg generally the friction coefficient is high for both the types of materials - the commercial magnesium and the composites based on it as shown in Fig.5.20 to 5.22. At a load of 2.5 kg, the friction coefficient in commercial magnesium is around 0.46 but those in composites containing 21 and 23 vol% alumina are 0.83 and 0.70 respectively. It appears that local melting and softening is there in commercial magnesium even at this low load. But in composites, the presence of alumina in substantial amount may have reduced the extent of melting for it to play a significant role. In the composite containing 23 vol% alumina, relatively higher inhomogeneity in distribution of alumina particles may also be responsible for softening of magnesium in the particle deficient area similar to that in commercial magnesium. When the load increases, the friction coefficient reduces and at a load of 5.5 kg, the average friction coefficient of commercial magnesium is around 0.34 as shown in Fig. 5.23. The corresponding value in composite containing 23 vol% of alumina is similar, around 0.36 as shown in Fig. 5.25. But the average friction coefficient did not reduce below 0.60 even at the load of 5.5 kg in the composite containing 21 vol% of alumina as shown in Fig.5.24. It may indicate that this composite containing 21 vol% alumina has not softened to the same extent even at higher load of 5.5 kg, as it has been observed either in commercial magnesium or the composites containing 23 vol% of alumina. This difference in behaviour could be attributed to near absence of aluminate and relatively better particle distribution in the composite containing 21 vol% of alumina.

An examination of the sliding surface and wear debris shows that the sliding surface is covered with a transfer layer containing oxides and the softening of magnesium may have helped this compaction process. At higher loads the transfer layer flakes off creating a recessed region. The wear debris accumulates, gets compacted to reform the layer again in this region. At higher loads some bright metallic particles could also be observed which may be due to squeezing out of soft magnesium into the transfer layer during compaction in the process of formation of transfer layer or due to a small extent of metallic wear. However, the wear observed is primarily oxidative.

The wear coefficient that has been defined as the wear rate per unit area of contact, may be misleading for the purpose of comparison of wear behaviour of the materials. The composite containing 21 vol% of alumina shows a wear rate that is an order of magnitude lower than that in commercial magnesium. Since, the composite has higher hardness and consequently, a lower real area of contact, the wear coefficient of the composite is 0.30×10^{-4} similar to that in commercial magnesium which has wear coefficient of 0.36×10^{-4} . However, the composites containing 23 vol% of alumina has wear coefficient which is an order of magnitude higher than that in either commercial magnesium or the composite containing 21 vol% of alumina. However, the observed wear rates in the composite containing 23 vol% of alumina are similar to those observed in commercial magnesium. But the hardness of the composite being considerably higher than that of commercial magnesium, the real area of contact is expected to be significantly lower in the composite and it is responsible for increasing the wear coefficient. Thus the wear coefficient of the composite containing 23 vol% of alumina is higher than that in commercial magnesium.

The microstructure of AZ91 alloy based composites containing 24 vol% of alumina has inhomogeneous particle distribution resulting in particle rich and particle deficient regions as it has been observed also in commercial magnesium based composites. The inhomogeneity of particle distribution may be due to pushing of particles by the infiltrating molten alloy stream for making its way. This effect is observed even in infiltrated preforms although its better bonding could hold the dispersoids in place (Kamado, Kojima, 1997). In the particle deficient region, the solidification of the alloy is clearly dendritic and the last

freezing liquid has undergone eutectic solidification resulting in lamellar eutectic containing magnesium solid solution and $Mg_{17}Al_{12}$ as shown in Fig.5.7.and 5.8. It may be remembered that at higher applied pressure of squeeze casting eutectic temperature increases but eutectic composition shifts to lower aluminium content (Hu and Luo, 1997). In addition to these phases there are other phases which could be $MgAl_2O_4$ and/or $Mg_{32}(Al,Zn)_{49}$, as shown in Fig.5.9. The X-ray diffraction pattern as shown in Fig 5.11, clearly reveals the presence of Al_2O_3 and magnesium solid solution. Apart from these phases the composite containing 23 vol% alumina has $MgAl_2O_4$ as indicated by its (311) peak in the x-ray diffraction pattern of this composite as shown in Fig.5.11(b). But the composite containing 21 vol% of alumina does not show any presence of $MgAl_2O_4$ as expected from Mg-Al-O ternary phase diagram. MgO which is expected from phase diagram, is present in both the composites. The microstructure shows the presence of $Mg_{17}Al_{12}$ but it could not be looked for in the X-ray diffraction pattern as it is not available. The irregular surface contour of Al_2O_3 particles indicate that there is reaction between the matrix and the alumina particles during processing at high temperature. Therefore, the presence of $MgAl_2O_4$ and/or MgO is expected. However, it has been claimed that the presence of aluminium in magnesium alloy decreases the extent of matrix-particle reaction and results in better bonding of alumina particles with the matrix alloy in the composites based on magnesium alloy (Wilks, King and Wardlow, 1997).

The hardness of the composites containing 14, 16 and 24 vol% of alumina show that hardness increases with increasing amount of alumina particles as shown in Table 5.5. It may be noted that the hardness of the composite containing 24 vol% alumina is significantly higher than that observed in commercial magnesium based composite containing 21 or 23 vol% of alumina and it may be attributed to higher matrix hardness of AZ91 alloy. The microhardness of magnesium solid solution as given in Table 5.6, indicates that it increases with increasing amount of alumina in general which is an indication of solute segregation aggravated by reaction between the matrix and the alumina particles even when the matrix is AZ91 alloy. The composite containing 14 and 16 vol% of alumina has higher microhardness of alumina particles and the microhardnesses of magnesium solid solution are similar to that in the commercial magnesium based composite containing 21 vol% alumina. But the composite containing 24 vol% alumina

show a relatively lower hardness for Al_2O_3 particles and a higher microhardness in magnesium solid solution that could be attributed to significantly more chemical reaction between the particles and the matrix in this composite.

The composite containing 16 vol% of alumina has significantly lower volume loss in wear at different loads compared those in the composites containing 14 and 24 vol% as shown in Fig. 5.26 to 5.28. Earlier studies have revealed very weak dependence of volume loss in wear on alumina content in AZ91 alloy based composite (Shook and Green, 1985). The wear rates observed at different loads in the composite containing 16 vol% of alumina is also considerably lower than the other two AZ91 alloy based composites. If one compares the wear rates observed in the composite containing 16 vol% alumina with those observed in commercial magnesium based composites, the former composite has wear rates lower than the lowest observed in commercial magnesium based composites, i.e., in the composite containing 21 vol% alumina. This could be due to higher matrix hardness of the alloy. However, the composite containing 24 vol% of alumina has wear rates similar to those observed in the commercial magnesium based composite containing 23 vol% of alumina. But the composite containing 14 vol% of alumina has relatively lower wear rates compared to those in the composite containing 24 vol% of alumina. Thus, it appears that the composite based on commercial magnesium containing 21 vol% alumina and that containing 16 vol% alumina in the matrix of AZ91 alloy have better particle distribution and near absence of MgAl_2O_4 which are responsible for lower wear rates observed.

The sliding surface of AZ91 alloy based composites under lower load show a large number of voids from where alumina particles appear to have debonded as shown in Fig. 5.4 (a). such voids are not seen in the commercial magnesium based composites. It is possible that the relatively softer matrix of these composites may have flowed over the alumina particles during sliding and covered these particles before they could debond. At higher loads such voids are not visible even in AZ91 alloy based composites as shown in Fig. 5.4.1(a) and (b), which may be due to higher plastic flow at the sliding surface. There are some plowing marks in certain regions of the sliding surface and it may indicate a relatively slower rate of formation of the transfer layer. The transfer layer often flakes off from certain regions generating wear debris as shown Fig. 5.4.2 (b). The formation of

transfer layers containing oxides under the loads employed in this investigation show that the wear is primarily oxidative.

The wear coefficient in the composite containing 16 vol% of alumina is 0.21×10^{-4} that is the lowest wear coefficient observed amongst the composites investigated in this study, containing alumina in the matrices of commercial magnesium or AZ91 alloy. However, the wear coefficient in the composites containing 14 and 24 vol% alumina in AZ91 alloy are 2.25×10^{-4} and 3.89×10^{-4} respectively, which is due to high hardness of the composites resulting in lower real area of contact although the wear rates in these composites are relatively lower than that in commercial magnesium which shows a wear rate of 0.36×10^{-4} .

The results of the present investigation on magnesium or AZ91 alloy based composites containing alumina particles have shown that particle-matrix reaction may play a crucial role in determining the wear behaviour of composite containing alumina undergoing dry sliding wear. The distribution of particles are important but this effect has not been investigated qualitatively.

The results reported in this chapter indicate that for both the composites based on commercial magnesium and AZ91 alloy, the average coefficient of friction decreases with increasing load. A decrease in coefficient of friction with increasing load has also been observed in the composites containing steelwool as reported in chapter-4. Earlier workers have also reported similar results (Yang and Chang, 1989). If one compares Fig.5.23 with Fig.4.40 (a), it appears that vacuum cast magnesium has relatively higher coefficient of friction at lower load compared to that in squeeze cast magnesium. But the composites based on both the commercial magnesium and AZ91 alloy containing alumina have relatively higher coefficient of friction at lower load as compared to those observed in the corresponding matrix. This may be due to direct contact of alumina against steel counterface which appears to form strong junctions compared to magnesium-steel junctions. The exposed alumina particles on the sliding surface may also lead to their debonding. But at higher loads, the alumina may get covered with magnesium or its alloys in the matrix and the coefficient of friction decreases. The AZ91 alloy based composite

containing 24 vol% alumina has shown a relatively lower average friction which is indicative of the alumina getting covered by magnesium during sliding even at the lowest load of 2.5 kg. In other composites containing 14 and 16 vol% alumina this effect is not apparent at lower loads. Particle distribution may make this difference. If the dispersoids are well distributed it may restrain flow of magnesium particularly at lower load. But inhomogeneous distribution may result in easy flow of magnesium from the areas deficient in alumina. Particle debonding may also lead to lowering of coefficient of friction.

The wear volume of commercial magnesium based composite may decrease significantly depending on matrix-particle reaction during processing. If aluminate is formed during processing the volume loss in wear remains as high as in commercial magnesium. But even if there is interfacial reaction to produce MgO , there may be considerable decrease in volume loss. The composite containing 21 vol% alumina has wear volume about one tenth that of commercial magnesium at similar load. The wear rate also is affected by the presence of aluminate as one observes similar wear rates for the commercial magnesium and the composite containing 23 vol% alumina, particularly at higher loads. But in the composite without any significant presence of aluminate, shows that the wear rate decreases by an order of magnitude compared to that in commercial magnesium. Similar decrease of wear rate with reinforcement in a composite has also been observed by other workers (Roy, Venkatraman, Bhanuprasad, Mahajan and Sundararajan, 1992; Zamzam, 1989). If one observes the variation of wear rate with load as shown in Fig. 5.17 for squeeze cast magnesium, there is no discontinuity in the nonlinear variation. The load range for the tests are here different than that used for steelwool reinforced composites in chapter-4. The higher load range has been used because at lower loads one does not get enough volume loss for measurement in the composites reinforced with alumina. The discontinuity in wear rate has been observed in commercial magnesium and the composites based on it containing steelwool, between the loads of 1.5 kg and 2 kg. But the tests here start at a load of 2.5 kg.

Similarly, the volume loss in wear in AZ91 alloy based composites appears to be generally lower than those in composites based on commercial magnesium. The lowest volume loss at higher load has been observed in the AZ91 alloy based composite

containing 16 vol% alumina, lower than that observed in commercial magnesium based composite containing 21 vol% alumina. The wear rate is also the lowest in the AZ91 alloy based composite containing 16 vol% alumina, an order of magnitude lower than that in the commercial magnesium based composite containing 21 vol% alumina. In the other two AZ91 alloy based composites the wear rates are relatively higher. But there is no discontinuity in wear rates and the variation in wear rate with load is nonlinear with the exception of the composite containing 24 vol% alumina which has shown relatively higher wear loss and wear rates compared to other composites. Thus, it is clear from the above discussion that reinforcing both commercial magnesium and AZ91 alloy with alumina may provide composites with significantly lower volume loss and wear rate when compared those observed in either the composites containing steelwool or the corresponding matrix materials at similar loads. But the matrix-particle reaction and its product may be of critical importance as it has been observed that aluminate may significantly impair wear resistance. In general, the composites based on alloy matrix have relatively lower wear rates compared to composites based on commercial magnesium.

CHAPTER-6

HYBRID COMPOSITE BEARING GRAPHITE AND ALUMINA

This chapter describes the results on processing of magnesium and AZ91 alloy matrix composites containing both alumina and graphite and on their mechanical and tribological properties. In the end, the results have been discussed to develop a coherent understanding of these composites.

6.1 Results

1.1 Chemical Composition

The chemical compositions of AZ91 alloy based hybrid composites containing both graphite and alumina have been determined in wt% with respect to the weight of the composite and the results are reported in Table-6.1.

Table 6.1
Chemical Composition of AZ91 Alloy Based Hybrid Composites

Materials	Chemical Composition wt%			
	Al	Zn	Fe	Mn
I.AZ91 alloy based hybrid composite	8.48	0.54	0.033	0.15

6.1.2 Density of Composites and Particle Content

The densities of the composites, ρ_{com} , and the constituents - matrix, ρ_m , alumina, ρ_A , and graphite, ρ_{gr} , have been determined and the volume fractions of alumina and graphite in a composite, f_A and f_{gr} respectively, have been estimated using the following equations.

$$f_A = \frac{\rho_{com} - \rho_m(1 - x) - \rho_{gr}(x)}{\rho_A - \rho_{gr}} \quad (6.1)$$

$$x = f_A + f_{gr} \quad (6.2)$$

Where, x is the total volume fraction of particles that includes both alumina and graphite as determined by point counting technique. The density of matrix, ρ_m , has been taken as the density of commercial magnesium in magnesium based hybrid composites and the density of AZ91 alloy for AZ91 alloy based hybrid composites. The results are summarized in Table 6.2.

Table 6.2

Densities of Composites and Constituents and Estimated Particle Contents

Sample number	Sample designation	Matrix	Density kg/m ³ x10 ³	Alumina and Graphite (Vol%)
1	Mg	Mg	1.75	00 0.0
2	Sq111A	Mg	2.01	13 0.3
3	Sq111B	Mg	2.06	15 0.3
4	Sq111C	Mg	2.10	18 0.3
5	Sq1VA	AZ91	2.05	16 0.4
6	Sq1VB	AZ91	2.09	17 0.4
7	Sq1VC	AZ91	2.14	19 0.4

6.1.3 Microstructure of the Composites

The microstructures of alumina and graphite reinforced composites based on commercial magnesium and AZ91 alloy have been examined under optical microscope to find the amount and the distribution of phases in the matrix alloy, in the context of phase diagram and also the volume fraction of reinforcements as determined from measured densities given in Table 6.2.

(a) Magnesium-Alumina-Graphite Composites

Figure 6.1. shows the microstructures of commercial magnesium based hybrid composites containing 13 vol% alumina and 0.3 vol% graphite. The microstructure shows particle rich areas where particle distribution is fairly uniform. At higher magnification of X62.5 and X625 (X25 and X250 magnified 2.5 times) it is observed

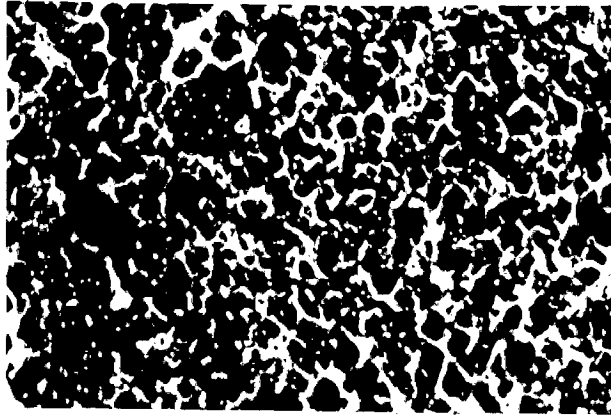


Fig.6.1 Microstructure of Squeeze cast hybrid composite based on commercial magnesium containing 13 vol % of alumina and ~0.3 vol% of graphite, showing fairly uniform particle distribution, X62.5.

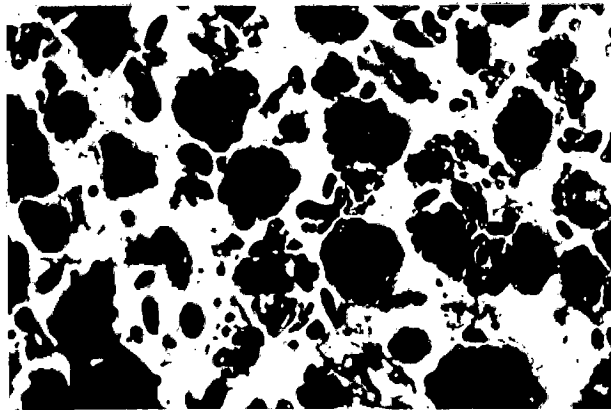


Fig.6.2 Microstructure of Squeeze cast hybrid composite based on commercial magnesium containing 13 vol % of alumina and ~0.3 vol% of graphite, showing longer but smaller graphite particles along with a relatively darker phase in the bright matrix, X250.

that smaller flakes of graphite are there between relatively larger particles of alumina as shown in Figs. 6.2. and 6.3. It may also be noted that dark phase has formed at the boundary of the particles.

Fig. 6.4. shows the microstructure of a commercial magnesium based composite which contains 15 vol% alumina and 0.3 vol% graphite. It is observed that the graphite flakes are confined only in certain regions where, at higher magnification, one may observe significantly more graphite than 0.3 vol% as shown in Fig. 6.5. and 6.6. At still higher magnification of X625 it is observed that dark phases are forming around the alumina particles and also in the matrix region between the particles. Formation of this dark phase could be evidence of reaction between alumina particles and magnesium matrix because the original matrix of commercial magnesium does not contain sufficient alloying elements to result in so much of precipitate.

Fig. 6.7. shows the microstructure of commercial magnesium based composite containing 18 vol% of alumina and 0.3 vol% graphite. The microstructure contains both particle rich and particle deficient regions. At higher magnification of X250 it is observed that the particles are surrounded by a relatively darker area of last freezing liquid, as shown in Fig. 6.8. The solute content of the last freezing liquid may have considerably higher aluminium released by reduction of alumina particles by molten magnesium during processing at higher temperature. One may also note that the graphite flakes are also surrounded by the relatively darker phase as shown in Fig. 6.9. The particle boundaries are highly irregular which may indicate matrix-particle reaction.

(b) AZ91 Alloy-Alumina-Graphite Composites

Figure 6.10. shows AZ91 alloy based hybrid composite containing 16 vol% alumina and 0.4 vol% graphite. The microstructure shows highly inhomogeneous distribution of particles. In the particle deficient regions the microstructure reveals the formation of aluminium rich phase at the boundary between the primary dendrites of magnesium solid solution as shown in Fig. 6.11(a) and (b). The dendrites are more clearly identified in this region where the particle concentration is relatively low. The graphite flakes and the alumina particles are surrounded by solute rich last freezing

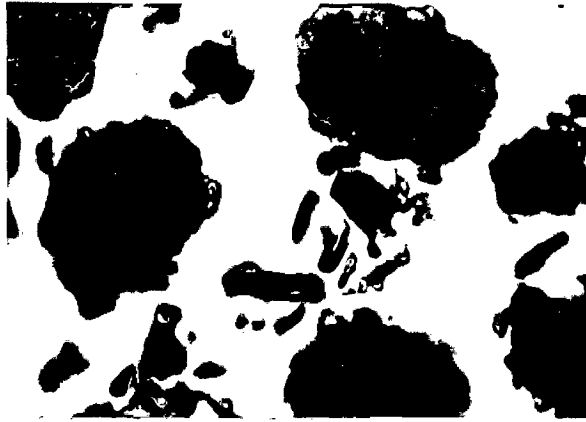


Fig.6.3 Microstructure of Squeeze cast hybrid composite based on commercial magnesium containing 13 vol % of alumina and ~0.3 vol% of graphite, show particle rich areas where particle distribution is fairly uniform, X625.

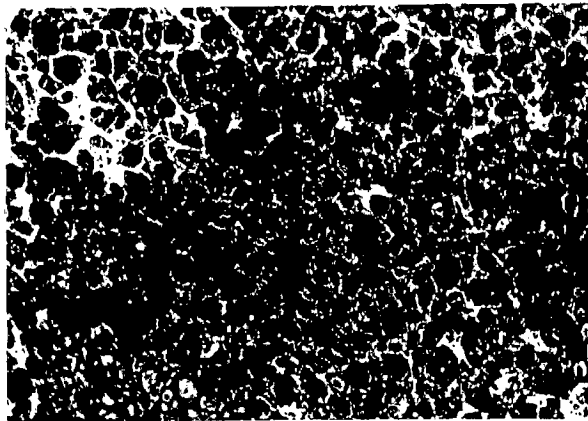


Fig.6.4 Microstructure of Squeeze cast hybrid composite based on commercial magnesium containing 15 vol % of alumina and ~0.3 vol% of graphite, showing darker regions of graphite flakes only in certain regions, X62.5.

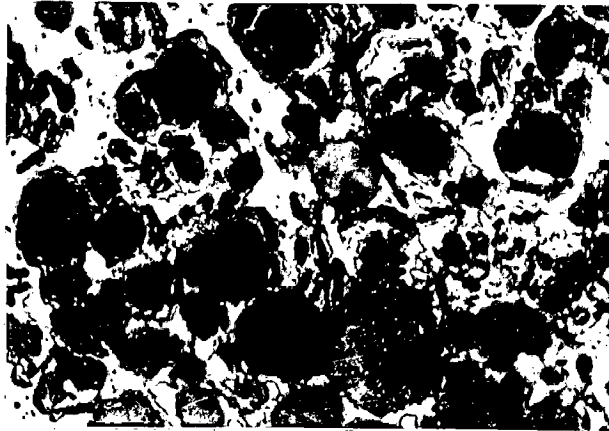


Fig.6.5 Microstructure of Squeeze cast hybrid composite based on commercial magnesium containing 15 vol % of alumina and ~0.3 vol% of graphite, showing the graphite flakes and solute rich phase, X250.

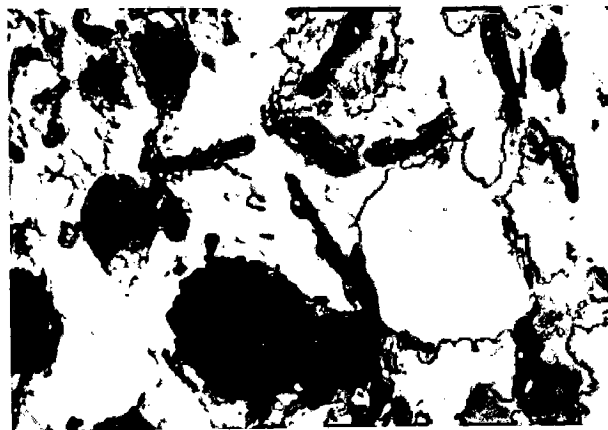


Fig.6.6 Microstructure of Squeeze cast hybrid composite based on commercial magnesium containing 15 vol % of alumina and ~0.3 vol% of graphite, showing dark graphite flakes and less dark solute rich phase in bright matrix, X625.

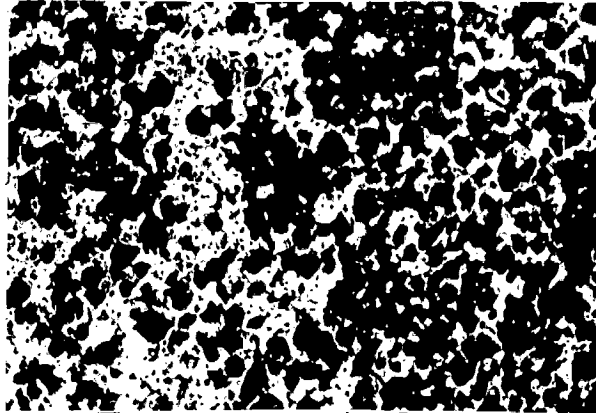


Fig.6.7 Microstructure of Squeeze cast hybrid composite based on commercial magnesium containing 18 vol % of alumina and ~0.3 vol% of graphite, showing both particle rich and particle deficient regions, X62.5.

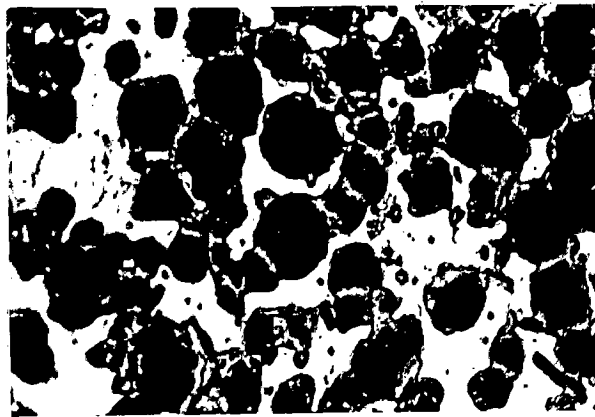


Fig.6.8 Microstructure of Squeeze cast hybrid composite based on commercial magnesium containing 18 vol % of alumina and ~ 0.3 vol% of graphite, showing relatively darker phase surrounding the alumina particles, X250.

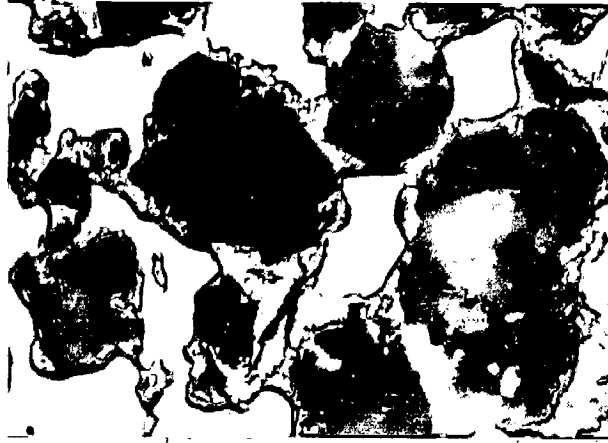


Fig.6.9 Microstructure of Squeeze cast hybrid composite based on commercial magnesium containing 18 vol % of alumina and ~ 0.3 vol% of graphite, showing graphite particles in the relatively darker solute rich area and irregular particle boundaries, X625.

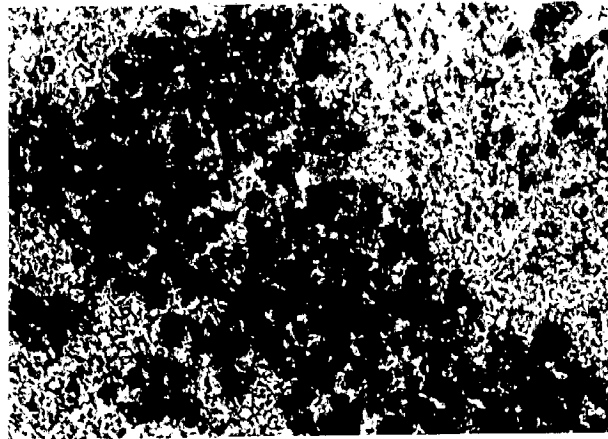


Fig.6.10 Microstructure of Squeeze cast hybrid composite based on AZ91 alloy containing 16 vol % of alumina and ~ 0.4 vol% of graphite, show the highly inhomogeneous particle distribution characterised by particle rich and the particle deficient regions in the matrix of AZ91 alloy, X62.5

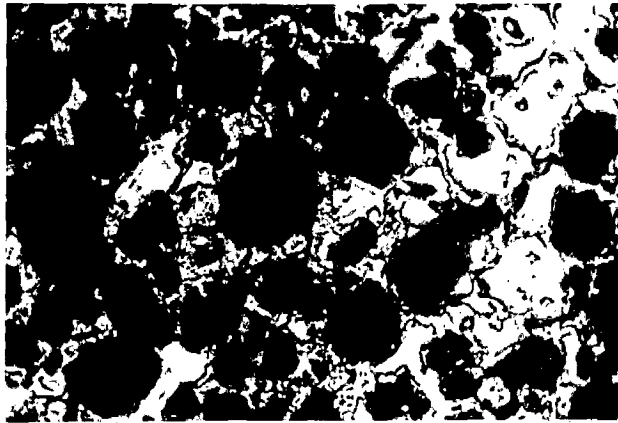


Fig.6.11(a) Microstructure of Squeeze cast hybrid composite based on AZ91 alloy, containing 16 vol % of alumina and ~ 0.4 vol% of graphite, showing dendritic solidification in particle areas, X250.

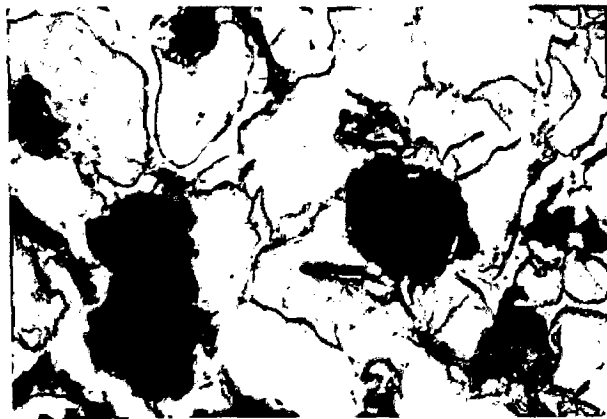


Fig.6.11(b) Microstructure of Squeeze cast hybrid composite based on AZ91 alloy, containing 16 vol % of alumina and ~ 0.4 vol% of graphite, showing the formation of relatively dark solute rich phase at the boundary between the primary of magnesium solid solution, X625.

liquid as it has been observed in Figs. 6.7. and 6.8, for commercial magnesium based composite containing alumina.

Fig. 6.12. shows the microstructure of AZ91 alloy base composite containing 17 vol% alumina and 0.4 vol% graphite. The microstructure shows inhomogeneous distribution of particles. At a higher magnification it is observed that lamellar eutectic has formed in the particle rich area as shown in Figs. 6.13. and 6.14. The particle boundaries are highly irregular which may indicate matrix-particle reaction.

6.1.4 Electron Probe Microanalysis

EPMA analysis has been carried out in commercial magnesium based hybrid composite containing 18 vol% alumina and 0.3 vol% graphite. It has already been observed in section 5.1.3 that commercial magnesium containing alumina is resulting in reaction of alumina particles with magnesium during processing at high temperature. It is expected that a similar phenomena may take place also during the processing of hybrid composites. Figs. 6.15 (a),(b) and (c). shows the line scan between the boundaries of two alumina particles. It is observed from the microstructure that the particles are surrounded by solute rich phase which is also indicated by enhanced aluminium signals near the boundary of alumina particles and magnesium solid solution is lying in the middle between aluminium rich areas as shown in Fig. 6.15 (a). The line scan showing distribution aluminium across gray areas next to white area as shown in Figure 6.15 (b) it is observed that the magnesium solid solution which represented by the bright area as relatively lower aluminium compared to the gray area. The network of gray area also contains higher aluminium and Zinc as shown in the line scan Figure 6.15 (c). The analysis of aluminium-magnesium-zinc in the gray area whether in a form of network or particles, as the same composition with atomic ratio of aluminium to magnesium to zinc as 2:14:1. The atom does not match with $Mg_{32}(Al,Zn)_{49}$ which could be expected on the bases of phase diagram.

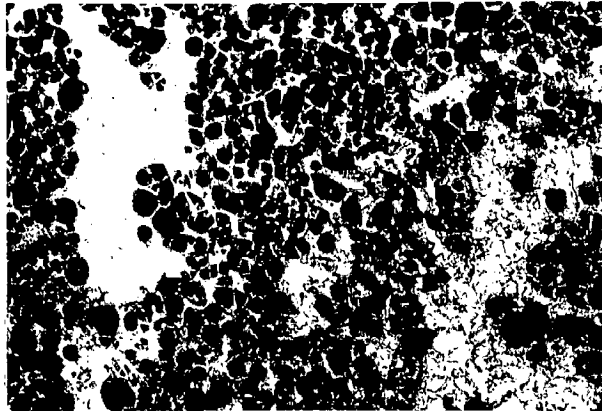


Fig.6.12 Microstructure of Squeeze cast hybrid composite based on AZ91 alloy, containing 17 vol % of alumina and ~0.4 vol% of graphite, showing inhomogeneous distribution of particles, X62.5.

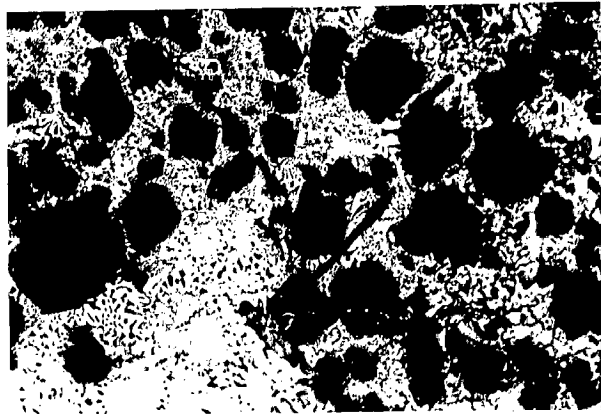


Fig.6.13 Microstructure of Squeeze cast hybrid composite based on AZ91 alloy containing 17 vol % of alumina and ~0.4 vol% of graphite, showing the lamellar eutectic formed in the last freezing liquid, X250.

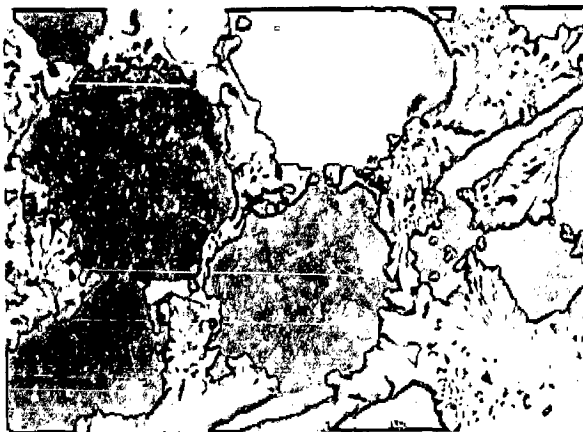


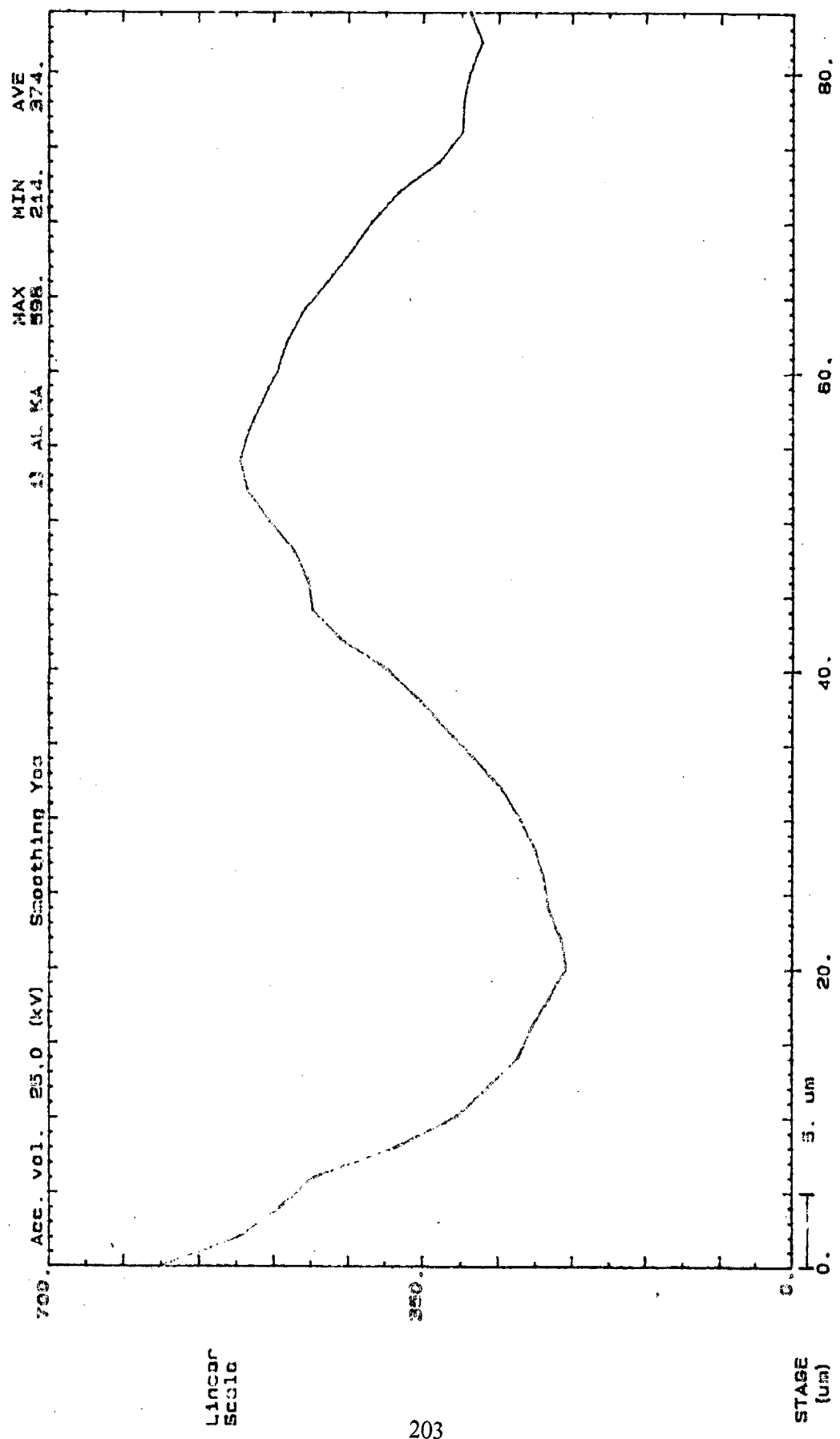
Fig.6.14 Microstructure of Squeeze cast hybrid composite based on AZ91 alloy containing 17 vol % of alumina and 0.4 vol% of graphite, showing the lamellar eutectic and irregular boundaries of alumina particles, X625.

LINE ANALYSIS

22-AUG-98

INTENSITY
(Counts)

File no. : 49
Comment : 9-AL



Acc. vol. 25.0 (kV) Smoothing 300
AL KA
MAX 598
MIN 214
AVE 374

Linear Scale

Fig.6.15(a) EPMA line scan shows distribution of aluminum across gray areas, next to white area.

LINE ANALYSIS

22-AUG-84

INTENSITY
(Counts)

File no. : 48
Comment : 10-MG

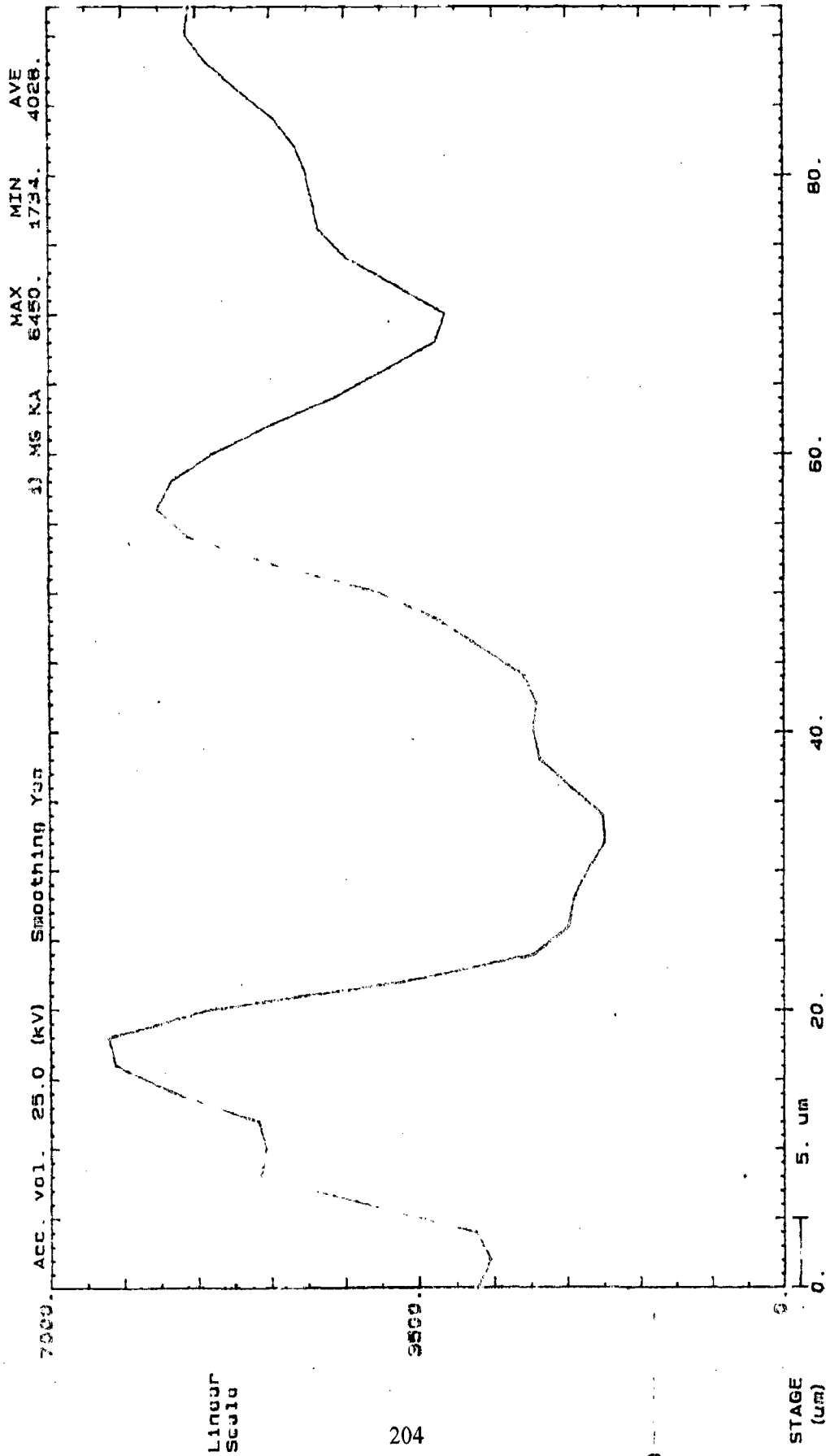


Fig.6.15(b) EPMA line scan shows that the magnesium solid solution which represented by the bright area.

Table 6.3**Composition of Magnesium Solid Solution (White Area)**

Element	Wt (%)	Wt% normalized to 100%
Al	0.662	1.649
Mg	39.425	98.170
Zn	0.073	0.182
Total	40.160	100.000

Table 6.3, indicates that there is more aluminium in magnesium in the composite than that present in commercial magnesium as shown Table 6.1. There is a small amount of zinc also in the solid solution.

6.1.5 X-Ray Diffraction Studies

The X-ray diffraction peaks in the interval of 2θ values between 31 and 71 degrees for the samples of hybrid composites based on commercial magnesium have been compared with the peaks obtained from commercial magnesium as shown in Fig.5.11, to identify the (hkl) of the different peaks obtained from the magnesium solid solution in the composites. The lattice parameters of the magnesium solid solution in different commercial magnesium based composites are shown in Table 6.4. Similarly, alumina peaks have been identified by comparing with the pattern obtained from alumina used in this investigation. A similar exercise has been carried out for AZ91 based hybrid composites and the lattice parameters for the magnesium solid solution have also been reported in Table 6.4. In the composites based on commercial magnesium the different peaks originating from different planes of the lattice of magnesium solid solution have been identified as shown in Figs. 6.16 (b), (a) and (c). In the composite containing 15 vol% alumina one observes the strongest peak from (311) plane of $MgAl_2O_4$. but this peak is not observed in the other two hybrid composites containing 13 or 18 vol% alumina. In the hybrid composites based on commercial magnesium, there are also peaks at $2\theta = 62.6$ and $2\theta = 43$ degrees which may be attributed respectively to diffraction from (220) having intensity $I/I_0 = 52$ and (200) of MgO having I/I_0 value of 100. But in composites based on AZ91 alloy these peaks may coincide with those coming from (103) of magnesium solid solution and $Mg_{32}(Al, Zn)_{49}$ respectively, if present. It appears that MgO may have formed due to

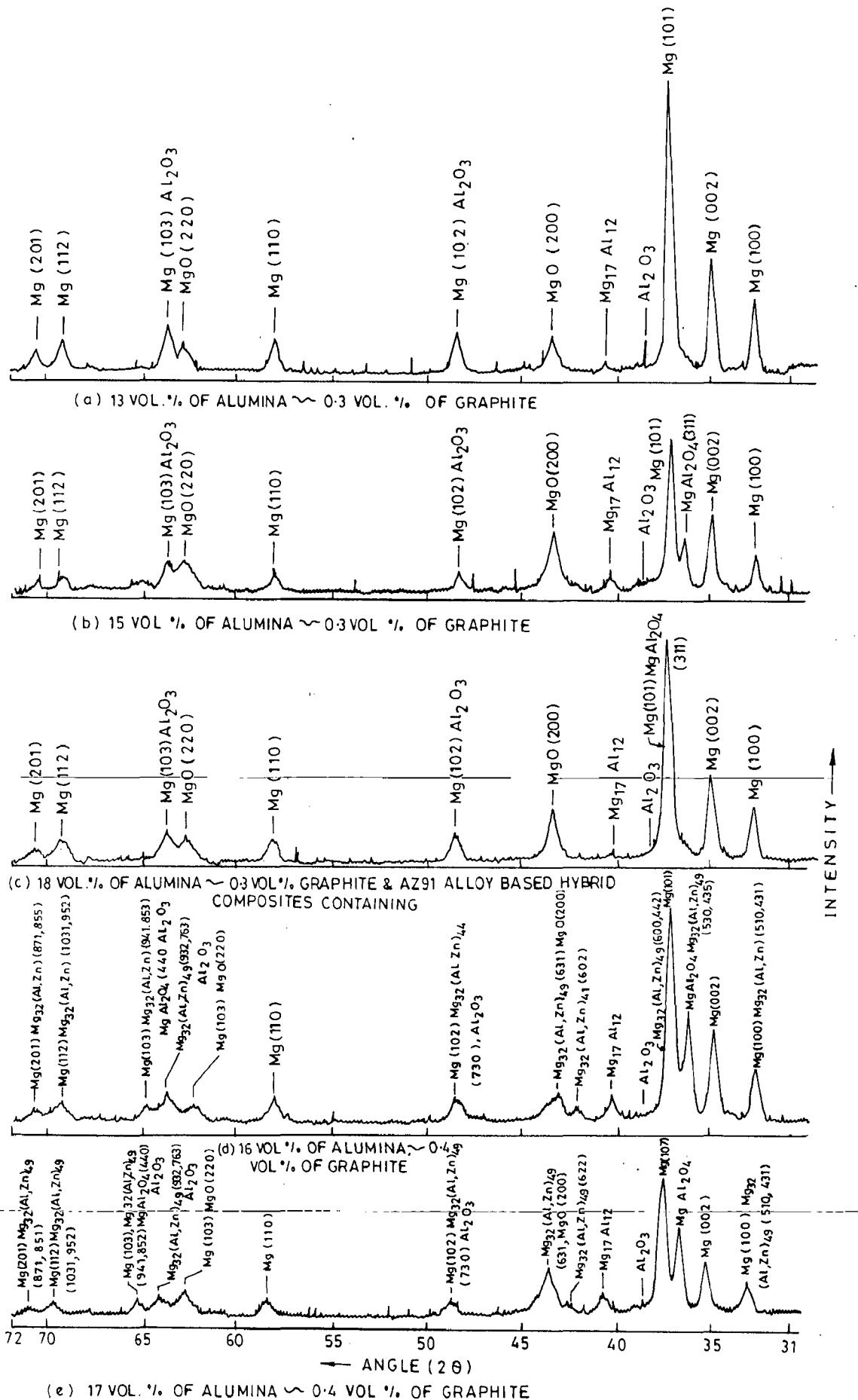


FIG. 6-16 X-RAY DIFFRACTION PATTERNS OF COMMERCIAL MAGNESIUM & AZ91 ALLOY BASED HYBRID COMPOSITES CONTAINING

reaction between molten magnesium and alumina particles during processing. The hybrid composites containing 16 and 17 vol% alumina show the (311) peak of $MgAl_2O_4$. There is a peak at $2\theta = 40.6$ in the patterns of AZ91 alloy based hybrid composites similar to that observed in AZ91 alloy based composite containing only alumina and it has been attributed to $Mg_{17}Al_{12}$ or $AlMnFe$.

Table 6.4
Lattice Parameters for Magnesium Solid Solution in Hybrid Composites

Material	Alumina content Vol%	a	c
Magnesium	00	3.208	5.1073
Magnesium-Alumina-Graphite	13	3.176	5.1580
Magnesium-Alumina-Graphite	15	3.176	5.1580
Magnesium-Alumina-Graphite	18	3.176	5.1580
AZ91Alloy-Alumina-Graphite	16	3.167	5.0942
AZ91Alloy-Alumina-Graphite	17	3.167	5.0942

6.1.6 Hardness of the composites

The macro-and micro-hardnesses have been measured and expressed in terms of Brinell and Vickers hardness respectively for commercial magnesium based and AZ91 alloy based composites.

The Brinell hardness of the commercial magnesium based composite and AZ91 alloy based composite containing different volume percents of particle are given in Table-6.5. Alumina is a hard constituent and the variation of Brinell hardness with alumina content in commercial magnesium based composites is shown in Fig. 6.17. The volume percent of graphite is about 0.3 vol% in these composites and graphite, being rest, is expected to lower the hardness of a composite. Since the composites have similar graphite content, hardness increases with alumina content in the composites as shown in Fig. 6.17. In AZ91 alloy based hybrid composites, the volume percent of graphite is about 0.4 and these composites have relatively higher hardness compared to magnesium based hybrid composites investigated here, as shown in Fig. 6.18.

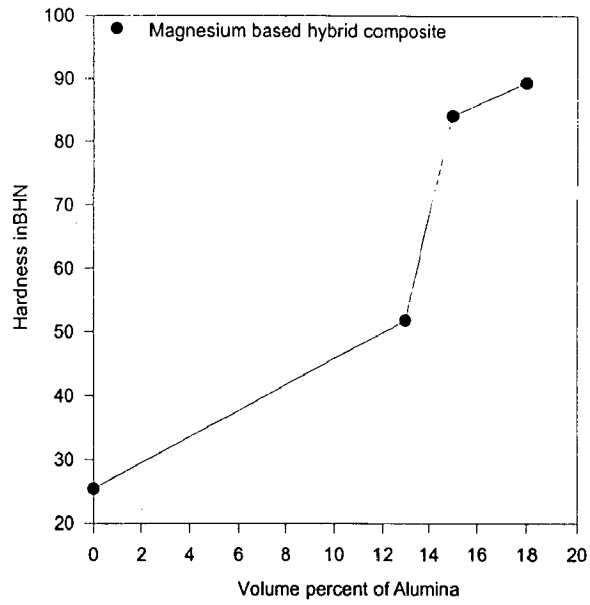


Fig.6.17 The variation of Brinell hardness with volume percent of alumina particles in commercial magnesium based hybrid composites containing ~0.3 vol.% of graphite.

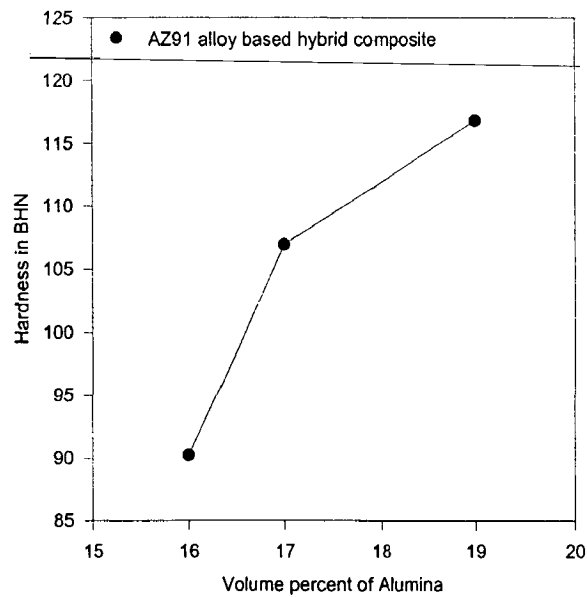


Fig.6.18 The variation of Brinell hardness with volume percent of alumina particles in AZ91 alloy based hybrid composite containing ~0.4 vol.% of graphite.

Table-6.5

Brinell Hardness of the Mg-Alumina Graphite Composites and AZ91-Alumina Graphite Composites

Sample number	Sample designation	Matrix	Alumina and Graphite content (vol%)		Brinell hardness (HB)
1	Mg	Mg	00	0.0	25.4
2	Sq111A	Mg	13	0.3	51.8
3	Sq111B	Mg	15	0.3	84.12
4	Sq111C	Mg	18	0.3	89.34
5	Sq1VA	AZ91	16	0.4	90.24
6	Sq1VB	AZ91	17	0.4	106.9
7	Sq1VC	AZ91	19	0.4	116.8

The Vickers microhardnesses for magnesium based hybrid composites and AZ91 alloy based hybrid composites have been measured. The Vickers hardness of these cast composites containing different particle contents are given in Table-6.6.

Table-6.6

Vickers Hardness of Mg-Alumina-Graphite Composites and AZ91-Alumina-Graphite Composites

Sample number	Sample designation	Matrix	Alumina & Graphite content Vol %		Vickers microhardness HV Primary phase/Alumina	
1	Mg	Mg	00	0.0	54.20	****
2	Sq111A	Mg	13	0.3	75.48	695.8
3	Sq111B	Mg	15	0.3	76.94	549.4
4	Sq111C	Mg	18	0.3	94.46	454.6
5	Sq1VA	AZ91	16	0.4	97.68	638.8
6	Sq1VB	AZ91	17	0.4	103.74	584.8
7	Sq1VC	AZ91	19	0.4	101.98	567.2

Fig. 6.19 shows the variation of microhardness in VHN with volume percent of alumina in squeeze cast magnesium based hybrid composite. It is observed that the hardness of primary phase increases by a little with alumina content. But it is

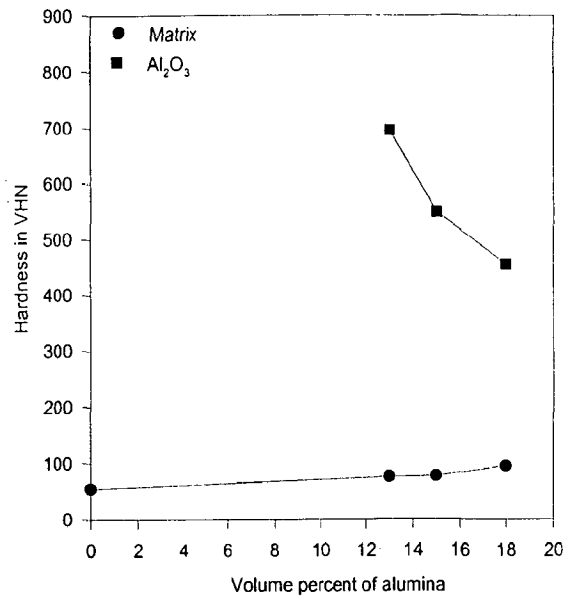


Fig.6.19 The variation of vickers hardness with volume percent of alumina particles in commercial magnesium based hybrid composites containing 0.3 vol.% of graphite.

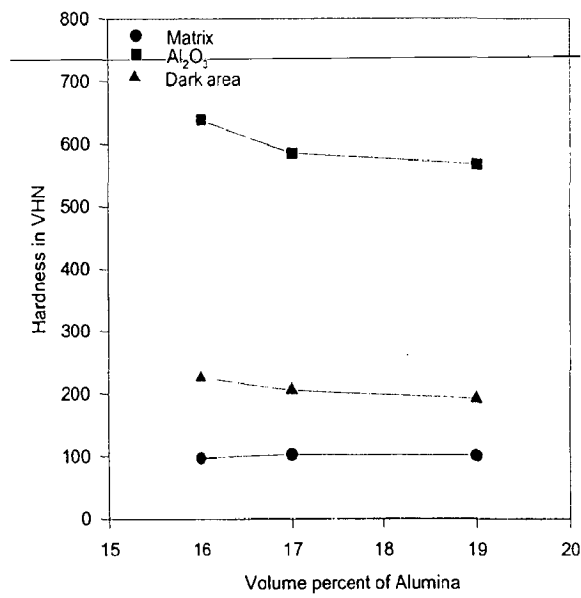


Fig.6.20 The variation of Vickers hardness with volume percent of alumina particles in AZ91 alloy based hybrid composites containing 0.3 vol.% of graphite.

interesting to note that the microhardness of alumina decreases with alumina content in the composite as shown in Fig.6.19. The variation of microhardness in VHN with volume percent of alumina in the AZ91 alloy based hybrid composites is shown in Fig.6.20. It is observed that the microhardness of the primary phase increases from 97 to 101 VHN when volume percent of alumina increases from 16 to 19 vol% in the composite. The microhardness of alumina decreases with alumina content similar to that observed for magnesium based hybrid composites.

6.1.7 Dry Sliding Friction and Wear

(a) Magnesium Based Hybrid Composites

Figs. 6.21 to 6.23 show the variation of cumulative volume loss with sliding distance for magnesium based hybrid composites containing 13, 15 and 18 vol% of alumina and about 0.3 vol% of graphite in each, tested under normal loads of 2.5, 3.5, 4.5 and 5.5 kg at contact and a sliding speed of 1.0 m/s. The cumulative volume loss increases more or less linearly with sliding distance at a given load and the least square fit for this variation at different loads are indicated by the lines drawn in these figures. It is observed that the volume loss in the composite containing 18 vol% of alumina and 0.3 vol% of graphite, shown in Fig. 6.23 is significantly lower than that in the other two magnesium based hybrid composites containing 13 and 15 vol% alumina respectively and 0.3 vol% graphite in both as shown in Figs. 6.21 and 6.22. The wear rate, i.e., volume loss in wear per unit sliding distance at a given load, has been determined from the slope of the linear least square fit lines at different loads in Figs. 6.21 to 6.23.

The variation of wear rate with normal load for magnesium based hybrid composites containing 13, 15 and 18 vol% of alumina respectively and 0.3 vol% graphite in each, are shown in Figs. 6.24 to 6.26. It is observed that the wear rate increases nonlinearly with contact load and the nonlinearity is more marked for the composites containing 15 and 18 vol% alumina and 0.3 vol% graphite in both. However, the wear rate in the composite containing 18 vol% alumina and 0.3 vol% graphite are an order of magnitude lower than those in the other two hybrid composites based on magnesium.

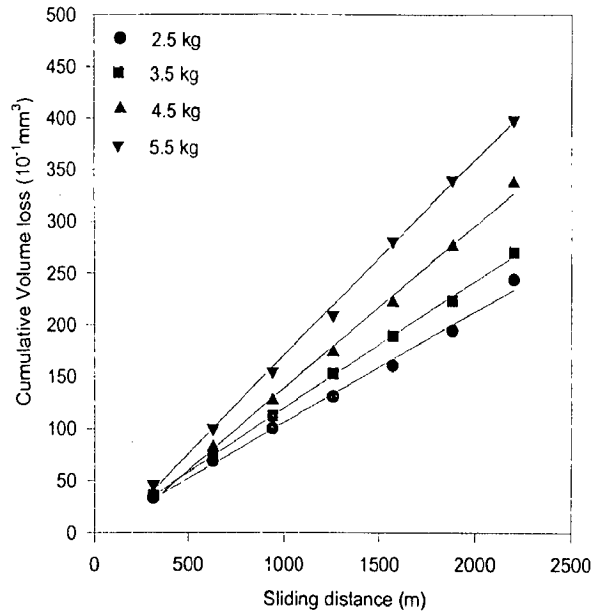


Fig.6.21 The variation of cumulative volume loss with sliding distance in commercial magnesium based hybrid composite containing 13 vol.% of alumina and ~0.3 vol.% of graphite, during dry sliding under constant sliding speed of 1.0 m/s against conterface of hardened steel

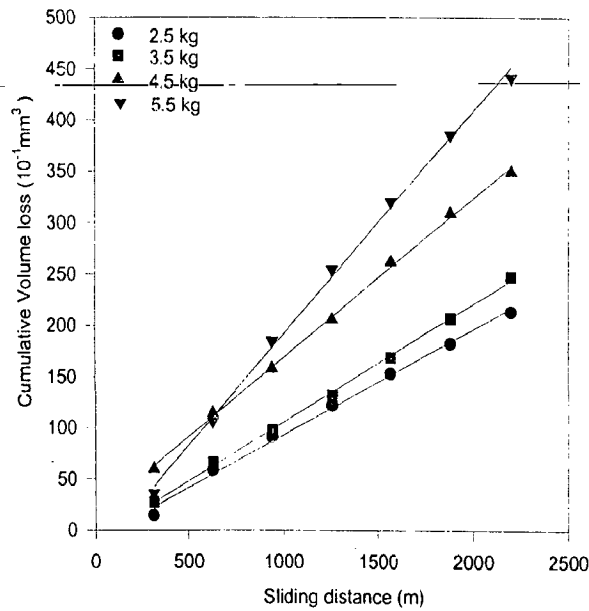


Fig.6.22 The variation of cumulative volume loss with sliding distance in commercial magnesium based hybrid composite containing 15 vol.% of alumina and ~0.3 vol.% of graphite, during dry sliding under a constant sliding speed of 1.0 m/s against conterface of hardened steel.

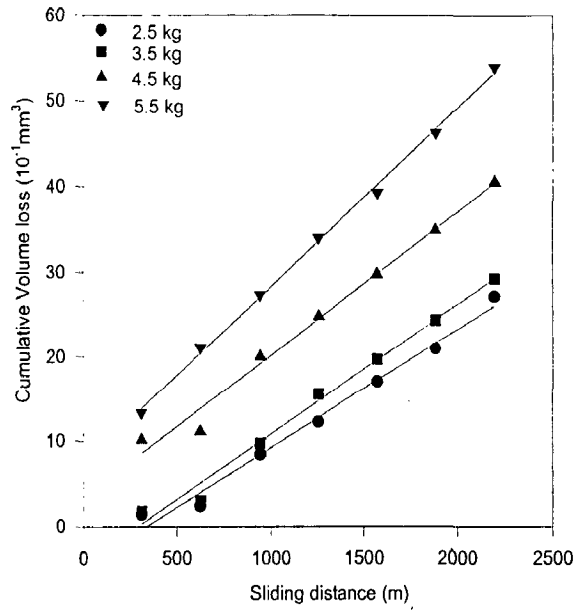


Fig.6.23 The variation of cumulative volume loss with sliding distance in commercial magnesium based hybrid composite containing 18 vol.% of alumina and ~0.3 vol.% of graphite, during dry sliding under a constant sliding speed of 1.0 m/s against conterface of hardened steel.

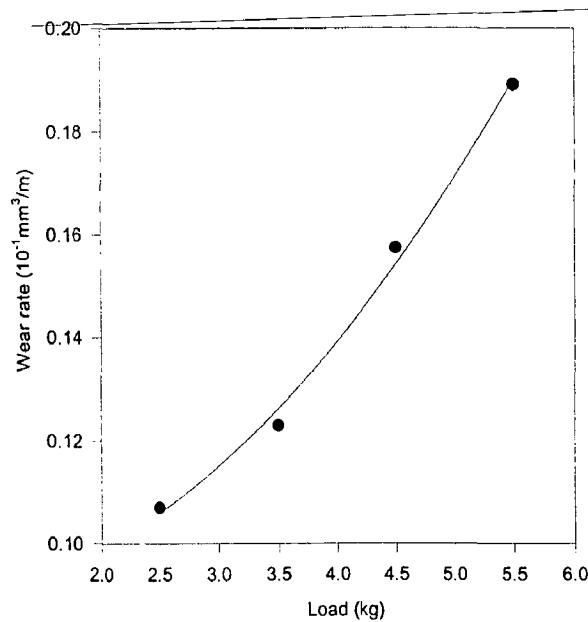


Fig.6.24 The variation of wear rate with normal load in commercial magnesium based hybrid composite containing 13 vol.% of alumina and ~0.3 vol.% of graphite, during dry sliding at a fixed sliding speed of 1.0 m/s against conterface of hardened steel.

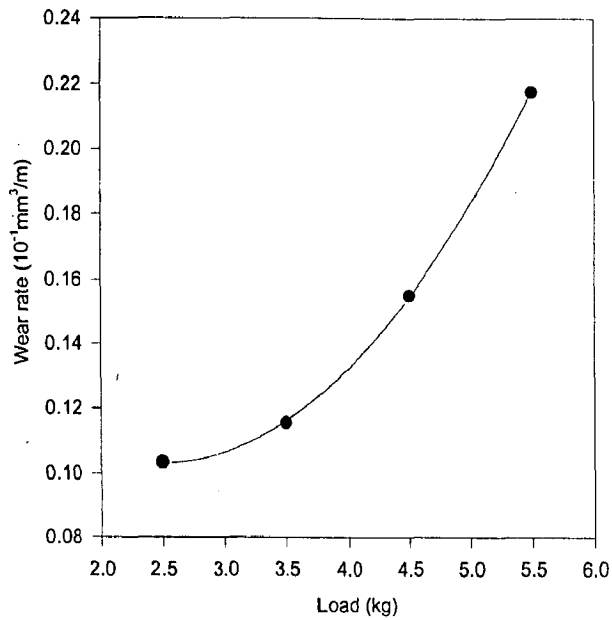


Fig.6.25 The variation of wear rate with normal loads in commercial magnesium based hybrid composite containing 15 vol.% of alumina and ~0.3 vol.% of graphite, during dry sliding at a fixed sliding speed of 1.0 m/s against conterface of hardened steel

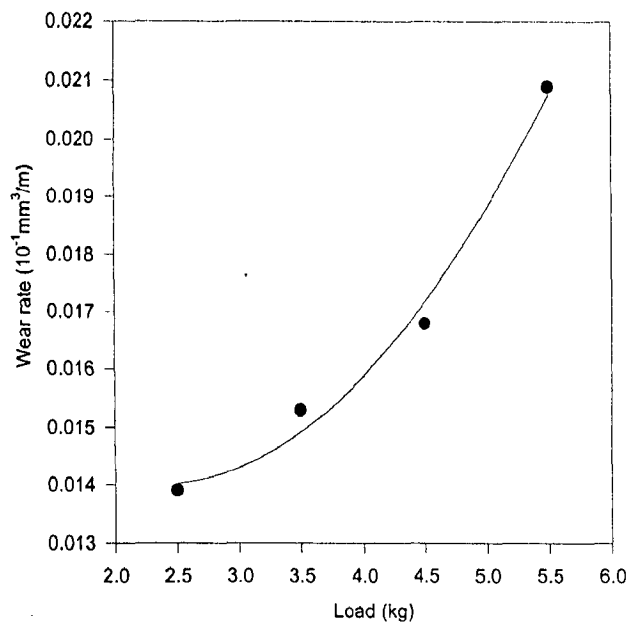


Fig.6.26 The variation of wear rate with normal loads in commercial magnesium based hybrid composite containing 18 vol.% of alumina and ~0.3 vol.% of graphite, during dry sliding at a fixed sliding speed of 1.0 m/s against conterface of hardened steel

Fig. 6.27 to 6.29 shows the variation of coefficient of friction with sliding distance in squeeze cast magnesium based composites containing 13, 15 and 18 vol% of alumina respectively and 0.3 vol% of graphite in each, for different applied loads ranging between 2.5 kg to 5.5 kg varied in steps of 1.0 kg. It is observed that at the lower load of 2.5 kg, the coefficient of friction is around 0.48 in the hybrid composite containing 13 vol% of alumina. The composite containing 18 vol% alumina has shown a higher coefficient of friction of 0.8 at lower loads and it decreases to 0.65 at higher loads. Figs. 6.30 to 6.32 shows the variation of the coefficient of friction averaged over sliding distance, with load for different magnesium based hybrid composites. When load increases from 2.5 kg, there is a drop in coefficient of friction as it has been observed for magnesium, its alloys and composites based on them. The decrease in coefficient of friction with load is almost linear in the hybrid composite containing 13 vol% alumina and 0.3 vol% graphite but for the other composites the variation is nonlinear.

The wear coefficient of the commercial magnesium based hybrid composite containing 18 vol% of alumina is 0.18×10^{-4} that is lower than 0.36×10^{-4} , the wear coefficient of commercial magnesium. However, the wear coefficients in the hybrid composites containing 13 and 15 vol% of alumina are considerably higher at 1.45×10^{-4} and 3.21×10^{-4} respectively.

(b) AZ91 Alloy Based Hybrid Composites

Figs. 6.33 to 6.35 show the variation of cumulative volume loss with sliding distance for AZ91 alloy based hybrid composites containing 16, 17 and 19 vol% of alumina and about 0.4 vol% of graphite in each, tested at different normal loads of 2.5, 3.5, 4.5 and 5.5 kg under a sliding speed of 1.0 m/s. The cumulative volume loss increases more or less linearly with sliding distance at a given load and the least square fit for this variation at a given load is indicated by the lines drawn in these figures.

The wear rate has been calculated from the slope of the linear least square fit lines at different loads as outlined earlier. Figs. 6.36 to 6.38 show the variation of the wear rate with normal load for AZ91 alloy based hybrid AZ91 alloy composites containing 16, 17 and 19 vol% of alumina and about 0.4 vol% of graphite in each the

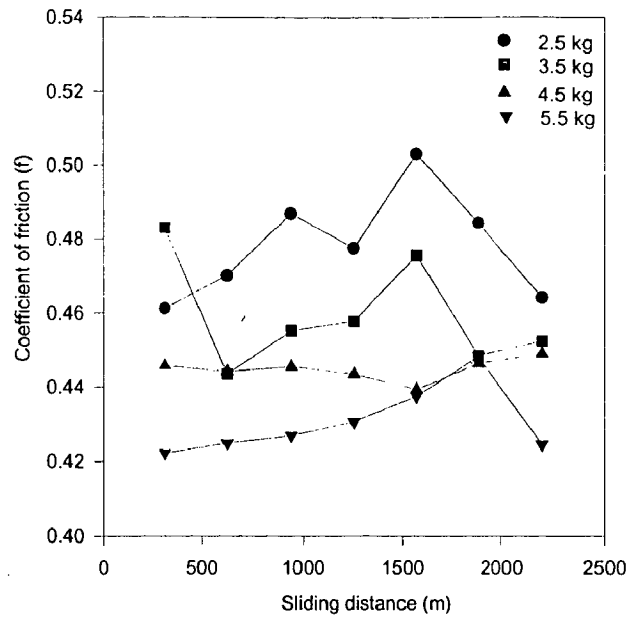


Fig.6.27 The variation of coefficient of friction with sliding distance in commercial magnesium based hybrid composite containing 13 vol.% of alumina and ~0.3 vol.% of graphite, during dry sliding under a constant sliding speed of 1.0 m/s against conterface of hardened steel

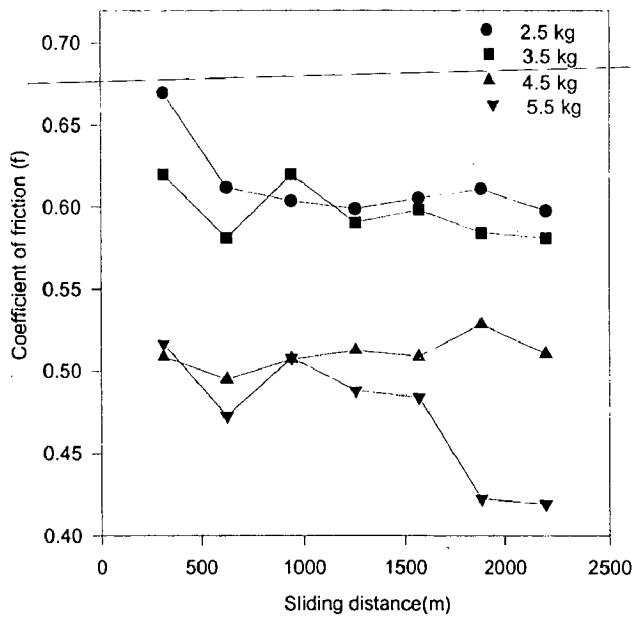


Fig.6.28 The variation of coefficient of friction with sliding distance in commercial magnesium based hybrid composite containing 15 vol.% of alumina and ~0.3 vol.% of graphite, during dry sliding under a constant sliding speed of 1.0 m/s against conterface of hardened steel.

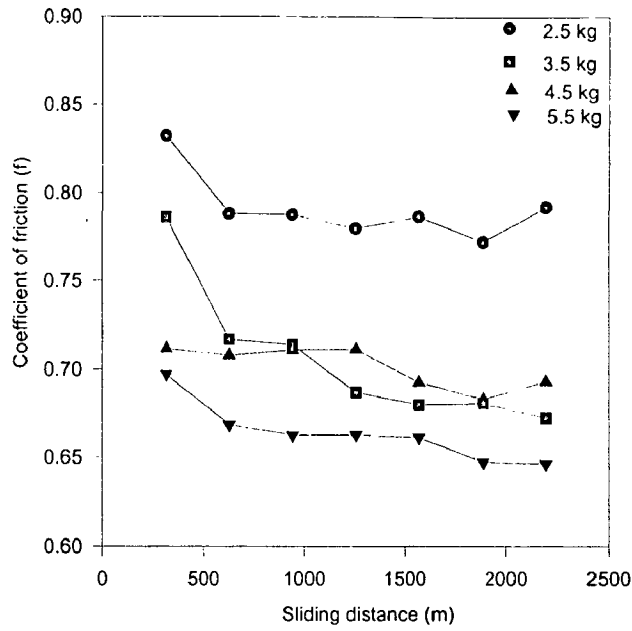


Fig.6.29 The variation of coefficient of friction with sliding distance in commercial magnesium based hybrid composite containing 18 vol.% of alumina and ~0.3 vol.% of graphite, during dry sliding under a constant sliding speed of 1.0 m/s against conterface of hardened steel

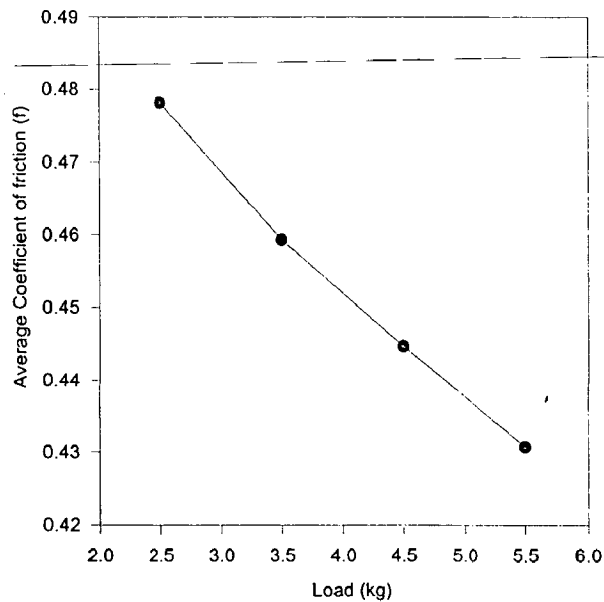


Fig.6.30 The variation of coefficient of friction averaged over sliding distance, with normal load in commercial magnesium based hybrid composite containing 13 vol.% of alumina and ~0.3 vol.% of graphite, during dry sliding at a fixed sliding speed of 1.0 m/s against conterface of hardened steel

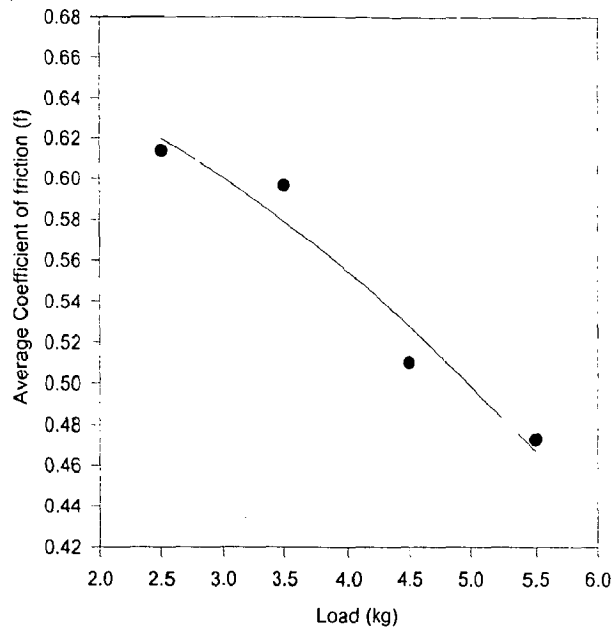


Fig.6.31 The variation of coefficient of friction averaged over sliding distance, with normal load in commercial magnesium based hybrid composite containing 15 vol.% of alumina and ~0.3 vol.% of graphite at a fixed sliding speed of 1.0 m/s against conterface of hardened steel

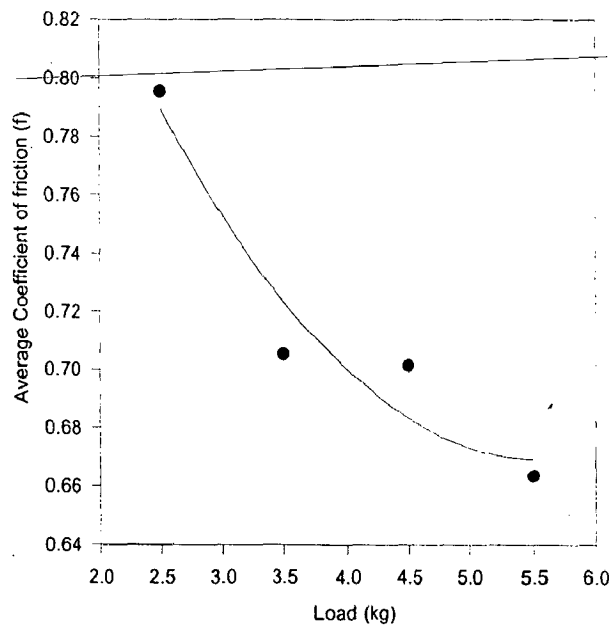


Fig.6.32 The variation of coefficient of friction averaged over sliding distance, with normal load in commercial magnesium based hybrid composite containing 18 vol.% of alumina and ~0.3 vol.% graphite, during dry sliding at a fixed sliding speed of 1.0 m/s against conterface of hardened steel.

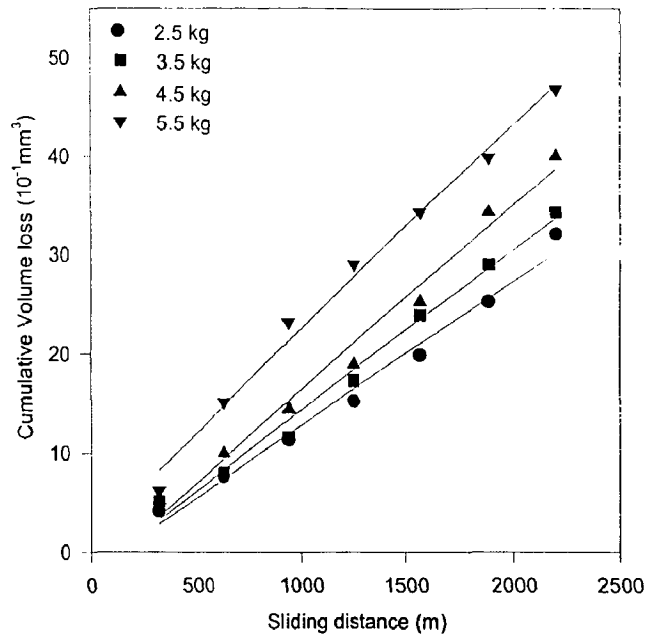


Fig.6.33 The variation of cumulative volume loss with sliding distance in AZ91 alloy based hybrid composite 16 vol.% alumina and ~0.4 vol.% of graphite, during dry sliding under a constant sliding speed of 1.0 m/s against counterface of hardened steel.

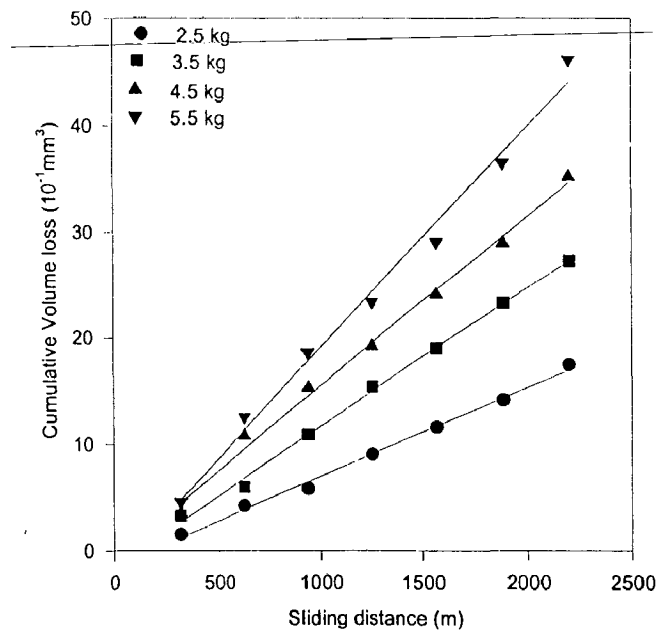


Fig.6.34 The variation of cumulative volume loss with sliding distance in AZ91 alloy based hybrid composite containing 17 vol.% of alumina and ~0.4 vol.% of graphite, during dry sliding under constant sliding speed of 1.0 m/s against counterface of hardened steel.

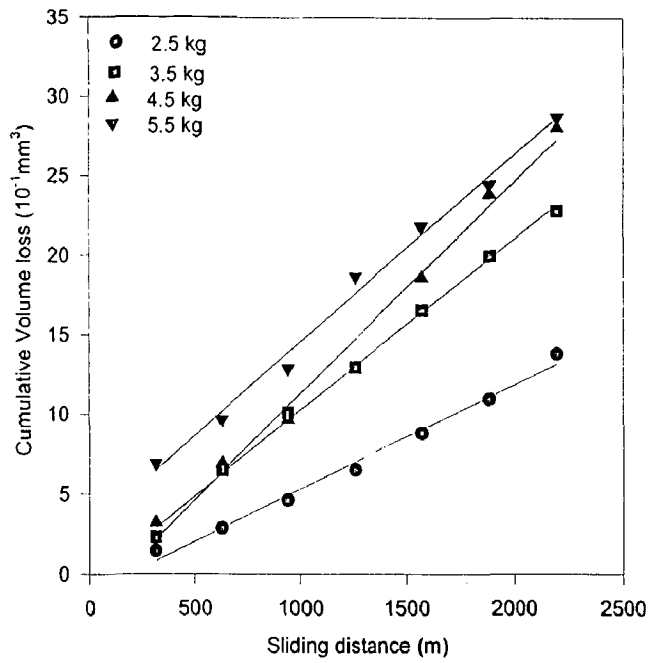


Fig.6.35 The variation of cumulative volume loss with sliding distance in AZ911 alloy based hybrid composite containing 19 vol.% alumina and ~0.4 vol.% graphite, during dry sliding under a constant sliding speed of 1.0 m/s against counterface of hardened steel.

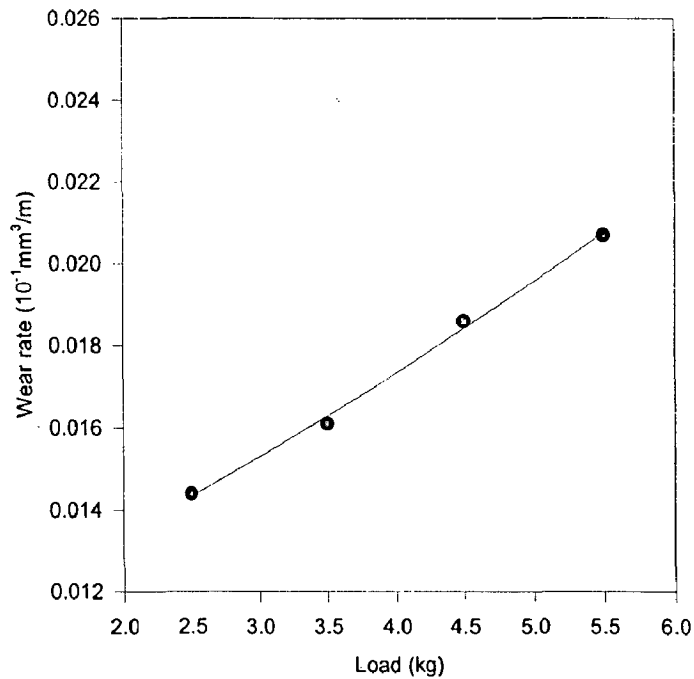


Fig.6.36 The variation of wear rate with normal load in AZ911 alloy based hybrid Composite containing 16 vol.% of alumina and ~0.4 vol.% of graphite, during dry sliding at a fixed sliding speed 1.0 m/s against counterface of hardened steel.

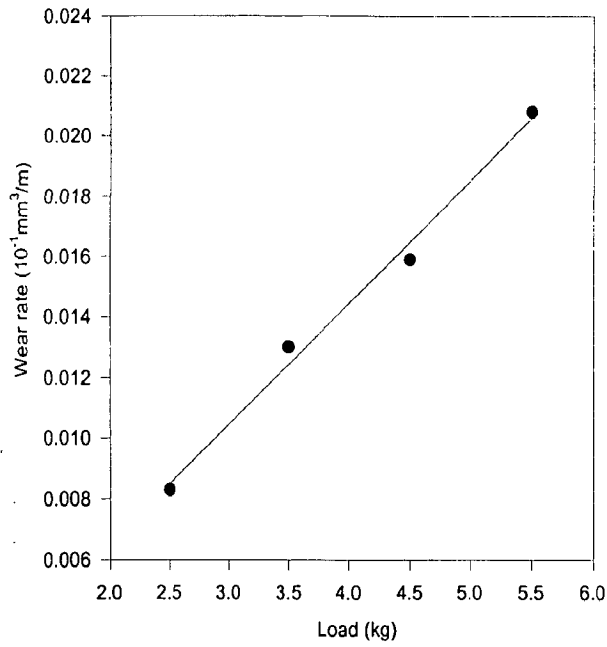


Fig.6.37 The variation of wear rate with normal load in AZ91 alloy based hybrid composite containing 17 vol.% of alumina and ~0.4 vol.% of graphite, during dry sliding at a fixed sliding speed of 1 m/s against conterface of hardened steel.

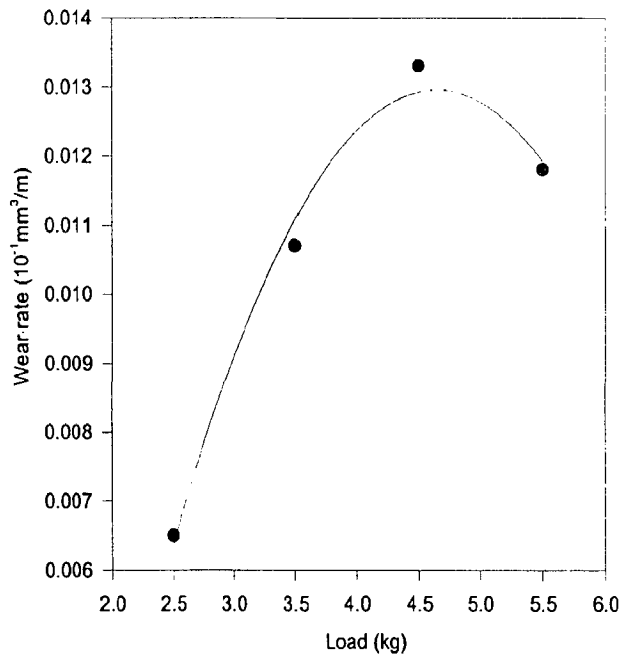


Fig.6.38 The variation of wear rate with normal loads in AZ91 alloy based hybrid composite containing 19 vol.% of alumina and ~0.4 vol.% of graphite, during dry sliding at a fixed sliding speed of 1.0 m/s against conterface of hardened steel.

wear rate increases linearly with load for the hybrid composite containing 17 vol% alumina but in the hybrid composites containing 16 and 19 vol% of alumina, the wear rate increases nonlinearly with load.

Fig. 6.39 to 6.41 shows the variation of coefficient of friction with sliding distance for different applied loads ranging between 2.5 kg to 5.5 kg varied in steps of 1.0 kg, in AZ91 alloy hybrid based composites containing 16, 17 and 19 vol% respectively. It is observed that at a lower load of 2.5 kg, the coefficient of friction varies significantly in the range between 0.80 to 0.85 in the hybrid composites containing 16 and 19 vol% alumina but in the composite containing 17 vol% alumina the coefficient of friction remains steady around 0.82 to 0.83 which reduces to around 0.74 as the load increases to 5.5 kg. For the AZ91 alloy based hybrid composites containing 16 and 19 vol% alumina there is significant variation of coefficient of friction at higher loads and at 5.5 kg the coefficient of friction decreases to around 0.76 and 0.74 respectively. Figs. 6.42 to 6.44 shows the variation of coefficient of friction averaged over sliding distance, with load for AZ91 alloy based hybrid composites. When load increases from 2.5 kg to 5.5 kg, the coefficient of friction decreases nonlinearly in all these hybrid composites.

The wear coefficients of the AZ91 alloy hybrid composites containing 16 and 19 vol% of alumina are 0.18×10^{-4} and 0.21×10^{-4} which is lower than 0.36×10^{-4} , the wear coefficient of vacuum cast AZ91 alloy. However, the wear coefficient in the AZ91 alloy hybrid composite containing 17 vol% of alumina is considerably higher at 0.42×10^{-4} which is higher than the values observed in the other two composites.

6.1.8 Examination of Sliding Surface and Wear Debris

The results of examination of the sliding surface under scanning electron microscope and wear debris under optical microscope for the hybrid composites based on commercial magnesium and AZ91 alloy are described below.

(a) Hybrid Magnesium-Alumina-Graphite

Figures 6.45 (a), (b) and (c) show a typical sliding surface of commercial magnesium based hybrid composite containing 13 vol% alumina at magnifications of

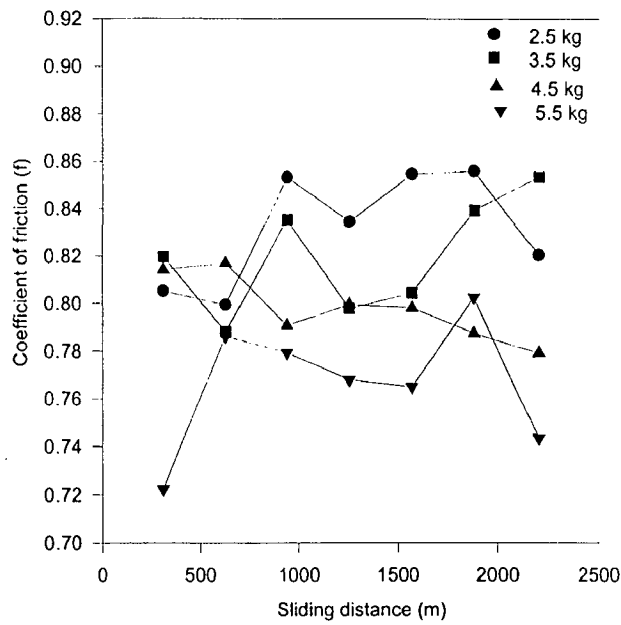


Fig.6.39 The variation of coefficient of friction with sliding distance in AZ91 alloy based hybrid composite containing 16 vol.% of alumina and ~0.4 vol.% of graphite, during dry sliding under a constant speed of 1.0 m/s against conterface of hardened steel.

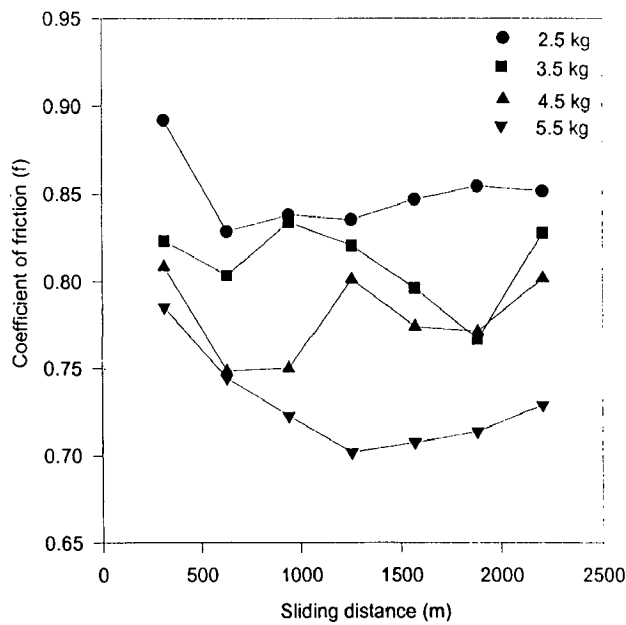


Fig.6.40 The variation of coefficient of friction with sliding distance in AZ91 alloy based hybrid composite containing 17 vol.% of alumina and ~0.4 vol.% of graphite, during dry sliding under a constant sliding speed of 1.0 m/s against conterface of hardened steel.

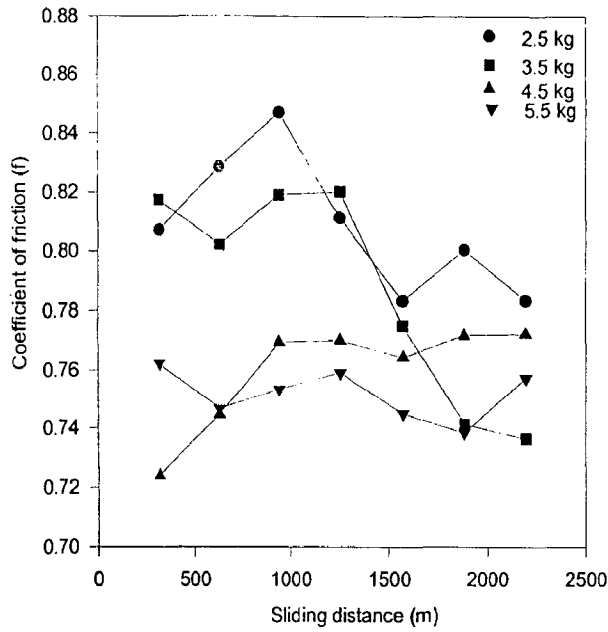


Fig.5.41 The variation of coefficient of friction with sliding distance in AZ91 alloy based hybrid composite containing 19 vol.% of alumina and ~0.4 vol.% of graphite, during dry sliding under a constant sliding speed of 1.0 m/s against conterface of hardened steel.

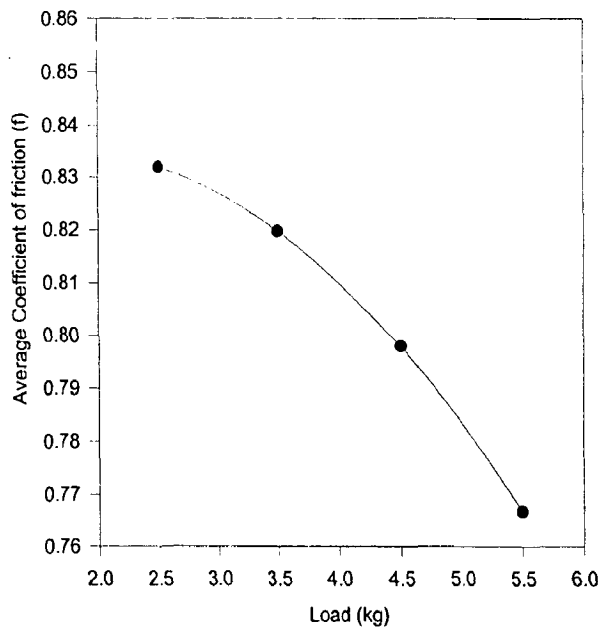


Fig.6.42 The variation of coefficient of friction averaged over sliding distance, with normal load in AZ91 alloy based hybrid composite containing 16 vol.% of alumina and ~0.4 vol.% of graphite, during dry sliding at a fixed sliding speed of 1.0 m/s against conterface of hardened steel.

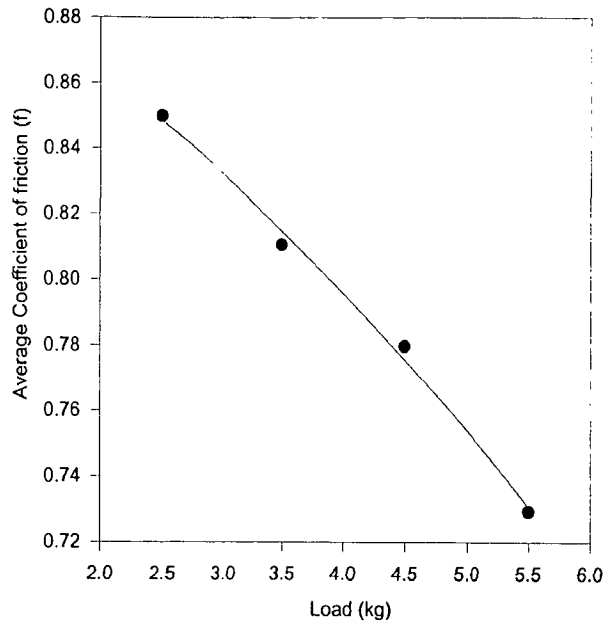


Fig.6.43 The variation of coefficient of friction averaged over sliding distance, with normal load in AZ91 alloy based hybrid composite containing 17 vol.% of alumina and ~0.4 vol.% of graphite, during dry sliding at a fixed sliding speed of 1.0 m/s against conterface of hardened steel.

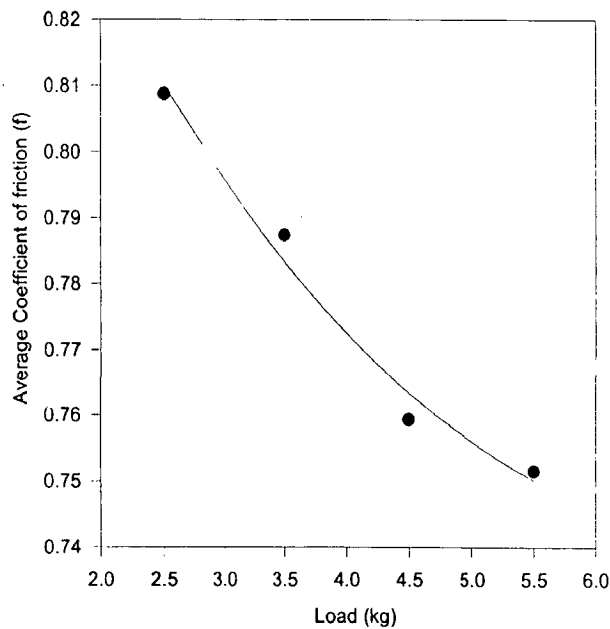
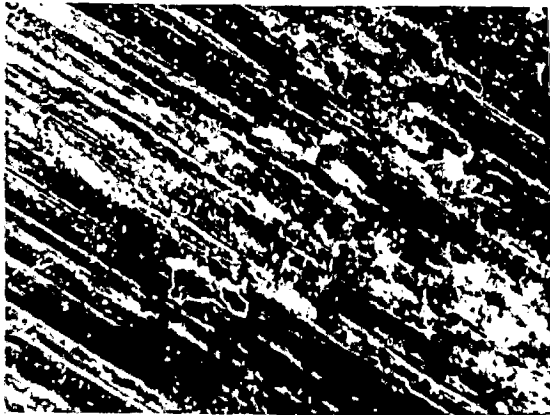
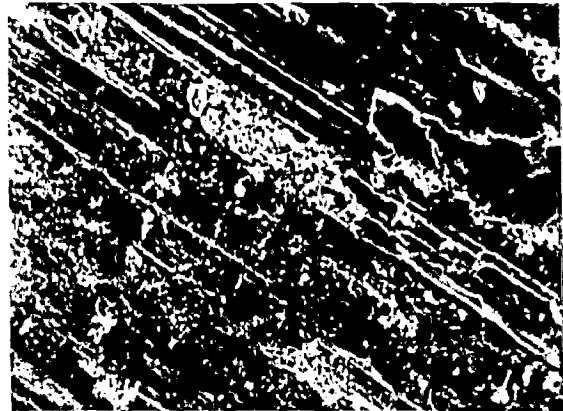


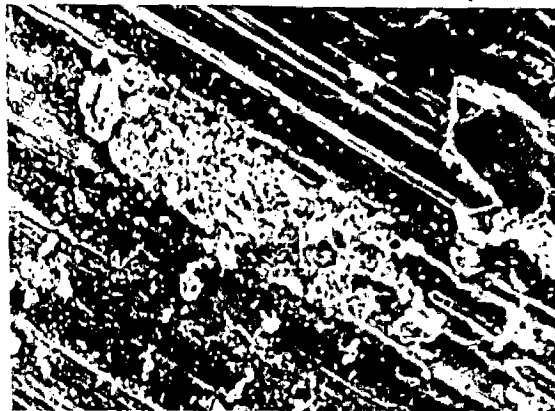
Fig.6.44 The variation of coefficient of friction averaged over sliding distance, with normal load in AZ91 alloy based hybrid composite containing 19 vol.% of alumina ~0.4 vol.% of graphite, during dry sliding at a fixed sliding speed of 1.0 m/s against conterface of hardened steel



(a)



(b)



(c)

Fig.6.45 SEM micrograph of the surface of commercial magnesium based hybrid composite containing 13 vol% alumina and ~0.3 vol% of graphite after dry sliding at a normal load of 2.5 kg, (a) X77 (b) X200 and (c) X400.

X77, X220 and X400 respectively. No graphite could be detected on the sliding surface and one may observe the formation of transfer layer containing oxides. At higher loads of 5.5 kg, one observes that the oxides are dominant on the sliding surface and graphite, if any does not have any significant role as shown in Figs. 6.46 (a), (b) and (c) at magnifications of X77, X22 and X400 respectively.

The wear debris at lower load of 2.5 kg from the same hybrid composite containing 13 vol% alumina appear to consist of flaked transfer layers as shown in Fig. 6.47(a). The transfer layer has oxide particles primarily apart from a few dark particles of graphite in it. At higher load of 5.5 kg the wear debris also contain a few bright metallic particles as shown in Fig.6.47 (b).

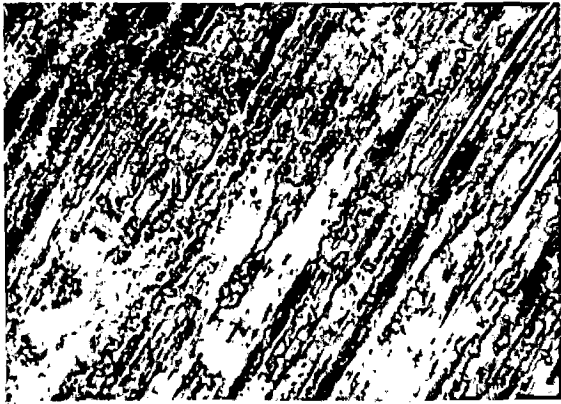
(b) Hybrid AZ91 Alloy-Alumina-Graphite

When the matrix is AZ91 alloy that is not as soft as commercial magnesium the sliding surface reveals that at a load of 2.5 kg there is smearing of graphite on the sliding surface as shown in Figs.6.48 (a) and (b) at magnifications of X200 and X400 respectively. This hybrid composite contains 16 vol% alumina and 0.4 vol% graphite. The sliding surface has large amount of oxide but graphite inspite of its low amount could play a role as observed in Fig. 6.48 (a) and (b). At higher loads of 5.5 kg one may observe significant cover provided by well formed transfer layer which cracks to generate wear debris and possibly forms again as shown in Fig 6.49. But the graphite could not be detected because of dominating oxidative wear at this load because of high temperature due to friction.

The wear debris at low loads of 2.5 kg as shown in Fig. 6.50 (a), appear similar to that observed for commercial magnesium based hybrid composite in Fig.6.47 (a). But at higher loads the flaked off transfer layer appear to be better consolidated and there are very few bright particles in it as shown in Fig.6.50 (b).

6.2 Discussion

The hybrid composites have been synthesized to examine the effect of graphite during processing and on the tribological behaviour. But it is observed that the graphite



(a)



(b)



(c)

Fig.6.46 SEM micrograph of the surface of commercial magnesium based hybrid composite containing 13 vol% alumina and ~0.3 vol% of graphite after dry sliding at a normal load of 5.5 kg, (a) X77 (b) X200 and (c) X400.

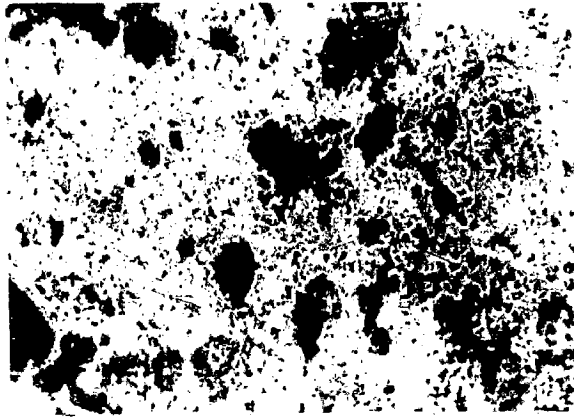


Fig.6.47(a) Stereo microphotograph showing the wear debris of commercial magnesium based hybrid composite containing 13 vol% of alumina and ~ 0.3 vol% of graphite generated during dry sliding against steel disc at load of 2.5 kg, X16.



Fig.6.47(b) Stereo microphotograph showing the wear debris of commercial magnesium based hybrid composite containing 13 vol% of alumina and ~ 0.3 vol% of graphite generated during dry sliding against steel disc at load of 5.5 kg, X16.

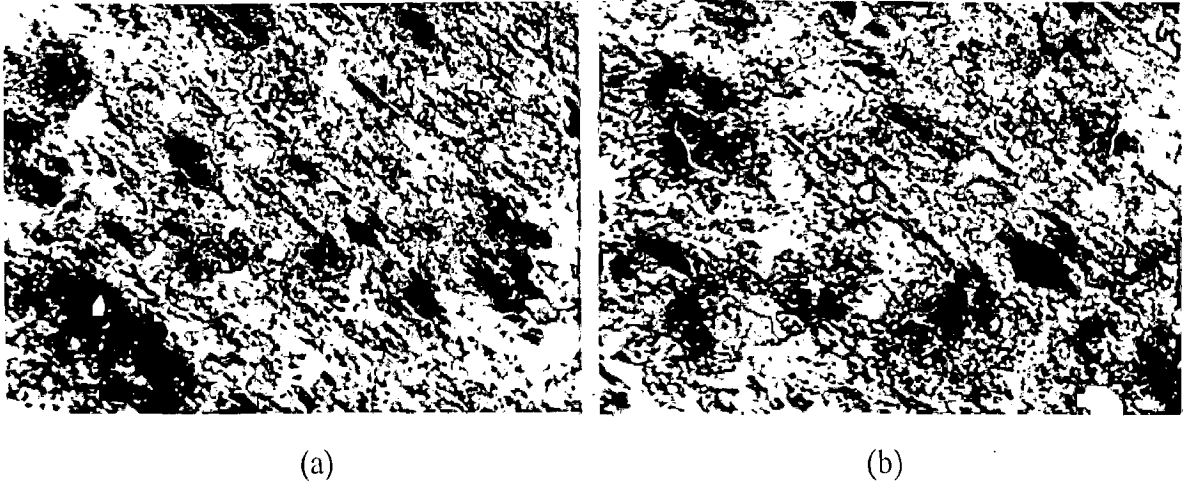


Fig.6.48 SEM micrograph of the surface of AZ91 alloy based hybrid composite containing 16 vol% of alumina and ~0.4 vol% of graphite after dry sliding at a normal load of 2.5 kg, (a) X200 and (b) X400.

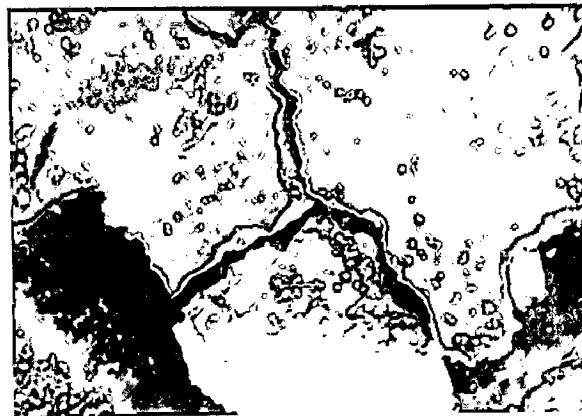


Fig.6.49 SEM micrograph of the surface of AZ91 alloy based hybrid composite containing 17 vol% of alumina and ~0.4 vol% of graphite after dry sliding at a normal load of 5.5 kg, X200.



Fig.6.50(a) Stereo microphotograph showing the wear debris of AZ91 alloy based hybrid composite containing 16 vol% of alumina and ~0.4 vol% of graphite generated during dry sliding against steel disc at different load of 2.5 kg, X16.

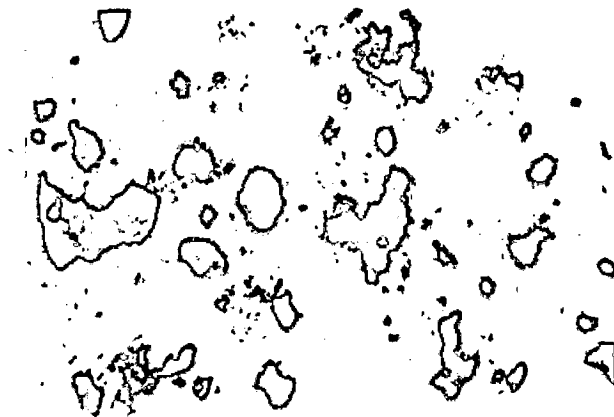


Fig.6.50(b) Stereo microphotograph showing the wear debris of AZ91 alloy based hybrid composite containing 16 vol% of alumina and ~0.4 vol% of graphite generated during dry sliding against steel disc at different load of 5.5 kg, X16.

added have mostly floated out during squeeze casting and the composites have more or less similar low levels of graphite between 0.3 and 0.4 vol% as shown Table 6.2.

The microstructures of the hybrid composite based on commercial magnesium have revealed graphite at higher magnification of 250X as shown in Fig. 6.2, 6.5 and 6.8. But graphite particles which have relatively higher l/d ratio than alumina particles, appear to have entrapped between the alumina particles in certain areas as shown Fig. 6.4. At higher magnification there is a very important distinction observed between the microstructures of the three composites. Although there has been matrix-particle reaction in all the three composites as indicated by irregular surface contour of alumina particles, it is only in the composite containing 18 vol% alumina, both the alumina and graphite particles are surrounded by a thick network of solute rich phase. The X-ray diffraction patterns of the composites containing 15 and 18 vol% of alumina show no indication of the strongest diffraction peak from $MgAl_2O_4$, but there are peaks from MgO, that are fairly strong. The spotted appearance of the network may be due to MgO particles which may have formed due to reaction between molten magnesium and alumina during processing and got detached from the alumina particles due to fluid flow during infiltration. These MgO particles may have nucleated $Mg_{17}Al_{12}$ during eutectic solidification of the last freezing liquid resulting in a network of $Mg_{17}Al_{12}$ containing small MgO particles as part of a divorced eutectic. This network is thick and may have engulfed graphite and alumina covered by MgO, both of which may also have nucleated the solute rich second phase. However, the composite containing 13 vol% of alumina does not show any such network and it is possible that the extent of matrix-particles reaction is not as much or the fluid flow in the relatively larger pores have not been as severe to break away MgO particles from the surface of reacted alumina. In the composite containing 15 vol% of alumina, there is $MgAl_2O_4$ in addition to MgO as indicated by the presence (311) peak of $MgAl_2O_4$ in Figs 6.16. However, there are no thick network similar to that observed in the composite containing 18 vol% of alumina.

The EPMA of the bright phases shows that the magnesium in the matrix of commercial magnesium based hybrid composites has aluminium in it exceeding the original level present in the commercial magnesium used as shown in Table 6.3. It appears to have been provided by matrix-particle reaction and the lattice parameters of

the magnesium solid solution in the hybrid composite based on commercial magnesium, change from the values observed for commercial magnesium by X-ray diffraction as shown Table 6.4. This is also an indirect proof of reaction between magnesium and alumina particles during processing at high temperature reducing alumina to aluminium that gets dissolved in commercial magnesium to result in magnesium solid solution. In most of the composites, the reaction product appears to be MgO, but there is presence of MgAl₂O₄ in some of the composites. The commercial magnesium based hybrid composite containing 15 vol% alumina shows (311) peak from MgAl₂O₄ in its X-ray diffraction pattern. Since there is so much magnesium, it is possible that MgO is the primary product of reaction following magnesium rich end of ternary Mg-Al-O system. If MgO remains on the alumina particle it may react with unreacted alumina inside to form MgAl₂O₄. But fluid flow during infiltration may erode the MgO forming on the particles before it may react with alumina and thereby, reducing the possibility of MgAl₂O₄ formation.

The BHN of the composites based on commercial magnesium increases with increasing alumina content as shown in Table 6.5. A comparison of the hardness of hybrid composites with those containing alumina alone shows that the hardness of the hybrid composites has not been significantly affected by the presence of small amount of graphite. It is possible that the degree of the matrix-particle reaction depends on the amount of the alumina in the composites and the hardness of the primary solid solution of magnesium increases with increasing alumina content as shown in Table 6.6. The composites containing 21 and 23 vol% of alumina shown in Table 5.6, has higher microhardness compared to the hybrid composites containing lower levels of alumina of 13, 15 and 18 vol%. However, the alumina particles have a lower hardness when the amount of particles increases as shown in Table 6.6. Many a times graphite particles are observed adjacent to the alumina particles which may have lowered the hardness of alumina particles relatively more in hybrid composites as shown in Table 6.6, compared to that in composites containing alumina alone as given in Table 5.6.

The dry sliding wear of the hybrid composite containing 18 vol% of alumina and 0.3 vol% of graphite has significantly lower volume loss in wear compared to the other two composites containing 13 and 15 vol% of alumina. The hybrid composite containing 15 vol% of alumina has an amount of MgAl₂O₄ which has been found

harmful for dry sliding wear as it has been reported in chapter 5 in the context of composites containing alumina alone. But the hybrid composite containing 13 vol% of alumina also shows a relatively higher volume loss compared to that in the hybrid composite containing 18 vol% alumina when both these composites do not show presence of $MgAl_2O_4$, possibly because of relatively lower alumina content in the former. The variation of wear rate with normal load is nonlinear in both the hybrid composites containing 15 and 18 vol% of alumina. But the one with 13 vol% alumina shows almost linear variation of wear rate with load following Archard's law. If one compares the lower wear rates observed in commercial magnesium based hybrid composite containing 18 vol% of alumina with those observed in the composite containing 21 vol% of alumina alone, it is observed that the wear rates are comparable as shown in Figs 6.26 and 5.18. However, the wear rates in the hybrid composites containing 13 and 15 vol% of alumina are an order of magnitude higher than those observed in the hybrid composite containing 18 vol% of alumina.

The coefficient of friction in the hybrid composites increases with alumina content at low load of 2.5 kg and it varies in the range between 0.46 to around 0.80. However, the coefficient of friction decreases with increasing load. But at a load of 5.5 kg, it reaches only 0.65 in the composite containing 18 vol% of alumina but those with lower amounts of alumina, the friction coefficients are still lower as shown in Figs 6.30 to 6.32. If one compares the variation of coefficient of friction with load in the hybrid composite containing 18 vol% of alumina with that observed in the composite containing 21 vol% of alumina alone, it is observed that in the hybrid composite, the coefficient of friction is a little lower at lower load which may be due to lower alumina content or due to the presence of small amount of graphite. But at higher loads of 5.5 kg, the coefficient of friction in the hybrid composite is higher at 0.66 but that for composite containing 21 vol% of alumina is also high at 0.6.

The increase in coefficient of friction with alumina content at low loads in the hybrid composites may indicate that alumina has higher coefficient of friction with the counterface of hardened steel as compared to that of magnesium or its oxide. In this context it should be remembered that magnesium has negligible solubility for iron and may have low interfacial shear strength particularly at elevated temperatures due to frictional heating at contacts. Since the wear is primarily oxidative as it has been

indicated by the sliding surface and wear debris shown in Figs.6.40 to 6.42, the interfacial strength of MgO with hardened steel should be lower than that for alumina. But at higher loads, the soft magnesium may flow under shear stress and cover alumina particles and so, one observes similar coefficient of friction at high loads in the composites containing 13 and 15 vol% alumina. But the composite containing 18 vol% alumina shows a higher coefficient of friction showing that a relatively larger area of alumina still remains exposed at the sliding surface at higher load of 5.5 kg.

The wear coefficient of the hybrid composite containing 15 vol% of alumina is the highest at 3.22×10^{-4} but those for the hybrid composites containing 13 and 18 vol% of alumina are respectively 1.4×10^{-4} and 0.18×10^{-4} . It is clearly observed that the hybrid composites containing 13 and 15 vol% of alumina have similar wear rates but the higher hardness of the hybrid composite containing 15 vol% of alumina has increased the value of wear coefficient. The lower wear rate of hybrid composite containing 18 vol% of alumina is still reflected in its low wear coefficient inspite of its higher hardness.

The AZ91 alloy based hybrid composites containing alumina and graphite contain a very low level of graphite. During squeeze casting, the graphite particles may have floated similarly as it has been inferred for the commercial magnesium based hybrid composites. However, some graphite particles get mechanically entrapped and are retained in the composites as shown in Figs. 6.11, 6.13 and 6.14. From the density measurements it has been determined that the amount of graphite in the AZ91 alloy based hybrid composite is about 0.4 vol% as shown in Table 6.2.

The microstructure of the AZ91 alloy based hybrid composite containing 16 vol% of alumina shows primary solid solution of magnesium which appears bright and relatively darker solute rich interdendritic areas, as shown Fig 6.11(a). At higher magnification, one could clearly see the solute rich grey area as shown in Fig. 6.11 (b). EPMA analysis indicates that there are higher aluminium and zinc in the grey area and it could be a ternary intermetallic compound. It is observed that both the alumina and graphite particles are in the last freezing liquid, i.e., interdendritic region. The hybrid composite containing 17 vol% of alumina has a distinctly different structure. One could observe lamellar eutectic almost in the entire region between alumina particles in the

area shown in Fig. 6.13. But there is considerable variation in cast structure of the composites depending on the particle content in the area as shown in Fig. 6.12.

The X-ray diffraction pattern of these AZ91 alloy based hybrid composites clearly shows that there is an amount MgO which has formed due to chemical reaction between alumina particles and the AZ91 alloy as it has been observed in all the composites containing alumina investigated here. The hybrid composites containing 16 and 17 vol% alumina show the (311) peak of $MgAl_2O_4$. There is one peak at $2\theta = 40.2$ which has not been identified. This peak could come from either $Mg_{17}Al_{12}$ which is more abundant in AZ91 alloy based composites compared to that in the composites based on commercial magnesium. This peak is also there in the AZ91 alloy based composite containing 14 vol% alumina alone, whose X-ray diffraction pattern has been reported in Fig. 5.11(b) in chapter 5. This peak may have come from compounds resulting out of reaction between the matrix and the particles which may be ruled out since this peak is not present in commercial magnesium based composites.

The BHN of AZ91 alloy based hybrid composites shows that the hardness increases with alumina content as shown in Table 6.5. But the hybrid composites have relatively lower hardness if one compares the hardness of hybrid composite containing 16 vol% of alumina with that in the composite containing 16 vol% of alumina alone as given in Table 5.5. It appears that graphite although the amount is small, could have played some role to reduce the hardness in the hybrid composites. The hardness of primary magnesium solid solution in the hybrid composites based on AZ91 alloy as shown in Table 6.6, is similar to the hardness of the same phase in the matrix of AZ91 alloy based composite containing alumina alone as reported in Table 5.6. However, the hardness of the primary solid solution of the composite appeared to increase with increasing alumina content as it has been observed also in other composites containing alumina. But the hybrid composite containing 19 vol% alumina has magnesium solid solution with hardness slightly lower than that of hybrid composite containing 17 vol% alumina. The hardness of alumina particles in hybrid composites decreases with increasing alumina content as it has observed in other composites containing alumina.

The volume loss in the hybrid composites based on AZ91 alloy are similarly low in all these composites but the composite containing 19 vol% alumina has a

relatively lower volume loss compared to the other two composites. The wear rates in the AZ91 alloy based hybrid composites containing 17 and 19 vol% of alumina are an order of magnitude lower than that observed in hybrid composite containing 16 vol% alumina. The composite containing 19 vol% of alumina has the lowest range of wear rate observed even in comparison to the composite containing 17 vol% of alumina. The variation of wear rate with load for both the AZ91 alloy based hybrid composites containing 16 and 19 vol% of alumina are nonlinear. But that in the composite containing 17 vol% of alumina is almost linear. If one compares the wear rates of the hybrid composite containing 16 vol% of alumina with that in the composite containing the same amount of alumina alone it is observed that the hybrid composite has shown a little higher wear rate which could be due to weakening by graphite. The composite containing 16 vol% of alumina alone has wear rates similar to those in the hybrid composite containing 19 vol% of alumina.

The coefficient of friction in the hybrid composite decreases with increase in the load. However, at higher load of 5.5 kg, the coefficient of friction in the AZ91 alloy based hybrid composites has been observed to be in the range between 0.73 to 0.77 as shown in Figs 6.42 to 6.44. It is surprising that the coefficient of friction in the AZ91 alloy based composite containing alumina alone is relatively lower at higher load compared to those observed in hybrid composites.

The increase in coefficient of friction with alumina content at low loads in the hybrid composites containing AZ91 alloy is not clearly established as the alumina contents are fairly close. But the wear is primarily oxidative in all these composites as it has been indicated by the sliding surface and wear debris shown in Figs.6.42 to 6.44. At higher loads, the AZ91 alloy does not flow as readily as soft magnesium under shear stress and cover alumina particles. Thus, the coefficient of friction at higher load of 5.5 kg is higher in the AZ91 alloy based hybrid composites shown in Figs.6.42 to 6.44, compared to those observed in the hybrid composites based on commercial magnesium as shown in Figs. 6.30 to 6.32. However, there is lowering of coefficient of friction with load which indicates that even the alloys flow and cover the relatively high friction constituent of alumina.

The wear coefficient in all these AZ91 alloy based hybrid composites are relatively lower and varies in a narrow range. The composites containing 16 and 19 vol% of alumina have wear coefficients of 0.19×10^{-4} and 0.21×10^{-4} respectively. But the wear coefficient in the composite containing 17 vol% of alumina is double of that observed in the composite containing 19 vol% of alumina. The lower wear rate in the composite containing 19 vol% of alumina has been able to result in lower wear coefficient inspite of its increased hardness. If one compares the wear coefficient of AZ91 alloy based composite containing 16 vol% alumina with that in the hybrid containing the same amount of alumina it appears that graphite even in low amount helps to decrease wear coefficient and thus, increase wear resistance as it has been observed earlier by Ames and Alpas (1995).

The results of this chapter indicate that for both the hybrid composites based on commercial magnesium and AZ91 alloy, the average coefficient of friction decreases with increasing load similar to that reported for other composites in chapters 4 and 5. Earlier workers have also observed similar results (Yang and chung, 1989). In the hybrid composite based on commercial magnesium, the observed coefficient of friction at the low load of 2.5 kg, increases with increasing alumina content. A similar trend is not clear in AZ91 alloy based composites. If one compares the average coefficient of friction in squeeze cast magnesium as reported in Chapter 5, Fig. 5.22 and that observed in the hybrid composite containing 13 vol% alumina in Fig. 6.45, it is evident that the coefficient of friction has not increased to the extent expected due to the presence of alumina. The graphite, although present in small amount, might have helped to reduce the coefficient of friction (Rohatgi, Ray and Liu, 1994) and kept it similar to that in squeeze cast magnesium. But when the amount of alumina increased to 15 and 18 vol% the coefficient of friction increased. In AZ91 alloy based hybrid composites the effect of graphite appears to be there as evident from the average friction in composites containing 16 vol% alumina without and with graphite as shown in Figs. 5.35 and 6.42

The wear volume of commercial magnesium based hybrid composite may also decrease significantly depending on matrix-particle reaction during processing as it has been stressed in the context of commercial magnesium based composite containing alumina in chapter-5. The higher volume loss in wear observed in commercial

magnesium based hybrid composites containing 15 vol% alumina appears to have been caused by aluminate. But in the hybrid composite containing 13 vol% alumina has higher volume loss than the in the hybrid composite containing 18 vol% alumina similar to observed in the composite containing 21 vol% alumina alone as shown in Fig.5.14. The higher volume loss in the hybrid composite containing 13 vol% alumina may be due to relatively lower alumina content. But all the hybrid composites show presence of MgO as a result of interfacial reaction between the alumina particles and the matrix magnesium. The wear rate also is affected by the presence of aluminate as it has been already pointed out in chapter-5. The hybrid composite containing 18 vol% alumina has similar wear rates shown in Fig. 6.26 as it has been observed in the composite containing 21 vol% alumina alone as shown in Fig. 5.18 The other hybrid composites based on commercial magnesium have wear rates an order of magnitude higher.

Similarly, the volume loss in wear in all the three AZ91 alloy based hybrid composites appear to be consistently low inspite of different processing history. The volume loss is similar to the lowest observed in the commercial magnesium based hybrid composites inspite of the presence of $MgAl_2O_4$ in the hybrid composites containing 16 and 17 vol% alumina. The wear rates in these composites are also lowest similar to that in magnesium based hybrid composite containing 18 vol% alumina. The wear rate decreases with increasing amount of alumina and the lowest has been observed in the hybrid composite containing 19 vol% alumina shown in Fig. 6.38 which has similar wear rates obtained in the composite containing 16 vol% alumina as shown in Fig. 5.30 Thus, it is clear from the above discussion that reinforcing both commercial magnesium and AZ91 alloy with alumina and graphite may provide composites with significantly lower volume loss and wear rate but the lower graphite content in the hybrid composites has not revealed its role clearly.

CHAPTER - 7

CONCLUSIONS

The present investigation on magnesium and AZ91 alloy based cast composites and their tribological characteristics have been presented in three segments as given in chapter 4, 5 and 6 outlining the results on the composites containing respectively the steelwool, the alumina and the hybrid of alumina and graphite. For each type of these dispersoids, singly or combined, two matrices of commercial magnesium and AZ91 alloys have been used. The study has led to the following conclusions presented in three segments pertaining to each type of dispersoid.

7.1 The Composite Containing Steelwool

- (1) Vacuum infiltration through a loosely packed bed of steelwool results into inhomogeneous distribution of steelwool creating steelwool deficient and steelwool rich regions, due to pushing by the infiltrating stream of molten metal or alloy.
- (2) The microstructure indicates dendritic solidification clearly revealed in the steelwool deficient region in the AZ91 alloy matrix and there is eutectic solidification in the last freezing liquid, often resulting into divorced eutectic consisting of a network of $Mg_{17}Al_{12}$ phase.
- (3) The magnesium based composites sometimes show shrinkage cavities at the boundary of infiltrating streams and often there are circular marks outlined by relatively darker solute rich region at the boundary of infiltrating streams.
- (4) The Brinell hardness of the composites based on either commercial magnesium or AZ91 alloy, increases with increasing steelwool content but the hardness appear to be lower than that estimated by the rule of mixture. AZ91 alloy based composites have higher hardness than those based on commercial magnesium.
- (5) The ultimate tensile strength (UTS) in magnesium based composite increases with increasing steelwool content but the increase is quite substantial when the steelwool content increases from 4.5 to 6.5 vol%. In AZ91 alloy based composite, the UTS is higher than those obtained in the composites based on commercial magnesium at comparable steelwool content.

- (6) The dry sliding wear in both commercial magnesium and AZ91 alloy based composites is mild and oxidative in the load range between 0.5 to 2.5 kg and under sliding speed of 1 m/s against the counterface of hardened steel.
- (7) The average coefficient of friction in both commercial magnesium and AZ91 alloy based composites decreases with increasing load which has been attributed to increasing cover of magnesium during sliding at higher loads over steelwool, replacing strong steel-steel (counterface) junctions by weak magnesium-steel (counterface) junctions.
- (8) The volume loss in wear in AZ91 alloy based composites is lower than that in commercial magnesium based composites at comparable steelwool content and load. AZ91 alloy has lower volume loss in wear compared to commercial magnesium at comparable steel wool content and load.
- (9) The wear rates in AZ91 alloy based composites are lower than that in commercial magnesium based composites at comparable steel wool content and load. There appears to be a discontinuity in wear rate between loads of 1.5 and 2 kg and beyond this load the rate of increase in wear rate with load decreases in commercial magnesium based composite but remains similar in AZ91 alloy based composites.
- (10) The wear coefficient is not a good index of wear resistance as increase in hardness and the consequent lowering of real area of contact, increases wear coefficient resulting in similar or higher wear coefficients in the composites and the base materials.
- (11) The wear rates calculated for composites at different loads on the basis of sharing of load by constituent phases, are much higher than those determined experimentally indicating considerable synergy between the constituents lowering the observed wear rate.

7.2 The Composite Containing Alumina

- (1) squeeze casting through a bed of alumina results into inhomogeneous distribution of alumina creating alumina deficient and alumina rich regions, due to pushing by the infiltrating stream of molten metal or alloy.
- (2) The microstructure indicates dendritic solidification, clearly revealed in the alumina deficient region in the AZ91 alloy matrix and there is eutectic solidification

resulting into lamellar eutectic consisting of $Mg_{17}Al_{12}$ phase in a matrix of bright phase of magnesium solid solution.

- (3) The magnesium based composites sometimes show shrinkage cavities at the boundary of infiltrating streams and there is evidence of eutectic solidification in the last freezing liquid, often resulting into divorced eutectic consisting of a network of $Mg_{17}Al_{12}$ phase. This appears to have resulted from aluminium enrichment of commercial magnesium resulting from reaction between alumina and molten magnesium during synthesis of the composite.
- (4) The chemical reaction at the interface of alumina during solidification processing has resulted into reaction product of MgO but sometimes $MgAl_2O_4$ also forms as revealed by X-ray diffraction, although magnesium rich corner of Al-Mg-O ternary phase diagram indicates only MgO as the stable phase.
- (5) The Brinell hardness of the composites based on commercial magnesium is significantly higher than that of squeeze cast commercial magnesium. In AZ91 alloy based composite the Brinell hardness increases with increasing alumina content. For comparable particle content, the higher matrix hardness in AZ91 alloy based composite results in higher hardness compared to that in commercial magnesium based composite.
- (6) In the composite based on commercial magnesium the Vickers microhardness of the matrix increases significantly due to solution strengthening and solute rich phase in the matrix provided by aluminium released by particle matrix reaction during solidification processing of the composite.
- (7) The dry sliding wear in both commercial magnesium and AZ91 alloy based composites containing alumina is mild and oxidative in the load range between 2.5 to 5.5 kg and under sliding speed of 1 m/s against the counterface of hardened steel.
- (8) The average coefficient of friction in both commercial magnesium and AZ91 alloy based composites decreases with increasing load more so in the case of commercial magnesium, possibly due to increasing plastic flow of the matrix to cover the alumina particles on the sliding surface.
- (9) At lower load of 2.5 kg, more alumina particles are exposed on the sliding surface and are in direct contact with the counterface of steel resulting in higher coefficient of friction. Such exposed particles may get debonded during sliding resulting in lowering of coefficient of friction. In composites where distribution of particles are

not uniform may show a lower coefficient of friction because of easy flow of matrix around unrestrained by the alumina particles.

- (10) AZ91 alloy has higher yield stress and is difficult to flow during sliding. Thus, there is higher average coefficient of friction in composites based on AZ91 alloy compared to those based on commercial magnesium but with comparable alumina content.
- (11) The volume loss in wear appears to be sensitive to the nature of reaction product during solidification processing. Presence of aluminate appear to increase the volume loss in wear significantly in both commercial magnesium and AZ91 alloy based composites.
- (12) The wear rate increases with increasing load in both commercial magnesium and AZ91 alloy based composites but there does not appear any discontinuity in wear rates. However, the tests have been carried out at a relatively higher range of load.
- (13) The wear rate in AZ91 alloy based composites appear to be lower than that in commercial magnesium based composites at comparable alumina content and load.
- (14) The wear rates and the wear coefficients in the composites based on commercial magnesium or AZ91 alloy, without significant amount of aluminate in it, appear to be an order of magnitude lower than that in the composites containing aluminate.

7.3 The Hybrid Composite Containing Alumina and Graphite

- (1) squeeze casting through a bed of alumina and graphite results into most of the graphite floating out and inhomogeneous distribution of alumina and graphite due to pushing by the infiltrating stream of molten metal or alloy.
- (2) The microstructure in magnesium based hybrid composite indicate both the graphite and alumina particles in a matrix of magnesium solid solution containing some solute rich precipitates except in the composite containing 18 vol% alumina where the particles are surrounded by a network of solute rich phase which may be part of divorced eutectic.
- (3) The microstructure of AZ91 alloy based hybrid composite indicates dendritic solidification, clearly revealed in particle deficient region and there is eutectic solidification in the last freezing liquid resulting into lamellar eutectic consisting of $Mg_{17}Al_{12}$ phase in a matrix of bright phase of magnesium solid solution. In some

regions there is considerable amount of eutectic which may be caused also by the shift of eutectic composition under pressure.

- (4) The chemical reaction at the interface of alumina during solidification processing has resulted into reaction product of MgO. Sometimes $MgAl_2O_4$ has also formed as indicated by its strongest peak from (311) in the X-ray diffraction patterns of both magnesium and AZ91 alloy based hybrid composites although magnesium rich corner of Al-Mg-O ternary phase diagram indicates only MgO as the stable phase.
- (5) The Brinell hardness of the hybrid composites based on both AZ91 alloy and commercial magnesium increases with increasing alumina content. The Vickers microhardness of the matrix also increases with increasing alumina content which may be attributed to matrix-particle reaction.
- (6) Graphite particles, although small in amount, appears to decrease the Brinell hardness in AZ91 alloy based hybrid composite containing 16 vol% alumina as compared to that in the composite containing 16 vol% alumina alone. Similar effect is also expected in magnesium based hybrid composites.
- (7) The dry sliding wear in both commercial magnesium and AZ91 alloy based hybrid composites containing alumina and graphite is mild and oxidative in the load range between 2.5 to 5.5 kg and under sliding speed of 1 m/s against the counterface of hardened steel.
- (8) The average coefficient of friction in both commercial magnesium and AZ91 alloy based hybrid composites decreases with increasing load as it has been observed in other composites investigated. The average coefficient of friction in magnesium based hybrid composites at low load of 2.5 kg increases with increasing alumina content indicating that these particles are possibly exposed on the sliding surface.
- (9) In the magnesium based hybrid composite containing 13 vol% alumina the friction is similar to that in squeeze cast magnesium inspite the presence of alumina particles. This may be attributed to the contribution of graphite in lowering the coefficient of friction.
- (10) In magnesium based composite, the volume loss in wear appears to be sensitive to the nature of reaction product during solidification processing. Presence of aluminate appear to increase the volume loss in wear significantly as it has been observed in the composites containing alumina alone. But in AZ91 alloy based hybrid composites the volume loss does not appear to get affected by the presence of aluminate.

- (11) The wear rate generally increases with increasing load in both commercial magnesium and AZ91 alloy based hybrid composites but there does not appear any discontinuity in wear rates. However, the tests have been carried out at a relatively higher range of load.
- (12) The wear volumes and the wear rates in the AZ91 alloy based hybrid composites are consistently lower and similar to the lowest observed in magnesium based hybrid composites.
- (13) The wear coefficients in the hybrid composites based on AZ91 alloy are consistently an order of magnitude lower than that observed in vacuum cast AZ91 alloy and similar to the lowest wear rates observed in commercial magnesium based hybrid composite.
- (14) The present study indicates that one may develop a variety of tribological materials in the system of composites investigated but the AZ91 alloy based composite processed in presence of graphite has yielded a consistent quality and the maximum wear resistance in a relatively higher load range. The composite containing steelwool could also result in good wear resistance in terms of lower volume loss and lower wear rate but the load range for its application should be relatively lower. In the composites containing alumina, the matrix-particle reaction during processing may not result in consistent quality in respect of their tribological properties but its cause needs to be further identified.

REFERENCES

- Akbulut, A., Durman, M. and Yilmaz, F., (1998), "Dry Wear and Friction of δ -Al₂O₃ Short Fiber Reinforced Al-Si (LM13) Alloy Metal Matrix Composites", Wear, vol. **215**, pp. 170-179.
- Alahelisten, A., Bergman, F., Olsson, M. and Hogmark, S., (1993), "On the wear of aluminium and magnesium metal matrix composites", Wear, vol. **165**, pp. 221-226.
- Alpas, A.T. and Embury, J. D., (1990), Scripta Metall. Mater., Vol. **24**, pp. 931-935.
- Ames, W. and Alpas, A.T., (1995), "Wear Mechanisms in Hybrid Composites of Graphite-20 Pct SiC in A356 Aluminium Alloy (Al-7 Pct Si-0.3 Pct Mg)", Metallurgical and Materials Transactions, vol. **26A**, pp. 85-98.
- Anand, K. and Kishore., (1983), Wear, Vol. **85**, pp. 163-169.
- Archard, J.F., (1980), "Wear Theory and Mechanisms", Wear Control Hand book, Edited by Peterson, M., B., and Winer, W., O., ASME, NY, pp. 35.
- Arsenault, R.J., Wang, L., and Feng, C.R., (1991), "Strengthening of composites due to microstructural changes in the matrix", Acta Metall. Mater. vol. **39**, No.1, pp. 47-57.
- Aune, T.K., and Ruden, T.J., (1992), "High temperature properties of magnesium die casting alloys", SAE Journal, vol. **101**, pp. 1-7.
- Bengisu, M.T. and Akay, A., (1997), "Relation of Dry Friction to Surface Roughness", J. of Tribology, Vol. **119**, pp. 18-25.
- Bhattacharyya, S., (1980), "Wear and Friction in Steel, Aluminum and Magnesium Alloys", Wear, vol **61**, pp. 133-141.

Bowden, F.P. and Tabor, D., (1950), "The Friction and Lubrication of Solids", Oxford University Press., pp. 19.

Brady and Clauser () "Material Hand Book"; Eleventh Edition, No. 620.11, B78M.

Broutman, L.J. and Krock, R.H; (1967), "Modern Composite Materials", Addison-Wesley Publishing Co.

Carc , C. and Masounave, J., (1990), "A Literature Review on Fabrication Techniques of Particulate Reinforced Metal Composite", Proc. Conf. in "Fabrication of Particulates Reinforced Metal Composites". Edited by Masounave., J. and Hamel, F.G, Montreal Quebec, Canada, pp. 17-21.

Chadwick, G.A., and Stubbington., "High quality squeeze casting of monolithic and of reinforced aluminium alloys", Technical Paper, Hi-Tec Metals R&D Ltd.

Chen, L.H. and Rigney, D.A., (1990), "Adhesion Theories of Transfer and Wear During Sliding of Metals", Wear, Vol. 136, pp.223-235.

Chris, Suman., (1990), "The Effects of Direct Aging on Mechanical Properties and Corrosion Resistance of Diecast Magnesium Alloys AZ91D and AM60B", Journal of Materials and Manufacturing, SAE Transactions, vol. 99, pp849-859.

Daniel, J.Sakkinen., (1994), "Physical Metallurgy of Magnesium Die cast Alloys", Materials and Manufacturing, SAE Transaction; vol. 103, pp.558-569.

Das, A.A, Yacoub, M.M., Zantout, B. and Clegg, A.J., "Cast Metal-Matrix Composites", Loughborough, UK., pp.69-78.

- David, Ilham B.Sc.,C.Eng; MIM, MIBF, MBIM Managing Director-Thom: "Fast Loop Moulding for Premium Quality Magnesium and Aluminium Alloy Castings" (1991), *The Foundryman*, pp.109-113.
- Eyre, T.S., (1976), "Wear Characteristics of Metals"., *Tribology International*, pp.203-212.
- Fukusako, T., Itsuo, O. and Yamauchi, I., (F 1266)"Vacuum suction casting process for aluminium and copper alloy pipes" pp.26-33.
- Ghosh, P.K. and Ray, S., (1988C), "Particle Dispersion and Fluid-Particle Interaction in a Slurry of Liquid Al-Mg Alloy and Al₂O₃ Particles"., *Trans. JIM*, Vol.29, pp.509-519.
- Ghosh, P.K. Ray, S. and Rohatgi, P.K; (1984A), "Incorporation of Alumina Particles in Aluminium-Magnesium Alloy by Stirring in Melt"., *Trans. of JIM*, Vol. 25, No. 6, pp.440-444.
- Guldberg, S., Westengen, H. and Albright, D.L; (1991), "Properties of squeeze cast magnesium based composites"., *SAE Journal*, vol. 100, pp.813-816.
- Hakon, Westengen., Albright, D.A. and Nygard, A., (1990), "Development of cast magnesium matrix composites"., *SAE Journal*, vol. 99, pp.606-612.
- Hallstedt, Z.K, Liu. and Agren., (1990), "Fibre-Matrix Interaction During Fabrication of Al₂O₃-Mg Metal Matrix Composites"., *Materials Science and Engineering*, vol A129, pp.135-145.
- Hansen., (1958),"Metallurgy and Metallurgical Engineering series"., constitution of Binary Alloys, McGraw-Hill Book Co.,pp.105, 662 & 927.

- Hanumanth, G.S., Irons, G.A. and Lafreniere, S., (1992), "Particle Sedimentation During Processing of Liquid Metal-Matrix Composites"; Metall. Trans; Vol. **23B**, pp. 753-763.
- Heine, R.W; Loper, C.,R. and Rosenthal, P.C., (1955), "Principle of Metal Casting", McGraw Hill, USA, pp.259.
- Henry, Hu. and Alan, Luo., (1997), "Recent developments in squeeze casting of magnesium alloys and their composites", Automotive alloys (ed. by S.K.Das and G.J.Kipouros), The Minerals, Metals and Materials society, pp.133-153.
- Hihara and Latanision. (1994), "Corrosion of metal matrix composites", International Materials Reviews, Vol **39**, No 6, pp.257-261.
- Hu, H. (1998), "Squeeze casting of magnesium alloys and their composites", Journal of materials science, vol **33**, pp.1579-1589.
- Inem, B. and Pollard, G., (1993), "Interface structure and fractography of a magnesium alloy, metal matrix composites reinforced with SiC particles", Journal of materials science, vol. **28**, pp.4427-4434.
- Iwai, Y., Yoneda, H. and Honda, T., (1995), "Sliding wear behavior of SiC whisker-reinforced aluminum composite", An International Journal on the Science and Technology of Friction, Lubrication and Wear, Wear **181-183**, pp.594-602.
- James, E. Hillis. and Scott, O. Shook., (1989), "Composition and Performance of an improved Magnesium AS41 Alloy", Journal of Materials and Manufacturing, SAE Transactions; vol.**98**. pp.11-18.

- James, D. Shearouse III and Barry, A. Mikucki., (1994), "The Origin of Microporosity in Magnesium Alloy AZ91"., Journal of Materials and Manufacturing, SAE Transactions, vol. **103**, pp.542-552.
- Jokinen, A. and Andersson, P.,(1990), Proc. Powder Metallurgy Conf.Exhib., Metal Powder Industries Federation, Pittsburgh, PA.
- Kagawa, Y. and Nakata, E., (1992), "Some mechanical properties of carbon fiber reinforced magnesium matrix composites fabricated by squeeze casting"., Journal of materials science letters, vol. **11**, pp. 176-178.
- Kamado, S. and Kojima, Y., (1997), "Microstructure and tensile properties of magnesium-zinc based alloy composites reinforced with δ Al₂O₃ short fiber or 9 Al₂O₃ 2 B₂O₃ whisker"., Proc. third international magnesium conference(ed. by G.W.Lorimer), Inst. of Materials, London, pp.613-625.
- Kimberly, Gaw., David, H. and Thomas, R., (1994), "The compatibility of Magnesium Alloys with Automatic Transmission Fluids"., Journal of Materials and Manufacturing, SAE Transactions, vol. **103**, pp.200-205.
- Klier,E.M., Mortensen, A., Cornie, J.A. and Flemings; (1991), "Fabrication of cast particle-reinforced metals via pressure infiltration"., Journal of Materials Science, vol. **29**, pp.2519-2526.
- Krishnan, B.P., Surappa, M.K. and Rohatgi, P.K., (1981), "The UPAL Process: a direct method of preparing cast aluminium alloy-graphite particle composites"., Journal of Materials Science, vol. **16**, pp.1209-1216.
- Lakhtin, Yu., (1990),"Engineering Physical Metallurgy and Heat-Treatment"., Mir Publishers Moscow., pp.392-397.

- Laurent, V. Jarry, and Regazzoni, G., (1992), "Processing microstructure relationships in compocast magnesium/SiC", Journal of materials science, vol. **27**, pp.4447-4459.
- Ledbetter, H.M., Datta, S.K. and Kyono., (1989), "Elastic constants of a graphite-magnesium composite", J.Appl. Phys., vol. **65**, No. 9, pp.3412-3416.
- Liu, Y.B., Lim, S.C., Ray, S. and Rohatgi, P.K., (1992), "Friction and Wear of Aluminium-Graphite Composite: The Smearing Process of Graphite During Sliding", Wear, Vol. **159**, pp.201-205.
- Lloyd, D.J., (1994), "Particle Reinforced Aluminium and Magnesium Matrix Composites", International Materials Reviews, vol. **39**, No. 1, pp.1-23.
- Luo, A., (1994), "Processing, microstructure and mechanical behaviour of cast magnesium metal matrix composites", Met. and Mater. Trans., vol. **26A**, pp.2445-2455.
- Marianne, V.and Hansen,R.S., (1994), "Metallurgical considerations for Machining Magnesium Alloys", Journal of Materials and Manufacturing, SAE Transactions, vol. **103**, pp.213-220.
- Masuo, E. and Takashige. H., Tadayoshi. H. and Hideaki, U., (1991), "Production Process of Metal Matrix Composite (MMC) Engine Block", SAE Technical paper Series, pp.1-13.
- Mileiko, S.T., (1969), "The Tensile Strength and Ductility of Continuous Fiber Composite", J. Mater. Sci; Vol. **4** No. **11**, pp. 974-981.
- Mikucki, B.A., MercerII, W.E. and Green, W.G., (1990), "Extruded magnesium alloys reinforced with ceramic particles", SAE Journal, vol. **99**, pp.597-605.

- Mortensen, L.J., Masur, J.A., Cornie and Flemings, M.C., (1989), "Infiltration of Fibrous Preforms by a Pure Metal: Part 1. Theory"., *Met. Transactions*, vol. **20A**, pp.2535-2546.
- Olav, H. and Hakon, W. and Albright. D., (1994), "High Purity Magnesium die casting Alloys: from Ingot to Cast Product"., *Journal of Materials and Manufacturing, SAE Transactions*, vol. **103**, pp.221-225.
- Peter, B.M., (1983), "The Friction Behaviour of Materials"., *wear*, Vol. **83**, pp.191-206.
- Polonsky, I.A. and Keer, L.M., (1996), "Scale Effects of Elastic-Plastic Behavior of Microscopic Asperity Contacts"., *Journal of Tribology, Transactions of the ASME*, vol. **118**, pp.335-340.
- Rabinowicz, E., (1965), "Friction and Wear of Metals"., John Wiley and Sons, Inc; New York.
- Rabinowicz, E., (1977), "Proceedings of International conference on Wear of Materials"., Louis, ASME, Newyork, pp.36-40.
- Ramesh, C.S., Seshadri, S.K. and Iyer, K.J.L., (1991), "A survey of aspects of wear of metals"., *Indian Journal of Technology*, vol. **29**, pp.179-185.
- Rana, F. and Stefanescu, D. M.,(1989), *Metall. Trans. A*, Vol. **20A**, pp.1564-1566.
- Rangachary, T., Chatterji, B. and Ganesha H.S; (1996), "Non-Destructive Testing of Magnesium Alloy Castings for Aerospace Application"; *Indian Foundry Journal*, pp. 6-9.
- Ray, S.,(1995), "Cast Metal Matrix Composites-Challenges in Processing and Design"., *Bull. Mater. Sci*; vol. **18**, No. 6, pp.693-709.

- Ray, S., (1995), "Casting of Metal Matrix Composites", Key Engg. Mater., Vol. 104-107, pp.417-446.
- Ray, S., (1994), "Casting of Metal Matrix Composite Components From slurry", J. of Indian Foundry, June, pp.37-44.
- Ray, S., (1993), "Review Synthesis of Cast Metal Matrix Particulate Composites", J. of Mater. Sci. vol. 28, pp.5397-5413.
- Ray, S., (1988), "Cast Reinforced Metal Composites", Proc. World Materials Congress, Chicago, IL, Sept. 24-30, 1988, Fishman S.G. and Dhingra A.K; Eds. ASM International.,Metals Park, OH, 1988, pp.61-66.
- Reed-Hill. R.E. and Abbaschian, R., (1994), "Physical Metallurgy Principles", PWS, Boston, pp.467-468.
- Roberts, Sheldon. C, (1960), "Magnesium and Its Alloys",John. Wiley and Sons, Inc.,pp-71-73.
- Ronald, F. Gibson., (1992), "Dynamic Mechanical Behavior of Composite materials and Structures"; Journal of Materials and Manufacturing, SAE Transactions, vol. 101, pp728-744.
- Rohatgi, P.K., Ray, S. and Liu, Y., (1992), "Tribological Properties of Metal Matrix-Graphite particle Composites", International Materials Reviews, Vol. 37, No. 3, pp.129-149.
- Rohatgi,P.K.,Ray,S. and Liu,Y., (1994), "Metal Matrix-Solid Lubricant Composites", Handbook of Lubrication and Tribology, vol 3, pp.149-163.

- Rohatgi, P.K., Ray, S. and Liu, Y., (1992), "Friction and Wear of Metal-Matrix Composites", ASM Handbook, Edited by Scott, D. Henry., Vol. **18**, pp.802-811.
- Rohatgi, P.K., Ray, S. and Liu, Y., (1992), "Friction and Wear of Metal-Matrix Composites", ASM Handbook, Edited by Scott, D. Henry, vol.**18**, pp.802-811.
- Rohatgi, P.K., Asthana, R. and Das, S., (1986), "Solidification, Structures, and Properties of Cast Metal- Ceramic particle Composites", International Metals Reviews, Vol. **31**, pp.115-139.
- Roy, M., Venkataraman, B., Bhanuprasad, V. and Mahajan, Y.R., (1992), "The Effect of Particulate Reinforcement on the Sliding Wear Behaviour of Aluminium Matrix Composites", Metall. Trans. Vol. **23A**, pp.2833-2847.
- Sarkar, A.D., (1980), "Friction and Wear", Academic press Inc; London.
- Sato, A. and Mehrabian, R., (1976), Metall. Trans. B, Vol. **7B**., pp.443-451.
- Sin, H.C., Saka, N. and Suh, N.P., (1979), " Abrasive Wear Mechanisms and Grit Size effect", Wear, vol, **55**, pp.163-190.
- Shook, S.O., and Green, W.G., (1985), "Improving magnesium's wear resistance - A composite approach", SAE Proc, Paper No. 850421, pp.1-8.
- Stefanescu, D.M., Baswas, B.K., Kacar and Moitra., (1988), "Behaviour of Ceramic Particles at the Solid-Liquid Metal Interface in Metal Matrix Composites", Metall. Trans.Vol. **19A**, pp.2847-2855.
- Suh, N.P; (1977), "An Overview of the Delamination Theory of Wear"; Wear, Vol. **44**, pp.1-16.

- Suh, N.P. and Sin, H.C., (1981), "The genesis of friction" wear, Vol, **69**, pp. 91-114.
- Surappa, M.K., Prasad, S.V. and Rohatgi, P.K., (1982), "Wear and Abrasion of Cast Al-Alumina Particle composites", Wear, Vol. **77**, pp-295-302.
- Tamala, R. Jomas, James, A. Cornie. and Kenneth, C. Russell., (1995), "Infiltration and wetting of alumina particulate preforms by aluminium and aluminium-magnesium alloys", Met. and Mater. Trans., vol. **26A**, pp.1491-1497.
- VijaiMohan, .V. and Gopalakrishna, V., (1996), "Technology for magnesium metal matrix composites", Indian Foundry Journal, pp.5-9.
- Wilks, T.E., King, J.F. and Wardlow, G.D., (1997), "The commercialisation of particle reinforced magnesium alloy composites", Proc. third international magnesium conference(Ed. by G.W.Lorimer), Inst. of Materials, London, pp.585-596.
- William, E. Mercer II. and James, E. Hillis., (1992), "The critical contaminate limits and salt water corrosion performance of Magnesium AE42 Alloy", Dow chemical co; Journal of Materials and Manufacturing, SAE Transactions, vol. **101**, pp.8-15.
- William, A. Glaeser., (1992), "Materials for Tribology", Tribology Series, **20**; pp. 114-129.
- Wolfgang, B., Weidinger, P., Watzinger, B., Sedlacek, R., Rosch, R. and Haldenwanger, H., (1997), "Time Dependent Deformation of the Magnesium Alloy AS21 and AZ91 around 100°C", Z. Metallkd, Vol. **88**, pp.636-641.
- Zam Zam, M. A., (1989), Metalwissenschaft Technik, Vol. **43**, pp.1158-1161.